Synthesis and Degradation of Biodegradable Polyurethanes

BLACKWELL, CATHERINE,JAYNE

Synthesis and Degradation of Biodegradable Polyurethanes

A thesis submitted for the degree of

Doctor of Philosophy

By

Catherine Jayne Blackwell

&

Department of Chemistry

Durham University

August 2016

Abstract

A series of biodegradable star poly(ε-caprolactone) (PCL)-based polyols and PCL-based diisocyanate prepolymers were synthesised and fully characterised. Biodegradable polyurethanes (PUs) were synthesised using star PCL-based polyols and either biodegradable diisocyanate prepolymers 4,4'-methylenebis(phenyl isocyanate) (MDI) or 2,4-toluene diisocyanate (TDI). The resulting polyols, diisocyanate prepolymers and PUs were subjected to enzymatic degradation using lipase for up to 30 days.

Chapter 1 is a general introduction to the reactions involved in the syntheses of PU foams and the ring-opening polymerisation of cyclic esters. The general components used in PU formulations including biodegradable polyols and diisocyanate prepolymers are discussed. Furthermore, polymer biodegradation testing methods and analytical methods to monitor degradation are investigated.

Chapter 2 includes the syntheses and enzymatic degradation of a series of biodegradable four- and six-arm star PCL polyols. This was achieved through the tin(II)octoate ($SnOct_2$) catalysed ring opening polymerisation (ROP) reaction of ε-caprolactone (ε-CL) using pentaerythritol, di(trimethylolpropane) and dipentaerythritol initiators. Furthermore, a series of six-arm star poly[(ε-caprolactone)-*co*-(β-butyrolactone)] were synthesised in a similar manner. Star PCL and star poly[(ε-CL)-*co*-(β-BL)] both exhibited almost 100% mass loss after 15 days of enzymatic degradation at a constant rate. Generally, an initial increase in % crystallinity ($\%\chi_c$) is seen for star PCL and star poly(ε-CL)-*co*-(β-BL) in the first few days (0-3 days) of enzymatic degradation. This was followed by a decrease in crystallinity ($\%\chi_c$), indicating amorphous regions of the polymer were preferentially degraded. This was supported by scanning electron microscopy (SEM) analyses showing surface pitting and occurrence of crystal spherulite structures within the first few days of enzymatic degradation.

Chapter 3 concerns the synthesis and enzymatic degradation of a series novel four-arm dumbbell-shaped copolymers $(PCL)_2$-(PEG)-$(PCL)_2$ bridged with 2,2'-bis(hydroxymethyl)propionic acid (bisMPA) moieties. This was achieved by the synthesis of a tetra-hydroxyl PEG macro-initiator through a coupling reaction of poly(ethylene glycol) (PEG) and acetyl-protected bisMPA using dicyclocarbodiimide (DCC) and 4-dimethylaminopyridine (DMAP). Subsequently, the four-arm star structure was synthesised with the $SnOct_2$ catalysed ROP of ε-CL using tetra-hydroxyl PEG macroinitiator. Contact

angle and %water uptake (%WU) indicated the copolymers containing a higher %PEG showed increased hydrophilic nature and surface wetting. A dispersity (Đ) of 1.32-1.51 and a small molecular weight shoulder were seen due to using a polydisperse PEG macro-initiator and the high viscosity of the reaction mixture under bulk conditions. The novel star copolymers showed >90% mass loss within 7 days and an increase in $\%\chi_c$ within the first few days of enzymatic degradation.

Chapter 4 entails the synthesis and enzymatic degradation of biodegradable seven arm star PCL with a central acetylated β-cyclodextrin (β-CD) moiety. This was achieved through a four step synthetic route involving the protection of 1° OH groups on the β-CD moiety, acetylation of the 2° OH groups on the β-CD moiety, removal of protecting group on the 1° OH group and subsequent ROP of ε-CL catalysed by $SnOct_2$. Contact angle and %WU analyses showed minimal surface wetting and high hydrophobicity. A very low rate of enzymatic degradation was seen with 7% mass loss and a general increase in $\%\chi_c$ in 20 days.

Chapter 5 involves the synthesis and enzymatic degradation of a series of biodegradable diisocyanate prepolymers containing a central PCL or PCL-*b*-PEG-*b*-PCL moiety and capped with either MDI or TDI moieties. This was achieved through the reaction of two molar equivalents of the diisocyanate moiety, MDI or TDI, and either PCL diol or PCL-PEG-PCL triblock copolymer. The diisocyanate prepolymers showed absorbances attributing to the C=N stretch in the NCO group as well as N-H and C-N in the urethane group in FT-IR spectra. Contact angle and %WU measurements of diisocyanate prepolymers with higher %PEG showed increased surface wetting and hydrophilicity. Generally the TDI-based diisocyanate prepolymer showing 100% mass loss in 4 days, degraded at a faster rate than MDI-based diisocyanate prepolymer of 23% in 40 days. Furthermore, the lower M_n MDI-based prepolymer showed a significantly faster rate of enzymatic degradation of 79% mass loss in 40 days than the higher M_n MDI-based prepolymer.

Chapter 6 concerns the synthesis and enzymatic degradation of a series of biodegradable PUs using biodegradable PCL-based star polyols and diisocyanate prepolymer components synthesised in Chapter 2-5. PU gels were produced as a result of a minimal amount of dichloromethane (DCM) solvent to ensure complete mixing. Generally, PUs showed the disappearance of the C=N stretch in fourier transform infrared spectroscopy (FT-IR) analyses, indicating all NCO groups successfully reacted to give urethane groups. PUs showed up to 18.5% mass loss over the 30 days of enzymatic degradation. Comparisons of

the PU degradation behaviour were made to demonstrate the effects of polyol type, diisocyanate type, and ratio of NCO:OH used, on the rate of PU enzymatic degradation.

Chapter 7 surmises and concludes the work covered in Chapter 2-6 and suggests further work.

Acknowledgements

I would like to thank Dr. Ezat Khosravi for his contributions during my PhD studies. I would also like to thank my industrial supervisor Mike Groombridge for his support and Michael McDonnell, Denis Gonzalez and Todd Underiner at P&G. I want to thank Doug Carswell for running the DSC and TGA experiments, the NMR service, CIS department, lab technicians in stores and lab attendants for their assistance.

I would also like to thank the members of the Khosravi research group, Dr. Peter King, Dr. David Cole, Dr. Russell Balster, Andrew Longstaff, Kieran Atter, Rose Simnett and Shenghui Hou. Further thanks to Vicki Linthwaite, Sam Lear, Hannah Bolt, Caitlin Mooney, Maria Czyzewska, Dr. Stephen Boothroyd, Brunella Maranesi, Dr. Tatiana Lovato, Dr. Asahi Cano-Marques, Dr Alex Hudson, Dr. Paul Brooks. Thanks also to Ustinov College Womens Basketball team.

I am extremely grateful for my family's support throughout my PhD, particularly my mum, dad, brother, sister, Rachel, Lucas and grandma. Finally I would like to say a big thank you to my partner Dr. Pete King who has constantly helped and supported me throughout my time at Durham in addition to sharing many memorable holidays!

Memorandum

The work reported in this thesis was carried out in the Department of Chemistry, Durham University, between October 2012 and June 2016. This work has not been submitted for any other degree in Durham and is the original work of the author except where acknowledged by means of appropriate reference.

Signed: _____ Date: _____

Financial Support

I gratefully acknowledge Proctor and Gamble for their funding of this research

Contents

Abbreviations

ASAP	Atmospheric Solids Analysis Probe Mass Spectrometry
AY	Candida cylindracea lipase
$BF_3.Et_2O$	Boron trifluoride diethyl etherate
bisHMPA	2,2'-Bis(hydroxymethyl)propionic acid
β-BL	β-Butyrolactone
CD	Cyclodextrin
$CDCl_3$	Deuterated chloroform
ε-CL	ε-Caprolactone
CLSM	Confocal scanning microscopy
COSY	Correlation spectroscopy
Đ	Dispersity
DCC	Dicyclocarbodiimide
DCM	Dichloromethane
dd	Double doublet
DMAP	4-Dimethylaminopyridine
DMF	Dimethylformaldehyde
DP	Degree of polymerisation
DP_{NMR}	Degree of polymerisation determined by NMR
DP_{SEC}	Degree of polymerisation determined by SEC
DP_{Th}	Theoretical degree of polymerisation
DSC	Differential scanning calorimetry

%EM	% Extracted material
FDA	US Food and Drug Administraion
FT-IR	Fourier transform infra-red spectroscopy
g	Gram(s)
GC-MS	Gas chromatography-Mass spectrometry
h	Hour(s)
ΔH_c	Enthalpy of crystallisation
HCl	Hydrochloric acid
ΔH_m	Enthalpy of melting
HMBC	Heteronuclear multiple-bond correlation
HMDI	1,1'-methylenebis(4-isocyanatocyclohexane)
HSQC	Heteronuclear single quantum coherence
Hz	Hertz
J	Coupling constant
kHz	Kilohertz
MALDI	Matrix-assisted laser desorption/ionisation mass spectrometry
MDA	Methylene dianiline
MDI	4,4'-Methylenebis(phenyl isocyanate)
MeOH	Methanol
MHz	Megahertz
mmol	Millimole(s)
min	Minute(s)
mL	Millilitre(s)

M_p	Peak molecular weight
M_n	Number average molecular weight
M_n^{NMR}	Number average molecular weight determined by NMR
M_n^{SEC}	Number average molecular weight determined by SEC
M_n^{Th}	Theoretical number average molecular weight
M_w	Weight average molecular weight
NaOH	Sodium hydroxide
NIPU	Non-isocyanate polyurethane
NMR	Nuclear magnetic resonance
PBS	Phosphate buffer saline
PCL	Poly(ε-caprolactone)
PCL-*b*-PEG-*b*-PCL	Poly[(ε-caprolactone)-*b*-(ethylene glycol)-*b*-(ε-caprolactone)]
PDI	1,4-phenylene diisocyanate
PEG	Poly(ethylene glycol)
PGA	Poly(glycolic acid)
PLA	Poly(lactic acid)
PLGA	Poly[(lactic)-*co*-(glycolic acid)]
PP	Porcine pancreatic lipase
ppm	Parts per million
PS	Pseudomonas cepacia
PU	Polyurethane
ROP	Ring-opening polymerisation
SAXS	Small-angle x-ray scattering

s	Second(s)
SEC	Size exclusion chromatography
$SnOct_2$	Tin (II) ethyl hexanoate
%SU	% Solvent uptake
TBDMS-Cl	*tert*-butylchlorodimethylsilane
T_c	Crystallisation temperature
T_d	Degradation temperature
TDI	Toluene-2,4-diisocyanate
T_g	Glass transition temperature
TGA	Thermogravimetric analysis
T_m	Melting point
υ	Wavenumber
%WU	% Water uptake
χ_c	Degree of crystallinity

1.0 General Background on Biodegradable Polyurethanes

Polyurethanes (PUs) are characterised by the NHCOO urethane group, formed by the reaction of an NCO group on a diisocyanate or polyisocyanate moiety and an OH group on a polyol moiety. The high commercial value of PU stems from the ability to fine tune the physical properties from a considered and balanced selection of components. Due to the numerous compounds that can be used in PU synthesis, there is a huge range of applications for PU materials.[1] The global production of the seven major PU materials in 2012 are shown in Figure 1.1, namely flexible foam, rigid foam, elastomers, coatings, adhesives, binders and sealants.

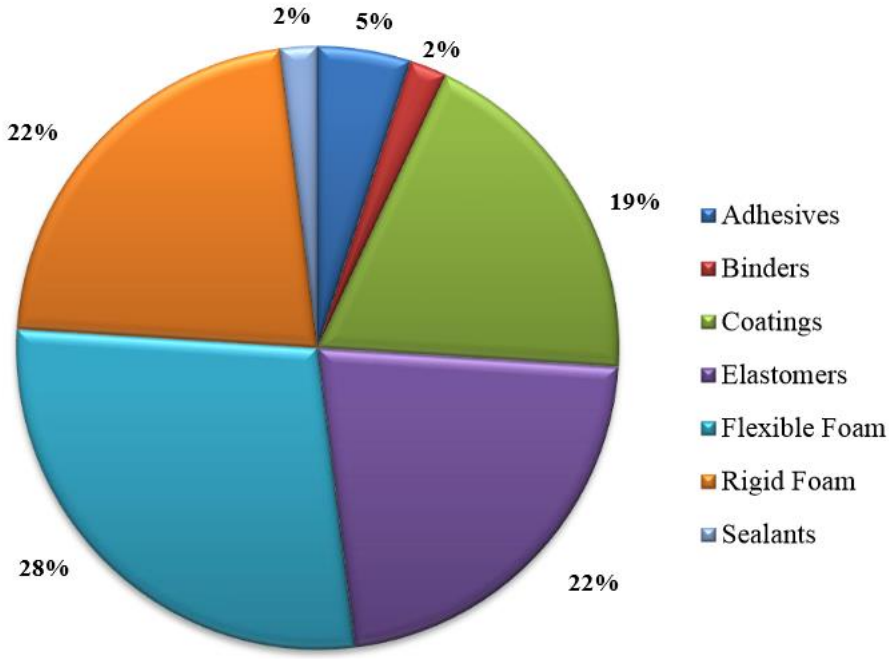

Figure 1.1: Global production of PU showing a range of applications in 2012[1]

In recent years, the demand for biodegradable polymers on a whole has largely increased as synthetic polymer wastes are disposed in landfills and incinerators, causing significant environmental problems.[2,3] Biodegradable PUs have been extensively researched for use in biomedical applications due to their tuneable rate of degradation and high mechanical strength.[4,5] However, for environmental reasons there is a commercial interest in producing biodegradable rigid PU foam. Furthermore, the use of ground particles of biodegradable rigid PU foam in personal products is of commercial interest for

companies such as P&G. The majority of research in the area of biodegradable rigid PU foam centres on using a biodegradable polyol component with a non-biodegradable aromatic diisocyanate, therefore, a compromise between the desired physical properties and biodegradability.

1.1 General Chemical Reactions in PU Foam Synthesis

The synthesis of PU foam comprises of two principle reactions in addition to several side reactions. The two key 'gelation' and 'blow' reactions are associated with the NCO group on the diisocyanate moiety and OH group on the polyol moiety, and with the NCO group on the diisocyanate moiety and water, respectively.

1.1.1 The Gelation Reaction

The exothermic gelation reaction is between multiple NCO groups on the diisocyanate moiety and multiple OH groups on the polyol moiety, forming urethane groups, Scheme 1.1.

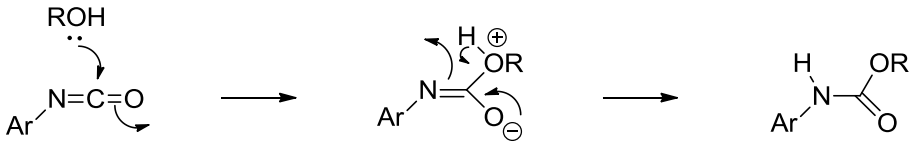

Scheme 1.1: Mechanism of the nucleophilic attack at an isocyanate

The OH group donates electrons to the electropositive carbon atom in the NCO group and the proton is exchanged to the nitrogen atom. It has been reported that the gelation reaction can either be autocatalytic, whereby the free electron pair located on the nitrogen atom acts as the catalytic species, or organo-tin catalysts such as dibutyltin dilaurate can be used.[6] The gel point can be defined as the point in time in which a critical amount of polymer chains are physically or chemically bonded so that at least one large polymer chain is coextensive with the polymer phase. Literature suggests the gel strength significantly increases as the length between the cross-links are decreased.[7]

1.1.2 The Blow Reaction

The exothermic 'blow' reaction involves the NCO group on the diisocyanate moiety **1.1** and water *via* the formation of an unstable carbamic acid **1.2**, which subsequently decomposes yielding an NH_2 group **1.3** and gaseous CO_2, Scheme 1.2.

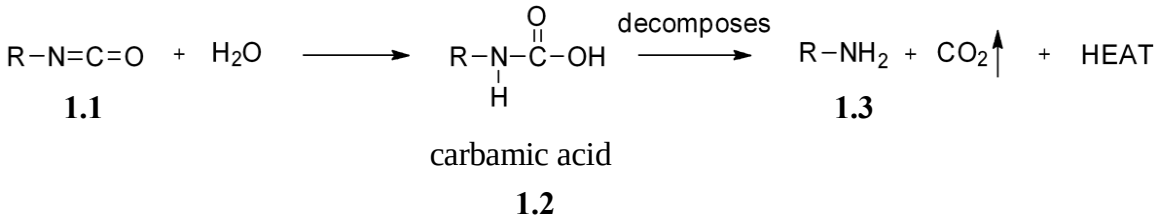

Scheme 1.2: The blow reaction

The generation of heat during the exothermic blow reaction causes the expansion of gaseous CO_2 and thus can blow the viscous liquid into foam. However, the relative rates of the blow and gelation reactions can significantly affect the foam structure and so must be carefully balanced. The use of a solvent in the syntheses of PU using multi-functional diisocyanate and polyol components results in a cross-linked PU gel. This is due to the gaseous CO_2 escaping due to the lower viscosity of the reaction mixture.

The electropositive carbon in the NCO group **1.1** will react with any labile hydrogen atom in the system, e.g. the newly formed NH_2 group **1.3** to generate a disubstituted urea group **1.4**, Scheme 1.3.[8] This reaction could introduce additional covalent cross-linking points to the PU structure if a poly-functional isocyanate or amine is used.

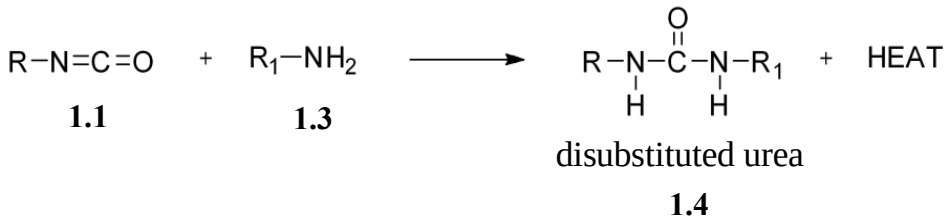

Scheme 1.3: Formation of disubstituted urea

Furthermore, the electropositive carbon atom in the NCO group **1.1** could react with the hydrogen atoms on the disubstituted urea **1.4** and urethane groups **1.5** to form biuret **1.6**, Scheme 1.4a, and allophanate groups **1.7**, Scheme 1.4b. The formation of biuret **1.6** and

allophonate **1.7** groups in the PU structure generates additional cross-linking sites. It has been reported that the reversible reaction in the formation of the biuret group **1.6** occurs at high temperatures between 100-135 °C, and decomposes at temperatures in excess of 135 °C.[9] Furthermore, the generation of the allophanate group **1.7** occurs at temperatures in the region of 110-135 °C.[6,9] This suggests the probability of additional cross-linking during PU syntheses is increased with higher reaction temperatures, through the generation of disubstituted urea **1.4**, biuret **1.6** and allophonate **1.7** groups.

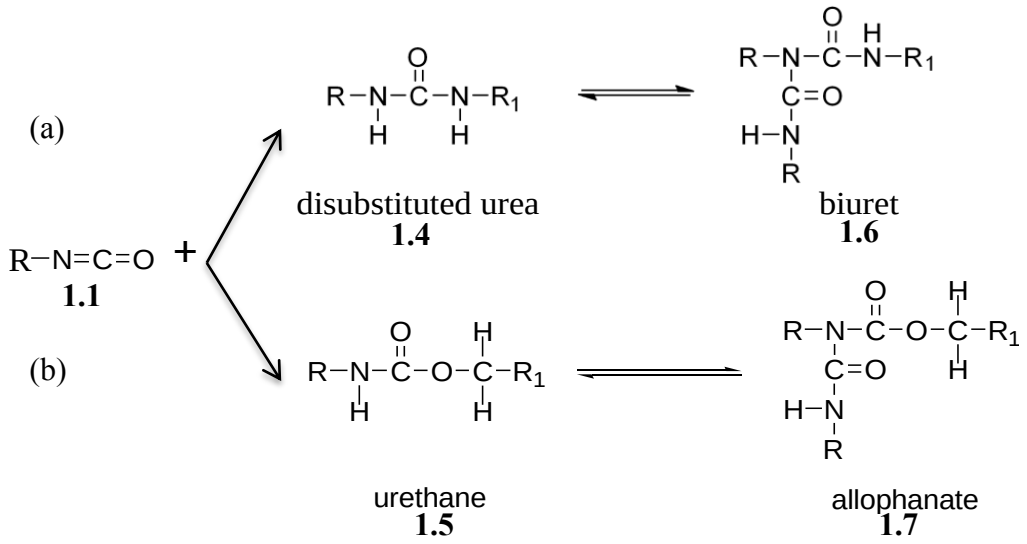

Scheme 1.4: Formation of (a) biuret **1.6** and (b) allophonate **1.7**

1.2 Basic Polyurethane Components

Polyols bearing a least two OH groups and isocyanate compounds bearing at least two NCO groups comprise the major components in the syntheses of PU. Di-functional or poly-functional polyol and isocyanate components can be used to produce either linear or cross-linked materials, respectively. Commonly, polyethers or polyesters are employed as the polyol component and aliphatic or aromatic diisocyanates are used as the isocyanate component. Furthermore, components such as chain-extenders, cross-linkers, catalysts, silicone surfactants and other additives can be used to achieve the desired characteristics of the resulting PU.

1.2.1 Catalysts

To promote the rate of the gelation and blow reactions in PU syntheses, catalysts such as nitrogen containing compounds with at least one tertiary nitrogen atom, organometallic

compounds or Lewis acids are used. Varying catalytic blends are often employed depending on the desired physical properties of the resulting PU. Tertiary amines such as *N*,*N*-dimethyl cyclohexylamine **1.8**,[10] Figure 1.2(a), and organo-tin catalysts such as dibutyltin dilaurate **1.9**,[11,12] Figure 1.2(b), have been shown to catalyse the blow reaction and the gelation reaction, respectively.

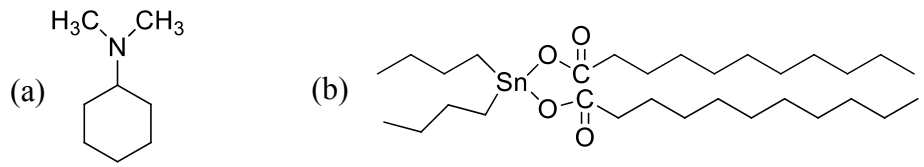

N,*N*-dimethyl cyclohexylamine **1.8**

Dibutyltin dilaurate **1.9**

Figure 1.2: Structures of catalysts used in PU synthesis (a) *N*,*N*-dimethyl cyclohexylamine **1.8** and (b) dibutyltin dilaurate **1.9**

1.2.2 Surfactants

Organo-silicon surfactants can be added to the PU foam formulation to help both emulsify the mixture of components and stabilise the expanding cells. Consequently, physical properties such as structure, size and open or closed character of the cells can be selected through modification or amount of surfactant used.[13,14,15] Organo-silicone surfactants consist of a polydimethylsiloxane (PDMS) backbone and poly(ethylene oxide-*co*-propylene oxide) (PEO-PPO) random copolymer grafts. Studies have shown that these surfactants do not alter the reaction kinetics in the PU foaming process, but have significant effects on the cell window stabilisation stage of the cell formation process. However, it can be noted that the effect of the surfactant is not greatly understood.[16]

1.2.3 Chain Extenders

Diamines or low molecular weight diols such as ethylene glycol, 1,4-butanediol and 1,6-hexanediol are commonly used as chain extenders in PU formulations. Studies have shown that the degradation rate and mechanical properties of PUs can be controlled by the structure and length of chain extenders.[17,18] Degradable chain extenders have been synthesised based on DL-lactic acid and ethylene glycol to increase the rate of PU degradation.[19] Skarja and Woodhouse studied the effect of novel amino acid based

degradable chain extenders in the degradation of PUs.[20] The results showed that the PUs containing the degradable chain extenders were more susceptible to enzyme-mediated degradation, but had no significant effect on the hydrolytic degradation of PU in buffer alone solution.

1.2.4 Biodegradable Polyols

Biodegradable polyols can be divided into two groups of enzymatically degradable and hydrolytically degradable polymers. It has been suggested that most naturally occurring polymers undergo enzymatic degradation due to their inherent bioactivity and presence of receptor-binding ligands.[21] Hydrolytically degradable polymers contain chemical bonds susceptible to hydrolysis in their backbone, for example functional groups such as esters, carbonates, anhydrides, amides and urethanes.

Biodegradable PUs have been synthesised through the incorporation of hydrolytically labile aliphatic polyester components, such as poly(ε-caprolactone) (PCL) **1.10**,[22] Figure 1.3(a), and poly(lactic acid) (PLA) **1.11**,[23] Figure 1.3(b).

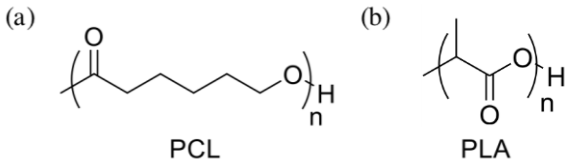

Figure 1.3: Structures of biodegradable aliphatic polyesters (a) poly(ε-caprolactone) **1.10** and (b) poly(lactic acid**) 1.11**

Biodegradable aliphatic polyesters PCL **1.10** and PLA **1.11** have found use in many biomedical applications such as resorbable sutures and drug-delivery systems. The hydrolysable ester groups located in the backbone allows the polymer to be fragmented into smaller, water soluble compounds that can be metabolised by enzymes and therefore, increase the rate of polymer biodegradation.[24,25]

It has been suggested that the degradation mechanism for aliphatic polyesters is primarily bulk erosion, showing an initial period of no significant mass loss, followed by spontaneous rapid mass loss in a short period of time.[26]

1.2.4 Ring Opening Polymerisation of Cyclic Esters

Polyesters can be prepared either by a polycondensation technique using compounds with hydroxyl and carboxylic acid groups or by the ring-opening polymerisation (ROP) of cyclic esters. It is difficult to obtain high molecular weight polymers using the polycondensation technique. Therefore, the facile ROP technique has been extensively used in the syntheses of a range of well-defined polyesters with architectures such as graft or star structures.

The ROP of cyclic esters in bulk conditions are commonly catalysed using the US Food and Drugs Administration (FDA) approved $SnOct_2$ **1.12**,[27,28] Figure 1.4(a). This is due to good solubility in common organic solvents, good control of the polymerisation reaction and commercial availability. However, other suitable catalysts have been reported such as aluminium isopropoxide **1.13**,[29] Figure 1.4(b), and an organocatalytic system based on 4-dimethylaminopyridine (DMAP) **1.14**,[30] Figure 1.4(c).

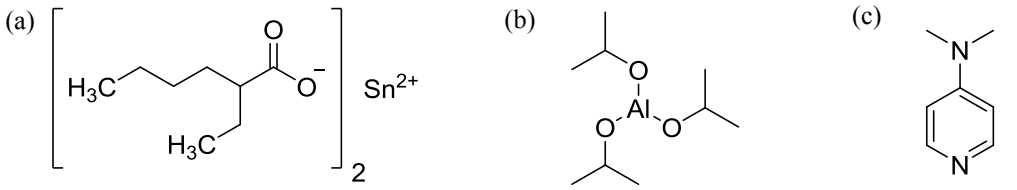

Tin (II) 2-ethylhexanoate **1.12**

Aluminium isopropoxide **1.13**

DMAP **1.14**

Figure 1.4: Structures of (a) $SnOct_2$ **1.12** (b) aluminium isopropoxide **1.13** and (c) DMAP **1.14** used as catalysts in the ROP of cyclic esters

There have been several proposals for the mechanism of $SnOct_2$ **1.12** in the ROP of cyclic esters, however it still remains unclear. The most accepted mechanism is the coordination-insertion mechanism whereby a hydroxyl functional group coordinates to $SnOct_2$ **1.12** to give an initiating tin-complex, Scheme 1.5.[31,32,33,34,35]

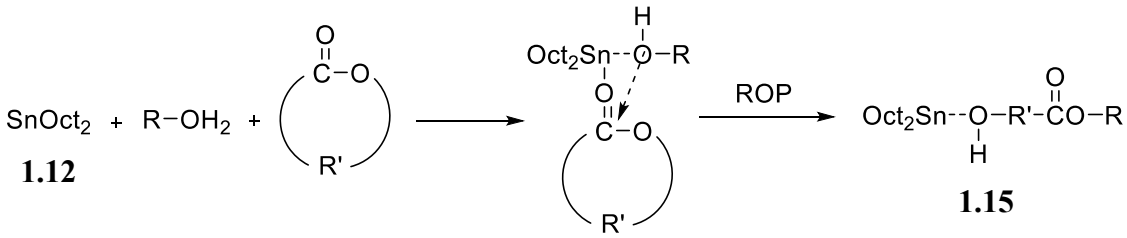

Scheme 1.5: ROP mechanism using $SnOct_2$ **1.12** catalyst and showing the complexation of a cyclic ester monomer and OH group to give initiating tin complex **1.15**

It has been suggested that propagation proceeds through the coordination of the cyclic ester monomer to the metal atom, followed by monomer insertion into the metal chain end and cleavage of the acyl-oxygen bond. Propagation of the growing polymer polymer chain proceeds by the insertion of a new cyclic ester monomer. PCL can be synthesised in the facile ROP of ε-caprolactone (ε-CL) in bulk, catalysed by $SnOct_2$ **1.12**.[36,37] A possible problem with using $SnOct_2$ **1.12** is the high reaction temperatures required which increases the probability of intramolecular and intermolecular transesterification reactions. This could lead to an increase in dispersity (Đ).[38]

1.2.4.2 Star Polyesters

Linear and star PCL polyols have been synthesised by the ROP of ε-CL catalysed by $SnOct_2$ **1.12** using di-hydroxyl and multi-hydroxyl initiators, respectively.[39] Common multi-hydroxyl initiators include glyercol **1.16**, trimethylolpropane **1.17**, pentaerythritol **1.18**, di(trimethylolpropane) **1.19** and dipentaerythritol **1.20** to give star polymers with 3-6 arms, Figure 1.6(a-e).[39,40,41,42,27]

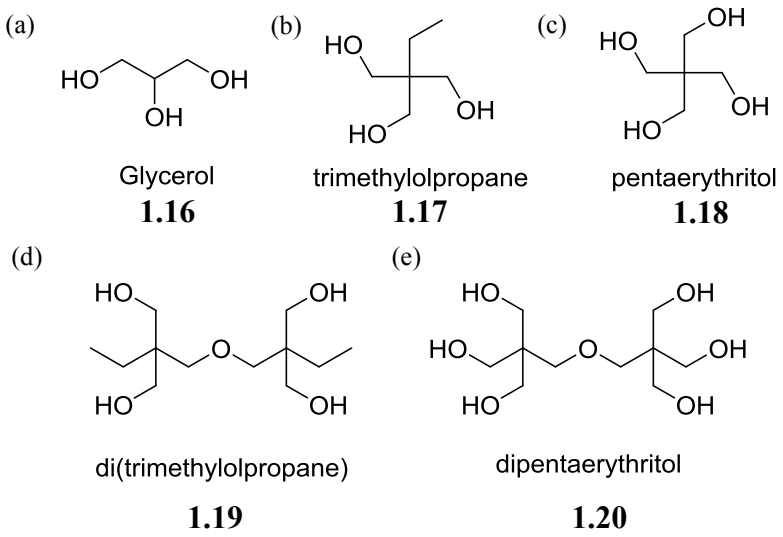

Figure 1.5: Structures of multi-hydroxyl initiators (a) glycerol **1.16** (b) trimethylolpropane **1.17** (c) pentaerythritol **1.18** (d) di(trimethylolpropane) **1.19** and (e) dipentaerythritol **1.20**

It has been reported that star PCL structures with longer arms show enhanced thermal properties and % crystallinity (%χ_c). However, little effect was observed on the %χ_c or glass transition temperature (T_g) of the star PCL with an increase in the number of arms.[43,40] The lengths of the arms on the star polyester can be controlled by varying the molar ratio of cyclic ester monomer to multifunctional initiator.[40] However, the lengths of the arms on the star polyester are an average of all the arms in the structure.

1.243 Cyclodextrin

Cyclodextrins (CD) are naturally occurring cyclic oligosaccharides containing six, seven and eight linked glucose units in α-, β- and γ-CD, respectively, Figure 1.6. Their inherent biodegradability and biocompatibility as well as their unique basket-shaped topology has led to research in their use in a variety of applications, including use in cosmetics, food and drug delivery.[44]

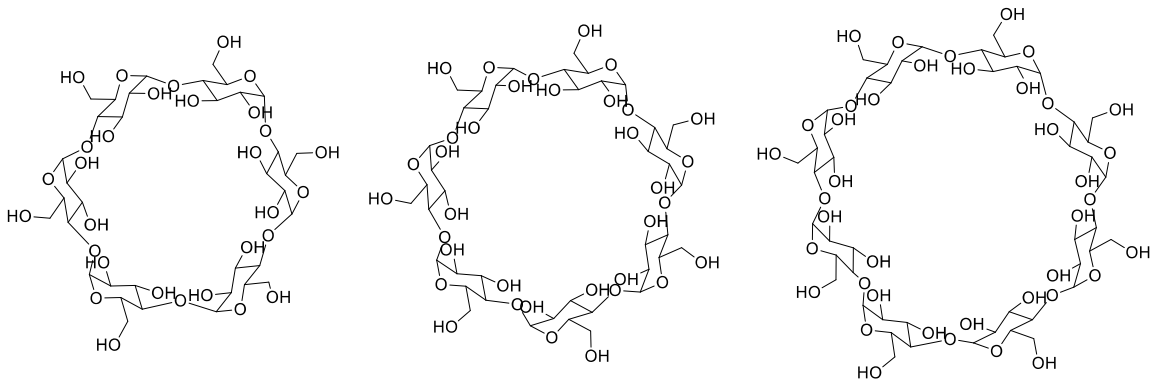

1.21 **1.22** **1.23**

Figure 1.6: Structures of α-CD **1.21**, β-CD **1.22** and γ-CD **1.23**

The seven 1° OH groups on the β-CD **1.22** moiety have been used directly as a cross-linking agent in the synthesis of PU.[45,46] However, the extent to which the OH groups react is unknown. β-CD **1.22** has been used as a multi-hydroxyl initiator in the ROP of ε-CL to give star PCL architectures.[47,48] However, β-CD **1.22** has been shown to form inclusion complexes with its inner cavity and PCL which could have implications on the degradation behaviour.[49] The seven arm star PCL polyols containing a biodegradable β-CD core could be used as the polyol component in the synthesis of biodegradable PU, Figure 1.7.

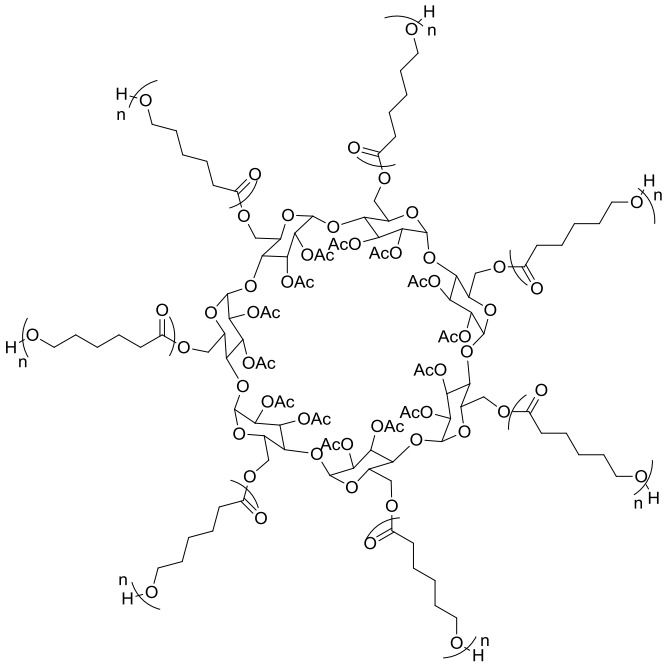

1.24

Figure 1.7: Seven-arm star PCL with acetylated β-CD core **1.24** [47]

1.244 Natural Oils

The synthesis of polymers from renewable resources such as natural vegetable oils have been of interest due to economic and environmental concerns.[50,51] Vegetable oils are triglycerides and can be functionalised to form polyols for the use in PU syntheses. This can be achieved through an epoxidation followed by a ring opening reaction to give OH groups.[52,53] Studies show that castor oil **1.25** can be used directly in the synthesis of biodegradable PU due to the 2° OH groups present in its structure, Figure 1.8.[54,55]

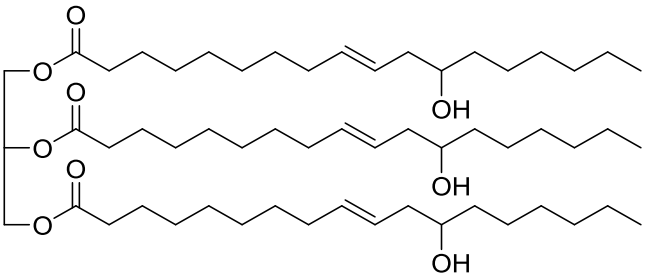

1.25

Figure 1.8: Structure of castor oil **1.25**

The presence of ester groups in natural vegetable oils renders the resulting PU biodegradable. However, the hydrophobic nature of natural vegetable oils mean that these PUs generally exhibit a slow rate of degradation.[54,56]

1.2.4.5 Incorporation of a Hydrophilic Poly(ethylene glycol) moiety

Studies have shown the incorporation of a hydrophilic poly(ethylene glycol) (PEG) moiety can increase the rate of degradation of PUs.[57,54] Yeganeh *et al*. reported that a range of PUs synthesised with PCL and PEG polyol components with HDI, showed increased surface and bulk hydrophilicity with increasing PEG content.[54] Furthermore, studies have shown that the rate of hydrolytic degradation of PCL-PEG copolymers increased with an increase in hydrophilic PEG content.[58,59] However, it must be noted that the PEG moiety in the PCL-PEG copolymer will remain intact throughout the degradation experiments. Degradation data of the tested films can show up to 100% mass loss, despite the water soluble PEG moiety not undergoing any degradation.

It has been reported that PU surface hydrophilicity has been related to good adhesion of bacteria on the polymer surface and therefore is an important factor to consider in the rate of biodegradation under composting conditions.[60]

Moreover, it has been reported that increasing the molecular weight of the hydrophobic PCL polyol used in the syntheses of PUs decreases the rate of hydrolytic degradation in a buffer solution (pH = 7.4) at 37 °C.[61] It was suggested that the decrease in the rate of degradation was due to a decrease in the PU water absorption ability. Furthermore, it was reported that the rate of degradation increased with time as a result of increased content of hydroxyl and carboxylic acid groups generated at the surface during degradation. However, the study did not identify any degradation products and PUs showed a very slow rate of degradation of up to 12% mass loss after 6 months. It has been suggested that polymer degradation is significantly affected by crystallinity and polymer chain mobility.[62] Furthermore, it has been observed in the literature that a PCL-PEG copolymer exhibits lower $\%\chi_c$ than PCL homopolymer.[63]

1.2.5 Isocyanates

The term 'isocyanate' is used to refer to compounds containing the NCO functionality. The electropositive carbon atom readily reacts with any labile hydrogen atom in the system and this high reactivity can be explained by the resonance structures of the NCO group, Figure 1.9. The electronegative oxygen and nitrogen atoms withdraw electron density from the neighbouring electropositive carbon atom. This allows a suitable nucleophile containing a hydrogen atom to add to the carbon atom with the subsequent transfer of the hydrogen atom to the nitrogen atom.

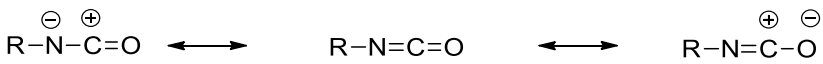

Figure 1.9: Resonance structures of isocyanate

Either aliphatic or aromatic isocyanates can be used in the syntheses of PU, depending on the desired properties of the polymer product. The aromatic compounds 2,4-toluene diisocyanate (TDI) **1.26**, Figure 1.10a, and 4,4′-methylenebis(phenyl isocyanate) (MDI) **1.27**, Figure 1.10b, are the most commonly used diisocyanates in PU foam formulations.[4]

The NCO groups on aromatic isocyanates have comparatively faster reaction rates than the aliphatic equivalents, such as hexamethylene diisocyanate (HDI) **1.28**, Figure 1.10c and lysine diisocyanate (LDI) **1.29**, Figure 1.10d. This is due to the stabilisation of the negative charge on the nitrogen atom by the neighbouring aromatic ring.

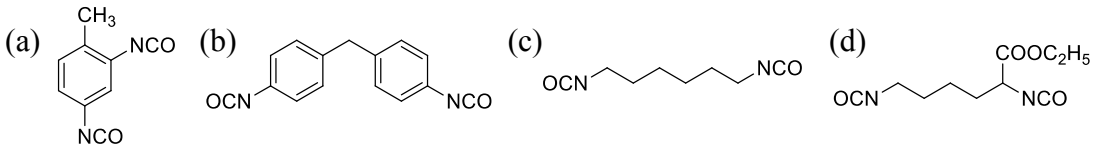

2,4-TDI **1.26** | 4,4-MDI **1.27** | 1,6-HDI **1.28** | LDI **1.29**

Figure 1.10: Structures of common diisocyanates used in the synthesis of PU (a) TDI **1.26** (b) MDI **1.27** (c) HDI **1.28** and (d) LDI **1.29**

Polyisocyanates such as polymeric methylene diphenylene diisocyanate (PMDI) have also been used in PU foam formulations and have an average NCO functionality in the range of 2.5-3.2.[55,64] The higher number of NCO groups results in an extensive cross-linked PU network.

MDI **1.27** is commercially desirable due to its crystalline nature and fast reaction with labile hydrogen atoms, however, a notable disadvantage is the possibility of producing highly toxic, carcinogenic methylene dianiline (MDA) **1.31** as a degradation product.[4,65,66,67,68] The proposed formation of MDA **1.31** *via* thermohydrolytic degradation is outlined in Scheme 1.6.[69] To avoid this toxic metabolite, isocyanates have been synthesised from L-lysine or other amino acids and found that they degraded *via* the ester linkage, and did not produce any non-biodegradable toxic metabolites.[67,70,21]

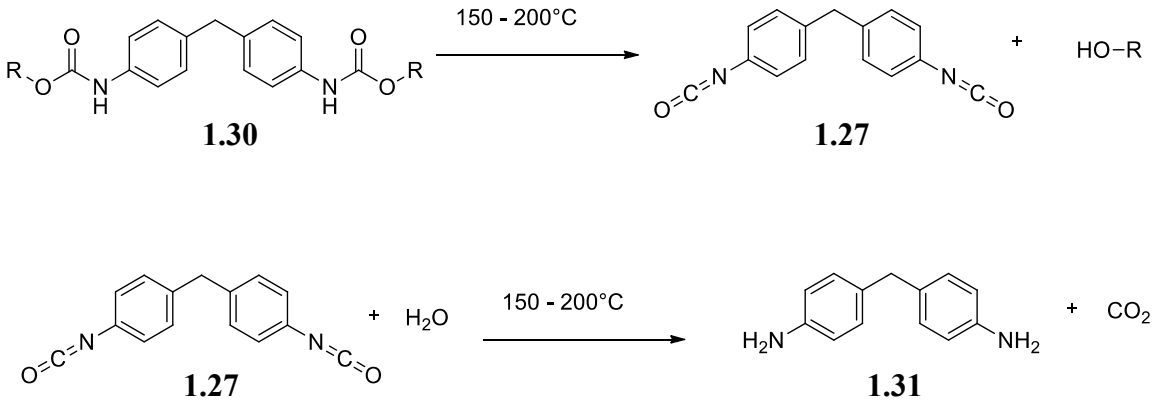

Scheme 1.6: Proposed thermolytic degradation of MDI based PUs **1.30** leading to the formation of MDA **1.31** [69]

1.2.5.1 Reactions of Isocyanates

It is important to note the numerous competing reactions in the formation of PU foam, as the NCO group can react with an OH group, water or another NCO group, Figure 1.11.[71]

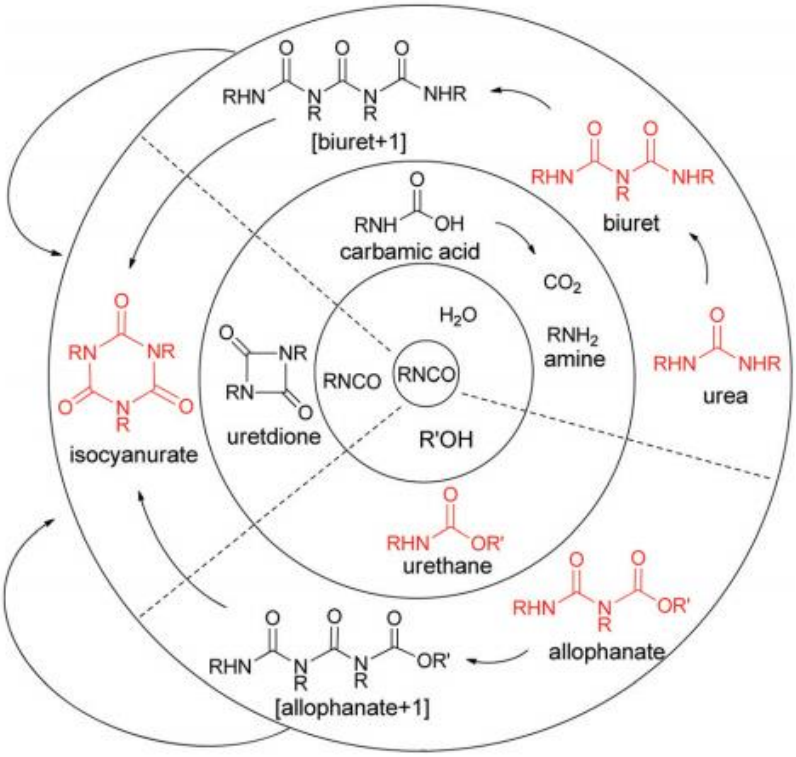

Figure 1.11: Competing reactions in PU foam formation. If R and R' are polyfunctional these reactions lead to cross-linked PU. Sites of cross-linking are shown in red.[71]

Diisocyanates can undergo self-addition dimerisation and trimerisation reactions to generate uretidiones **1.32**, Scheme 1.7, and isocyanurates **1.33**, Scheme 1.8.[9,6,71] The exothermic self-addition reactions proceed at low temperatures but become increasingly likely with increasing temperatures, during PU syntheses. The generation of 4-membered and stable 6-membered cyclic structures of uretidione **1.32** and isocyanurate **1.33** groups, respectively, increases the functionality of the polymer therefore, increasing the cross-linking potential.

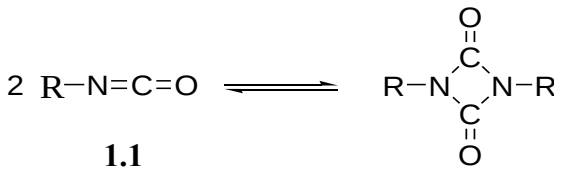

1.1 uretidione **1.32**

Scheme 1.7: Dimerisation of an isocyanate **1.1** to form uretidione **1.32**

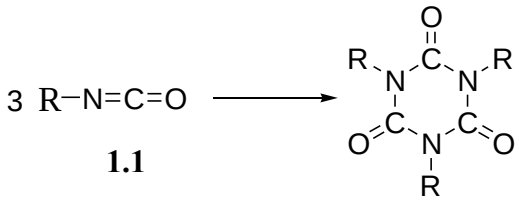

1.1 isocyanurate **1.33**

Scheme 1.8: Trimerisation of an isocyanate **1.1** to form isocyanurate **1.33**

The reactivity of the NCO group **1.1** is strongly dependent on its electronic environment; electron withdrawing groups increase the reactivity as the carbon atom becomes increasingly electropositive, whilst electron donating groups lower the reactivity. For this reason, aromatic isocyanates undergo trimerisation more readily than aliphatic isocyanates. Furthermore, the steric hindrance of the NCO group can greatly limit the reactivity of the isocyanate. Moreover, the reactivity of the two NCO groups in the diisocyanate compound towards nucleophiles can be different, despite their symmetry, Scheme 1.9. This is due to the formation of a urethane isocyanate **1.34** after the reaction of the first NCO group (K_1). The second NCO group has a decreased reactivity (K_2) due to the electron donating effect of the urethane group.

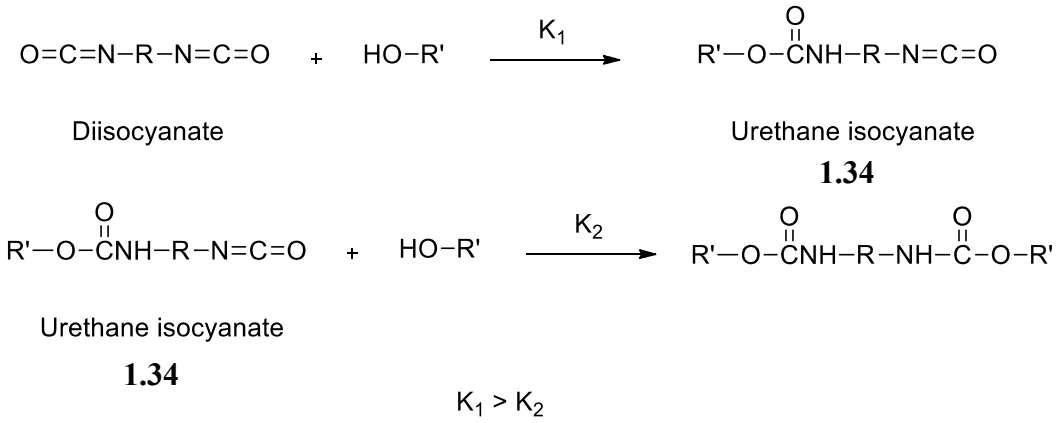

Scheme 1.9: Reactivities of the NCO groups in diisocyanate and urethane isocyanate **1.34** compounds

1.2.5.1 Biodegradable Diisocyanate Prepolymers

Diisocyanate prepolymers have been employed in the synthesis of multi-block copolymers.[72] This has been achieved through the synthesis of telechelic PCL containing NCO end groups, which are subsequently reacted with PLLA to form PLLA-PCL multi-block copolymers. The NCO-capped PCL moiety was synthesised by the reaction of two molar equivalents of HDI with PCL diol after heating at 80 °C for 3 h. However, the large Đ of 1.89-2.49 seen for the PLLA-PCL multi-block copolymers suggests poor synthetic control. Furthermore, the possibility of cross-linking or other competing reactions of the NCO group have not been considered in this investigation and could have a huge impact on the physical properties of the resulting copolymer.

Khan *et al*. prepared multi-block biodegradable PCL-based PU through the synthesis of a diisocyanate prepolymer using a series of PCL-diols with different M_n and either MDI, TDI, 1,4-phenylene diisocyanate (PDI) or 1,1'-methylenebis(4-isocyanatocyclohexane) (HMDI).[73] It was reported that the M_n and Đ of the resulting PUs were significantly influenced by both the reaction time and temperature, showing an increase in both M_n and Đ with an increase in reaction time. The high temperatures used in the syntheses of PUs ranging from 160-170 °C for up to 48 h indicate the NCO groups are likely to react further and form potential cross-linking sites.

Diisocyanate prepolymers have been employed as part of a two-step synthetic procedure in the synthesis of PU, with the aim to improve miscibility and reduce phase separation of

the polyol and diisocyanate components.[74] This has been achieved through the synthesis of a prepolymer containing NCO end-groups, followed by a reaction with the polyol component. Moreover, diisocyanate prepolymers containing a central hydrolytically degradable moiety between two aromatic isocyanate moieties could enhance the degradation of the resulting PU. This is due to the spacing of the rigid hydrophobic aromatic diisocyanate moieties with a more flexible linear polymer moiety.

1.2.6 Non-isocyanate Polyurethane

Recent studies have shown the syntheses of PU without the use of an isocyanate compound. This area of research has arisen from the environmental and health concerns in the manufacture of PU materials which use toxic, moisture sensitive and phosgene-based isocyanate components.[75] Furthermore, the production of toxic MDA as a degradation product of PUs containing MDI, has been well documented.[69]

Non-isocyanate polyurethane (NIPU) can be obtained through step-growth polyaddition, polycondensation and ROP methods. The step-growth polyaddition reaction of multi-functional cyclic carbonates **1.35** with aliphatic 1° diamines **1.36** or polyamines is the most popular industrial method to produce NIPUs, so will be discussed in further detail.[76,77]

The reaction of a cyclic carbonate **1.35** and 1° amine **1.36** to give compounds containing a urethane group **1.37** can be seen in Scheme 1.10. Furthermore, the production of an OH group can lead to intermolecular and intramolecular hydrogen bonding between the hydrogen atom on the OH group and the oxygen atom in the carbonyl of the urethane group. It has been reported that these hydrogen bonds decrease the susceptibility of urethane groups to hydrolysis by shielding the carbonyl carbon atom.[78] Moreover, the absence of thermally labile allophanate **1.7** and biuret **1.6** groups increases the thermal stability of NIPUs, in comparison to PUs synthesised with an isocyanate component. This could have an effect on the rate of hydrolytic or enzymatic degradation of NIPUs.

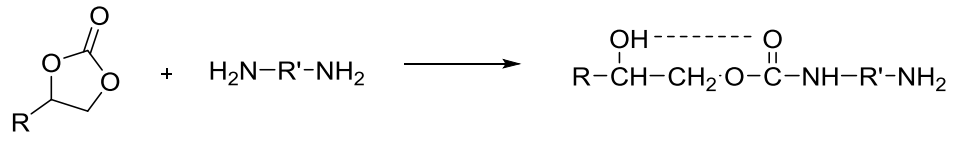

1.35 **1.36** **1.37**

Scheme 1.10: Reaction of cyclic carbonate **1.35** and diamine **1.36** to give **1.37**

1.3 Biodegradation Testing Methods

Biodegradation has been described as the process by which organic substances are broken down by living organisms.[79] The ultimate degradation products in this process include water, carbon dioxide and biomass.[80]

Polymer degradation has been categorised as processes inducing changes in polymer properties due to either chemical, physical or biological reactions that result in bond scission and chemical transformations.[79] Polymer characteristics such as chain mobility, crystallinity, molecular weight and types of functional groups present, have all been reported to play a vital role in polymer degradation.[62] The literature suggests polymers undergo surface and/or bulk erosion during the degradation period. Surface erosion can be identified by visible surface pitting and roughening while the polymer sample retains its original geometrical shape, but decreases in size. Bulk erosion can be identified as erosion not restricted to the surface of the sample and can cause cracking and disintegration of the whole polymer sample. Common biodegradation testing methods include soil burial, hydrolytic degradation and enzymatic degradation.

1.3.1 Soil Burial

Polymers can be degraded by immersing samples into a soil medium that is maintained at constant moisture. The microorganisms naturally present in the soil have been shown to degrade polymer samples. Soil burial has been used as a representative method to show polymer degradation behaviour similar to natural environmental conditions.[60] However, it must be taken into consideration the large variations in soil type, depending on the soil location and microorganisms present.

Ikata *et al.* reported the degradation of PCL films by exposing the samples to soils taken from farms and a coastal location for 50 days. The soils were maintained at constant moisture and the PCL films showed the appearance of surface cracks, indicating polymer degradation.[81] However, surface morphology changes determined by SEM analyses was the only analytical method used in this study, and only indicates the onset of PCL degradation. Therefore, it is difficult to measure the rate and extent of polymer degradation over time. Moreover, Dutta *et al*. carried out biodegradation tests of PU thin films using three different soils from three different locations for 2, 4 and 6 months.[56] Three repeat sample measurements were taken in addition to using positive and negative

control samples, to avoid any irregular measurements. A low carbon content of the soils suggests that PU is the major carbon source for the microorganisms present in the soil. The PU films showed up to 16% weight loss after 6 months and showed splits and cracks on the film surface after 4 months of soil burial, indicating biodegradation had occurred. Furthermore, TGA analyses were used as evidence of polymer degradation to show the conversion from a two-step degradation curve before biodegradation, to one-step after biodegradation. It was suggested this was due to a decrease in the amount of ester linkages during biodegradation. However, there is very little difference between the TGA curves before and after biodegradation, therefore provides little support for the claims.

Studies have shown soil burial is a suitable and representative method for monitoring polymer degradation in the environment, however, the long time period required to generate results is a major disadvantage.

1.3.2 Hydrolytic Degradation

Hydrolytic degradation is a commonly used facile method to degrade polymer samples through the hydrolysis of susceptible groups in the polymer backbone chain. The functional groups susceptible to hydrolysis include esters, anhydrides, carbonates, amides, urethanes etc. Polymer samples are commonly immersed in a buffer solution and maintained at a constant temperature throughout the testing period.

Hydrolysable bonds can be cleaved in the absence of enzymes, catalysed by acids, bases or salts.[82] Hydrolytic cleavage occurs by the direct contact of water molecules, indicating the hydrophilic nature of the polymer has a significant effect on the rate of degradation. Geng *et al.* reported that the PCL component in PCL-PEG micelles undergoes hydrolytic degradation *via* a polymer chain end cleavage mechanism.[83] Moreover they suggested the degradation rate could be tuned by temperature, pH and M_n of polymer sample.

Hydrolytic degradation of PCL-based PU, Novosorb^{TM}, in PBS buffer solution (pH = 7.4) at 37 °C showed up to 34% mass loss over 9 months.[84] Several studies reported the very slow rate of hydrolytic degradation of PCL of 2-3 years.[21] The long time duration required for hydrolytic degradation of PCL-based polymers and PUs under physiological conditions, is a major disadvantage to this testing method.

1.3.3 Enzymatic Degradation

Heterotrophic microorganisms including bacteria and fungi can be used to degrade polymeric materials, however, there is a distinct lack of information available on the degradation mechanisms in the literature.[85] It has been suggested that the degradation process is a four-step progression, beginning with the attachment of the microorganism to the polymer surface. The microorganism grows from utilising the polymer carbon source and consequently, the main polymer chain is cleaved, followed by further chain scission and the generation of absorbable products.[86] The molar mass of the polymer must be sufficiently reduced to generate oligomers and monomers that are water soluble and therefore, can be transported through the semi-permeable bacterial membrane. The polymer degradation products can then be assimilated as a carbon or nitrogen source through a metabolic pathway.[62] A proposed enzymatic degradation pathway whereby micoorganisms secrete extracellular enzymes that can degrade the polymer outside the cells is shown in Figure 1.12.[87] The extracellular enzymes attach to the surface of the polymer to form an enzyme-polymer complex, followed by polymer chain scission described as depolymerisation. When the molar mass of the polymer is sufficiently reduced to produce water soluble degradation products, they can be transported through the semi-permeable bacterial membrane and be assimilated as a carbon or nitrogen source. Furthermore, these extracellular enzymes are too large to penetrate into the bulk of the polymer therefore, only act on the surface, resulting in surface erosion.

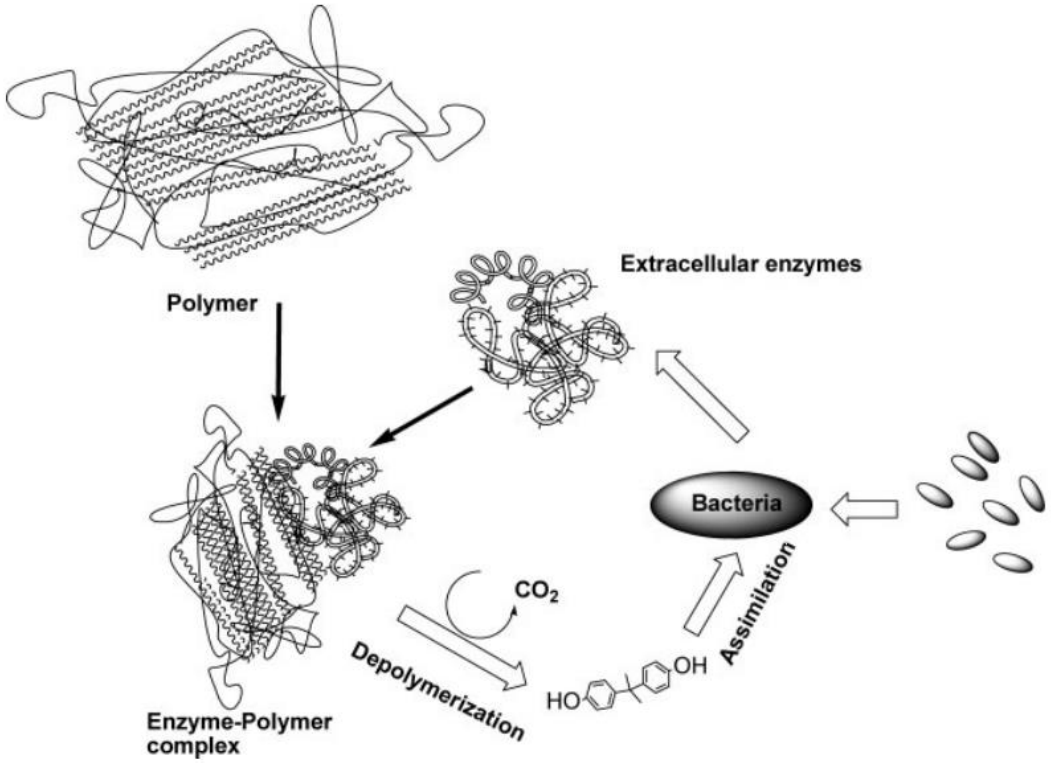

Figure 1.12: Enzymatic degradation pathway of polymers by the use of extracellular enzymes[62]

Middleton *et al*. described enzymatic polymer degradation as a two-stage process.[88] The first phase involves water penetration, preferentially attacking the hydrolysable groups in the amorphous region and converting long polymer chains into shorter, water-soluble fragments. Initially, the reduction in molecular weight does not affect the physical properties of the polymer as the crystalline regions retain the general structure. The second phase involves the enzymatic degradation and metabolism of polymer fragments leading to rapid mass loss. Initially degradation occurs more rapidly at the surface of the polymer due to the greater water availability.

The literature suggests that certain lipases such as *pseudomonas cepacia* lipase enhance the degradation of PCL when compared to hydrolytic degradation with incubation in buffer solution alone.[89] Activated sludge has been shown to successfully degrade aliphatic polyesters due to the action of multiple micoorganisms present in the media.[81] Furthermore, studies have been conducted into enzymatically modulating the polymer by incorporating enzymatic recognition sites such as amino acids into the polymer backbone.[20]

Artham *et al*. summarises the key factors that influence polymer biodegradation, Figure 1.13.[62] Parameters such as abiotic factors, type of microorganism used and polymer characteristics play an important role in the mechanism and rate of degradation.

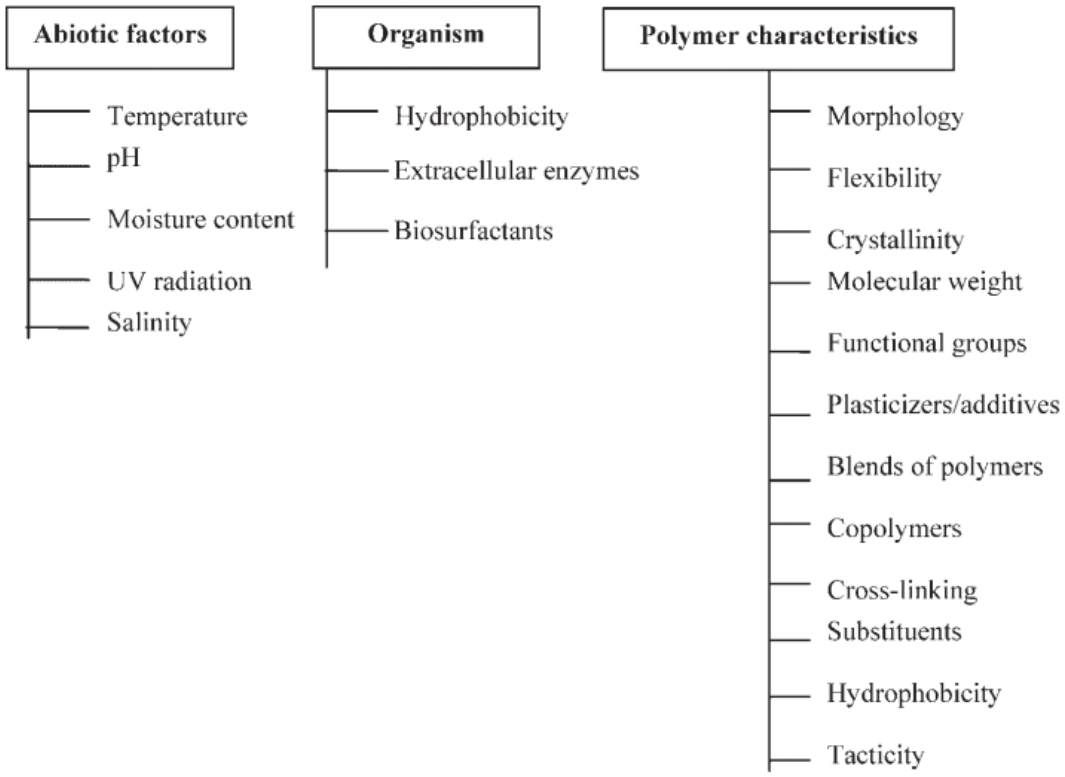

Figure 1.13: Parameters influencing polymer biodegradation[62]

Several studies have indicated that the crystalline nature of polymers have a significant effect on enzymatic degradation, as highly ordered crystalline structures can restrict access for enzymatic attack.[90,62] Moreover, structural features such as branching or cross-linking can have a similar effect in the restriction of enzyme access to the polymer chains.

1.3.3.1 Enzymatic Degradation of Polyurethane

Wales and Sagar proposed that PU degradation involves the synergistic activity of enzymes endopolyurethanases and exopolyurethanases. These enzymes hydrolyse the PU chain at random points and remove monomer units from chain ends, respectively.[91]

Huang and Roby synthesised PUs with long repeating units of alternating amide and urethane groups.[92] It was discovered that the long repeating units and hydrophilic groups

on the polymer are less likely to pack into crystalline areas and these PUs were degraded in a selective manner. The amorphous regions were preferentially degraded before the crystalline regions, implying they are more enzyme-accessible to degradation. Moreover, Tang *et al*. reported that degradation of polycarbonate PUs were highly dependent on the concentration of cholesterol esterase enzyme and significantly influenced by the structure and surface chemistry of the PU.[93] Moreover, the cholesterol esterase enzyme has been shown to increase the extent of degradation in PUs by approximately 10 times in comparison to degradation in buffer solution alone.[94]

Gautam *et al*. investigated the biodegradation of polyester PU foam using *P.chlororaphis* ATCC 55729.[95] It was found that concentrations of the degradation products, diethylene glycol and ammonia, increased over time in line with an increase of bacterial growth and decrease in PU mass. Nakajima-Kambe *et al*. found that the products of degradation of polyester PU were produced by esterase activity.[96] GC-MS analysis revealed these products as diethylene glycol, trimethylolpropane and adipic acid from the polyester segments of the PU, arising from the hydrolysis of ester groups. 2,4-Diaminotoluene was also detected which was derived from the polyisocyanate segments, demonstrating hard segment degradation. Studies on the strain TB-35 revealed that only the cell-surface-bound secreted esterase catalyses the degradation in polyester PU.

Akutsu *et al*. purified a PU degrading cell-bound esterase enzyme from a bacterium which utilises polyester PU as the sole carbon source.[97] The degradation products were shown to be diethylene glycol and adipic acid and the results indicated that this particular enzyme degrades PU in a two-step process, initially hydrophobic adsorption onto the surface followed by hydrolysis of the ester group. Interestingly, a mathematical model has been proposed that describes the *in vitro* enzymatic degradation of biomedical polyurethanes by a single enzyme, but more information is needed to apply this approach to other polymeric systems.[98]

1.4 Analytical Methods to monitor Polymer Degradation

A variety of analytical methods can be employed to monitor the physical and chemical changes during polymer degradation and to determine the rate and extent of degradation. The analyses of visible physical changes in degraded polymers can be used as a method

of evaluation in almost all polymer degradation tests. Common examples include roughening of the surface, formation of holes and cracks, defragmentation and changes in colour.[79] Furthermore, mass loss measurements can be used to determine the extent of polymer degradation, however, inaccurate results can occur with excessive fragmentation or ineffective cleaning of the specimens. Changes in thermal properties or chemical composition can also be analysed to monitor the degradation process. It is clear that a combination of the methods should be used to build a comprehensive polymer degradation profile and give an insight into the degradation mechanism involved.

1.4.1 Changes in Thermal Properties

The changes in physical properties of polymers during degradation such as the degree of crystallinity ($\%\chi_c$), can indicate the onset and the mechanism of degradation. Differential scanning calorimetry (DSC) and thermal gravimetric analyses (TGA) can be used to detect any thermal changes throughout the polymer degradation period. Studies have shown that $\%\chi_c$ generally increases during the initial stages of degradation due to preferential degradation of amorphous regions of the polymer.[99,100] Furthermore, studies suggest that the initial $\%\chi_c$ of polymers can have a significant impact on the rate of hydrolytic[11] and enzymatic[101] degradation.

1.4.2 Changes in Molecular Weight

The changes in polymer molecular weight can be determined throughout the degradation period to monitor the extent of degradation. This can be achieved by using Size exclusion chromatography (SEC) and Matrix-assisted laser desorption/ionisation mass spectrometry (MALDI). Goepferich reported the SEC analyses of poly[(lactic acid)-*co*-(glycolic acid)] polymer discs during degradation in PBS solution (pH = 7.4).[26] The result showed a decrease in polymer molecular weight before any significant mass loss was detected. This implies the method of degradation involves the random chain scission of polymer chains, generating lower molecular weight fragments prior to the formation of smaller water soluble compounds that would result in mass loss.

1.4.3 Change in Chemical Structures

Fourier transform infrared spectroscopy (FT-IR) and nuclear magnetic resonance (NMR) can be used to detect changes in functional groups during polymer degradation.[56] A decrease in the hydrolytically susceptible groups such as esters and an increase in functional groups found in the degradation products such as carboxylic acids and alcohols, could indicate the extent of polymer degradation.

1.4.4 Change in Surface Morphology

Several studies report significant changes in the surface morphology of polymer films or discs during degradation, including surface pitting and formation of fissures.[56] Domanska *et al.* reported the appearance of macro- and micro-pores in the surfaces of PU samples after degradation in PBS solution at 37 °C after 1, 3 and 6 months.[12] Furthermore, it was reported that a higher number of pores were observed in the PU samples that exhibited a faster rate of degradation. Scanning electron microscopy (SEM) is the preferred method used to visualise the surface of degraded materials.[81] It must be taken into consideration that an initial smooth and flat polymer surface is required in order to visibly detect changes in surface erosion throughout the degradation process. However, it may not be practical to form polymer discs or films for SEM analyses, depending on the nature of the polymeric sample.

1.4.5 Mass Loss

A common and facile method of monitoring polymer degradation is to determine mass loss throughout the degradation period.[102,11] Studies have shown the mass loss profiles commonly seen for aliphatic polyesters exhibit two stages, comprising of an initial lag phase followed by rapid mass loss, typical of a bulk erosion mechanism.[26] It should be noted that inaccurate results could be obtained due to inefficient removal of impurities when washing samples after degradation testing. Furthermore, in cases of excessive fragmentation, small solid polymer fragments may be difficult to collect and measure, therefore, producing misleading results.

1.5 Aims

This project involves the development of biodegradable rigid PU foams with a target of 60% degradation after 10 days and 90% degradation after 1 month. The rigid PU foam will be ground into particles for use as a 'soft' abrasive in various cleaning products such as surface cleaning spray. The resulting PU particles will have a unique brush-like geometry originating from the foam cell structure, and have the capacity to remove dirt whilst not damaging surfaces. There is an increasing interest in the development of biodegradable PUs due to environmental concerns of plastic waste disposal. After the surface cleaning product has been used, the final destination of the PU particles will likely be the sewage system and/or other bodies of water. It is important these polymer particles can biodegrade in the natural environment under aqueous conditions and ambient temperature. Moreover, the PU particles must not produce toxic degradation products.

The biodegradable rigid PU foams will be synthesised using biodegradable polyol and diisocyanate prepolymer components. Four- and six-arm star PCL polyols will be synthesised through the $SnOct_2$ catalysed ROP of ε-CL using multi-hydroxyl initiators pentaerythritol, di(trimethylolpropane) and dipentaerythritol. A hydrophilic PEG moiety will be incorporated into the star PCL polyol by the synthesis of a tetra-hydroxyl PEG macro-initiator with subsequent $SnOct_2$ catalysed ROP of ε-CL. The incorporation of a hydrophilic PEG moiety is anticipated to increase the overall hydrophilicity and therefore increase the rate of biodegradation. Six-arm star poly(ε-CL)-co-(β-BL) will be synthesised by the random copolymerisation of ε-CL and β-BL using dipentaerythritol initiator. It is anticipated that the lower crystallinity exhibited by the star copolymer will increase the rate of biodegradation. Seven-arm star PCL with an acetylated β-CD core will be synthesised with the aim to increase biodegradation through the use of a biocompatible and biodegradable β-CD core. The biodegradable diisocyanate prepolymers will be synthesised using two molar equivalents of either MDI or TDI and PCL-diol. The aromatic diisocyanates MDI or TDI must be used in the syntheses of rigid PU due to the current processes used in industry. It is anticipated that the incorporation of a central biodegradable PCL moiety spaced between two aromatic isocyanate moieties, will increase the rate of biodegradation. Furthermore, the incorporation of a hydrophilic PEG moiety into the diisocyanate prepolymer is expected to increase the rate of PU biodegradation, due to an overall increase in hydrophilicity. This will be achieved

through the synthesis of a PCL-*b*-PEG-*b*-PCL moiety and subsequent reaction with two molar equivalents of either MDI or TDI. The biodegradation of synthesised star polyols, diisocyanate prepolymers and PUs will be investigated using *Pseudomonas Cepacia* lipase over 30 days. The extent of degradation will be determined using % mass loss, DSC and SEM analyses.

1.6 References

(1) Available at http://utech-polyurethane.com. Accessed on 21/5/2016.
(2) Koenig, M. F.; Huang, S. J. *Abstr. Pap. Am. Chem. Soc.* **1993**, *206*, 131.
(3) Elidrissi, A.; Krim, O.; Ouslimane, S.; Berrabeh, M.; Touzani, R. *J. Appl. Polym. Sci.* **2007**, *105*, 1623.
(4) Gunatillake, P. A.; Adhikari, R. *Eur. Cell. Mater.* **2003**, *5*, 1.
(5) Kulkarni, A.; Reiche, J.; Hartmann, J.; Kratz, K.; Lendlein, A. *Eur. J. Pharm. Biopharm.* **2008**, *68*, 46.
(6) Behrendt, G., Naber, B. W. *J. Chem. Tecnol. Metall.* **2009**, *44*, 3.
(7) Chambon, F.; Petrovic, Z. S.; Macknight, W. J.; Winter, H. H. *Macromolecules* **1986**, *19*, 2146.
(8) Dounis, D. V.; Wilkes, G. L. *Polymer* **1997**, *38*, 2819.
(9) Ionescu, M. *Chemistry and technology of polyols for polyurethanes*; Rapra Technology Limited, 2005.
(10) Pengjam, W.; Saengfak, B.; Ekgasit, S.; Chantarasiri, N. *J. Appl. Polym. Sci.* **2012**, *123*, 3520.
(11) Hong, J. H.; Jeon, H. J.; Yoo, J. H.; Yu, W.-R.; Youk, J. H. *Polym. Degrad. Stabil.* **2007**, *92*, 1186.
(12) Domanska, A., Boczkowska, A., *Polym. Degrad. Stabil.* **2014**, *108*, 175.
(13) Herrington, R., Hock, K. *Flexible Polyurethane Foams, Chemistry and Technology*; 2nd ed.; Springer 1982: Essex, England, 1982.
(14) Jones, R. E., Fesman, G. *J. Cell. Plast* **1965**, *1*.
(15) Zhang, X. D., Macosko, C. W., Davis, H. T., Nikolov, A. D., Wasan, D. T. *J. Colloid Interface Sci.* **1999**, *215*, 270.
(16) Yasunaga, K.; Neff, R. A.; Zhang, X. D.; Macosko, C. W. *J. Cell. Plast.* **1996**, *32*, 427.
(17) Oprea, S. *Polym. Bull.* **2010**, *65*, 753.
(18) Sarkar, D.; Lopina, S. T. *Polym. Degrad. Stabil.* **2007**, *92*, 1994.
(19) Tatai, L.; Moore, T. G.; Adhikari, R.; Malherbe, F.; Jayasekara, R.; Griffiths, I.; Gunatillake, P. A. *Biomaterials* **2007**, *28*, 5407.
(20) Skarja, G. A.; Woodhouse, K. A. *J. Biomater. Sci.-Polym. Ed.* **2001**, *12*, 851.
(21) Nair, L. S.; Laurencin, C. T. *Prog. Polym. Sci.* **2007**, *32*, 762.
(22) Kylma, J.; Seppala, J. V. *Macromolecules* **1997**, *30*, 2876.
(23) Wang, W.; Ping, P.; Chen, X.; Jing, X. *Eur. Polym. J.* **2006**, *42*, 1240.
(24) Chandra, R.; Rustgi, R. *Prog. Polym. Sci.* **1998**, *23*, 1273.
(25) Azevedo, H. S., Reis, R. L. *Understanding the Enzymatic Degradation of Biodegradable Polymers and Strategies to Control Their Degradation Rate*; CRC Press, 2004.
(26) Göpferich, A. *Macromolecules* **1997**, *30*, 2598.
(27) Sobczak, M. *Polym. Bull.* **2012**, *68*, 2219.
(28) Liu, L.; Wang, Y.; Shen, X.; Fang, Y. e. *Biopolymers* **2005**, *78*, 163.
(29) Dubois, P.; Jacobs, C.; Jerome, R.; Teyssie, P. *Macromolecules* **1991**, *24*, 2266.
(30) Kadota, J.; Pavlovic, D.; Hirano, H.; Okada, A.; Agari, Y.; Bibal, B.; Deffieux, A.; Peruch, F. *RSC Advances* **2014**, *4*, 14725.
(31) Kowalski, A.; Duda, A.; Penczek, S. *Macromol. Rapid Commun.* **1998**, *19*, 567.
(32) Schwach, G.; Coudane, J.; Engel, R.; Vert, M. *Journal of Polymer Science Part A: Polymer Chemistry* **1997**, *35*, 3431.
(33) Dong, C.-M.; Qiu, K.-Y.; Gu, Z.-W.; Feng, X.-D. *Macromolecules* **2001**, *34*, 4691.
(34) Kowalski, A.; Libiszowski, J.; Biela, T.; Cypryk, M.; Duda, A.; Penczek, S. *Macromolecules* **2005**, *38*, 8170.
(35) Storey, R. F.; Sherman, J. W. *Macromolecules* **2002**, *35*, 1504.
(36) Chen, Y.-J.; Fang, H.-J.; Hsu, S. C. N.; Jheng, N.-Y.; Chang, H.-C.; Ou, S.-W.; Peng, W.-T.; Lai, Y.-C.; Chen, J.-Y.; Chen, P.-L.; Kao, C.-H.; Zeng, Z.-X.; Chen, J.-L.; Chen, H.-Y. *Polym. Bull.* **2013**, *70*, 993.

(37) Baimark, Y., Molloy, R. *ScienceAsia* **2004**, *30*, 327.
(38) Möller, M.; Kånge, R.; Hedrick, J. L. *J. Polym. Sci. Part A: Polym. Chem.* **2000**, *38*, 2067.
(39) Sisson, A. L.; Ekinci, D.; Lendlein, A. *Polymer* **2013**, *54*, 4333.
(40) Choi, J.; Kim, I.-K.; Kwak, S.-Y. *Polymer* **2005**, *46*, 9725.
(41) Wang, J. L.; Wang, L.; Dong, C. M. *J. Polym. Sci. Pol. Chem.* **2005**, *43*, 5449.
(42) Xue, L.; Dai, S.; Li, Z. *Macromolecules* **2009**, *42*, 964.
(43) Cameron, D. J. A.; Shaver, M. P. *Chem. Soc. Rev.* **2011**, *40*, 1761.
(44) Mellet, C. O.; Fernandez, J. M. G.; Benito, J. M. *Chem. Soc. Rev.* **2011**, *40*, 1586.
(45) Potolinca, V. O.; Oprea, S.; Ciobanu, A.; Lungu, N. C. *J. Optoelectron. Adv. M.* **2011**, *13*, 1246.
(46) Zia, F.; Zia, K. M.; Zuber, M.; Kamal, S.; Aslam, N. *Carbohydr. Polym.* **2015**, *134*, 784.
(47) Gou, P. F.; Zhu, W. P.; Shen, Z. Q. *Biomacromolecules* **2010**, *11*, 934.
(48) Miao, Y.; Rousseau, C.; Mortreux, A.; Martin, P.; Zinck, P. *Polymer* **2011**, *52*, 5018.
(49) Kawaguchi, Y.; Nishiyama, T.; Okada, M.; Kamachi, M.; Harada, A. *Macromolecules* **2000**, *33*, 4472.
(50) Uyama, H.; Kuwabara, M.; Tsujimoto, T.; Kobayashi, S. *Biomacromolecules* **2003**, *4*, 211.
(51) Tsujimoto, T.; Uyama, H.; Kobayashi, S. *Macromolecules* **2004**, *37*, 1777.
(52) Allauddin, S.; Somisetti, V.; Ravinder, T.; Rao, B.; Narayan, R.; Raju, K. *Ind. Crop. Prod.* **2016**, *85*, 361.
(53) Miao, S.; Wang, P.; Su, Z.; Zhang, S. *Acta Biomaterialia* **2014**, *10*, 1692.
(54) Yeganeh, H.; Hojati-Talemi, P. *Polym. Degrad. Stabil.* **2007**, *92*, 480.
(55) Bernardini, J.; Cinelli, P.; Anguillesi, I.; Coltelli, M.-B.; Lazzeri, A. *Eur. Polym. J.* **2015**, *64*, 147.
(56) Dutta, S.; Karak, N.; Saikia, J. P.; Konwar, B. K. *J. Polym. Environ.* **2010**, *18*, 167.
(57) Lee, S.-I.; Yu, S.-C.; Lee, Y.-S. *Polym. Degrad. Stabil.* **2001**, *72*, 81.
(58) Yeganeh, H.; Lakouraj, M. M.; Jamshidi, S. *Eur. Polym. J.* **2005**, *41*, 2370.
(59) Santerre, J. P.; Woodhouse, K.; Laroche, G.; Labow, R. S. *Biomaterials* **2005**, *26*, 7457.
(60) Kim, Y. D.; Kim, S. C. *Polym. Degrad. Stabil.* **1998**, *62*, 343.
(61) Yeganeh, H.; Lakouraj, M. M.; Jamshidi, S. *J. Polym. Sci. Part A: Polym. Chem.* **2005**, *43*, 2985.
(62) Artham, T.; Doble, M. *Macromol. Biosci.* **2008**, *8*, 14.
(63) Bogdanov, B.; Vidts, A.; Schacht, E.; Berghmans, H. *Macromolecules* **1999**, *32*, 726.
(64) Liu, G.-C.; He, Y.-S.; Zeng, J.-B.; Xu, Y.; Wang, Y.-Z. *Polym. Chem.* **2014**, *5*, 2530.
(65) Bruin, P.; Veenstra, G. J.; Nijenhuis, A. J.; Pennings, A. J. *Macromol. Chem. Rapid Comm.* **1988**, *9*, 589.
(66) Gogolewski, S.; Pennings, A. J. *Macromol. Chem. Comm* **1982**, *3*, 839.
(67) Hettrich, W.; Becker, R. *Polymer* **1997**, *38*, 2437.
(68) Spaans, C. J.; de Groot, J. H.; Dekens, F. G.; Pennings, A. J. *Polym. Bull.* **1998**, *41*, 131.
(69) Szycher, M. *J. Biomat. App.* **1988**, *3*, 297.
(70) Hassan, M. K.; Mauritz, K. A.; Storey, R. F.; Wiggins, J. S. *J. Polym. Sci. Part A: Polym. Chem.* **2006**, *44*, 2990.
(71) Gibb, J. N.; Goodman, J. M. *Org. Biomol. Chem.* **2013**, *11*, 90.
(72) Teng, C.; Yang, K.; Ji, P.; Yu, M. *J. Polym. Sci. Part A: Polym. Chem.* **2004**, *42*, 5045.
(73) Khan, F.; Valere, S.; Fuhrmann, S.; Arrighi, V.; Bradley, M. *J. Mater. Chem. B* **2013**, *1*, 2590.
(74) Guelcher, S. A.; Srinivasan, A.; Dumas, J. E.; Didier, J. E.; McBride, S.; Hollinger, J. O. *Biomaterials* **2008**, *29*, 1762.
(75) Nakashima, K.; Takeshita, T.; Morimoto, K. *Environ. Health Prev. Med.* **2002**, *7*, 1.
(76) Rokicki, G.; Parzuchowski, P. G.; Mazurek, M. *Polym. Adv. Technol.* **2015**, *26*, 707.
(77) Poussard, L.; Mariage, J.; Grignard, B.; Detrembleur, C.; Jérôme, C.; Calberg, C.; Heinrichs, B.; De Winter, J.; Gerbaux, P.; Raquez, J. M.; Bonnaud, L.; Dubois, P. *Macromolecules* **2016**, *49*, 2162.
(78) Guan, J.; Song, Y.; Lin, Y.; Yin, X.; Zuo, M.; Zhao, Y.; Tao, X.; Zheng, Q. *Ind. Eng. Chem. Res.* **2011**, *50*, 6517.

(79) Shah, A. A.; Hasan, F.; Hameed, A.; Ahmed, S. *Biotechnol. Adv.* **2008**, *26*, 246.
(80) Arutchelvi, J., Sudhakar, M., Arkatkar, Doble, M., Bhaduri, S., Uppara, P. V., *Indian J Biotechnol* **2008**, *7*, 9.
(81) Ikada, E. *J. Environ. Polym. Degrad.* **1999**, *7*, 197.
(82) Williams, D. F.; Zhong, S. P. *Int. Biodeterior. Biodegrad* **1995**, *34*, 95.
(83) Geng, Y.; Discher, D. E. *J. Am. Chem. Soc.* **2005**, *127*, 12780.
(84) Sgarioto, M.; Adhikari, R.; Gunatillake, P. A.; Moore, T.; Malherbe, F.; Nagel, M.-D.; Patterson, J. *J. Biomed. Mater. Res. Part B: Appl. Biomater.* **2014**, *102*, 1711.
(85) Gu, J.-D. *Int. Biodeterior. Biodegrad.* **2003**, *52*, 69.
(86) Rahmouni, M.; Chouinard, F.; Nekka, F.; Lenaerts, V.; Leroux, J. C. *Eur. J. Pharm. Biopharm.* **2001**, *51*, 191.
(87) Howard, G. T.; Ruiz, C.; Hilliard, N. P. *Int. Biodeterior. Biodegrad.* **1999**, *43*, 7.
(88) Middleton, J. C.; Tipton, A. J. *Biomaterials* **2000**, *21*, 2335.
(89) Gan, Z.; Liang, Q.; Zhang, J.; Jing, X. *Polym. Degrad. Stabil.* **1997**, *56*, 209.
(90) Mochizuki, M.; Hirano, M.; Kanmuri, Y.; Kudo, K.; Tokiwa, Y. *J. Appl. Polym. Sci.* **1995**, *55*, 289.
(91) Wales, D. S., Sagar, B. R. *Mechanistic aspects of polyurethane deterioration* 7th ed.; Elsevier Applied Science, London, 1988.
(92) Huang, S. J., Roby, M. S. *J. Bioact. Compat. Polym.* **1986**, *1*, 61.
(93) Tang, Y. W.; Labow, R. S.; Santerre, J. P. *J. Biomed. Mater. Res.* **2001**, *56*, 516.
(94) Santerre, J. P.; Labow, R. S.; Duguay, D. G.; Erfle, D.; Adams, G. A. *J. Biomed. Mater. Res.* **1994**, *28*, 1187.
(95) Gautam, R.; Bassi, A. S.; Yanful, E. K.; Cullen, E. *Int. Biodeterior. Biodegrad.* **2007**, *60*, 245.
(96) Nakajima-Kambe, T.; Shigeno-Akutsu, Y.; Nomura, N.; Onuma, F.; Nakahara, T. *Appl. Microbiol. Biotechnol.* **1999**, *51*, 134.
(97) Akutsu, Y.; Nakajima-Kambe, T.; Nomura, N.; Nakahara, T. *Appl. Environ. Microbiol.* **1998**, *64*, 62.
(98) Duguay, D. G., Labow, R. S., Santerre, J. P., McLean, D. D. *Polym. Degrad. Stabil.* **1995**, *47*, 229.
(99) You, Y.; Min, B.-M.; Lee, S. J.; Lee, T. S.; Park, W. H. *J. Appl. Polym. Sci.* **2005**, *95*, 193.
(100) Zong, X.-H.; Wang, Z.-G.; Hsiao, B. S.; Chu, B.; Zhou, J. J.; Jamiolkowski, D. D.; Muse, E.; Dormier, E. *Macromolecules* **1999**, *32*, 8107.
(101) Seretoudi, G.; Bikiaris, D.; Panayiotou, C. *Polymer* **2002**, *43*, 5405.
(102) Gorna, K.; Gogolewski, S. *Polym. Degrad. Stabil.* **2002**, *75*, 113.

2. Synthesis and Degradation Studies of Poly(ε-caprolactone)

2.1 Introduction

Polyurethanes (PUs) are synthesised by the reaction of diols or polyols and diisocyanates. To achieve biodegradable PU, biodegradable polyol and diisocyanate reactive intermediates were firstly synthesised.

Star polymers can be defined as having multiple linear chains connecting to a central core unit. They are of particular interest due to the increased functional chain-end density, compact structures and decreased crystallinity. This can increase the rate of degradation, in comparison to linear polymers.[1] The stars can be synthesised through two methods; an arm-first technique, or a core-first approach. The arm-first technique uses pre-synthesised linear polymers which can then attach to the core unit *via* a crosslinking agent or a multifunctional molecule.[2] The core-first approach utilises a multifunctional initiator from which polymer chains are grown.[3]

An important class of biodegradable polymer stars are made from aliphatic polyesters such as ε-caprolactone (ε-CL), β-butyrolactone (β-BL), lactide and trimethylene carbonate. These polymers can be easily hydrolysed using enzymes to produce hydroxyacids, many of which are metabolised through the citric acid cycle.[4,5] Ring-opening polymerisations (ROP) are driven by the loss of enthalpy associated with the loss of ring strain. This is even observed with 7-membered lactones where the ring strain is *ca*. 6 J mol^{-1}.[6] For both industrial production and academic research, the most commonly used catalyst for the ROP of ε-CL is tin (II) octoate ($SnOct_2$) *via* a tin complex-induced coordination/insertion mechanism.[7,8] The advantages of using $SnOct_2$ range from increased control of polymer structure, kinetic enhancement and solubility in organic solvents.[9,10] Moreover, it is accepted by the US Food and Drug Administration (FDA).[11] It must be noted however, the high toxicity of $SnOct_2$ has provoked environmental concerns and has led to research into alternate low toxicity metal catalysts for ROP of ε-CL.[12,13]

Commonly, multi-hydroxyl discrete core molecules such as glycol, pentaerythritol, di(trimethylolpropane) and dipentaerythritol have been used to produce 3 to 6-arm star structures.[4,14] Xie *et al*. reported the synthesis of star PCL with 2 to 5 arms using the ROP of ε-CL with $SnOct_2$ and multi-hydroxyl initiators ethylene glycol, glycerol, erythritol and xylitol.[15] ^{1}H NMR analysis confirmed the presence of the initiator moiety and well as the

PCL end groups, however, they failed to show the respective degrees of polymerisation ($\overline{DP}$) as well as confirming the initiator moiety is indeed attached to the PCL moiety.

Trollsas *et al*. reported the synthesis of 6-, 12- and 24-arm PCL dendrimer-like star structures, using a 2,2-bis(hydroxymethyl)propionic acid (bisHMPA) derivative as the initiating species.[16] The polymers were analysed by SEC, DLS and SAXS showing low dispersity (Đ) and good agreement with expected molecular weight values. However, there was insufficient analysis to confirm the number of PCL arms, the $\overline{DP}$ or number of terminal OH groups present in the structure.

PCL has significant use in biomedical applications due to its biodegradability, low melting point (T_m) and low glass transition temperature (T_g).[4] Studies on the crystallisation and biodegradation characteristics of star PCL have been reported, showing that increasing the arm length (from $M_n = 2 \times 10^3$ to 1×10^4 g mol^{-1}) of the star polymers increases the T_m, whereas, increasing the number of arms (from 1 to 5) causes a decrease in T_m.[15] Interestingly, the rate of enzymatic degradation of star PCL increased with increasing arm number from 1-3, however, the rate of degradation decreased with a further increase in arm number from 3-5. It was reported that the decrease in T_m with increasing arm number was due to the limited effect of the central core on chain mobility of each arm. Furthermore, it was suggested that the different rates of enzymatic degradation on arm number from 1-3 and 3-5, reflect the corresponding roles of crystal size and central cores in degradation behaviour.

Cameron *et al*. reported that there was little effect on crystallinity when increasing the number of aliphatic polyester arms including PCL in a star structure.[4] Furthermore, the degree of crystallinity (%χ_c) of PCL is affected by molecular weight, as an increase in the length of polymer arms leads to an increase in %χ_c.

The random copolymerisation of ε-CL and β-BL increases the amorphous content of the polymer, as opposed to block copolymerisation, therefore, show improved degradation characteristics.[4] There are limited studies involving the copolymerisation of ε-CL and β-BL as well as degradation characteristics in the literature. Olsen *et al*. have shown that ring size and degree of substitution have a large influence on the thermodynamic equilibrium polymerisation behaviour of lactones.[17] Therefore, it is expected that this will have implications on the final composition of a ε-CL / β-BL random copolymer.

Polymer chain mobility can be a principal factor in determining the rate of polymer degradation.[18] Therefore, the restricted mobility of the PCL chains in a star architecture due to the central core unit, has a significant effect on the polymer degradation rate. This implies the rate of degradation will increase with the number of arms in a polymer star structure.

The enzymatic degradation of PCL films using different lipases, namely *pseudomonas* lipase (PS), *porcine pancreatic* lipase (PP) and candida cylindracea lipase (AY), in phosphate buffer solutions has been reported.[19] The studies showed very slow PCL degradation and no weight loss after one week for PP and AY lipases, however, PS showed rapid and complete weight loss after only 4 days. Furthermore, PCL films have been degraded using lipases from *Aspergillus oryzae* and *Bacillus subtilis* showing up to 10% weight loss in 42 days.[20] The degradation was monitored by weight loss, FTIR, DSC and CLSM analyses and showed a decrease in molecular weight, a decrease in crystallinity and cracks in the surface of the PCL films during degradation. However, monitoring the carbonyl index through FTIR analyses at band 1726 cm^{-1} did not show any conclusive evidence of a decrease in the number of ester bonds in PCL during degradation.

Enzymatic degradation of PCL films occurs over the whole polymer surface[21] and primarily takes place in amorphous regions of the polymer *via* random scission of ester bonds on the polymer chains.[22,18]

Chapter 2 concerns the syntheses of a series of star PCL and star poly[(ε-CL)-*co*-(β-BL)] polyols. Four and six-arm star PCL **2.4 – 2.7**, **2.9 – 2.10** and **2.12** were synthesised in the ROP of ε-CL catalysed by $SnOct_2$ using pentaerythritol **2.11**, di(trimethylolpropane) **2.8** and dipentaerythritol **2.3** initiators with a $\overline{DP}_{Th}$ of 10, 20 50 and 100 per arm. Six-arm star poly[(ε-CL)-*co*-(β-BL)] **2.14 – 2.16** were synthesised in a similar manner using dipentaerythritol **2.3** initiator and a mixture of ε-CL and β-BL monomers with a $\overline{DP}_{Th}$ of 10. The molar ratios of 7:3, 8:2 and 9:1 were used for ε-CL:β-BL to determine the effect β-BL incorporation. For comparative analysis, linear PCL **2.2** and linear poly[(ε-CL)-*co*-(β-BL)] **2.13** were synthesised in a similar manner using ethylene glycol **2.1** initiator. PCL-based polyols were fully characterised using NMR, SEC and DSC. Linear PCL **2.2**, star PCL **2.7** with a $\overline{DP}_{Th}$ of 100 and star poly[(ε-CL)-*co*-(β-BL)] **2.14** with a $\overline{DP}_{Th}$ of 10 and ratio of 7:3 for ε-CL:β-BL, were subjected to enzymatic degradation using *pseudomonas cepacia* lipase in PBS solution (pH 7.4) and monitored using % mass loss, DSC and SEM.

2.2 Experimental

2.2.1 Materials

Tin (II) octoate ($SnOct_2$), ε-caprolactone (ε–CL), β-butyrolactone (β–BL) di(trimethylolpropane) **2.8**, dipentaerythritol **2.3**, pentaerythritol **2.11**, ethylene glycol **2.1**, *pseudomonas cepacia* lipase and phosphate buffer saline salts (pH = 7.4) were purchased from Sigma Aldrich and used without further purification unless otherwise stated. ε–CL and β–BL were distilled over calcium hydride under reduced pressure prior to use. All dry solvents were obtained from Durham Chemistry Department Solvent Purification System (SPS). All other solvents were analytical grade and used without any purification. The NMR solvent used was deuterated chloroform ($CDCl_3$) purchased from Apollo Scientific.

2.2.2 Characterisation Techniques

^1H Nuclear magnetic resonance (NMR) spectra were recorded using an Avance-400 or VNMRS 600 that operate at 400 MHz and 600 MHz, respectively. ^{13}C NMR spectra were recorded using an Avance-400 or VNMRS 600 that operate at 100 MHz and 150 MHz, respectively. Measurements of NMR spectra were conducted under ambient temperature in $CDCl_3$ and Tetramethylsilane (TMS) was used as the internal chemical shift reference.

Size Exclusion Chromatography (SEC) was carried out on a Viscotek TDA 302 with triple detection (refractive index, viscosity and light scattering), using 2 × 300 mL PLgel 5 μm C columns using THF as the eluent at a flow rate of 1 mL min^{-1} (30 °C). The system was calibrated with narrowly polydisperse polystyrene standards.

Differential Scanning Calorimetry (DSC) was carried out on a TA Instruments DSC Q1000 over a temperature range of -80 °C to 150 °C at a rate of 10 °C min^{-1}. The heating scans of the samples before and after enzymatic hydrolysis with *pseudomonas cepacia* lipase were recorded. The enthalpy of fusion (ΔH_m) was calculated from the heating scans and degree of crystallinity ($\%\chi_c$) calculated from the cooling scans. Three repeat scans were taken for every sample.

Fourier-transform Infrared Spectroscopy (FT-IR) was performed on a PerkinElmer 1600 series FT-IR.

Scanning Electron Microscopy (SEM) was performed on a Hitachi SU-70 FEG. The films were first sputter-coated in gold to provide good conductivity of the electron beam. A voltage of 25 kV and a probe current of 90 μA were used.

2.2.3 Enzymatic Degradation

Films (10 × 20 × 0.5 mm^3, ~110 mg) of PCL samples were prepared using a heat press. The films were placed in sealed vials containing a solution of phosphate buffer saline (PBS) (5 mL, 0.2 M, pH = 7.4) and *pseudomonas cepacia* lipase (0.2 mg mL^{-1}). The vials were placed in an oven at 37 ±1°C for up to 15 days and the solutions were replaced every 24 h. After a specified time, the films were removed from the solution, washed thoroughly with distilled water and dried under reduced pressure until a constant weight was obtained. As a control, the experiment was repeated under the same conditions in the absence of enzyme. The enzymatic degradation was analysed by % mass loss, DSC and SEM. The reported % mass losses are the averages of three repeat measurements.

2.2.4 Typical method for the synthesis of PCL

Linear and star PCL were synthesised by the ring-opening polymerisation (ROP) of ε-CL based on the procedure in the literature,[25] using ethylene glycol **2.1**, pentaerythritol **2.11**, di(trimethylolpropane) **2.8** and dipentaerythritol **2.11** initiators to give linear, four-, four- and six-arm stars, respectively.

Dipentaerythritol **2.11** initiator (0.044 g, 0.11 mmol) was added to an oven-dried Schlenk tube equipped with a suba seal and stirrer bar and purged with nitrogen for 10 min. Distilled ε-CL (12.47 g, 111.6 mmol) was added, followed by catalyst stock solution (2.5 mL) [$SnOct_2$ (0.0876 g) in dry toluene (5 mL)]. The reaction mixture was stirred and heated at 120 °C for 24 h. The Schlenk tube was then allowed to cool to ambient temperature and dichloromethane (DCM) (8 mL) was added to dissolve the residue which was then added to methanol (120 mL) at 0 °C precipitating a white solid. The product was filtered and dried under reduced pressure at 40 °C until a constant weight was obtained. All polymers were purified by a second precipitation from DCM into methanol at 0 °C.

2.2.4.1 Synthesis of Linear PCL using Ethylene Glycol Initiator 2.2

Synthesised using a ratio of ε-CL:ethylene glycol of 400:1 to produce linear PCL **2.2** with a $\overline{DP}_{Th}$ of 200 on each arm.

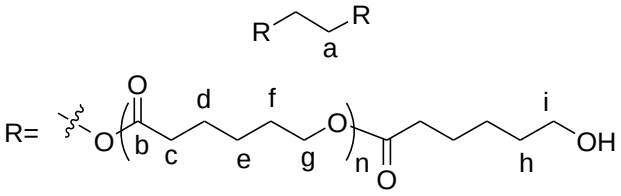

Figure 2.1: Linear PCL **2.2** using ethylene glycol initiator

Collected as a white powder **2.2** (7.47 g, 99% yield). ^{1}H NMR (400 MHz, $CDCl_3$, TMS): δ = 1.36 (m, 354H, H_e), 1.61 (m, 716H, H_d, H_f, H_h), 2.29 (t, *J* = 7.5 Hz, 358H, H_c), 3.62 (t, *J* = 6.5 Hz, 4H, H_i), 4.04 (t, *J* = 6.7 Hz, 352H, H_g), 4.25 (m, 4H, H_a). ^{13}C NMR (400 MHz, $CDCl_3$, TMS): δ = 24.7 (d), 25.6 (e), 28.5 (f), 32.4 (h), 34.2 (c), 62.2 (i), 64.2 (g), 173.6 (b). T_m = 55 - 57 °C. FT-IR: ν_{max} = 3442 (O-H), 2940, 2860 (C-H), 1720 (C=O), 1296, 1238, 1170 (C-O), 1040, 956, 732 cm^{-1}. SEC: M_n = 2.44 × 10^4 g mol^{-1}, M_w = 3.81 × 10^4 g mol^{-1}, Đ = 1.56. The ^{1}H and ^{13}C NMR data were in good agreement with the literature.[25]

2.2.4.2 Synthesis of Six-arm Star PCL using Dipentaerythritol Initiator 2.4 – 2.7

The six-arm star polymers were synthesised following the procedure described for the linear PCL **2.2**.[25]

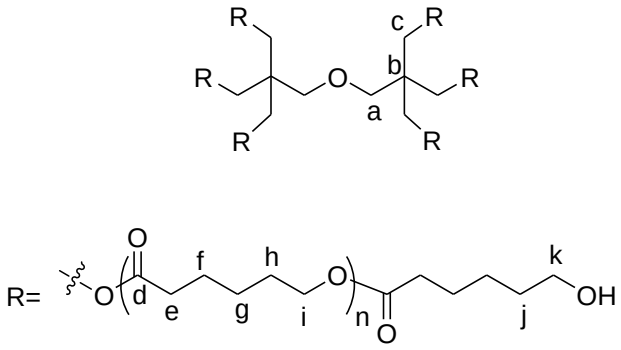

Figure 2.2: Six-arm star PCL **2.4 – 2.7** using dipentaerythritol initiator

2.2.4.2.1 $\overline{DP}$ of 10 per arm 2.4

Synthesised using a ratio of ε-CL : dipentaerythritol **2.3** of 60:1to produce six-arm star PCL **2.4** with a $\overline{DP}_{Th}$ of 10 per arm.

Collected as a white powder **2.4** (12.2 g, 93% yield). ^{1}H NMR (400 MHz, $CDCl_3$, TMS): δ = 1.38 (m, 78H, H_g), 1.63 (m, 196H, H_f, H_h), 2.29 (t, *J* = 7.6 Hz, 78 H, H_e), 3.49 (s, 4H, H_a), 3.65 (t, *J* = 6.4 Hz, 8H, H_k), 4.06 (t, *J* = 6.4 Hz, 77H, H_i, H_c). ^{13}C NMR (400 MHz, $CDCl_3$, TMS): δ = 24.4 (f), 25.4 (g), 28.2 (h), 32.3 (j), 34.0 (e), 41.5 (b), 62.3 (k), 64.0 (c), 64.2 (i), 72.1 (a), 173.3 (d). T_m = 50 - 55 °C. FT-IR: ν_{max} = 3438 (O-H), 2944, 2866 (C-H), 1721 (C=O), 1366, 1293, 1239, 1172 (C-O), 1045, 961, 732 cm^{-1}. SEC: M_n = 7.30 × 10^3 g mol^{-1}, M_w = 8.32 × 10^3 g mol^{-1}, Đ = 1.14. The ^{1}H and ^{13}C NMR data were in good agreement with the literature.[25]

2.2.4.2.2 $\overline{DP}$ of 20 per arm 2.5

Synthesised using a ratio of ε-CL : dipentaerythritol **2.3** of 120:1to produce six-arm star PCL **2.5** with a $\overline{DP}_{Th}$ of 20 per arm.

Collected as a white powder **2.5** (12.8 g, 99% yield). ^{1}H NMR (400 MHz, $CDCl_3$, TMS): δ = 1.37 (m, 179H, H_g), 1.64 (m, 356H, H_f, H_h), 2.29 (t, *J* = 7.6 Hz, 179H, H_e), 3.32 (m, 4H, H_a), 3.63 (t, *J* = 6.4 Hz, 8H, H_k), 4.05 (t, *J* = 6.8 Hz, 180H, H_i, H_c). ^{13}C NMR (400 MHz, $CDCl_3$, TMS): δ = 24.7 (f), 25.6 (g), 28.5 (h), 32.3 (j), 34.1 (e), 41.5 (b), 62.7 (k), 64.2 (c), 64.3 (i), 72.1 (a), 173.6 (d). T_m = 51 - 55 °C. FT-IR: ν_{max} = 3542 (O-H), 2943, 2866 (C-H), 1721 (C=O), 1239, 1168 (C-O), 1046, 732 cm^{-1}. SEC: M_n = 1.38 × 10^4 g mol^{-1}, M_w = 1.67 × 10^4 g mol^{-1}, Đ = 1.22. The ^{1}H and ^{13}C NMR data were in good agreement with the literature.[25]

2.2.4.2.3 $\overline{DP}$ of 50 per arm 2.6

Synthesised using a ratio of ε-CL : dipentaerythritol **2.3** of 300:1to produce six-arm star PCL **2.6** with a $\overline{DP}_{Th}$ of 50 per arm.

Collected as a white solid **2.6** (9.50 g, 94% yield). ^{1}H NMR (400 MHz, $CDCl_3$, TMS): δ = 1.34 (m, 564H, H_g), 1.61 (m, 1128H, H_f, H_h), 2.26 (t, *J* = 7.5 Hz, 564H, H_e), 3.34 (m, 4H, H_a), 3.60 (t, *J* = 6.5 Hz, 12H, H_k), 4.02 (t, *J* = 6.7 Hz, 564H, H_i, H_c). ^{13}C NMR (400 MHz, $CDCl_3$, TMS): δ = 24.6 (f), 25.5 (g), 28.3 (h), 32.3 (j), 34.1 (e), 41.5 (b), 62.5 (k), 64.1 (c), 64.2 (i), 173.5 (d). T_m = 52 - 58 °C. FT-IR: ν_{max} = 3542 (O-H), 2954, 2858 (C-H), 1720 (C=O), 1366, 1236, 1160 (C-O), 1048, 958, 728 cm^{-1}. SEC: M_n = 2.65 × 10^4 g mol^{-1}, M_w =

3.30×10^4 g mol^{-1}, Đ = 1.25. The ^{1}H and ^{13}C NMR data were in good agreement with the literature.[25]

2.2.4.2.4 $\overline{DP}$ of 100 per arm 2.7

Synthesised using a ratio of ε-CL : dipentaerythritol **2.3** of 600:1to produce six-arm star PCL **2.7** with a $\overline{DP}_{Th}$ of 100 per arm.

Collected as a white solid **2.7** (11.8 g, 99% yield). ^{1}H NMR (400 MHz, $CDCl_3$, TMS): δ = 1.34 (m, 804H, H_g), 1.60 (m, 1608H, H_f, H_h), 2.26 (m, 804H, H_e), 3.35 (m, 4H, H_a), 3.59 (m, 12H, H_k), 4.02 (m, 804H, H_i, H_c). ^{13}C NMR (400 MHz, $CDCl_3$, TMS): δ = 24.6 (f), 25.6 (g), 28.4 (h), 32.3 (j), 34.2 (e), 41.5 (b), 62.6 (k), 64.2 (i), 173.6 (d). T_m = 53 - 58 °C. FT-IR: ν_{max} = 2948, 2866 (C-H), 1720 (C=O), 1366, 1240, 1166 (C-O), 1046, 962, 732 cm^{-1}. SEC: $M_n = 2.45 \times 10^4$ g mol^{-1}, $M_w = 5.59 \times 10^4$ g mol^{-1}, Đ = 2.28. The ^{1}H and ^{13}C NMR data were in good agreement with the literature.[25]

2.2.4.3 Synthesis of Four-arm Star PCL using Di(trimethylolpropane) Initiator 2.9 – 2.10

The four-arm star polymers were synthesised following the procedure described for the linear PCL **2.2**.[25]

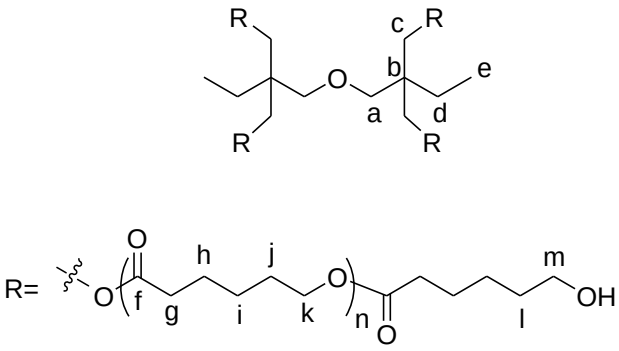

Figure 2.3: Four-arm star PCL **2.9 – 2.10** using di(trimethylolpropane) initiator

2.2.4.3.1 $\overline{DP}$ of 10 per arm 2.9

Synthesised using a ratio of ε-CL : di(trimethylolpropane) **2.8** of 40 : 1 to produce four-arm star PCL **2.9** with a $\overline{DP}_{Th}$ of 10 per arm.

Collected as a white powder **2.9** (3.62 g, 81% yield). ^{1}H NMR (400 MHz, $CDCl_3$, TMS): δ = 0.77 (t, *J* = 8.0 Hz, 6H, H_e), 1.31 (m, 99H, H_i, H_d), 1.58 (m, 206H, H_h, H_j, H_l), 2.24 (t, *J* = 8.0 Hz, 96H, H_g) 3.19 (s, 4H, H_a), 3.58 (t, *J* = 8.0 Hz, 8H, H_m), 3.97 (s, 8H, H_c), 3.99 (t, *J* = 8.0 Hz, 89H, H_k). ^{13}C NMR (400 MHz, $CDCl_3$, TMS): δ = 7.5 (e), 23.1 (d), 24.6 (h), 25.6 (i), 28.4 (j), 32.4 (l), 34.2 (g), 41.6 (b), 62.5 (m), 64.1 (c), 64.2 (k), 71.1 (a), 173.7 (f). T_m = 46 - 51 °C. FT-IR: ν_{max} = 3441 (O-H), 2945, 2865 (C-H), 1720 (C=O), 1365, 1293, 1238, 1173, 1107 (C-O), 1045, 961, 732 cm^{-1}. SEC: $M_n = 5.84 \times 10^3$ g mol^{-1}, $M_w = 6.12 \times 10^3$ g mol^{-1}, Đ = 1.05. The ^{1}H and ^{13}C NMR data were in good agreement with the literature.[25]

2.2.4.3.2 $\overline{DP}$ of 20 per arm 2.10

Synthesised using a ratio of ε-CL : di(trimethylolpropane) **2.8** of 80:1to produce four-arm star PCL **2.10** with a $\overline{DP}_{Th}$ of 10 per arm.

Collected as a white powder **2.10** (8.27 g, 95% yield). ^{1}H NMR (400 MHz, $CDCl_3$, TMS): δ = 0.83 (m, 6H, H_e), 1.37 (m, 206H, H_i, H_d), 1.63 (m, 400H, H_h, H_j, H_l), 2.30 (t, *J* = 7.6 Hz, 200H, H_g), 3.24 (m, 4H, H_a), 3.63 (t, *J* = 6.4 Hz, 8H, H_m), 3.97 (s, 8H, H_c), 4.05 (t, *J* = 8.5 Hz, 192H, H_k). ^{13}C NMR (400 MHz, $CDCl_3$, TMS): δ = 7.5 (e), 23.1 (d), 24.6 (h), 25.7 (i), 28.4 (j), 32.4 (l), 34.3 (g), 41.6 (b), 62.7 (m), 64.2 (c), 64.3 (k), 70.1 (a), 173.5 (f). T_m = 56 - 60 °C. FT-IR: ν_{max} = 3440 (O-H), 2945, 2866 (C-H), 1721 (C=O), 1293, 1239, 1174 (C-O), 1046, 961, 732 cm^{-1}. SEC: $M_n = 1.04 \times 10^4$ g mol^{-1}, $M_w = 1.25 \times 10^4$ g mol^{-1}, Đ = 1.20. The ^{1}H and ^{13}C NMR data were in good agreement with the literature.[25]

2.2.4.4 Synthesis of Four-arm Star PCL using Pentaerythritol Initiator 2.12

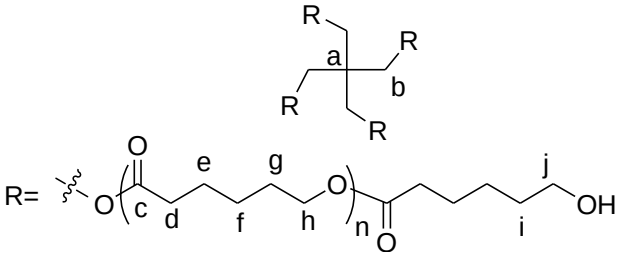

Figure 2.4: Four-arm star PCL **2.12** using pentaerythritol initiator

2.2.4.3.1 $\overline{DP}$ of 10 per arm 2.12

Synthesised using a ratio of ε-CL : pentaerythritol **2.11** of 40:1to produce four-arm star PCL **2.12** with a $\overline{DP}_{Th}$ of 10 per arm.

Collected as a white powder **2.12** (8.51 g, 97% yield). ^{1}H NMR (400 MHz, $CDCl_3$, TMS): δ = 1.37 (m, 114H, H_f), 1.64 (m, 222H, H_e, H_g, H_i), 2.30 (t, *J* = 7.6 Hz, 110H, H_d), 3.64 (t, *J* = 6.4 Hz, 8H, H_j), 4.05 (t, *J* = 6.8 Hz, 101H, H_h), 4.10 (s, 8H, H_b). ^{13}C NMR (400 MHz, $CDCl_3$, TMS): δ = 24.7 (e), 25.5 (a), 25.7 (f), 28.5 (g), 32.5 (i), 34.2 (d), 59.1 (j), 62.8 (b), 64.3 (h), 173.7 (c). T_m = 49 - 54 °C. FT-IR: ν_{max} = 3532 (O-H), 2940, 2864 (C-H), 1721 (C=O), 1365, 1293, 1238, 1171 (C-O), 1045, 961, 732 cm^{-1}. SEC: $M_n = 5.75 \times 10^3$ g mol^{-1}, $M_w = 6.35 \times 10^3$ g mol^{-1}, Đ = 1.10. The ^{1}H and ^{13}C NMR data were in good agreement with the literature.[25]

2.2.5 Typical method for the synthesis of Poly[(ε-CL)-*co*-(β-BL)] 2.13 – 2.16

Ring-opening co-polymerisations of ε-CL and β-BL using ethylene glycol **2.1** and dipentaerythritol **2.3** initiators to produce linear **2.13** and six-arm star **2.14 – 2.16** copolymers, respectively, were performed following a typical procedure described below.[24]

Dipentaerythritol **2.3** initiator (0.085 g, 0.033 mmol) and stirrer bar were added to an oven-dried Schlenk tube and purged with nitrogen for 10 min. Distilled ε-CL (1.60 g, 14.0 mmol) and distilled β-BL (0.52 g, 6.00 mmol) were added to the flask followed by catalyst stock solution (0.5 mL) [$Sn(Oct)_2$ (0.28g) in dry toluene (10 mL)]. The reaction mixture was stirred and heated to 110 °C for 96 h. The schlenk was allowed to cool, the product dissolved in DCM (~10 mL) and precipitated into methanol (~100 mL) at 0 °C using an ice bath. The solid product was filtered and dried under reduced pressure at 40 °C until a constant weight was obtained. The product was purified by a further precipitation from DCM into methanol at 0 °C.

2.2.5.1 Synthesis of Linear Poly(ε-CL)-*co*-(β-BL) using Ethylene Glycol Initiator 2.13

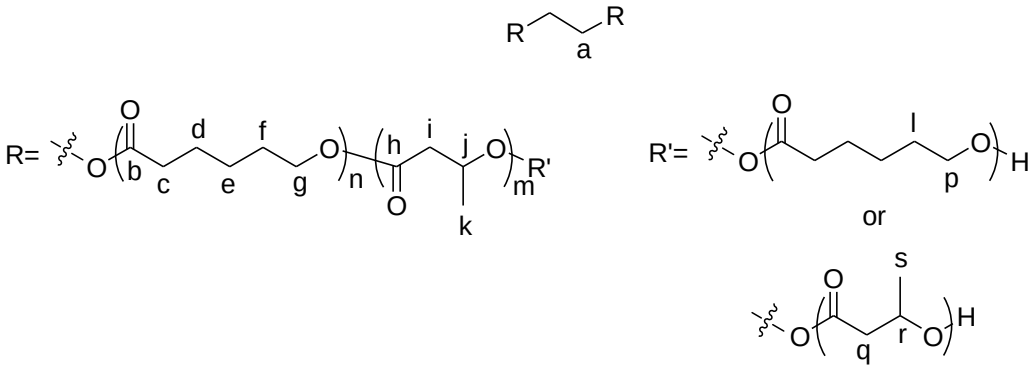

Figure 2.5: Linear poly[(ε-CL)-*co*-(β-BL)] **2.13** using ethylene glycol initiator

Synthesised using a ratio of ε-CL and β-BL monomer : ethylene glycol **2.1** of 20:1 to produce linear copolymer **2.13** with a $\overline{DP}_{Th}$ of 10 per arm, consisting of 7 ε-CL repeat units and 3 β-BL repeat units.

Collected as a off-white powder **2.13** (2.87 g, 41% yield). ^{1}H NMR (400 MHz, $CDCl_3$, TMS): δ = 1.18 (m, 3H, H_s), 1.22 (m, 12H, H_k), 1.32 (m, 72H, H_e), 1.52 (m, 6H, H_l), 1.59 (m, 146H, H_d, H_f), 2.25 (t, *J* = 7.4 Hz, 72H, H_c), 2.39-2.57 (m, 8H, H_m), 3.57 (t, *J* = 6.6 Hz, 4H, H_p), 4.00 (t, *J* = 6.6 Hz, 70H, H_g), 4.23 (t, *J* = 2.5 Hz, 4H, H_a), 5.20 (m, 4H, H_j). ^{13}C NMR (400 MHz, $CDCl_3$, TMS): δ = 19.8 (k), 22.5 (s), 24.5 (d), 25.5 (e), 28.3 (f), 32.3 (l), 34.1 (c), 40.8 (i), 42.8 (q), 62.0 (a), 62.5 (p), 64.1 (g), 67.2 (r), 67.6 (j), 169.1 (h), 173.5 (b). T_m = 45 - 51 °C. FT-IR: ν_{max} = 3484 (O-H), 2944, 2868 (C-H), 1722 (C=O), 1368, 1240, 1166 (C-O), 1048, 962, 732 cm^{-1}. SEC: $M_n = 4.57 \times 10^3$ g mol^{-1}, $M_w = 5.34 \times 10^3$ g mol^{-1}, Đ = 1.17. The ^{1}H and ^{13}C NMR data were in good agreement with the literature.[24]

2.2.5.2 Synthesis of Six-arm Star Poly(ε-CL)-*co*-(β-BL) using Dipentaerythritol Initiator 2.14 – 2.16

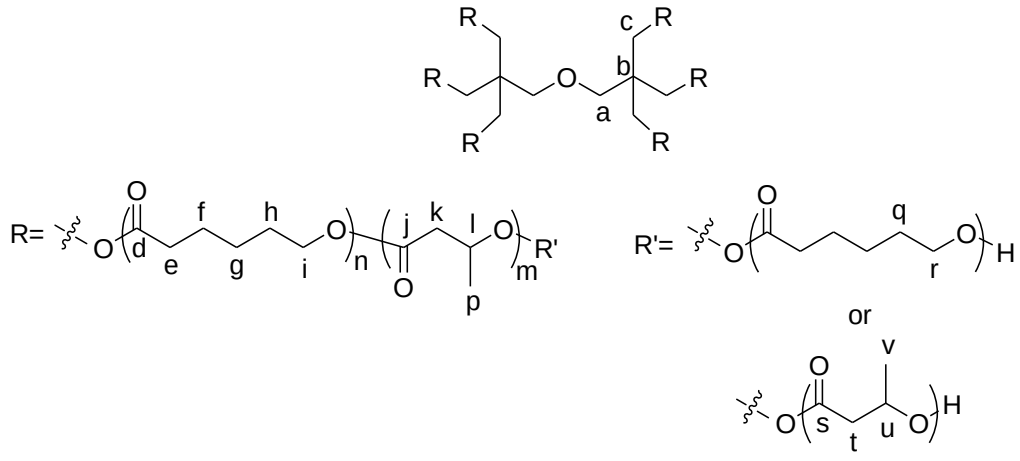

Figure 2.6: Six-arm star poly[(ε-CL)-*co*-(β-BL)] **2.14 – 2.16** using dipentaerythritol initiator

2.2.5.2.1 $\overline{DP}$ of 10 per arm 2.14 – 2.16

Synthesised using a ratio of ε-CL : β-BL : dipentaerytritol **2.3** of 42:18:1to produce a six-arm star copolymer **2.14** with a $\overline{DP}_{Th}$ of 10 per arm, consisting of 7 ε-CL and 3 β-BL units.

Collected as an off-white powder **2.14** (1.41 g, 64% yield). ^{1}H NMR (400 MHz, $CDCl_3$, TMS): δ = 1.16 (m, 9H, H_v), 1.23 (m, 9H, H_p), 1.33 (m, 68H, H_g), 1.60 (m, 138H, H_f, H_h, H_q), 2.26 (t, *J* = 7.1 Hz, 68H, H_e), 2.38 (m, 7H, H_t), 2.55 (m, 6H, H_k), 3.34 (m, 4H, H_a), 3.57 (t, *J* = 5.6 Hz, 2H, H_r), 4.01 (t, *J* = 6.2 Hz, 74H, H_i, H_c), 5.19 (m, 3H, H_l), 5.25 (m, 2H, H_u). ^{13}C NMR (400 MHz, $CDCl_3$, TMS): δ = 19.9 (p), 22.5 (v), 24.6 (f), 25.5 (g), 28.3 (h), 32.3 (q), 34.0 (e), 40.8 (k), 42.8 (b), 42.9 (t), 62.3 (c), 62.5 (r), 64.0 (i), 67.2 (l), 67.5 (u), 70.0 (a), 170.2 (j), 172.8 (s), 173.5 (d). T_m = 42 - 46 °C. FT-IR: ν_{max} = 3458 (O-H), 2946, 2868 (C-H), 2358, 1724 (C=O), 1368, 1292, 1238, 1176 (C-O), 1042, 962, 726 cm^{-1}. SEC: M_n = 8.29 × 10^3 g mol^{-1}, M_w = 9.42 × 10^3 g mol^{-1}, Đ = 1.14. The ^{1}H and ^{13}C NMR data were in good agreement with the literature.[24]

Synthesised using a ratio of ε-CL : β-BL : dipentaerytritol **2.3** of 48:12:1to produce a six-arm star copolymer **2.15** with a $\overline{DP}_{Th}$ of 10 per arm, consisting of 8 ε-CL and 2 β-BL units.

Collected as an off-white powder **2.15** (1.45 g, 64% yield). ^{1}H NMR (400 MHz, $CDCl_3$, TMS): δ = 1.18 (d, *J* = 6.0 Hz, 6H, H_p), 1.33 (m, 116H, H_g), 1.60 (m, 232H, H_f, H_h, H_q), 2.26 (t, *J* = 7.4 Hz, 116H, H_e), 2.45 (m, 4H, H_k), 3.04 (bs, 4H, OH), 3.34 (m, 4H, H_a), 3.59 (t, *J* = 6.6 Hz, 2H, H_r), 4.01 (t, *J* = 6.6 Hz, 116H, H_i, H_c), 5.21 (m, 2H, H_l). ^{13}C NMR (400 MHz, $CDCl_3$, TMS): δ = 19.9 (p), 22.5 (v), 24.6 (f), 25.5 (g), 28.3 (h), 34.1 (e), 40.8 (k), 42.8 (b), 42.9 (t), 62.3 (c), 64.1 (i), 67.2 (l), 67.4 (u), 69.9 (a), 172.8 (j), 173.5 (d). T_m = 47 - 51 °C. FT-IR: ν_{max} = 3548 (O-H), 2946, 2868 (C-H), 1722 (C=O), 1368, 1296, 1240, 1176 (C-O), 1046, 962, 732 cm^{-1}. SEC: $M_n = 7.32 \times 10^3$ g mol^{-1}, $M_w = 8.78 \times 10^3$ g mol^{-1}, Đ = 1.20. The ^{1}H and ^{13}C NMR data were in good agreement with the literature.[24]

Synthesised using a ratio of ε-CL : β-BL : dipentaerytritol **2.3** of 54:6:1to produce a six-arm star copolymer **2.16** with a $\overline{DP}_{Th}$ of 10 per arm, consisting of 9 ε-CL and 1 β-BL unit.

Collected as an off-white powder **2.16** (1.63 g, 71 % yield). ^{1}H NMR (400 MHz, $CDCl_3$, TMS): δ = 1.17 (d, *J* = 6.4 Hz, 9H, H_p), 1.33 (m, 132H, H_g), 1.60 (m, 264H, H_f, H_h, H_q), 2.26 (t, *J* = 7.6 Hz, 132H, H_e), 2.40 (m, 6H, H_k), 3.04 (bs, 4H, OH), 3.34 (m, 4H, H_a), 3.59 (t, *J* = 6.6 Hz, 6H, H_r), 4.01 (t, *J* = 6.6 Hz, 132H, H_i, H_c), 5.21 (m, 3H, H_l). ^{13}C NMR (400 MHz, $CDCl_3$, TMS): δ = 19.8 (p), 22.5 (v), 24.5 (f), 25.5 (g), 28.3 (h), 34.1 (e), 40.8 (k), 42.8 (b), 42.9 (t), 62.4 (c), 64.0 (i), 67.2 (l), 70.0 (a), 172.7 (j), 173.4 (d). T_m = 48 - 51 °C. FT-IR: ν_{max} = 2944, 2864 (C-H), 1722 (C=O), 1362, 1294, 1236, 1172 (C-O), 1042, 956, 730 cm^{-1}. SEC: $M_n = 8.38 \times 10^3$ g mol^{-1}, $M_w = 9.61 \times 10^3$ g mol^{-1}, Đ = 1.15. The ^{1}H and ^{13}C NMR data were in good agreement with the literature.[24]

2.3 Results and Discussion

2.3.1 Linear PCL 2.2

Linear PCL **2.2** was synthesised *via* ROP of ε-CL using ethylene glycol **2.1** and catalysed by $SnOct_2$, Scheme 2.1. A ratio of ε-CL to ethylene glycol of 400:1 was used to produce **2.2** with a $\overline{DP}_{Th}$ of 200 on each arm.

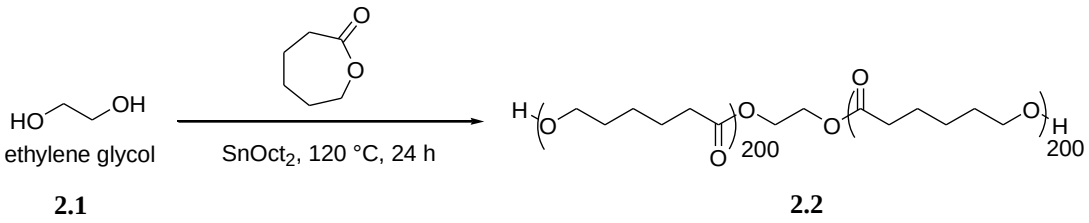

Scheme 2.1: Synthesis of linear PCL **2.2** using ethylene glycol

The ^{1}H NMR spectrum of **2.2**, Figure 2.7, shows a resonance at 4.25 ppm that can be attributed to methylene protons **a** on the central ethylene moiety, and a resonance at 2.28 ppm attributing to methylene protons **c** in the PCL repeat unit. The $\overline{DP}_{NMR}$ of **2.2** was calculated using Equation 2.1, where the integral of protons **c** located on the PCL repeat unit were compared to the integral of protons **a** located on the central ethylene unit. This was achieved by dividing ∫**c** by 2 (number of arms) multiplied by 2 (number of protons in methylene group). This value was then divided by ∫**a** over 4 (number of proton environments equal to **a**) multiplied by 1 (number of central unit). The calculated $\overline{DP}_{NMR}$ of 89 is notably lower than that of the theoretical $\overline{DP}_{Th}$ of 200. This could be due to the increase in viscosity as the ROP proceeds in bulk conditions. Therefore, polymer chain mobility is restricted and availability of initiating chain-end groups in the polymer limits $\overline{DP}$.

$$\overline{DP} = \frac{\left(\frac{\int \boldsymbol{c}}{2\times 2}\right)}{\left(\frac{\int \boldsymbol{a}}{4\times 1}\right)}$$

Equation 2.1

The resonances attributed to the methylene protons in ethylene glycol at 3.76 ppm are shifted downfield to 4.25 ppm in **2.2**, as methylene protons **a** neighbour an ester group in the central ethylene moiety, Figure 2.7. This shift in resonance suggests successful initiation and ROP of ε-CL from the OH groups on the ethylene glycol moiety.

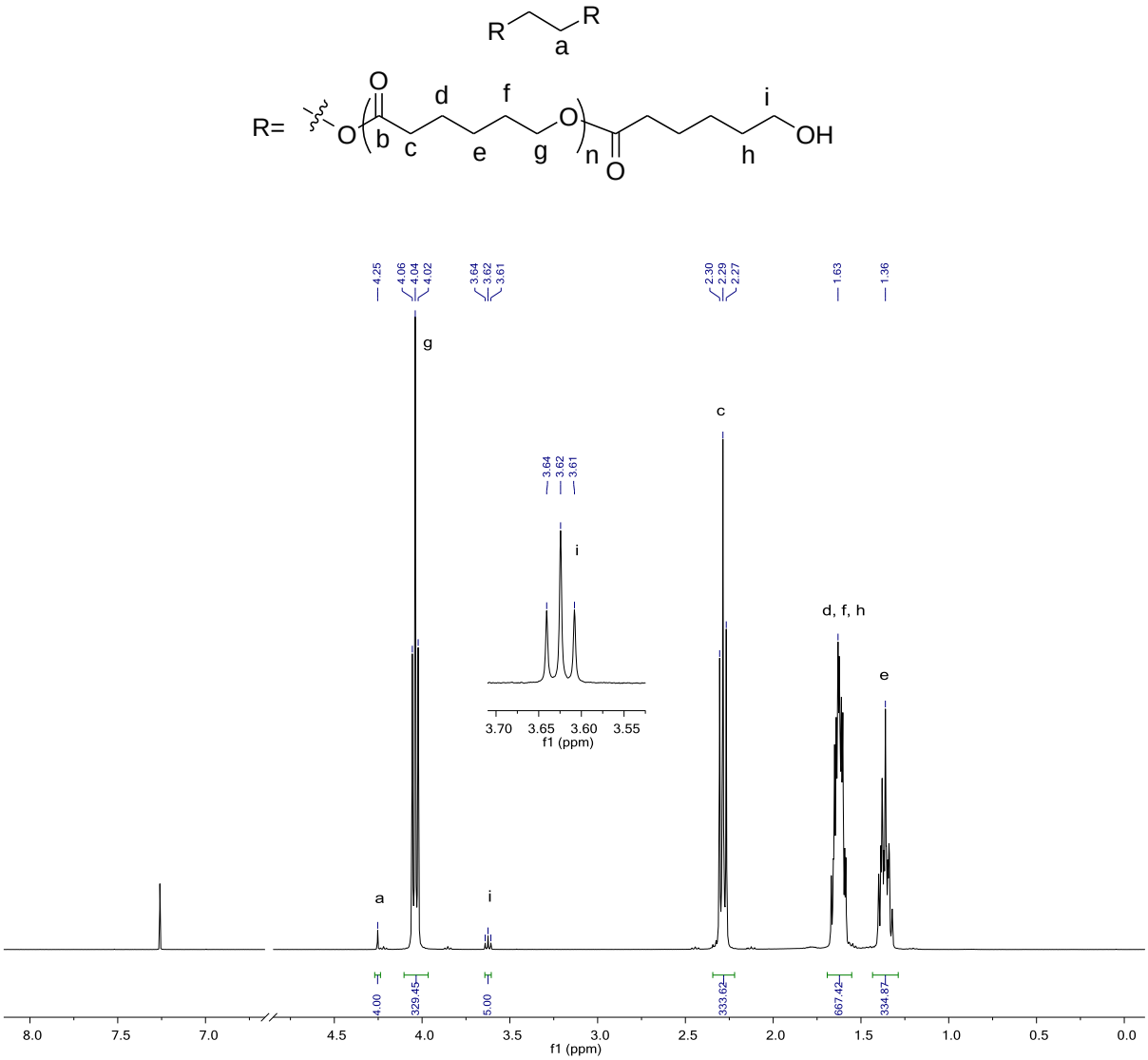

Figure 2.7: 400 MHz ^{1}H NMR spectrum of **2.2** in $CDCl_3$

The most shielded methylene protons **e** located on the PCL repeat unit, are seen as the resonance located furthest upfield at 1.36 ppm. Methylene protons **d**, **f** and **h** in PCL share a similar chemical environment and so are seen as an overlapped resonance at 1.63 ppm. Methylene protons **c** in PCL neighbouring the carbonyl atom of the ester group, are attributed to the triplet resonance at 2.29 ppm, due to splitting from the two neighbouring **d** protons. Further downfield, methylene protons **i** in PCL neighbouring the OH group, are

attributed to the triplet resonance at 3.62 ppm and are integrated to 4H. Moreover, the ^{1}H – ^{1}H COSY spectrum of **2.2**, Figure 2.8, shows methylene protons **i** at 3.62 ppm coupling to neighbouring methylene protons **h** at 1.63 ppm. Furthermore, methylene protons **g** in PCL located next to the oxygen atom of the ester group are attributed to the triplet resonance at 4.04 ppm.

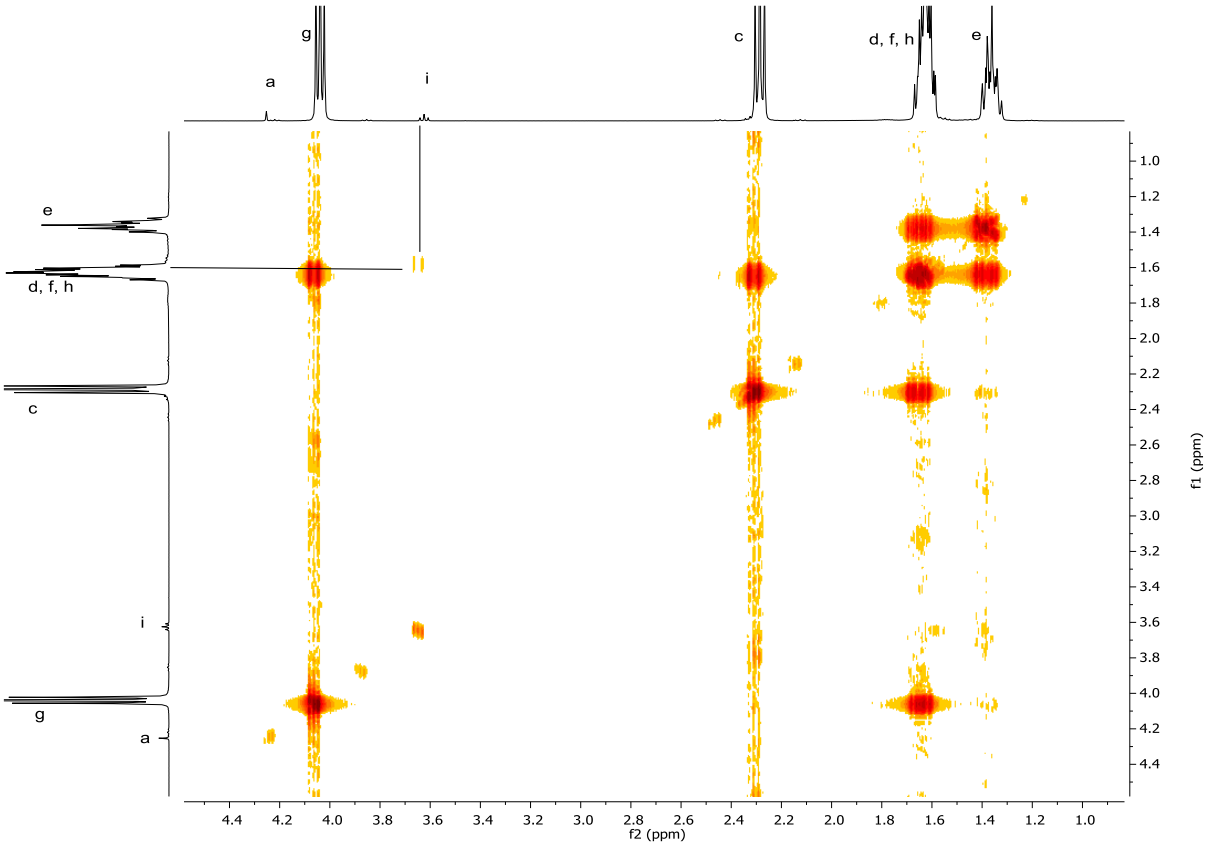

Figure 2.8: 400 MHz ^{1}H - ^{1}H COSY NMR spectrum of **2.2** in $CDCl_3$

The methylene carbon atom resonance in ethylene glycol at 63.8 ppm is seen to shift upfield to 62.7 ppm in the ^{13}C NMR spectrum of **2.2**, Figure 2.9. This is due to the carbon atoms **a** on the central ethylene moiety neighbouring an oxygen atom in an ester group. This indicates the successful ROP reaction using the ethylene glycol OH initiating groups. The characteristic PCL resonances are seen at 24.7 ppm, 25.6 ppm, 28.5 ppm, 34.2 ppm and 64.2 ppm, attributing to the methylene carbon atoms on the PCL backbone **d**, **e**, **f**, **c** and **g**, respectively. The downfield resonance at 173.6 ppm is attributed to carbonyl carbon atom **b**. Furthermore, the resonances seen at 32.4 ppm and 62.2 ppm are attributed to methylene carbon atoms **h** and **i**, in PCL carbon atoms neighbouring the OH group, respectively.

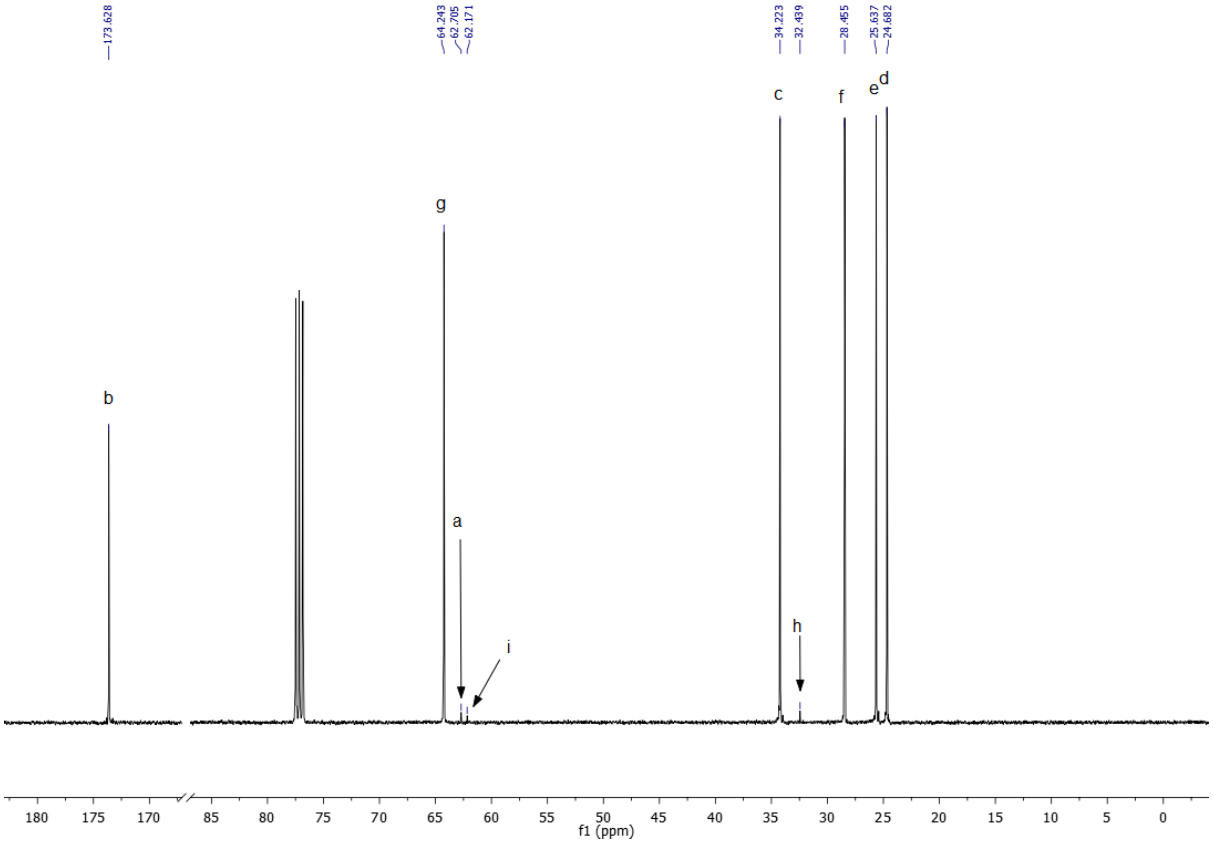

Figure 2.9: 100 MHz ^{13}C NMR spectrum of **2.2** in $CDCl_3$

2.3.2 Six-arm Star PCL using Dipentaerythritol Initiator 2.4 - 2.7

Six-arm star PCL was synthesised in a similar ROP reaction with ε-CL and dipentaerythritol **2.3** as the initiator to give stars **2.4 - 2.7**, Scheme 2.2. The ratio of ε-CL to dipentaerythritol initiator was varied to achieve six-arm stars with a $\overline{DP}_{Th}$ of 10, 20, 50 and 100 per arm in **2.4**, **2.5**, **2.6** and **2.7**, respectively.

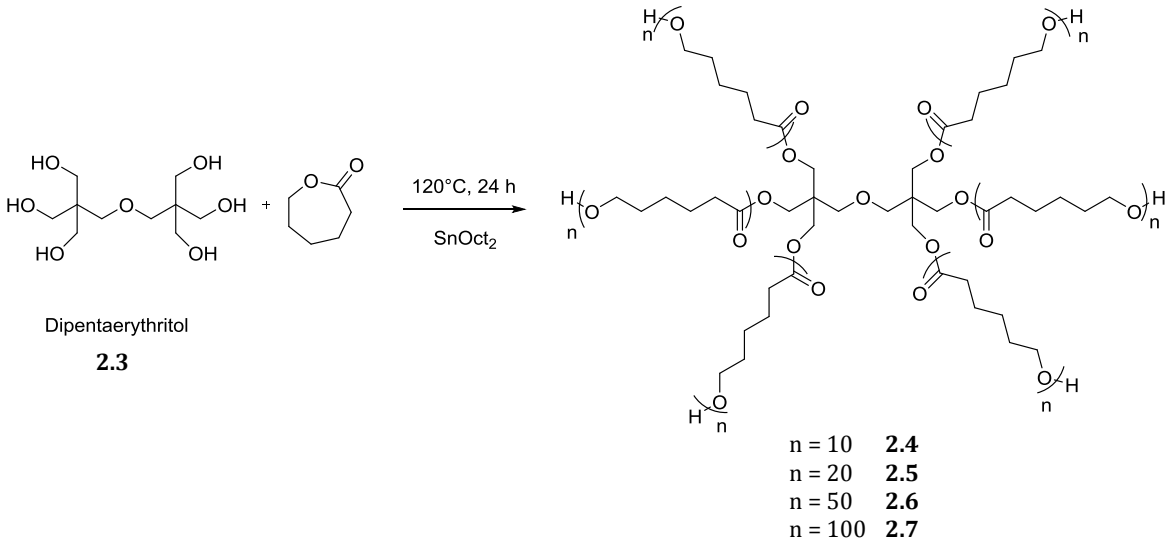

Scheme 2.2: Synthesis of six-arm star PCL **2.4 - 2.7** using dipentaerythritol initiator **2.3**

Figure 2.10 shows the ^{1}H NMR spectrum of **2.5** and the characteristic resonances attributing to methylene protons in the PCL repeat unit at 1.37 ppm, 1.64 ppm, 2.29 ppm and 4.05 ppm attributing to **g**, **f/h/j**, **e** and **i**, respectively. Methylene protons **a** and **c** located on the dipentaerythritol initiator moiety are seen at resonance 3.32 ppm and 4.05 ppm, respectively. The $\overline{DP}_{NMR}$ of **2.5** was determined using Equation 2.1, using dipentaerythritol initiator protons **a** at 3.32 ppm, and PCL repeat unit protons **e** at 2.29 ppm, and found to be $\overline{DP}_{NMR}$ = 20. The integration of 4H for dipentaerythritol methylene protons **a** to 12H for chain-end methylene protons **k**, indicates successful ROP from all six OH initiating groups on the dipentaerythritol moiety.

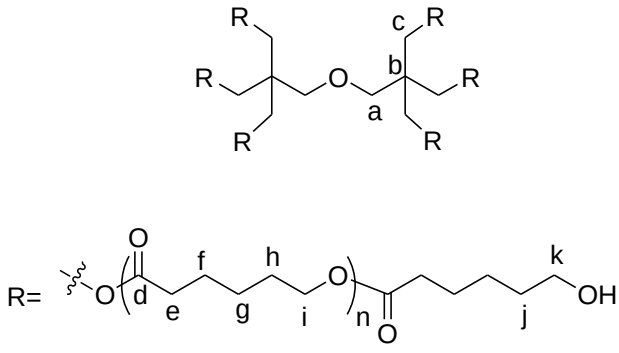

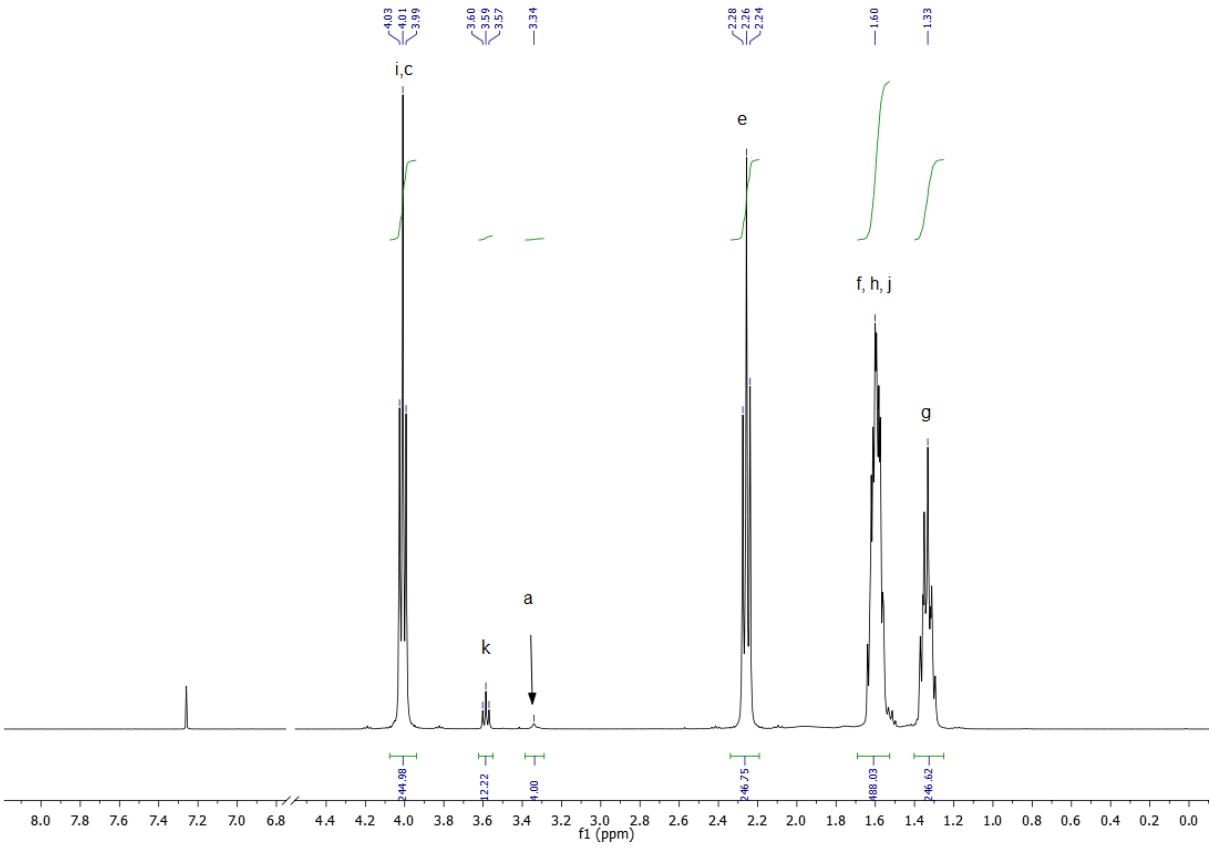

Figure 2.10: 600 MHz ^{1}H NMR spectrum of **2.5** in $CDCl_3$

The characteristic resonances for the methylene carbon atoms on the PCL repeat unit are seen in the ^{13}C NMR spectrum of **2.5**, Figure 2.11, at 24.7 ppm, 25.5 ppm, 28.5 ppm, 34.1 ppm and 64.1 ppm, attributing to carbon atoms **f**, **g**, **h**, **e** and **i**, respectively. The downfield resonance at 173.6 ppm can be attributed to carbonyl carbon atom **d**. Furthermore, methylene carbon atoms in PCL neighbouring the OH group, **j** and **k**, can be seen at 32.3 ppm and 67.2 ppm, respectively. The dipentaerythritol initiator carbon atom resonances **a**, **b** and **c** can be seen at 72.1 ppm, 41.5 ppm and 64.2 ppm, respectively. The presence of these resonances after two precipitations from DCM into methanol, indicate a successful reaction, as any unreacted dipentaerythritol would have been removed.

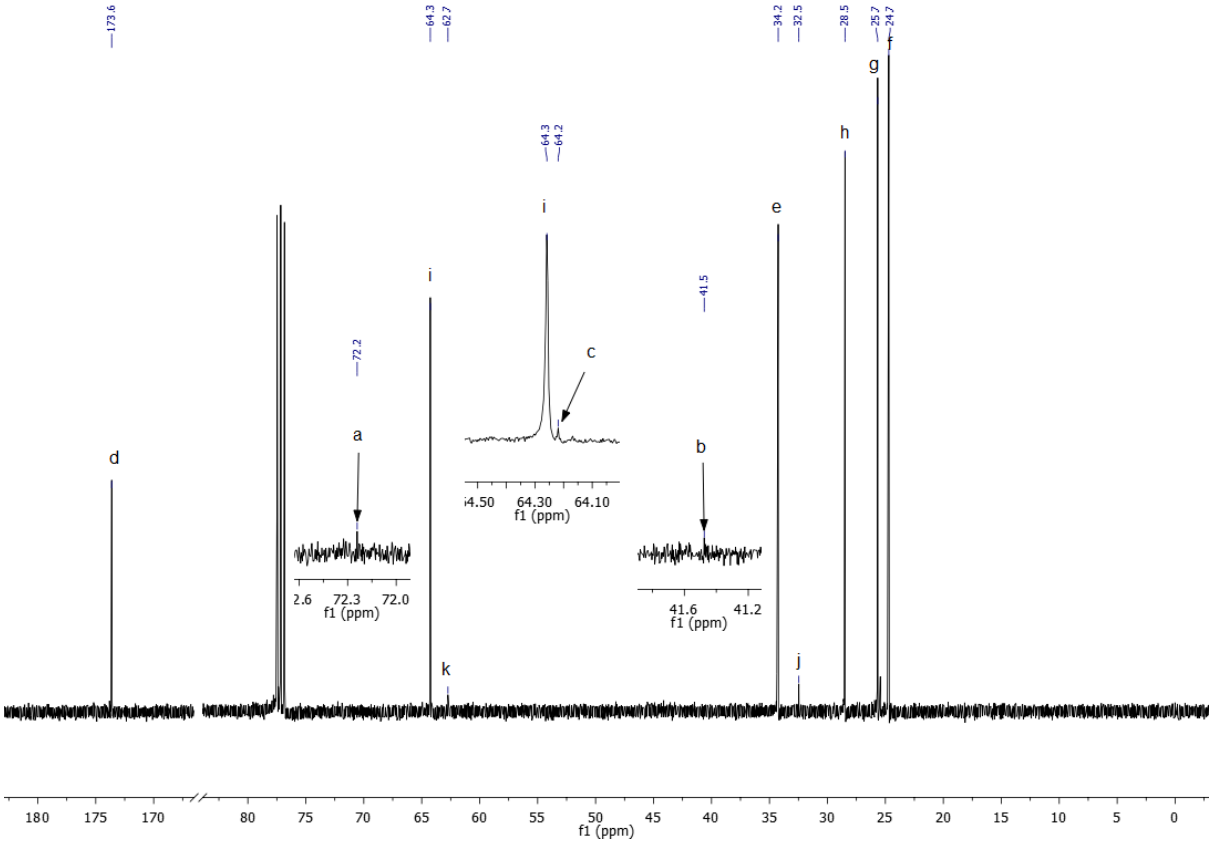

Figure 2.11: 150 MHz ^{13}C NMR spectrum of **2.5** in $CDCl_3$

Figure 2.12 depicts the normalised SEC chromatograms of six-arm star PCL **2.4 - 2.7**. An increase in M_n is observed in **2.4 – 2.7** from 0.73×10^4 g mol^{-1} to 2.45×10^4 g mol^{-1}, with an increase in $\overline{DP}$ from 1.14 to 2.28. A lower molecular weight shoulder can clearly be seen for the highest molecular weight star **2.7** with a $\overline{DP}_{NMR}$ of 67. This could be attributed to the decreased mobility of polymer chains during the ROP reaction performed in bulk conditions. As the ROP proceeds, the reaction mixture increases in viscosity, restricting mobility and decreasing the availability of initiating chain-end groups. This effect both limits the $\overline{DP}$ and produces a higher Đ. This is evident in Table 2.1, as the Đ significantly increases from 1.14 to 2.28 in **2.4 - 2.7**.

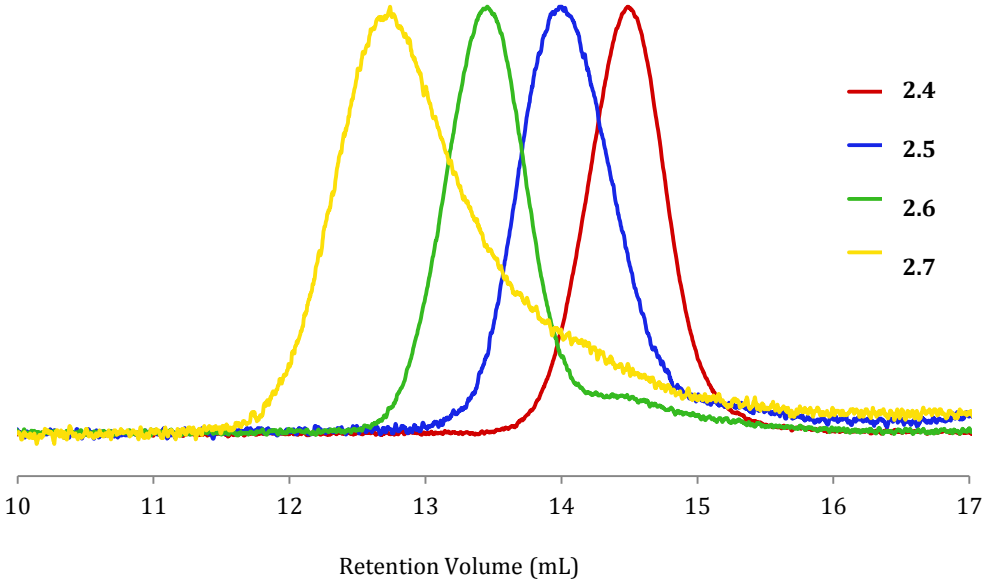

Figure 2.12: Overlayed normalised SEC chromatograms for **2.4 - 2.7**

The comparsion of M_n^{SEC}, M_n^{NMR} and M_n^{Th} for linear **2.2** and six-arm stars **2.4 - 2.7**, are shown in Table 2.1. The lower molecular weight stars **2.4 - 2.7** with $\overline{DP}_{NMR}$ values of 10, 22 and 47, are in good agreement with the $\overline{DP}_{Th}$ values of 10, 20 and 50, respectively. However, the highest molecular weight star **2.7** and linear **2.2** with $\overline{DP}_{NMR}$ values of 67 and 89, are in poor agreement with the $\overline{DP}_{Th}$ values of 100 and 200, respectively. This supports the previous hypothesis of decreased polymer chain mobility due to higher viscosity in bulk conditions, limiting the $\overline{DP}$.

Linear **2.2** and lower molecular weight stars **2.4 - 2.7** with M_n^{NMR} values of 2.04×10^4 g mol^{-1}, 0.71×10^4 g mol^{-1} and 1.53×10^4 g mol^{-1} are in good agreement with M_n^{SEC} values of 2.44×10^4 g mol^{-1}, 0.73×10^4 g mol^{-1} and 1.38×10^4 g mol^{-1}, respectively. However, higher molecular weight stars **2.6 - 2.7** with M_n^{NMR} values of 3.24×10^4 g mol^{-1} and 4.61×10^4 g mol^{-1}, show poor agreement with M_n^{SEC} values of 2.65×10^4 g mol^{-1} and 2.45×10^4 g mol^{-1}, respectively. The greater discrepancy in values for the larger star structures **2.6** and **2.7** can be explained by the method used for SEC analyses. The M_n is determined by the polymer's hydrodynamic volume and calibrated with linear polystryrene standards. For larger stars, the observed M_n^{SEC} will be a lower value than expected (M_n^{NMR}) due to a denser polymer structure and hence different hydrodynamic volumes.[23]

Table 2.1: Molecular weight and dispersities for linear **2.2** and six-arm star **2.4** - **2.7**

Sample	Initiator	[a]$\overline{DP}_{Th}$	[b]$\overline{DP}_{NMR}$	[a]M_n^{Th}	[b]M_n^{NMR}	[c]M_n^{SEC}	[c]Đ
				$\times 10^{-4}$ g mol^{-1}			
2.2	Ethylene Glycol **2.1**	200	89	4.57	2.04	2.44	1.56
2.4	Dipentae-rythritol **2.3**	10	10	0.71	0.71	0.73	1.14
2.5		20	22	1.40	1.53	1.38	1.22
2.6		50	47	3.45	3.24	2.65	1.25
2.7		100	67	6.87	4.61	2.45	2.28

[a]Determined by the feed ratio; [b]Determined by ^{1}H NMR analyses; [c]Determined by SEC analyses

The thermal properties of PCL stars **2.4** - **2.7** were measured using DSC, Table 2.2. An example thermogram of **2.6** is shown in Appendix 2.1. There were no observable T_g in the DSC thermograms for linear **2.2** and star PCL **2.4** - **2.7**. In general, the T_m increased from 50 - 55 °C to 53 - 58 °C and the T_c also increased from 23 - 27 °C to 29 - 35 °C with an increase in M_n and $\overline{DP}$ of the arms from **2.4** - **2.7**, respectively.

Table 2.2: Thermal analyses of six-arm star **2.4 - 2.7** determined by DSC analysis

Sample	$\overline{DP}_{NMR}$	T_m	T_c	ΔH_c	χ_c
		°C		$J\ g^{-1}$	%
2.4	10	50 - 55	23 - 27	120	86
2.5	22	51 - 55	26 - 29	38	27
2.6	47	52 - 58	30 - 34	41	29
2.7	67	53 - 58	29 - 35	37	27

The degree of crystallinity ($\%\chi_c$) was calculated using the enthalpy of crystallisation (ΔH_c) measured by DSC, Table 2.2. A large decrease in $\%\chi_c$ from 86% to 27% was observed with an increase in M_n and $\overline{DP}$ of arm for stars **2.4 - 2.5**, respectively. However, for stars **2.5 - 2.7** the $\%\chi_c$ remained unchanged with a further increase in M_n and $\overline{DP}$ of arm. This can be explained by **2.4** having shorter PCL arms, imparting greater chain mobility and therefore, greater ability to arrange into a more crystalline structure thus increasing the $\%\chi_c$. On the other hand, the longer PCL arms in stars **2.5 - 2.7** have a greater tendency to become entangled increasing amorphous in character and therefore, decreasing the overall polymer $\%\chi_c$.

2.3.3 Four-arm Star PCL using Di(trimethylolpropane) Initiator 2.9 - 2.10

Four-arm star PCL was synthesised by the ROP of ε-CL with di(trimethylolpropane) **2.8** as initiator and catalysed by $SnOct_2$, to give **2.9** and **2.10**, Scheme 2.3. The ratio of ε-CL to di(trimethylolpropane) initiator was varied to give four-arm stars with a $\overline{DP}_{Th}$ of 10 and 20 per arm in **2.9** and **2.10**, respectively.

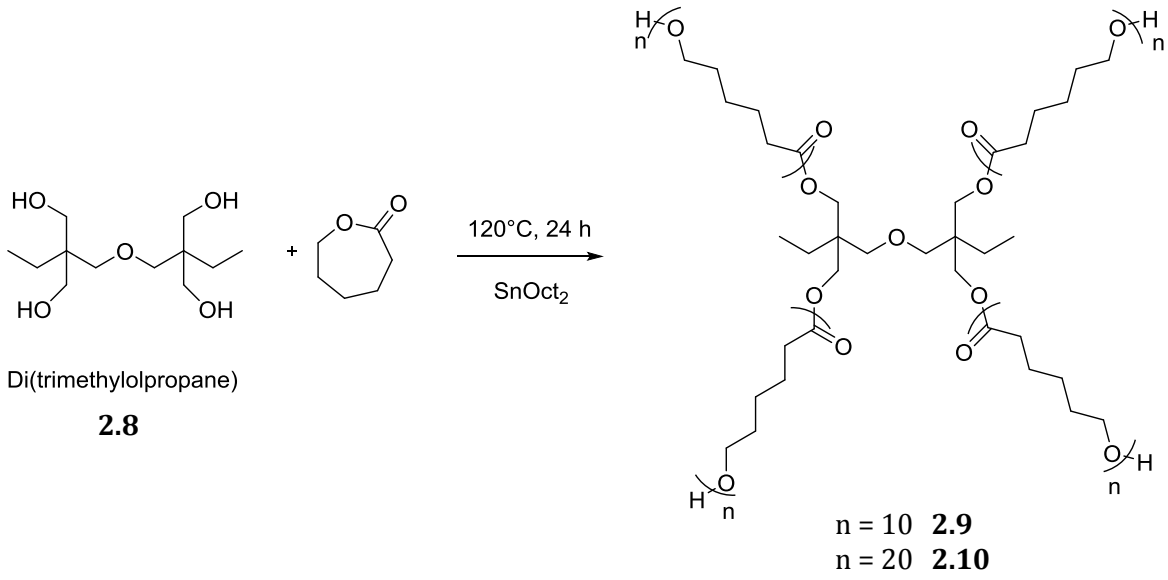

Scheme 2.3: Synthesis of four-arm star PCL **2.9 – 2.10** using di(trimethylolpropane) initiator **2.8**

The characteristic methylene protons in PCL can be seen in the ^{1}H NMR spectrum of **2.9**, Figure 2.13, at 1.31 ppm, 1.58 ppm, 2.24 ppm and 3.99 ppm for protons **i**, **h/j**, **g** and **k**, respectively. The $\overline{DP}_{NMR}$ was determined using Equation 2.1 with resonances of methylene protons **a** in the central di(trimethylolpropane) moiety at 3.19 ppm, and methylene protons **g** in the PCL repeat unit at 2.24 ppm. The $\overline{DP}_{NMR}$ of **2.9** and **2.10** was found to be 12 and 25, which are in good agreement with the $\overline{DP}_{Th}$ of 10 and 20, respectively, Table 2.3.

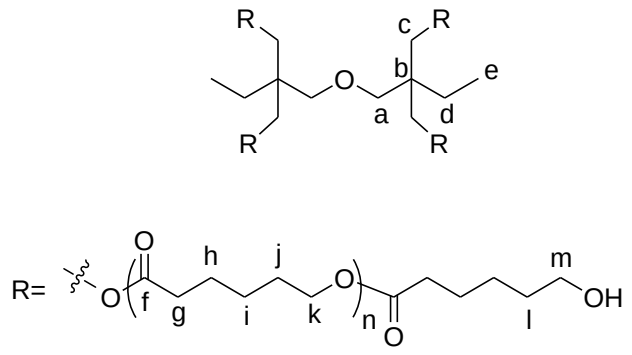

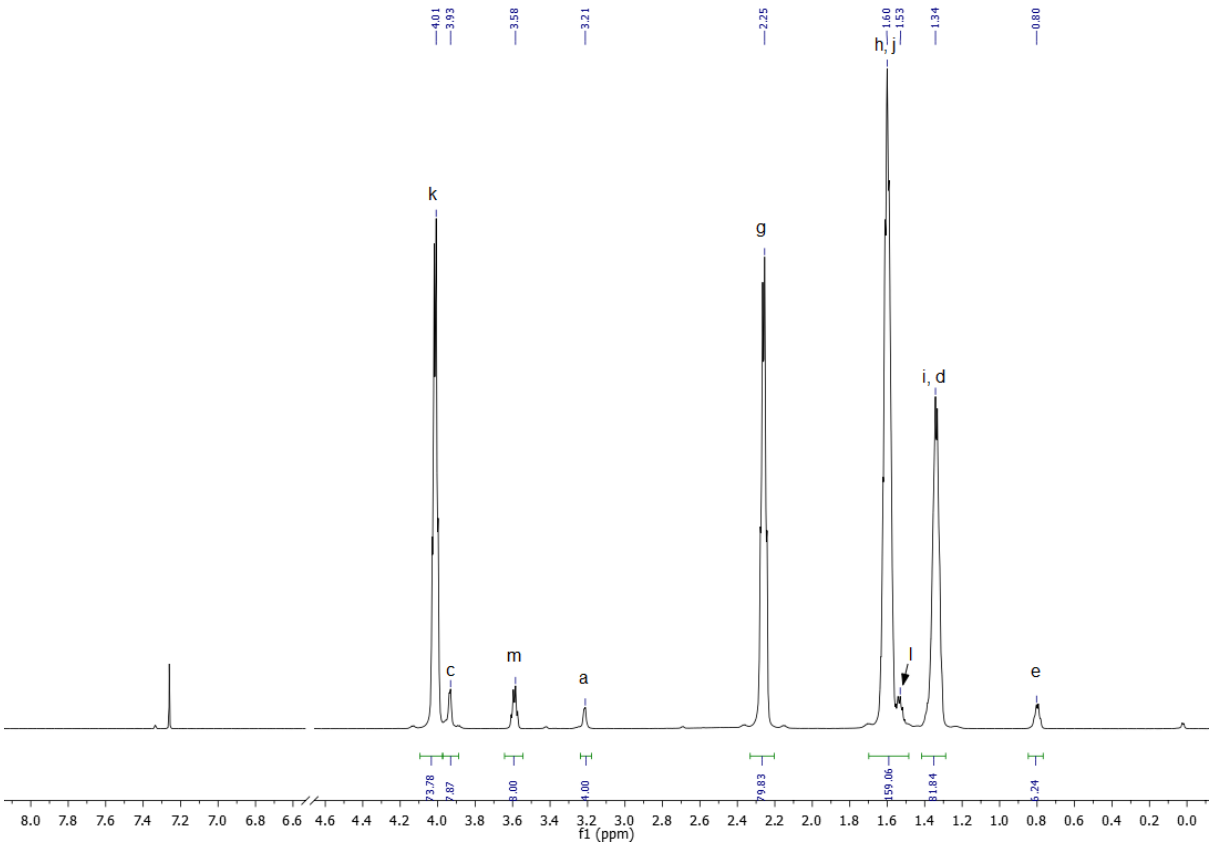

Figure 2.13: 600 MHz ^{1}H NMR spectrum of **2.9** in $CDCl_3$

Resonances at 3.19 ppm, 3.97 ppm, 1.31 ppm and 0.77 ppm are attributed to methylene protons **a**, **c**, **d** and methyl protons **e** in the central di(trimethylolpropane) moiety, respectively. The resonances attributing to methylene protons **l** and **m** in PCL protons neighbouring the OH group can be seen at 1.58 ppm and 3.58 ppm, respectively. Furthermore, resonance **m** at 3.58 ppm integrates to 8H, indicating ROP has occurred from all four OH initiating sites on the central di(trimethylolpropane) moiety.

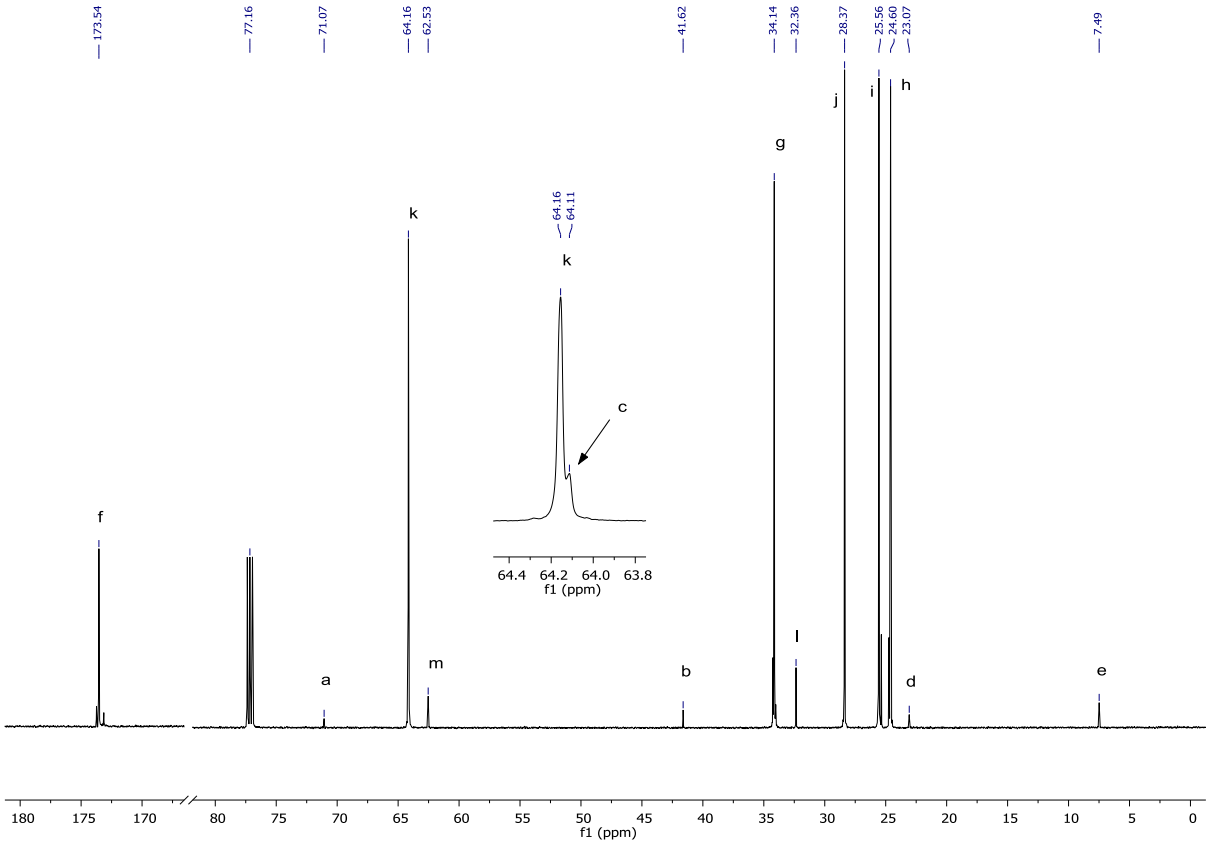

Figure 2.14: 150 MHz ^{13}C spectrum of **2.9** in $CDCl_3$

The characteristic carbon atom resonances of PCL at 24.6 ppm, 25.6 ppm, 28.4 ppm and 64.2 ppm are attributed to **h**, **i**, **j**, **g** and **k**, respectively, Figure 2.14. The downfield resonance at 173.7 ppm is attributed to carbonyl carbon atom **f**. Furthermore, resonances at 32.4 ppm and 62.5 ppm are attributed to methylene carbon atoms **l** and **m** in PCL neighbouring the OH group, respectively. The ^{1}H – ^{13}C HSQC spectra, Figure 2.15 and Figure 2.16, confirms this assignment, showing proton resonances at 1.58 ppm and 3.58 ppm attributed to **l** and **m**, correlate to carbon atom resonances at 32.4 ppm and 62.5 ppm attributed to **l** and **m**, respectively. Moreover, the ^{1}H – ^{13}C HMBC spectrum, Figure 2.17, shows proton resonance **m** at 3.58 ppm correlating to neighbouring carbon atom resonances **i** and **l** at 25.6 ppm and 32.4 ppm, respectively.

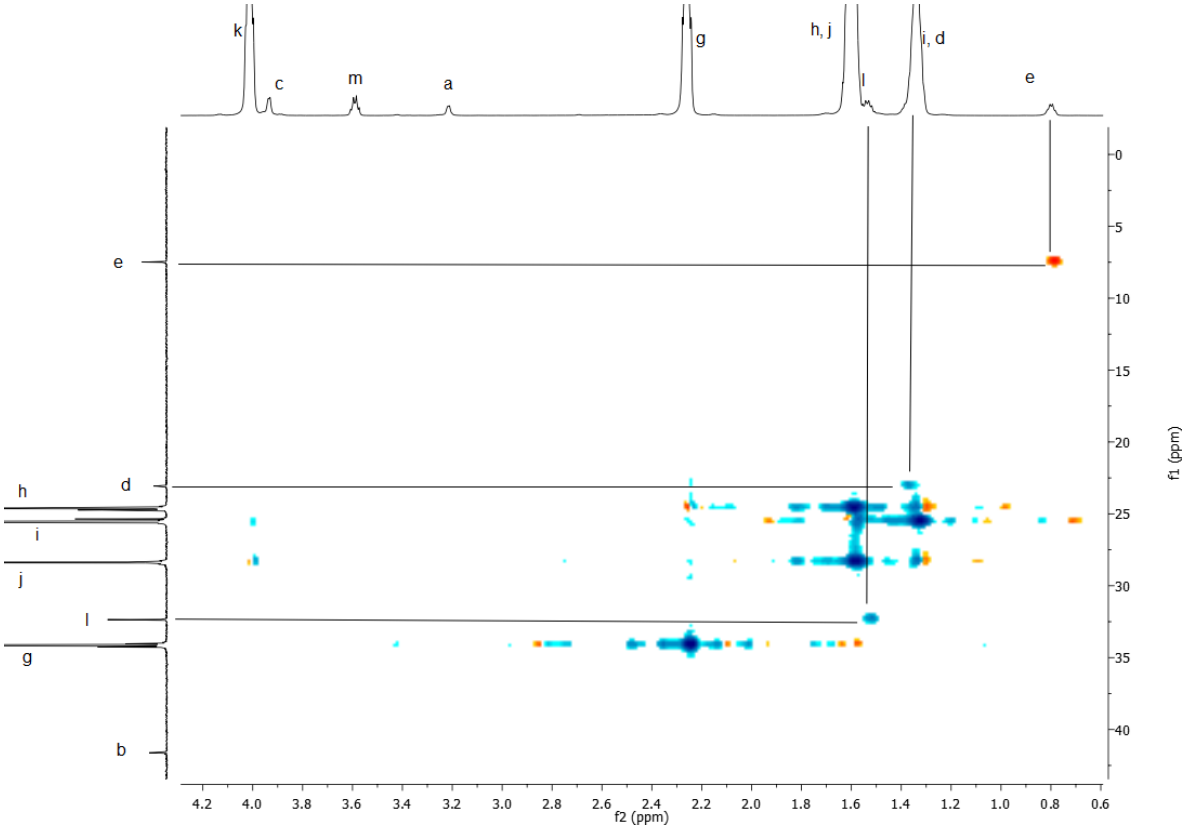

Figure 2.15: ^{1}H - ^{13}C HSQC spectrum of **2.9** in $CDCl_3$

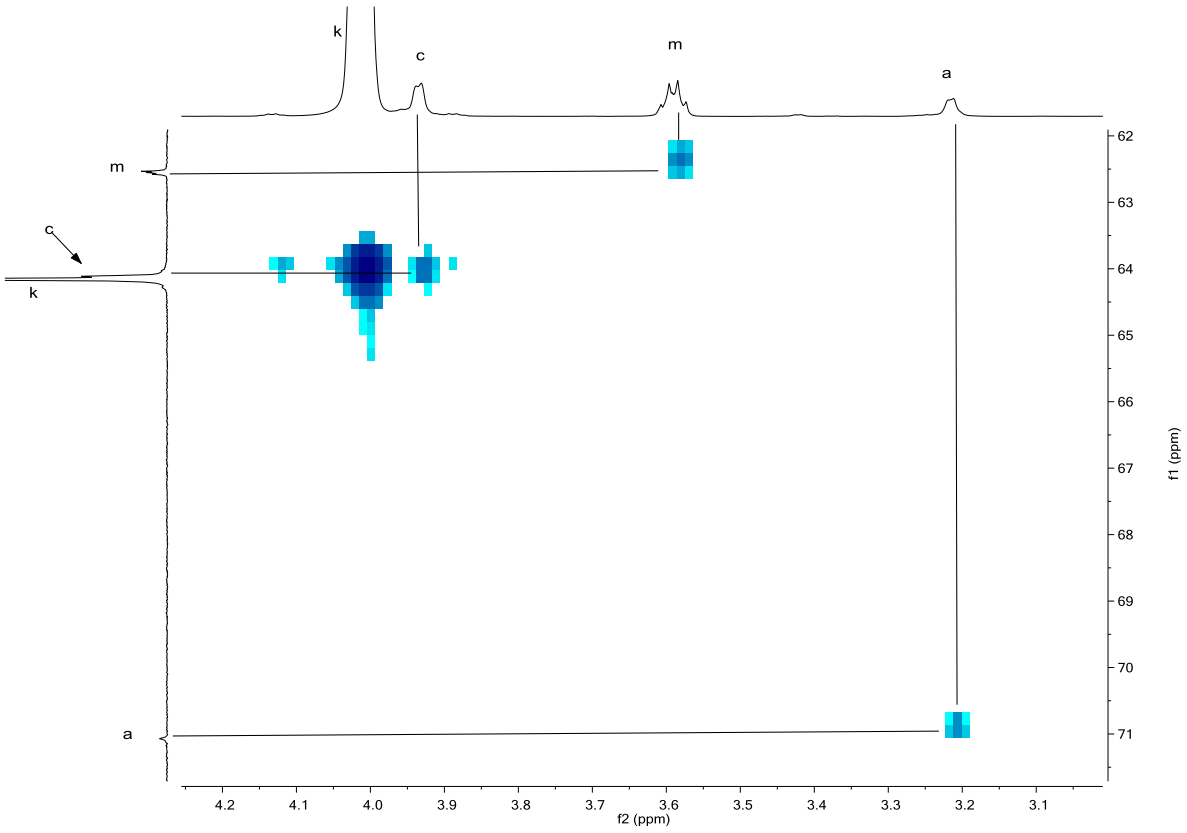

Figure 2.16: ^{1}H - ^{13}C HSQC spectrum of **2.9** in $CDCl_3$

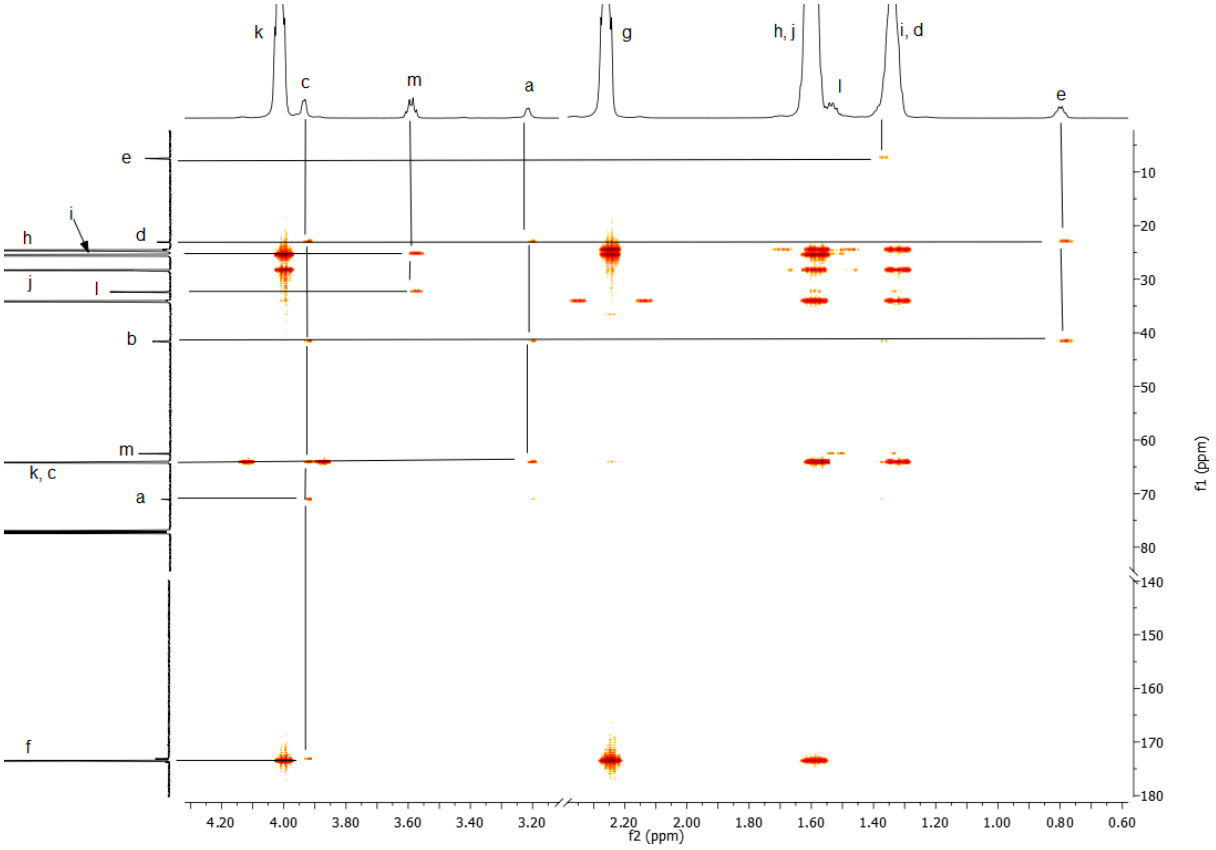

Figure 2.17: ^{1}H - ^{13}C HMBC spectrum of **2.9** in $CDCl_3$

The resonances at 71.1 ppm, 41.6 ppm, 64.1 ppm, 23.1 ppm and 7.5 ppm, correlate to carbon atoms located on the central di(trimethylolpropane) moiety **a**, **b**, **c**, **d** and **e**, respectively. The ^{1}H – ^{13}C HSQC spectrum for **2.9**, Figure 2.15, confirms the correlation between proton resonances **d** and **e** at 1.31 ppm and 0.77 ppm, with carbon atom resonances **d** and **e** at 23.1 ppm and 7.5 ppm, respectively. Moreover, ^{1}H – ^{13}C HSQC shows quaternary carbon atom **b** at 41.6 ppm correlates with no proton resonances. However, the ^{1}H – ^{13}C HMBC spectrum of **2.9**, Figure 2.17, shows quaternary carbon atom **b** correlating to neighbouring proton resonances **c**, **a** and **e** at 3.97 ppm, 3.19 ppm and 0.77 ppm, respectively. The downfield ^{1}H – ^{13}C HSQC spectrum of **2.9**, Figure 2.16, shows the central di(trimethylolpropane) proton resonances **a** and **c** at 3.19 ppm and 3.97 ppm correlating to carbon atom resonances **a** and **c**, at 71.1 ppm and 64.1 ppm, respectively.

2.3.4 Four-arm Star PCL 2.12 using Pentaerythritol Initiator

Four-arm star PCL was synthesised in the ROP reaction of ε-CL using pentaerythritol **2.11** initiator to give **2.12**, Scheme 2.4. A ratio of ε-CL to pentaerythritol of 40:1 was used to give four-arm star **2.12**, with a $\overline{DP}_{Th}$ of 10 per arm.

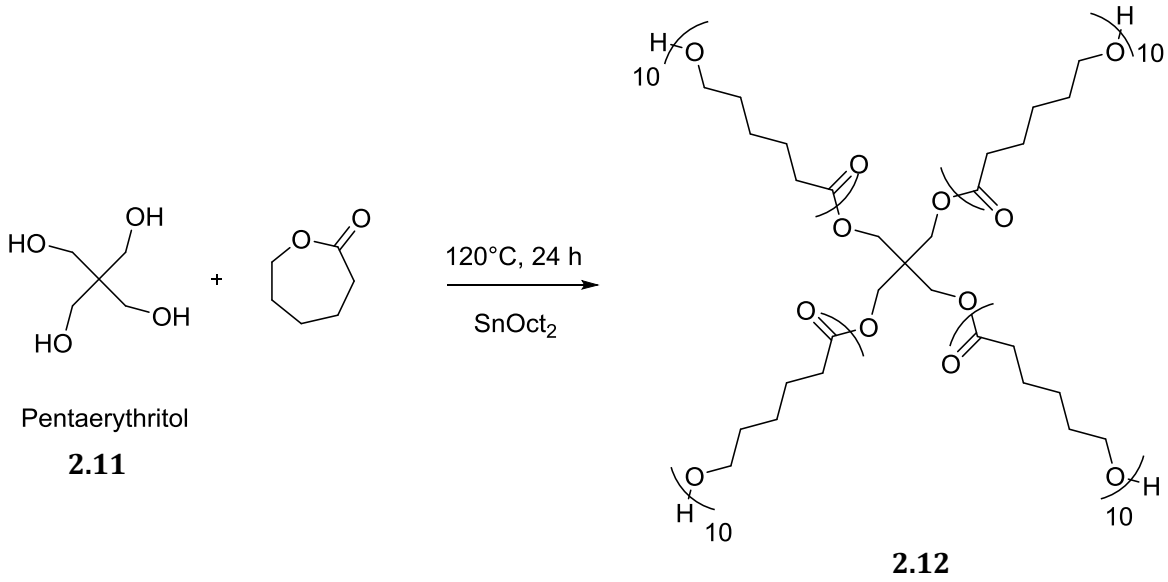

Scheme 2.4: Synthesis of four-arm star PCL **2.12** using pentaerythritol initiator

The ^{1}H NMR spectrum of **2.12**, Figure 2.18, shows the characteristic methylene proton resonances in PCL at 1.37 ppm, 1.64 ppm, 2.30 ppm and 4.05 ppm for protons **f**, **e**/**g**, **d** and **h**, respectively. Methylene protons **i** and **j** in PCL neighbouring the OH group, are attributed to resonances 1.64 ppm and 3.64 ppm, respectively. Furthermore, the resonance at 4.10 ppm is attributed to methylene protons **b** on the central pentaerythritol moiety. The $\overline{DP}_{NMR}$ could not be determined using the integral of proton resonance **b** at 4.05 ppm located on the pentaerythritol moiety, due to overlapping resonances with methylene protons **h** on the PCL moiety. Therefore, $\overline{DP}_{NMR}$ was estimated by Equation 2.1 using the resonances of methylene protons **j** in PCL neighbouring the OH group at 3.64 ppm, and methylene protons **d** in the PCL repeat unit at 2.30 ppm. It is assumed that the ROP of ε-CL has occurred from all four OH initiating sites on the pentaerythritol moiety. The $\overline{DP}_{NMR}$ of **2.12** was found to be 11, which is in good agreement with $\overline{DP}_{Th}$ of 10.

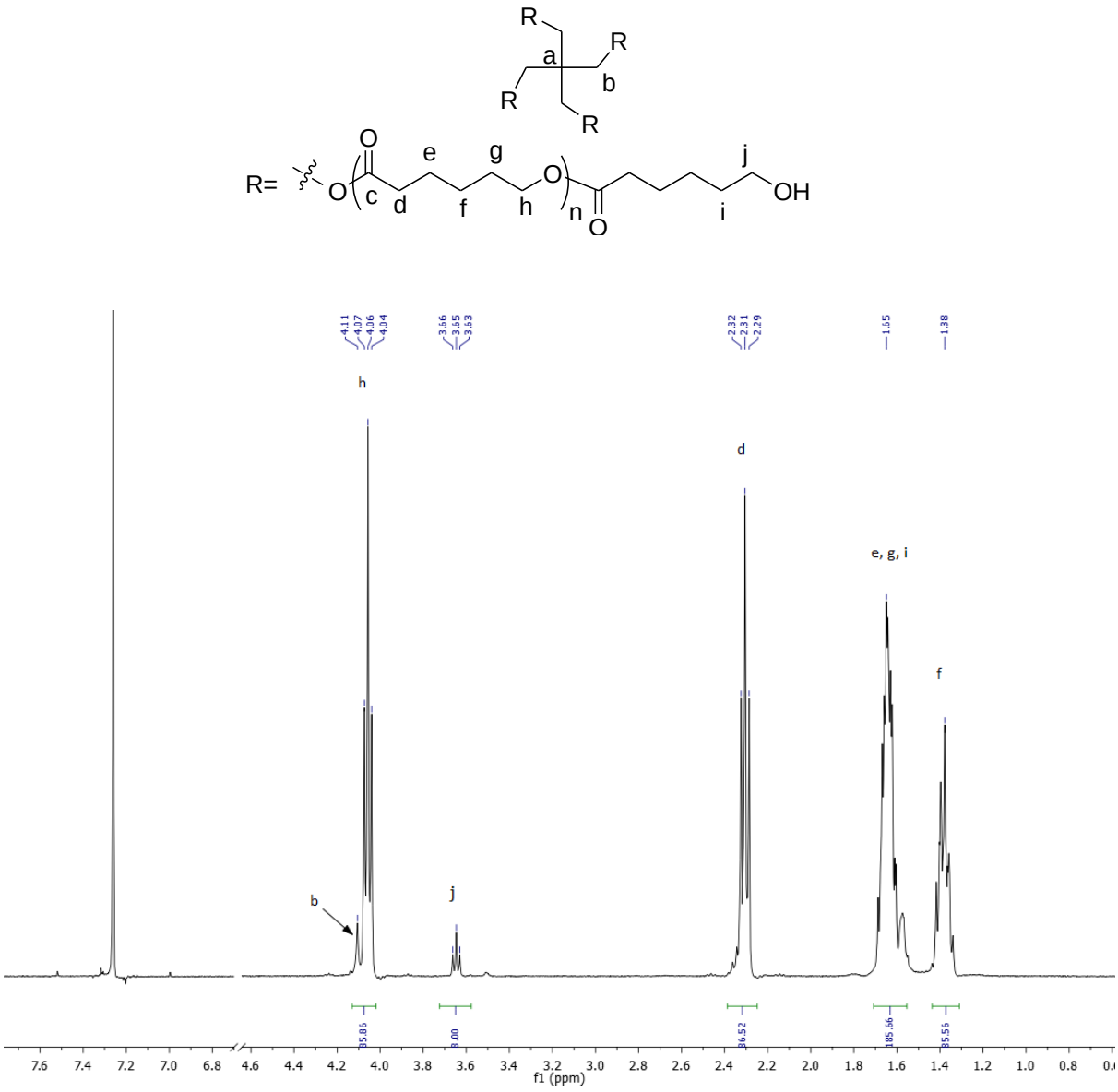

Figure 2.18: 400 MHz ^{1}H NMR spectrum of **2.12** in $CDCl_3$

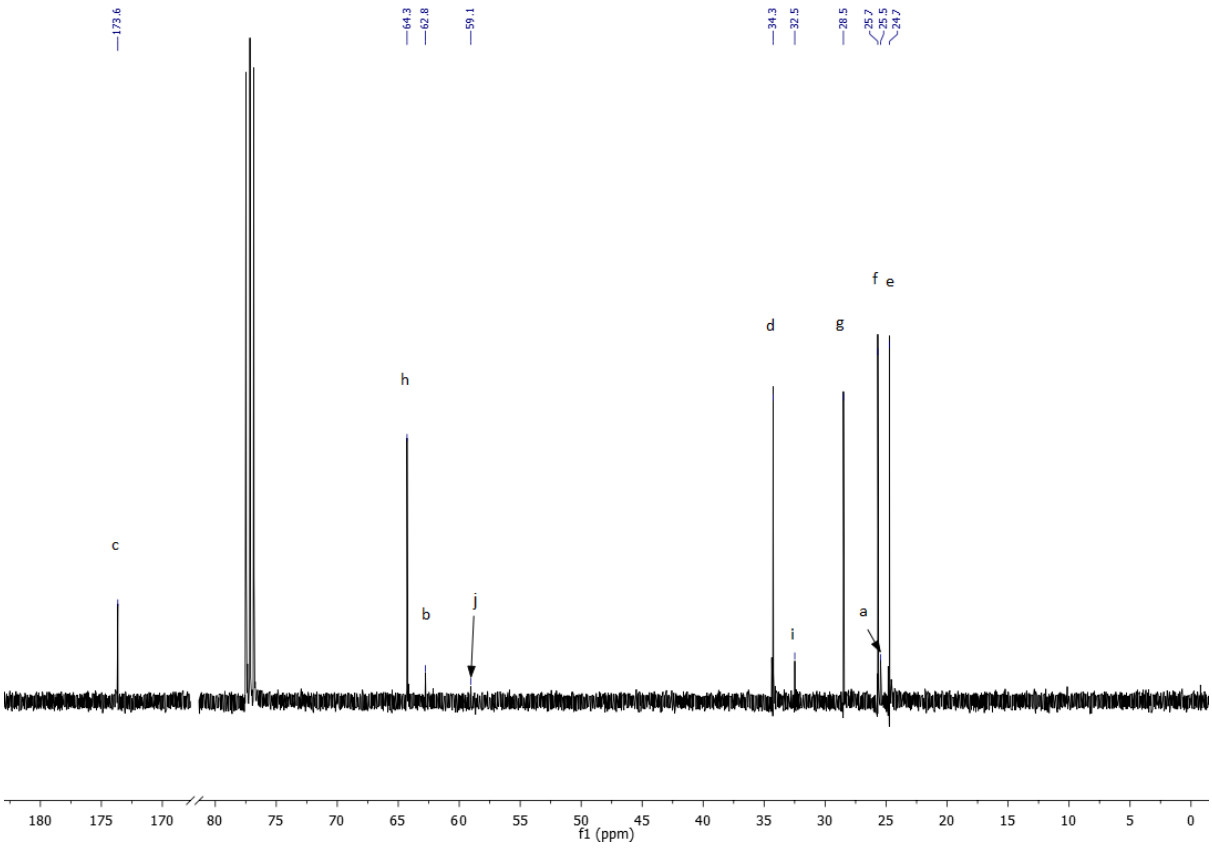

Figure 2.19: 100 MHz ^{13}C NMR spectrum of **2.12** in $CDCl_3$

The characteristic carbon atom resonances of PCL can be seen at 24.7 ppm, 25.7 ppm, 28.5 ppm, 34.3 ppm and 64.3 ppm, attributing to **e**, **f**, **g**, **d** and **h**, respectively, Figure 2.19. The downfield resonance at 173.6 ppm is attributed to carbonyl carbon atom **c** in PCL. Methylene carbon atoms **i** and **j** in PCL neighbouring the OH group, can be seen at resonances 32.5 ppm and 59.1 ppm, respectively. Furthermore, resonances at 25.5 ppm and 62.8 ppm are attributed to quaternary carbon atom **a** and methylene carbon atom **b**, on the central pentaerythritol moiety, respectively.

The M_n^{Th} for four-arm stars **2.9 - 2.10** and **2.12** are in good agreement with the calculated M_n^{NMR} and M_n^{SEC}, Table 2.3. As expected, an increase in Đ is seen with an increase in the $\overline{DP}$, from 1.05 to 1.20 and $\overline{DP}_{NMR}$ of 12 to 25, from four-arm stars **2.9** to **2.10** respectively.

Table 2.3: Molecular weights and average arm length of **2.2**, **2.9- 2.10** and **2.12** determined by ^{1}H NMR and SEC analyses

Sample	Initiator	$^{a}\overline{DP}_{Th}$	$^{b}\overline{DP}_{NMR}$	$^{a}M_n^{Th}$	$^{b}M_n^{NMR}$	$^{c}M_n^{SEC}$	$^{c}Đ$
				$\times 10^{-4}$ / g mol^{-1}			
2.2	Ethylene Glycol	200	57	4.57	1.31	2.44	1.56
2.9	Di(trimethylol propane)	10	12	0.47	0.56	0.58	1.05
2.10		20	25	0.93	1.15	1.04	1.20
2.12	Pentaerythritol	10	11	0.47	0.52	0.58	1.10

^{a}Determined by feed ratio; ^{b}Determined by ^{1}H NMR ; ^{c}Determined by SEC

2.3.5 Linear Poly[(ε-CL)-*co*-(β-BL)] using Ethylene glycol Initiator 2.13

Linear poly[(ε-CL)-*co*-(β-BL)] **2.13** was synthesised *via* ROP of ε-CL and β-BL monomers using ethylene glycol **2.1** initiator and catalysed by $SnOct_2$, Scheme 2.5. A ratio of ethylene glycol : ε-CL : β-BL of 1 : 14 : 6 was used to produce linear random copolymer **2.13** with a $\overline{DP}_{Th}$ of 10 per arm, consisting of 7 ε-CL units and 3 β-BL units.

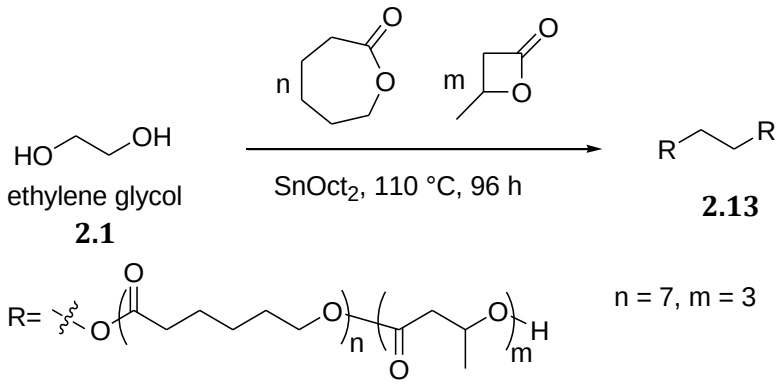

Scheme 2.5: Synthesis of linear poly[(ε-CL)-*co*-(β-BL)] **2.13** using ethylene glycol initiator **2.1**

The ^{1}H NMR spectrum for **2.13**, Figure 2.20, shows the resonances attributing to protons in the PCL repeat unit at 1.32 ppm, 1.59 ppm, 2.25 ppm and 4.00 ppm for methylene protons **e**, **d**/**f**, **c** and **g**, respectively. Resonances attributing to the β-BL repeat unit are seen at 1.22 ppm, 2.39-2.57 ppm and 5.20 ppm for methyl protons **k**, methylene protons **i** and methine protons **j**, respectively. The triplet at 4.23 ppm is attributed to the methylene protons neighbouring the ester group on the central ethylene moiety. This indicates successful ROP of either ε-CL or β-BL from the ethylene glycol initiating unit. Methylene protons **l** and **p** in PCL, neighbouring the OH group can be seen at 1.59 ppm and 3.57 ppm, respectively. Methyl protons **s** of the chain-end group in PBL near to the OH group are attributed to the resonance at 1.18 ppm. This suggests both PCL and PBL repeat units are located at the chain ends of **2.13**.

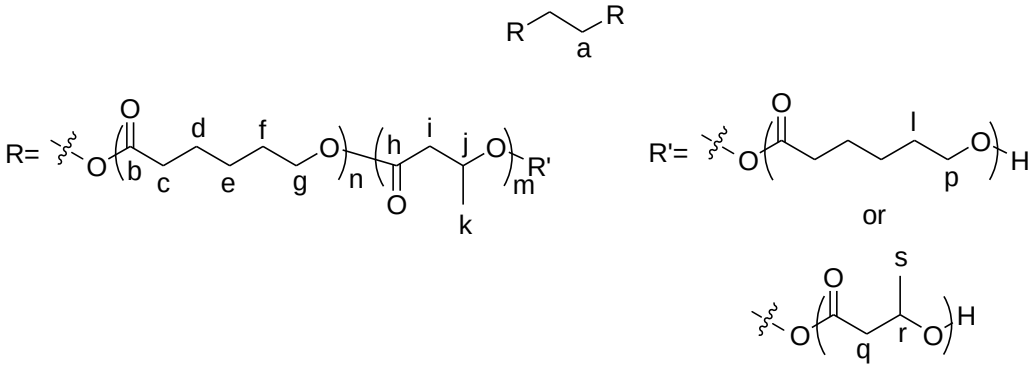

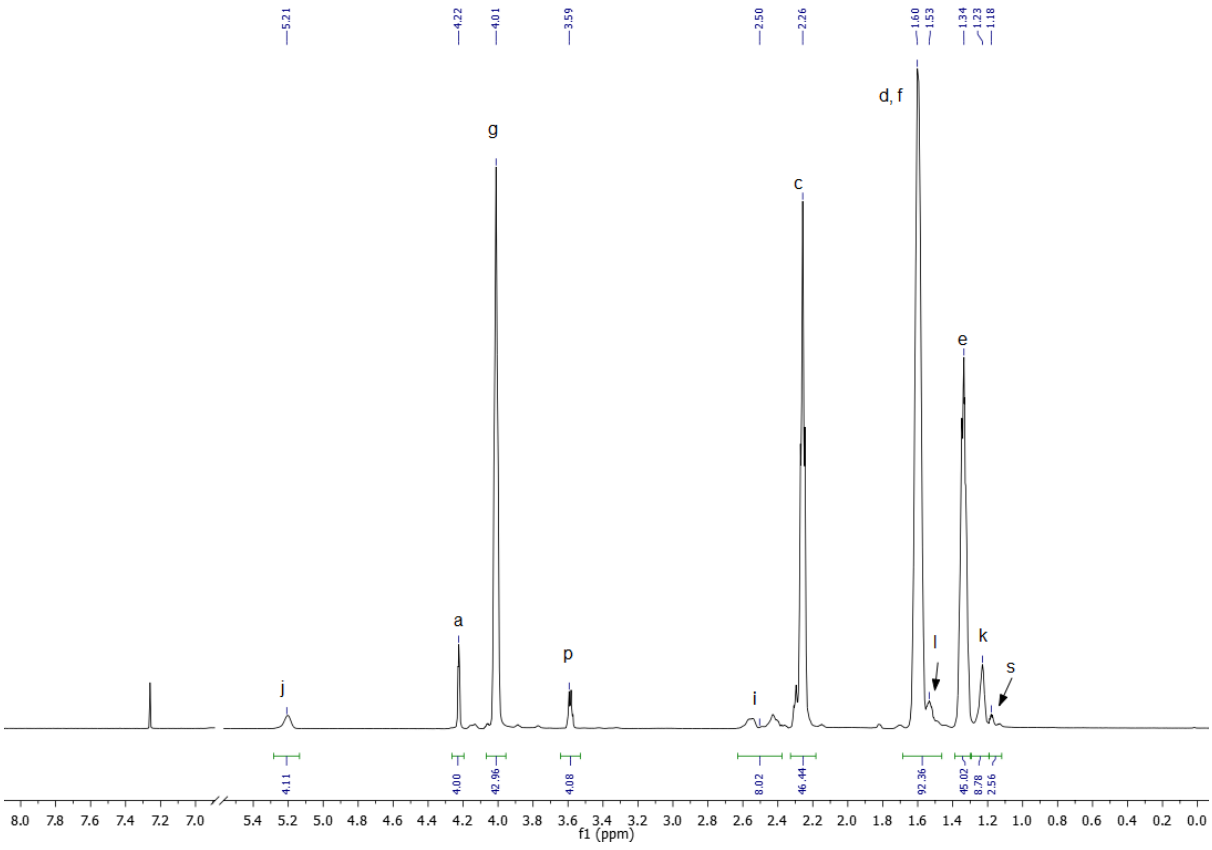

Figure 2.20: 600 MHz ^{1}H NMR spectrum of **2.13** in $CDCl_3$

The ^{13}C NMR spectrum of **2.13**, Figure 2.21, shows a resonance at 62.0 ppm that is attributed to methylene carbon atom **a** on the central ethylene moiety. The resonances corresponding to the methylene carbon atoms in the PCL repeat units at 24.5 ppm, 35.5 ppm, 28.3 ppm, 34.1 ppm and 64.1 ppm are attributed to **d**, **e**, **f**, **c** and **g**, respectively. Carbonyl carbon atom **b** on the PCL repeat unit is attributed to the resonance at 173.5 ppm. Methylene carbon atoms **l** and **p** on the PCL unit neighbouring the OH group, are attributed to resonances 32.3 ppm and 67.6 ppm, respectively. The carbon atom resonances in the PBL repeat unit at 19.8 ppm, 40.8 ppm 67.6 ppm and 169.1 ppm are attributed to **k**, **i**, **j** and **h**, respectively. A shift is seen for the resonances attributing to the PBL unit located at the polymer chain end for **s**, **q** and **r** at 22.5 ppm, 42.8 ppm and 67.2 ppm, respectively.

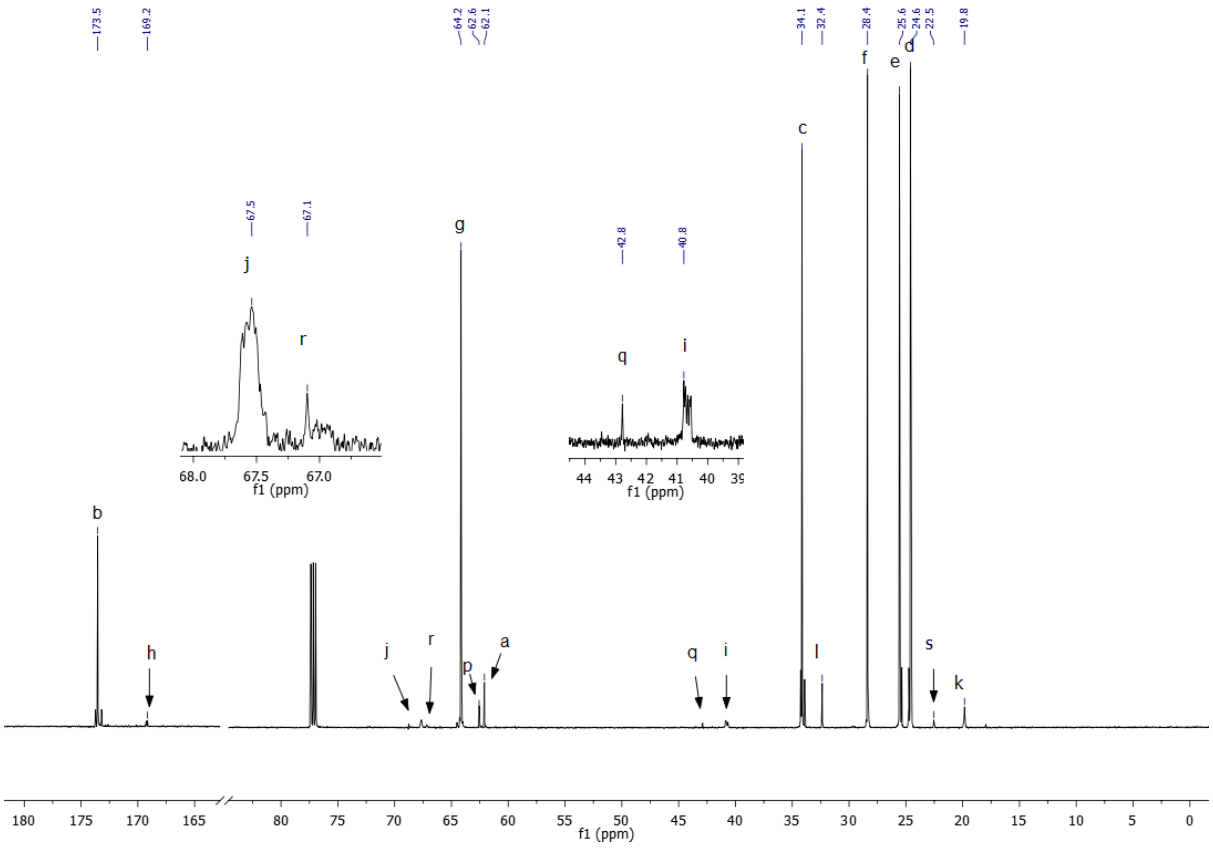

Figure 2.21: 150 MHz ^{13}C NMR spectrum of **2.13** in $CDCl_3$

2.3.6 Six-arm Star Poly[(ε-CL)-*co*-(β-BL)] using Dipentaerythritol Initiator 2.14 – 2.16

Six-arm star poly[(ε-CL)-*co*-(β-BL)] **2.14 - 2.16** were synthesised in a similar ROP reaction of ε-CL and β-BL, using dipentaerythritol **2.3** initiator and catalysed by $SnOct_2$, Scheme 2.6. The ratios of ε-CL : β-BL : dipentaerythritol were varied at 42:18:1, 48:12:1 and 54:6:1 to produce random six-arm star copolymers with 7 ε-CL and 3 β-BL units per arm, 8 ε-CL and 2 β-BL units per arm, and 9 ε-CL and 1 β-BL unit per arm, in **2.14**, **2.15** and **2.16**, respectively.

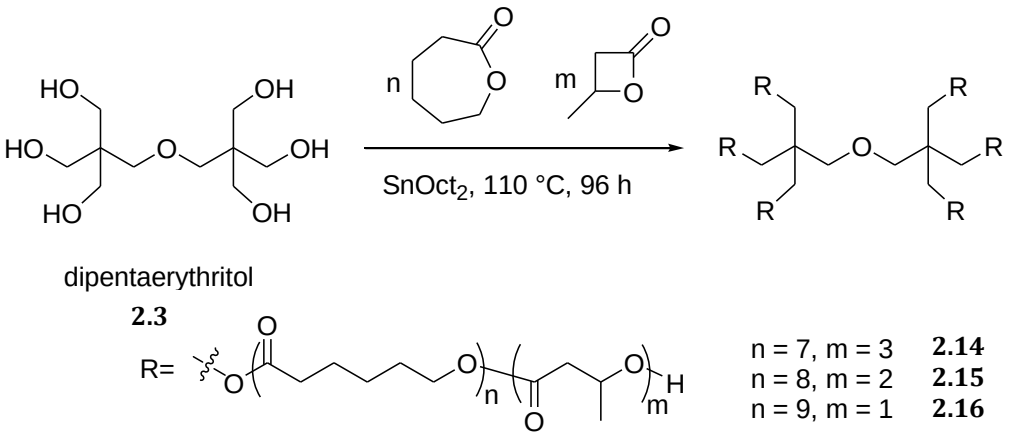

Scheme 2.6: Synthesis of six-arm star poly[(ε-CL)-*co*-(β-BL)] **2.14 - 2.16** using dipentaerythritol **2.3**

The ^{1}H NMR spectrum of **2.14**, Figure 2.22, shows resonances corresponding to methylene protons in the PCL repeat unit at 1.33 ppm, 1.60 ppm, 2.26 ppm and 4.01 ppm are attributed to **g**, **f/h/q**, **e** and **i**, respectively. The resonances at 1.23 ppm, 2.41-2.60 ppm and 5.22 ppm are attributed to methyl protons **p**, methylene protons **k** and methine protons **l** in the PBL repeat unit, respectively. The resonances at 3.34 ppm and 4.01 ppm correspond to methylene protons **a** and **c** on the central dipentaerythritol moiety, respectively. The resonances for the PBL chain-end unit at 1.16 ppm, 2.38 ppm and 5.25 ppm correspond to methyl protons **v**, methylene protons **t** and methine proton **u**, respectively. Furthermore, the resonances at 1.60 ppm and 3.57 ppm are attributed to methylene protons **q** and **r** on the PCL chain end moiety, neighbouring the OH group, respectively. This indicates both the PBL and PCL repeat units are found at the polymer chain ends.

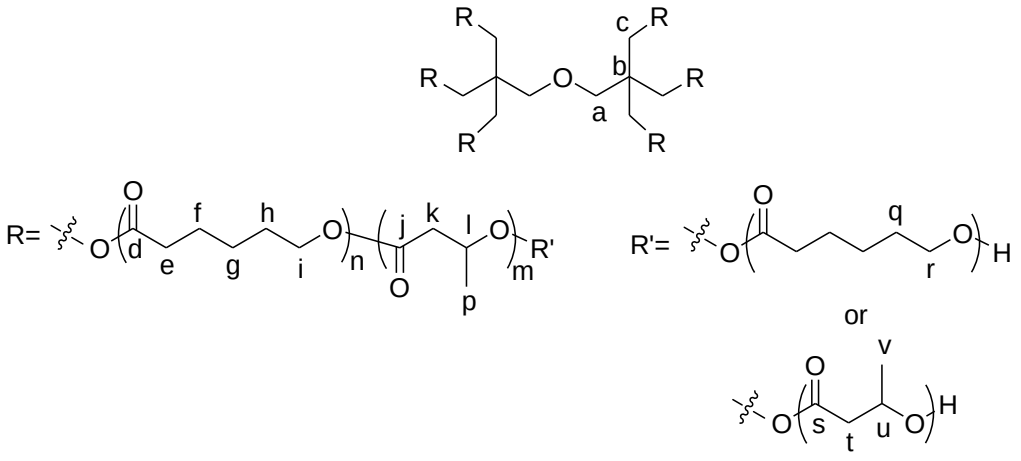

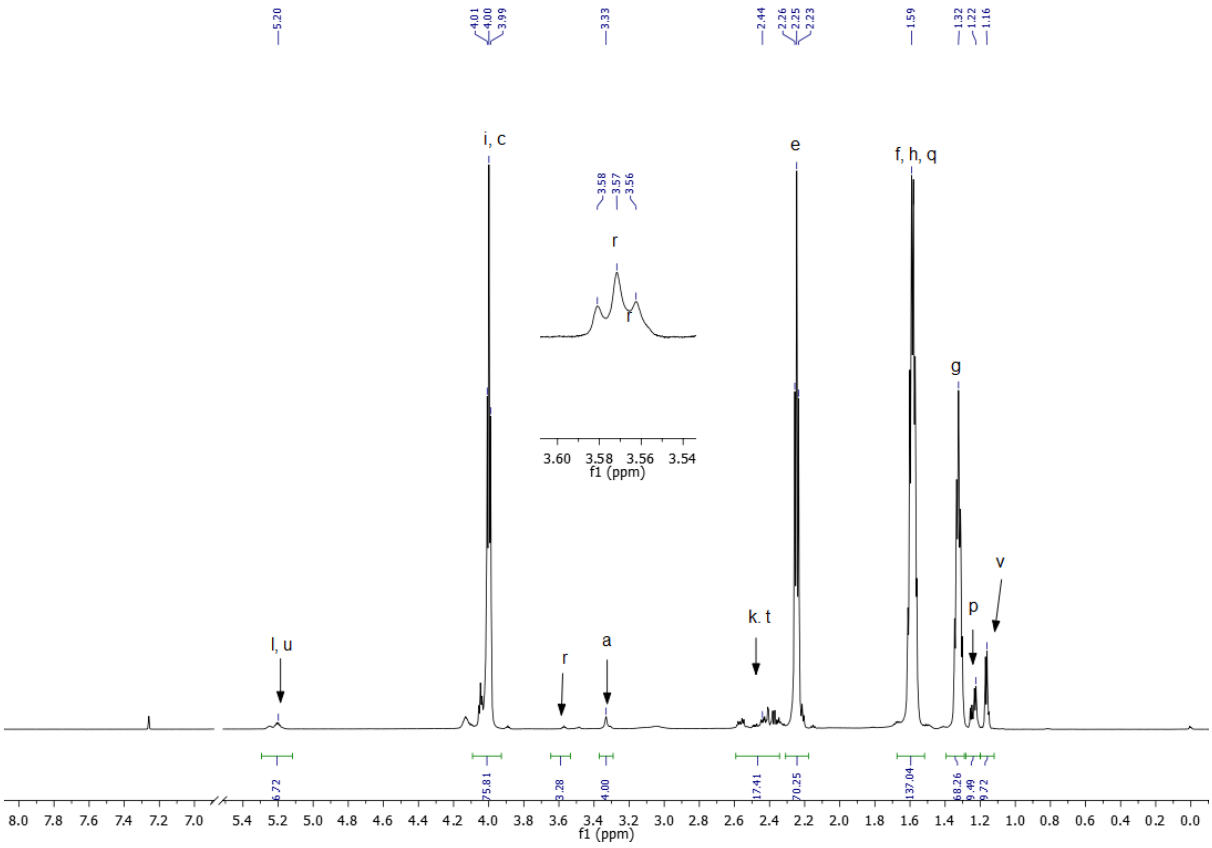

Figure 2.22: 600 MHz ^{1}H NMR spectrum of **2.14** in $CDCl_3$

The ^{13}C NMR spectrum for **2.14**, Figure 2.23, shows characteristic carbon atom resonances for PCL at 24.6 ppm, 25.5 ppm, 28.3 ppm, 34.0 ppm and 64.0 ppm that correspond to **f**, **g**, **h**, **e** and **i,** respectively. The downfield resonance at 173.5 ppm is attributed to the carbonyl carbon atom **d** on the PCL repeat unit. Central dipentaerythritol carbon atom resonances **a**, **b** and **c** are seen at 71.1 ppm, 41.6 ppm and 64.1 ppm, respectively. Furthermore, the ^{1}H – ^{13}C HSQC spectrum, Figure 2.24, confirms this assignment, as methylene protons **a** and **c** at 3.34 ppm and 4.01 ppm correlate to carbon atom resonances at 71.1 ppm and 64.1 ppm, respectively. Moreover, quaternary carbon atom **b** at 41.6 ppm on the central dipentaerythritol moiety shows no correlation to any proton resonances. Further confirmation can be seen in the ^{1}H – ^{13}C HMBC spectrum, Figure 2.25, showing protons **a** at 3.34 ppm correlating to neighbouring carbon atom resonances **b** and **c**, at 41.6 ppm and 71.1 ppm, respectively. Moreover, protons **c** at 4.01 ppm are correlated to neighbouring carbon atoms **b**, **a** and **d**, at 41.6 ppm, 71.1 ppm and 173.5 ppm, respectively. The proximity of methylene carbon atom **c** on the central

dipentaerythritol moiety to carbonyl carbon atom **d** on the PCL moiety confirms the successful ROP of ε-CL from the initiating OH groups on the dipentaerythritol moiety.

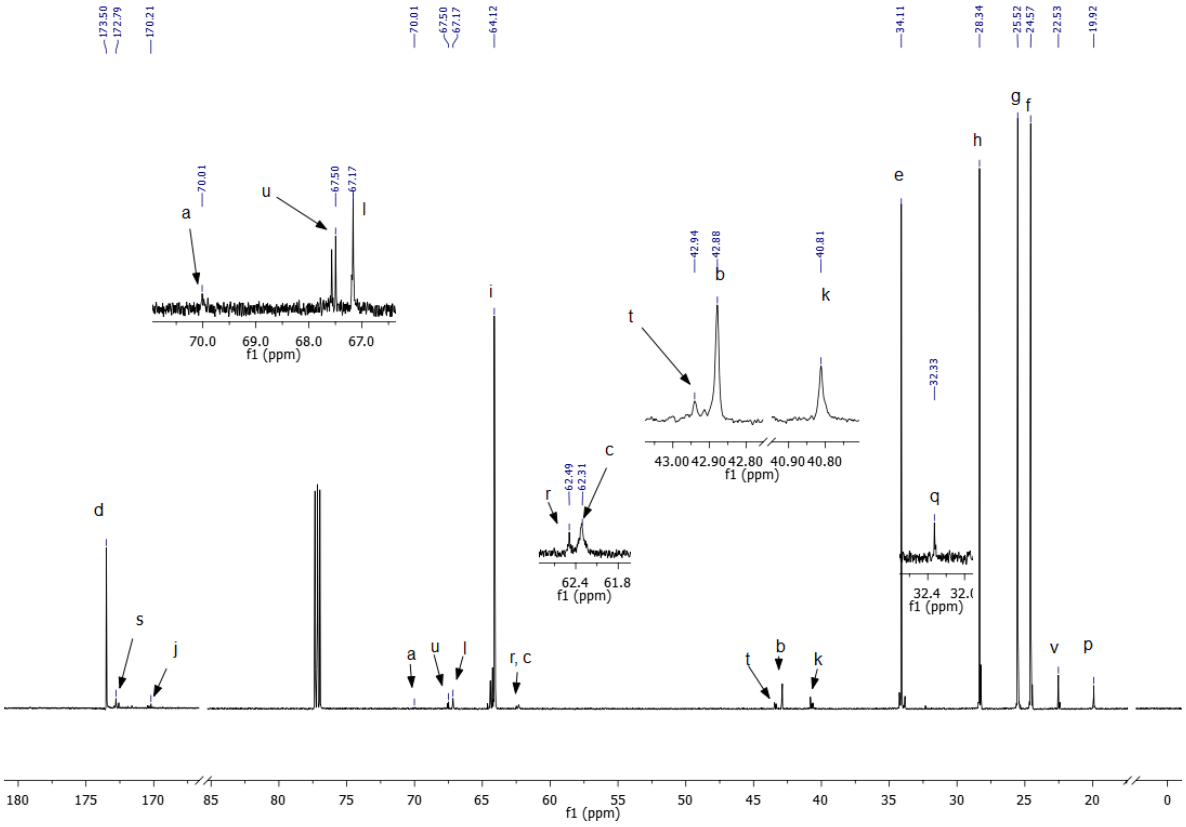

Figure 2.23: 150 MHz ^{13}C NMR spectrum of **2.14** in $CDCl_3$

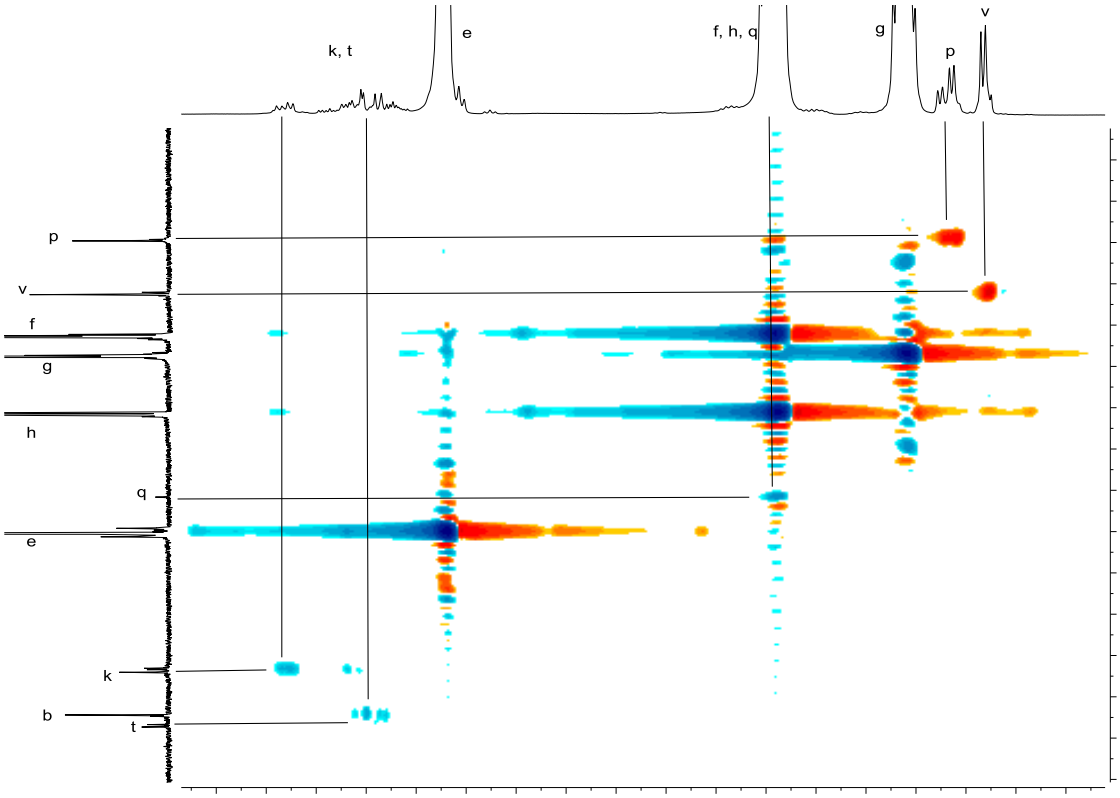

Figure 2.24: ^{1}H - ^{13}C HSQC spectrum of **2.14** in $CDCl_3$

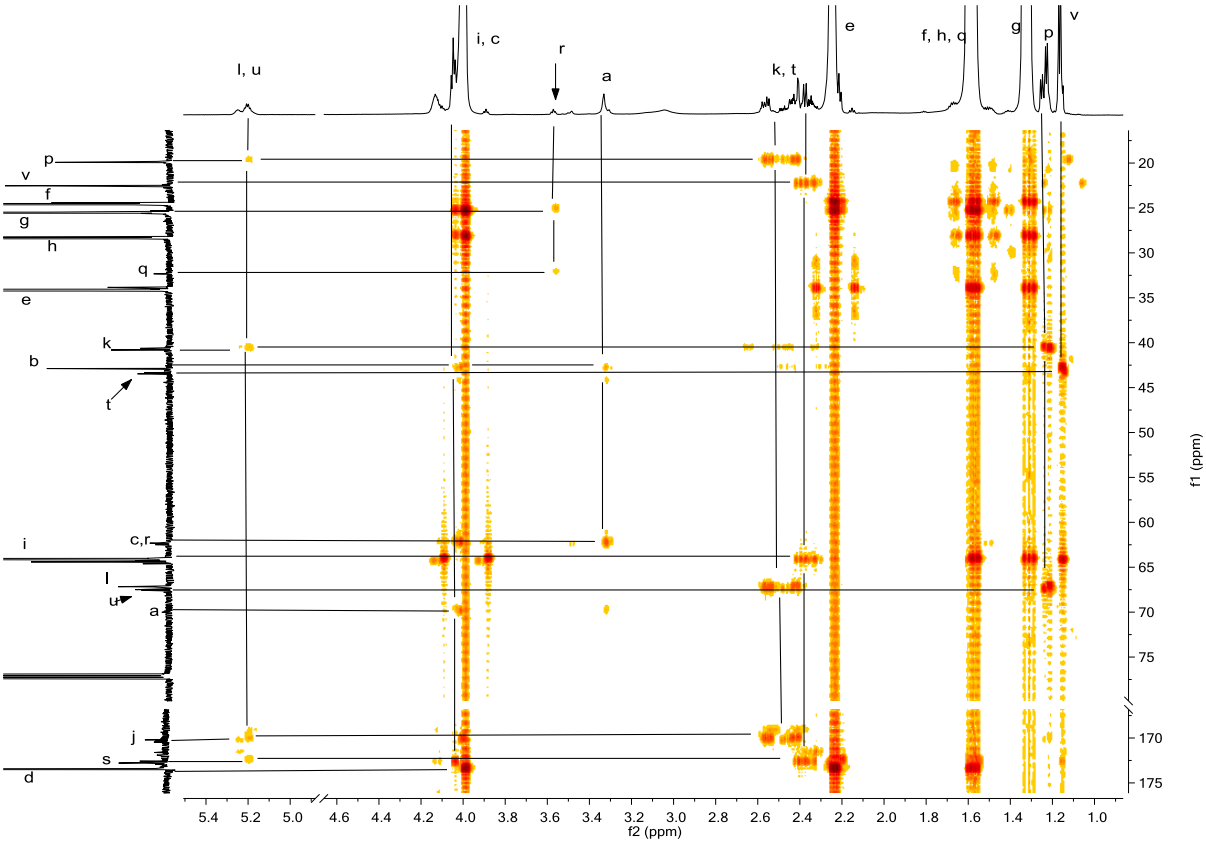

Figure 2.25: ^{1}H - ^{13}C HMBC spectrum of **2.14** in $CDCl_3$

Resonances at 22.5 ppm, 40.8 ppm, 67.2 ppm and 170.2 ppm correspond to methyl carbon atom **p**, methylene carbon atom **k**, methine carbon atom **l** and carbonyl carbon atom **j**, on the PBL moiety, respectively. These assignments are confirmed in the ^{1}H – ^{13}C HMBC spectrum, Figure 2.25, showing protons **p** at 1.23 ppm correlating to neighbouring carbon atom resonances **k** and **l** at 40.8 ppm and 67.2 ppm, respectively. Furthermore, protons **k** at 2.41-2.60 ppm correlate to neighbouring carbon atom resonances **p**, **l** and **j** at 22.5 ppm, 67.2 ppm and 170.2 ppm, respectively. Moreover, protons **l** at 5.22 ppm correlate to neighbouring carbon atom resonances **p**, **k** and **j** at 22.5 ppm, 40.8 ppm and 170.2 ppm, respectively.

The ^{13}C NMR spectrum of **2.14**, Figure 2.23, shows resonances for carbon atoms in the PBL chain-end unit at 19.9 ppm, 42.9 ppm, 67.5 ppm and 172.8 ppm, corresponding to **v**, **t**, **u** and **s**, respectively. These assignments are confirmed in the ^{1}H – ^{13}C HSQC spectrum, Figure 2.24, showing the correlation between protons **v** and **t** at 1.16 ppm and 2.38 ppm, and carbon atoms **v** and **t** at 19.9 ppm and 67.5 ppm, respectively. Furthermore, the downfield ^{1}H – ^{13}C HSQC spectrum of **2.14**, Figure 2.26, shows the correlation between protons **u** at 5.25 ppm and carbon atom **u**, at 67.5 ppm.

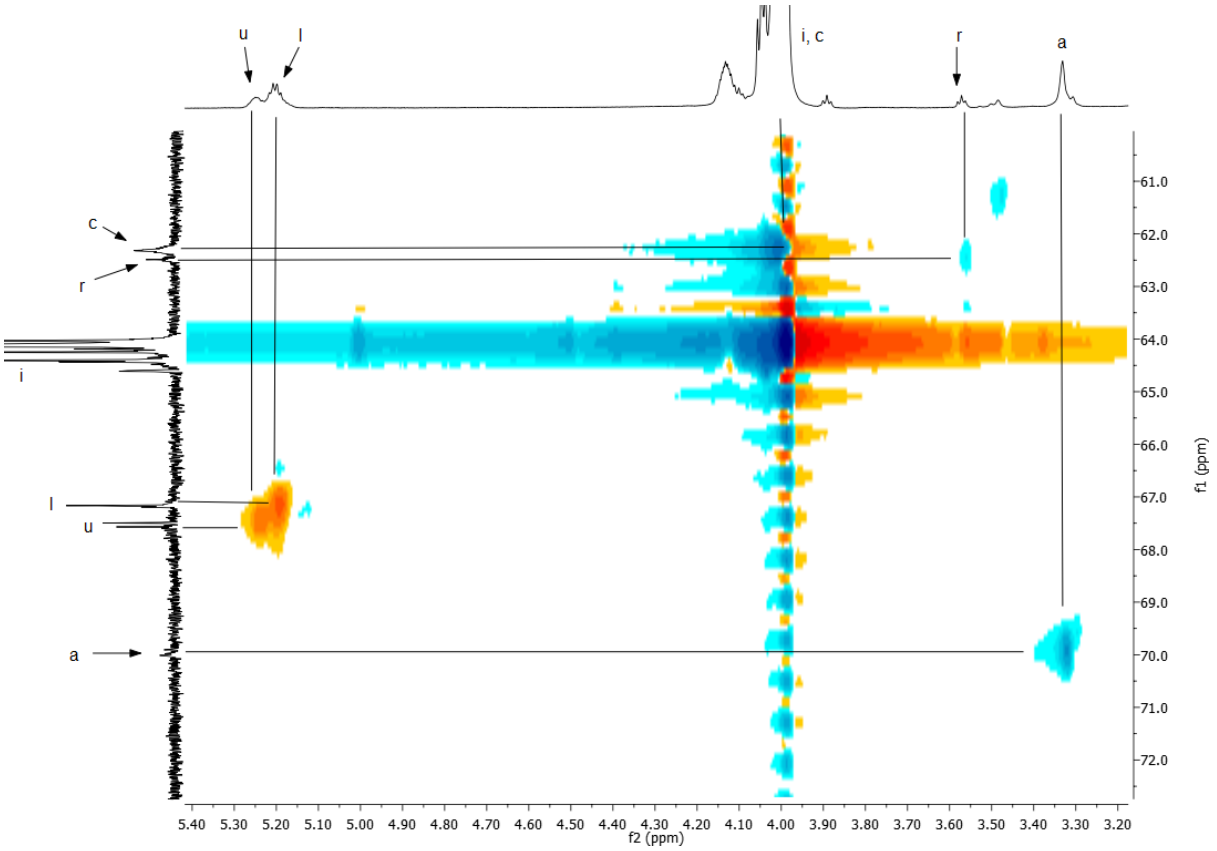

Figure 2.26: ^{1}H - ^{13}C HSQC spectrum of **2.14** in $CDCl_3$

The resonances attributed to methylene carbon atoms **q** and **r** in the PCL neighbouring the OH group, are seen at 32.3 ppm and 62.5 ppm, respectively, Figure 2.23. These assignments are confirmed in the ^{1}H – ^{13}C HSQC spectra, Figure 2.24 and Figure 2.26, showing protons **q** and **r** at 1.60 ppm and 3.57 ppm are correlated to carbon atoms **q** and **r** at 32.3 ppm and 62.5 ppm, respectively. Furthermore, the ^{1}H – ^{13}C HMBC spectrum, Figure 2.25, shows protons **r** at 3.57 ppm correlate to neighbouring carbon atoms **g** and **q**, attributed to resonances 1.33 ppm and 32.3 ppm, respectively.

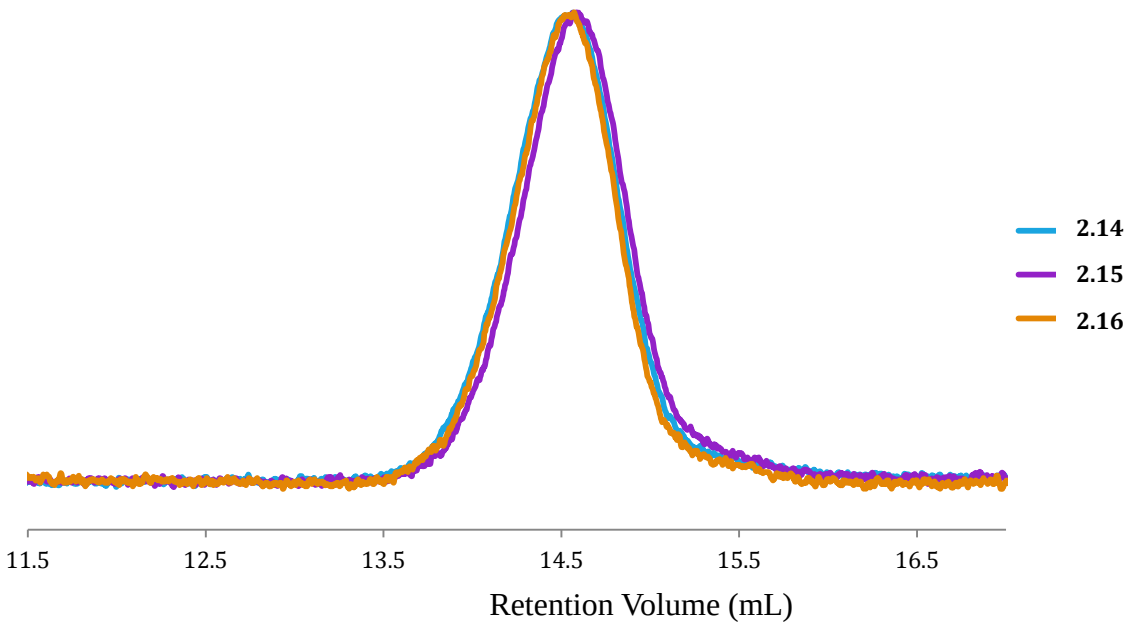

Figure 2.27: SEC chromatograms of normalised RI *vs* retention volume for **2.14 - 2.16**

It can be seen from the normalised SEC chromatograms for six-arm star copolymers **2.14 - 2.16**, Figure 2.27, with a $\overline{DP}$ of 10 per arm, show good correlation in both M_n^{SEC} and Đ, indicating good control in the ROP. Interestingly, the β-BL content in the product ratio for linear copolymer **2.13** and star copolymers **2.14 - 2.16** were much lower than in the feed ratio, Table 2.4. The product ratios were determined by ^{1}H NMR analyses of the copolymers after three precipitations, and showing no change in the ^{1}H NMR proton integrals. It should be noted that the filtrate collected after the first precipitation, generally showed oligomers of PCL and PBL with a higher β-BL content than that incorporated into the copolymer products **2.3 - 2.16**.

Table 2.4: Molecular weights and dispersities of **2.13 - 2.16** determined by ^{1}H NMR and SEC analyses

Sample	Initiator	ε-CL:β-BL Initial Feed Ratio	ε-CL:β-BL Product Ratio†	M_n^{Th}	M_n^{NMR}	M_n^{SEC}	Đ
				$\times 10^{-4}$ / g mol^{-1}			
2.13	Ethylene Glycol **2.1**	70:30	91:9	0.22	0.23	0.46	1.17
2.14	Dipentaerythritol **2.3**	70:30	93:7	0.66	0.86	0.83	1.14
2.15		80:20	94:6	0.68	0.70	0.73	1.20
2.16		90:10	96:4	0.69	0.70	0.84	1.15

†Determined by ^{1}H NMR

The thermal properties and $\%\chi_c$ of six-arm star poly[(ε-CL)-*co*-(β-BL)] **2.14 - 2.16** were determined by DSC, Table 2.5. As a comparison, linear PCL **2.2** and linear poly[(ε-CL)-*co*-(β-BL)] **2.13**, have also been included in Table 2.5. It can be seen that the incorporation of β-BL into the star PCL structure had a profound effect on the $\%\chi_c$ of the polymer. Linear PCL homopolymer **2.2** exhibits a $\%\chi_c$ of 71%, whereas all copolymers **2.13 - 2.16** exhibit a significantly lower $\%\chi_c$ ranging from 20-47%. The decrease in $\%\chi_c$ of a random copolymer of β-BL and ε-CL, compared to PCL homopolymer, has been reported by Li *et al.*[24]

Table 2.5: Thermal analysis data and $\%\chi_c$ for **2.2** and **2.13 - 2.16**, determined by DSC analyses at 10 °C min^{-1}

Sample	Initiator	% β-BL content†	T_m	T_c	ΔH_c	χ_c
			°C		$J\ g^{-1}$	%
2.2	Ethylene glycol **2.1**	0	55 - 57	32 - 38	100	71
2.13		9	45 - 51	25 - 31	35	25
2.14	Dipentaerythritol **2.3**	7	42 - 46	12 - 18	27	20
2.15		6	47 - 51	19 - 26	54	38
2.16		4	48 - 51	21 - 25	66	47

† Determined by ^1H NMR analyses

It can be seen that the T_m generally increases from 42 - 46 °C to 48 - 51 °C with decreasing β-BL content from 7% to 4% in star copolymers **2.14** to **2.16**, Table 2.5. Furthermore, the T_c increases with decreasing β-BL content from 12 - 18 °C to 21 - 25 °C in star copolymers **2.14** to **2.16**. The large increase in $\%\chi_c$ from 20% to 47% seen in star copolymers **2.14 - 2.16**, with a relatively small decrease in β-BL content from 7% to 4%**,** show that a small amount of β-BL incorporation significantly decreases the overall $\%\chi_c$ of PCL. Linear copolymer **2.13** with 9% β-BL exhibits a higher $\%\chi_c$ of 25% than that of star copolymer **2.14** at 20%, as well as a higher T_m, 45 - 51 °C and 42 - 46 °C, and a higher T_c, 25 - 31 °C and 12 - 18 °C, respectively. This suggests the linear structure has greater chain mobility and therefore, the linear polymer chains have a greater ability to arrange themselves into a regular crystal structure, compared to a star structure, thus increasing $\%\chi_c$.

2.3.7 Enzymatic Degradation

Linear PCL **2.2** with a $\overline{DP}_{NMR}$ of 89 per arm, six-arm star PCL **2.7** with a $\overline{DP}_{NMR}$ of 67 per arm, and six-arm star copolymer **2.14** with a $\overline{DP}_{NMR}$ of 10 per arm, were subjected to enzymatic degradation using *pseudomonas cepacia* lipase. Due to the brittle nature of films made from PCL homopolymer, the lower molecular weight samples **2.4 - 2.6** could not be used in the enzymatic degradation analyses. However, six-arm star copolymer **2.14** with a $\overline{DP}_{NMR}$ of 10 per arm, each containing 7 ε-CL and 3 β-BL repeat units, was more amorphous in character and remained intact when removed from the heat press mould, unlike star copolymers **2.15 - 2.16**.

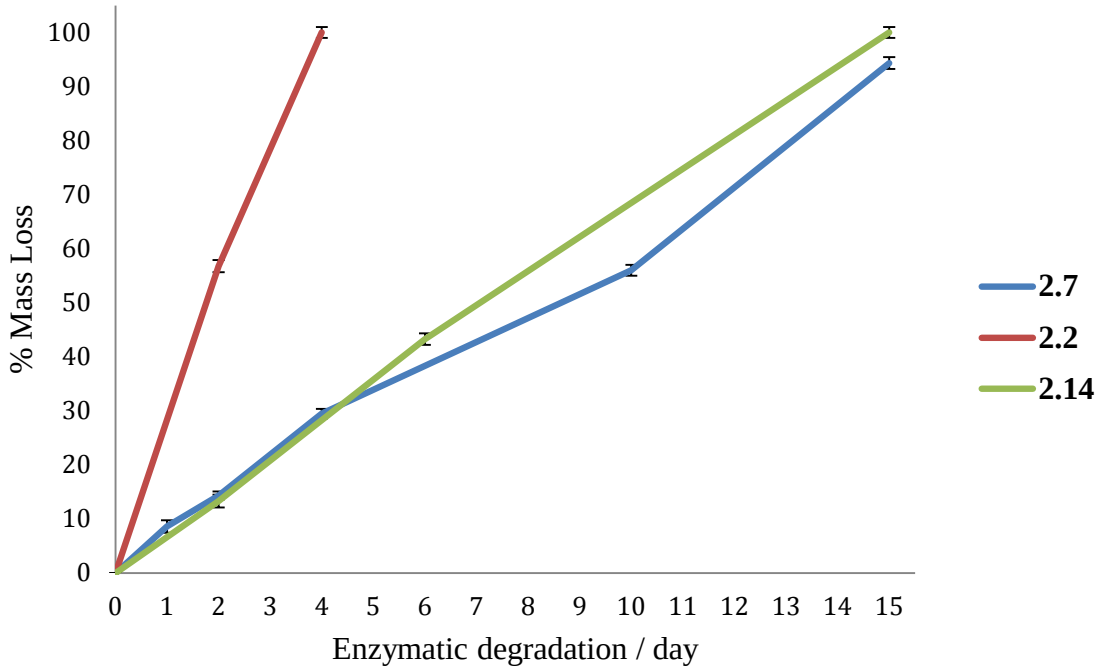

Figure 2.28: % Mass losses of **2.2**, **2.7** and **2.14** over 15 days of enzymatic degradation using *pseudomonas cepacia* lipase in PBS solution (pH 7.4). Each % mass loss is an average of 3 repeat experiments with error bars shown.

The rate of enzymatic degradation was determined by the mass loss of the polymer film over a period of 15 days. The mass loss of **2.2**, **2.7** and **2.14** expressed as a fraction (%) of the initial mass, as a function of time (days) is shown in Figure 2.28. A control was used whereby a polymer film of **2.2** was placed in PBS solution (pH 7.4) under the same conditions, in the absence of *pseudomonas cepacia* lipase. The polymer film showed negligible mass loss during the 15 day period, suggesting any mass loss was solely due to enzymatic degradation. Similar results have been reported in the literature, indicating that

PCL film samples showed negligible mass loss with no visible changes to the film surface after incubating the samples in PBS solution at 37 °C for several weeks.[5]

Figure 2.28 shows that polymers **2.2**, **2.7** and **2.14** exhibit a relatively linear progression in the rate of enzymatic degradation. This could indicate that enzymatic degradation using *pseudomonas cepacia* lipase takes place predominantly *via* a polymer surface erosion mechanism. Linear PCL **2.2** shows complete degradation (100% mass loss) after just 4 days of enzymatic degradation. However, six-arm star PCL **2.7** shows a slower degradation rate, reaching >94% mass loss after 15 days of enzymatic degradation. Similarly, star copolymer **2.14** showed 100% mass loss after 15 days of enzymatic degradation. The decrease in degradation rate from linear **2.2** (100% mass loss in 4 days) to stars **2.7** and **2.14** (>94% mass loss in 15 days) could be due to increased entanglement and decreased mobility of polymer chains, attributed to their star structures.

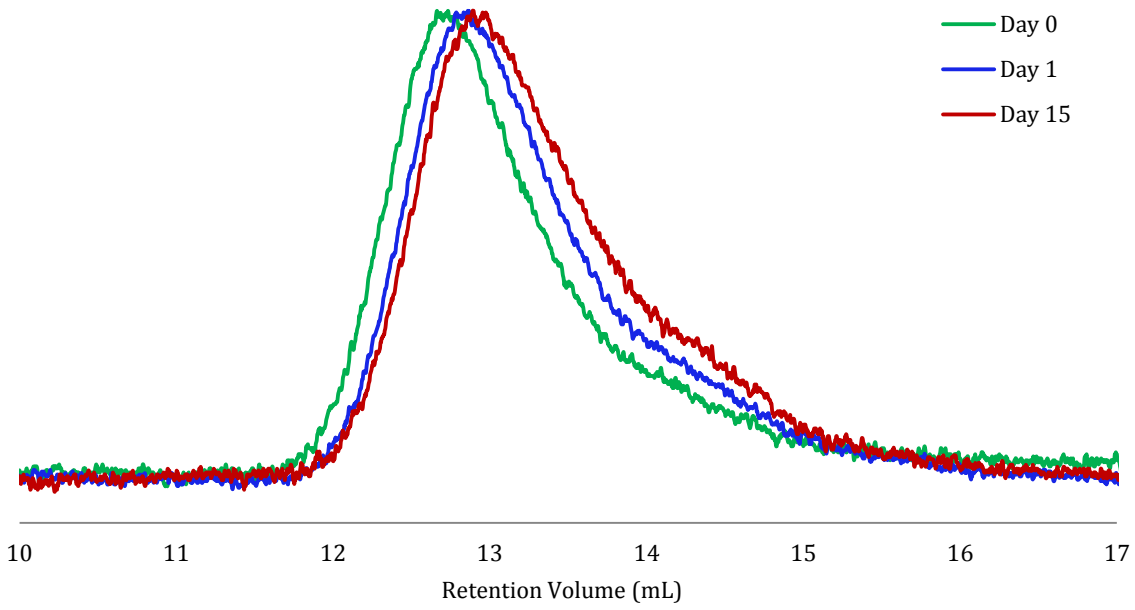

Figure 2.29: Normalised SEC chromatograms of star PCL **2.7** on day 0, 1 and 15 of enzymatic degradation using *pseudomonas cepacia* lipase in PBS solution (pH 7.4)

The normalised SEC chromatograms for star PCL **2.7** after 0, 1 and 15 days of enzymatic degradation using *pseudomonas cepacia* lipase are shown in Figure 2.29. It should be

noted that the SEC chromatograms for **2.7** after 2, 4 and 10 days of degradation have been omitted for clarity, as there was minimal change in M_n^{SEC} between days 1 to 15. A small decrease in M_p^{SEC} is seen from 6.73×10^4 g mol^{-1} to 5.84×10^4 g mol^{-1} from day 0 to day 15, respectively, indicating enzymatic degradation of the PCL arms. Furthermore, an increase in Đ is seen from day 0 to day 1 of 2.27 to 2.42, followed by a decrease in Đ from day 1 to day 15 of 2.42 to 1.86, respectively, Table 2.6. The initial increase in Đ could indicate random cleavage of ester groups in PCL during enzymatic degradation. The subsequent decrease in Đ could be due to further cleavage of PCL oligomer degradation products towards the end of enzymatic degradation. It must be noted that only the collected solid material after degradation was used for SEC analysis and therefore, lower molecular weight soluble degradation products were not detected. This explains the observed small decrease in M_n^{SEC} and small increase in Đ in SEC analyses, when compared with % mass loss data. These results are in line with studies by Buchholz *et al*. who reported that SEC analysis showed no change in PCL molar mass during enzymatic degradation.[5] This suggests a surface-erosion degradation mechanism, which is supported by the surface pitting seen in the SEM micrographs of **2.7** degraded films, Figure 2.30.

Table 2.6: SEC analyses of star PCL **2.7** after enzymatic degradation using *pseudomonas cepacia* lipase in PBS solution (pH 7.4)

Enzymatic degradation	M_n^{SEC}	M_w^{SEC}	M_p^{SEC}	Đ
Day	$\times 10^{-4}$ g mol^{-1}			
0	2.48	5.62	6.73	2.27
1	1.95	4.73	5.52	2.42
15	2.88	5.36	5.84	1.86

The SEM micrographs depicting the polymer film surface of **2.7** after 0, 1, 2 and 15 days of enzymatic degradation using *pseudomonas cepacia* lipase are shown in Figure 2.30. It must be noted that the polymer film of star PCL **2.7** remained intact throughout the

degradation period, unlike linear PCL **2.2** and star copolymer **2.14**. However, significant changes in surface morphology can be seen in the first day of enzymatic degradation (from day 0-1) such as increase in texture and surface pitting, clearly distinct from the smooth even film surface before enzymatic degradation.

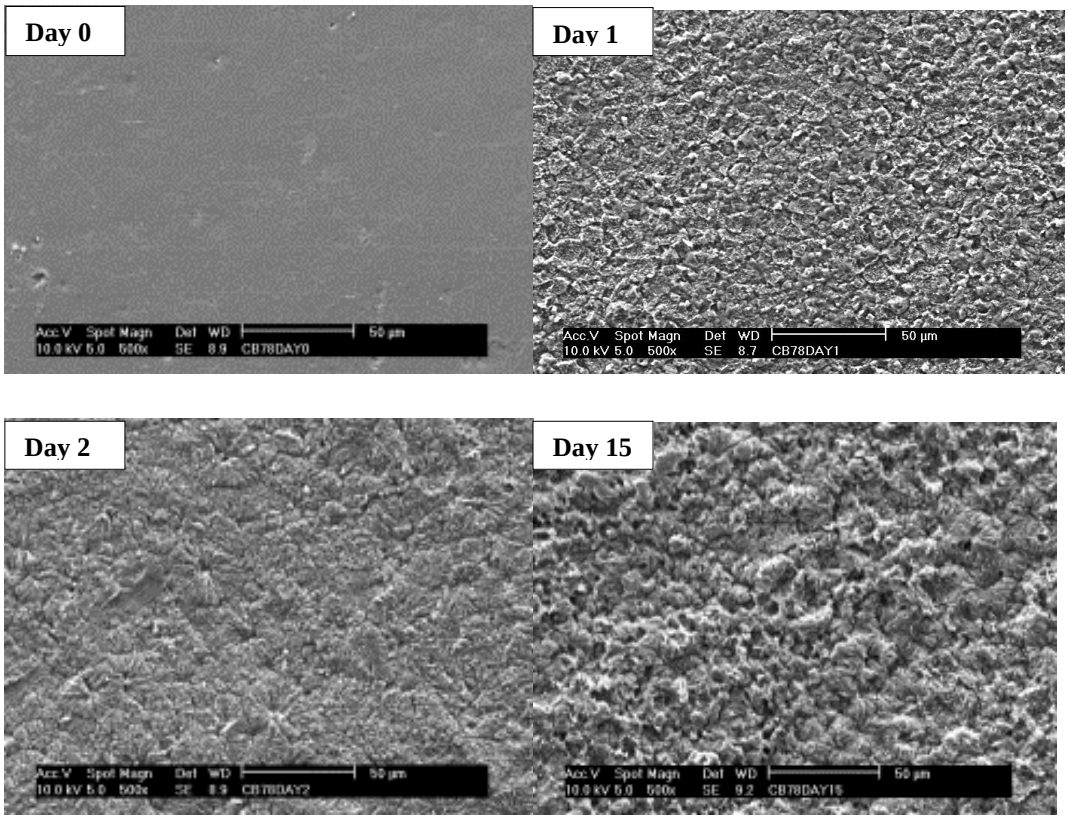

Figure 2.30: SEM micrographs showing films of PCL star **2.7** after 0, 1, 2 and 15 days of enzymatic degradation using *pseudomonas cepacia* lipase in PBS solution (pH 7.4). The scale bar used is 50 μm.

The SEM micrographs clearly show that enzymatic degradation occurs over the whole surface of the film, suggesting a surface-erosion degradation mechanism. The same observations have been previously made with the enzymatic degradation of aliphatic polyesters including PCL.[21]

It is possible to distinguish crystal spherulites in the SEM micrograph after just 2 days of enzymatic degradation. This phenomenon has been reported in the literature, indicating that degradation primarily takes place in the amorphous areas, therefore, increasing the

overall crystallinity of the substrate.[25,18,26] Furthermore, the formation of crystal spherulites slows the degradation process, by restricting the mobility and accessibility of the ester groups embedded in the crystal spherulites.

It is generally accepted that $\%\chi_c$ has a major impact on the rate of enzymatic degradation, due to amorphous regions being preferentially degraded before crystalline regions.[18] It has been suggested that in the initial stages of PCL degradation, water diffuses into amorphous regions resulting in random scission of the ester groups in the PCL chains. Furthermore, the production of shorter PCL chains may result in additional crystallisation, as the shorter polymer chains have greater mobility and ability to arrange themselves into regular crystalline structures. Both the affects of removal of amorphous regions and production of shorter polymer chains cause a net increase in the overall $\%\chi_c$ of the polymer.

The changes in thermal properties $\%\chi_c$ and of linear PCL **2.2**, star PCL **2.7** and star copolymer **2.14** throughout enzymatic degradation are shown in Table 2.7. Linear PCL **2.2** shows an increase in $\%\chi_c$ from 71% to 81% from 0 days to 2 days of enzymatic degradation, respectively. The DSC thermograms for linear PCL **2.2** after 0 and 1 day of enzymatic degradation can be found in Appendices 2.2 and 2.3, respectively. However, star PCL **2.7** shows an initial decrease in $\%\chi_c$ from 73% to 29% at 0 and 1 day of enzymatic degradation, respectively. Subsequently, an increase in $\%\chi_c$ of **2.7** is seen from 29% to 34% in day 1 to day 2 of enzymatic degradation, respectively. Star copolymer **2.14** shows a small decrease in $\%\chi_c$ from 20% to 18%, in day 0 to day 2 of enzymatic degradation, respectively. Due to inconsistent results from several repeat measurements in DSC analyses of **2.14** after 6 days and 15 days of enzymatic degradation, these results have been omitted from Table 2.7. A decrease in the enthalpy of melting (ΔH_m) and enthalpy of crystallisation (ΔH_c) is seen in **2.2**, **2.7** and **2.14**, with a decrease in $\%\chi_c$ throughout enzymatic degradation. Furthermore, an initial increase in T_m (from day 0-2) was observed for **2.2** and **2.7**, followed by a decrease in T_m (from day 2-15), in correlation with the initial increase and subsequent decrease in $\%\chi_c$ throughout enzymatic degradation. Linear PCL **2.2** and star PCL **2.7** showed little change in T_c throughout enzymatic degradation. However, star copolymer **2.14** showed a significant increase in T_c from 12 - 18 °C to 18 - 22 °C from day 0 to day 2 of enzymatic degradation, respectively.

Table 2.7: Thermal properties of linear PCL **2.2**, star PCL **2.7** and star copolymer **2.14** throughout enzymatic degradation using *pseudomomas cepacia* lipase in PBS solution (pH 7.4), determined by DSC at 10 °C min^{-1}

Sample	Enzymatic Degradation	ΔH_m	ΔH_c	χ_c	T_m	T_c
	day	J g^{-1}		%	°C	
2.2	0	98	100	71	55 - 57	32 - 38
	2	111	113	81	55 - 58	33 - 37
2.7	0	90	101	73	53 - 58	29 - 35
	1	36	41	29	54 - 59	30 - 34
	2	42	48	34	54 - 58	30 - 34
	4	10	11	8	55 - 57	31 - 35
	15	4	5	3	54 - 56	31 - 35
2.14	0	35	27	20	42 - 46	12 - 18
	2	24	25	18	39 - 41	18 - 22

2.4 Conclusion

A series of biodegradable star PCL **2.4 – 2.7** and star poly[(ε-CL)-*co*-(β-BL)] **2.14 – 2.16** were synthesised *via* the ROP of ε-CL and a mixture of ε-CL/ β-BL monomers, catalysed by $SnOct_2$, respectively. Multi-functional hydroxyl initiators pentaerythritol, di(trimethylolpropane) and dipentaerythritol were used to give four- and six-arm structures. For comparative analysis, linear PCL **2.2** and linear poly[(ε-CL)-*co*-(β-BL)] **2.13** were synthesised in a similar manner using di-hydroxyl initiator, ethylene glycol. All polymers were fully characterised using NMR, SEC and DSC.

Linear PCL **2.2** exhibited a higher $\%\chi_c$ than star PCL **2.5 – 2.6** due to increased chain entanglement and restricted mobility of arms connected to a central core moiety. The $\%\chi_c$ decreased in star PCL with an increase in M_n and of $\overline{DP}$ of arm in **2.4 – 2.7**, respectively. Star poly[(ε-CL)-*co*-(β-BL)] **2.14** exhibited a lower $\%\chi_c$ than linear PCL **2.2** and star PCL **2.4 – 2.7** due to the incorporation of the β-BL monomer.

The enzymatic degradation behaviour of linear PCL **2.2**, star PCL **2.7** and star poly[(ε-CL)-*co*-(β-BL)] **2.40** were investigated using *pseudomonas cepacia* lipase. The rate of enzymatic degradation was determined by % mass loss, DSC, SEC and SEM analyses. Linear PCL **2.2** was seen to degrade at a faster rate than that of the star structures, due to increased mobility and decreased entanglement of polymer chains in the linear structure. Star PCL **2.7** and star poly[(ε-CL)-*co*-(β-BL)] **2.14** showed very similar rates of enzymatic degradation. Both linear and star structures showed changes in thermal properties during enzymatic degradation, with an increase in $\%\chi_c$ seen in the initial few days of degradation (0-3 days), subsequently followed by a decrease in $\%\chi_c$. This suggests enzymatic degradation occurs primarily in the amorphous regions of the polymer, therefore increasing the overall $\%\chi_c$ of the polymer. The SEM micrographs of the degraded polymer films supports this result, showing significant changes in surface morphology including surface pitting and occurrence of crystal spherulite structures, in the first few days of enzymatic degradation.

2.5 References

(1) Zhang, X.; Xiao, Y.; Lang, M. *Polym J* **2013**, *45*, 420.
(2) Roovers, J.; Zhou, L. L.; Toporowski, P. M.; van der Zwan, M.; Iatrou, H.; Hadjichristidis, N. *Macromolecules* **1993**, *26*, 4324.
(3) Knischka, R.; Lutz, P. J.; Sunder, A.; Mülhaupt, R.; Frey, H. *Macromolecules* **2000**, *33*, 315.
(4) Cameron, D. J. A.; Shaver, M. P. *Chem. Soc. Rev.* **2011**, *40*, 1761.
(5) Buchholz, V.; Agarwal, S.; Greiner, A. *Macromol. Biosci.* **2016**, *16*, 207.
(6) Nuyken, O.; Pask, S. *Polymers* **2013**, *5*, 361.
(7) Kricheldorf, H. R.; Kreiser-Saunders, I.; Stricker, A. *Macromolecules* **2000**, *33*, 702.
(8) Kowalski, A.; Duda, A.; Penczek, S. *Macromolecules* **2000**, *33*, 689.
(9) Arbaoui, A.; Redshaw, C. *Polym. Chem.* **2010**, *1*, 801.
(10) Thomas, C. M. *Chem. Soc. Rev.* **2010**, *39*, 165.
(11) Pitt, G. G. G., M. M.; Kimmel, G. L.; Surles, J.; Sohingler, A. *Biomaterials* **1981**, *2*, 215.
(12) Sobczak, M. *Polimery* **2009**, *54*, 114.
(13) Dubois, P.; Jacobs, C.; Jerome, R.; Teyssie, P. *Macromolecules* **1991**, *24*, 2266.
(14) Kim, S. H.; Han, Y.-K.; Ahn, K.-D.; Kim, Y. H.; Chang, T. *Macromol. Chem.* **1993**, *194*, 3229.
(15) Xie, W.; Jiang, N.; Gan, Z. *Macromol. Biosci.* **2008**, *8*, 775.
(16) Trollsås, M.; Hedrick, J. L. *J. Am. Chem. Soc.* **1998**, *120*, 4644.
(17) Olsén, P.; Odelius, K.; Albertsson, A.-C. *Biomacromolecules* **2016**, *17*, 699.
(18) Marten, E.; Müller, R.-J.; Deckwer, W.-D. *Polym. Degrad. Stabil.* **2003**, *80*, 485.
(19) Gan, Z.; Liang, Q.; Zhang, J.; Jing, X. *Polym. Degrad. Stabil.* **1997**, *56*, 209.
(20) Hermanová, S.; Bálková, R.; Voběrková, S.; Chamradová, I.; Omelková, J.; Richtera, L.; Mravcová, L.; Jančář, J. *J. Appl. Polym. Sci.* **2013**, *127*, 4726.
(21) Bikiaris, D. N. *Polym. Degrad. Stabil.* **2013**, *98*, 1908.
(22) Kulkarni, A.; Reiche, J.; Kratz, K.; Kamusewitz, H.; Sokolov, I. M.; Lendlein, A. *Langmuir* **2007**, *23*, 12202.
(23) Gaborieau, M.; Castignolles, P. *Anal. Bioanal. Chem.* **2011**, *399*, 1413.
(24) Li, S. M.; Pignol, M.; Gasc, F.; Vert, M. *Macromolecules* **2004**, *37*, 9798.
(25) Wang, J. L.; Wang, L.; Dong, C. M. *J. Polym. Sci. Pol. Chem.* **2005**, *43*, 5449.
(26) Mochizuki, M.; Hirano, M.; Kanmuri, Y.; Kudo, K.; Tokiwa, Y. *J. Appl. Polym. Sci.* **1995**, *55*, 289.

3 Synthesis and Degradation Studies of Poly[(ε-caprolactone)-*co*-(ethylene glycol)]

3.1 Introduction

Poly(ε-caprolactone) (PCL) has been shown to be non-toxic, biocompatible and biodegradable.[1,2,3] It has received significant attention in applications for biomedical use, due to its tuneable degradation rate and good mechanical properties.[2] It can be synthesised by the facile ring-opening polymerisation (ROP) of ε-caprolactone (ε-CL) using a nucleophilic initiator such as hydroxyl groups and tin (II) ethyl hexanoate ($SnOct_2$) catalyst.[4,5] Hydrophilic poly(ethylene glycol) (PEG) has been recognised as a biocompatible water soluble polymer with important biological or pharmaceutical applications.[6]

PEG has been copolymerised with hydrophobic aliphatic polyesters poly(lactide-*co*-glycolide) (PLGA) to increase the hydrophilic nature and therefore increase the rate of hydrolytic degradation of the hydrophobic polyester block.[7] However, some studies have shown that the rate of enzymatic degradation of PCL was not affected by the incorporation of a hydrophilic PEG unit.[8,9]

Multi-hydroxyl initiators have been derived from the dendritic building block 2, 2 bis(hydroxymethyl) propionic acid (bisHMPA)[10,11] Furthermore, Y-shaped copolymers have been synthesised by the 1° alcohol protection of bisHMPA, coupling with mono-methylether PEG and subsequent deprotection of the 1° alcohol group on the bisMPA moiety. The di-hydroxyl PEG initiator was then used in the ROP of cyclic monomers such as lactide.[12] Moreover, Bensaid *et al*. reported the synthesis of Y-shaped copolymer Me-(PEG)-*b*-$(PLA)_2$ using a bisMPA linakge.[13] However, there is no characterisation for the benzyl-protected Me-PEG precursor. Furthermore, there are insufficient ^{1}H and ^{13}C NMR analyses of the benzyl-deprotection to give Me-PEG di-hydroxyl initiator. The extent of benzyl-deprotection is unknown, in addition to potential cleavage of the ester bond in the bisMPA moiety under the acidic conditions. Additionally, the research lacked FTIR analyses to support the full benzyl-protection (disappearance of O-H stretch) and deprotection of the 1° alcohol groups (appearance of O-H stretch) on the bisMPA moiety in the Me-PEG di-hydroxyl precursor.

Four-arm star copolymers with a central PEG unit and PLA arms have been synthesised by the ROP of lactide using commercially available 1,3,4-triphenyl-4,5-dihydro-1*H*-1,2,4-triazol-5-yliadene and a Me-PEG-$(NH_2)_2$ initiator.[14] However, impurities can be seen in the ^{1}H NMR spectrum of the product and also ^{13}C NMR spectrum of the product is not shown.

The synthesis and hydrolytic degradation of star copolymers consisting of a central PEG unit with 2, 4 and 8 poly(lactic-*co*-glycolic acid) (PLGA) arms have been reported.[7] These star copolymers were degraded in PBS solution (pH = 7.4) at 37 °C left for up to 40 days and monitored only by mass loss. The results showed the degradation rate increased with the increase of number of arms or with the decrease of arm length. However, no thermal analyses on the degraded material were shown, to monitor the changes in $\%\chi_c$ during hydrolytic degradation. On the other hand, it has been reported that enzymatic degradation of PCL occurs though random chain scission of the polymer backbone chain and is irrespective of chain length.[15]

Complete degradation of PCL in the presence of *pseudomonas* lipase has been reported to occur within 4 days,[16] whereas hydrolytic degradation in the absence of enzymes lasts several years.[17] The enzymatic degradation of PCL has been extensively investigated using lipase.[18,19,9] It has been reported that only three kinds of lipases effectively accelerate the degradation of PCL which are all obtained from fungi or bacteria, namely from *rhizopus delemer* lipase,[20] *rhizopus arrhizus* lipase[21] and from *pseudomonas* PS lipase.[22,23] Different mechanisms of PCL degradation have been proposed; a surface erosion mechanism was observed during enzymatic degradation whereas a bulk erosion mechanism was observed in hydrolytic degradation.[24]

Enzymatic degradation of PCL has been shown to be dependent on crystallinity, as the degree of crystallinity ($\%\chi_c$) initially increases during degradation, indicating amorphous regions are primarily degraded.[25,26] Furthermore, it has been proposed that enzymatic degradation of PCL primarily occurs at the chain-ends, chain-folds and at the edge of crystals, where chain mobility is higher.[27] Generally, PCL-PEG copolymers show a decreased crystallinity in comparison to PCL homopolymer therefore would be expected to increase the rate of enzymatic degradation.

In this chapter, the synthesis of a series of novel four-arm star PCL with a central PEG moiety bridged with a bisMPA linkage will be discussed. Polymers were fully

characterised using NMR, SEC, DSC, FT-IR, contact angle and % water uptake (%WU). PCL-*b*-PEG-*b*-PCL linear triblock copolymer is synthesised and used as a comparison in analyses. The linear and four-arm star PCL-PEG copolymers were subjected to enzymatic degradation using *pseudomonas cepacia* lipase and monitored using % mass loss, DSC and SEM analyses.

3.2 Experimental

3.2.1 Materials

ε-Caprolactone (ε-CL), tin (II) ethyl hexanoate ($SnOct_2$), poly(ethylene glycol) PEG (M_n = 600 g mol^{-1}) **3.1** and (M_n = 3350 g mol^{-1}) **3.4**, 2,2'-Bis(hydroxymethyl)propionic acid (Bis-HMPA) **3.6**, 2,2'-Dimethoxypropane, 4-dimethylamino pyridine (DMAP), *pseudomonas cepacia* lipase and phosphate buffer saline salts (pH = 7.4) were purchased from Sigma Aldrich and used as received unless stated otherwise. ε-CL was distilled over CaH_2 under reduced pressure prior to use. All dry solvents were obtained from Durham Chemistry Department Solvent Purification System (SPS). All other solvents were analytical grade and used without any purification. The NMR solvent used was deuterated chloroform ($CDCl_3$) purchased from Apollo Scientific.

3.2.2 Characterisation Techniques

^{1}H and ^{13}C Nuclear magnetic resonance (NMR), Size Exclusion Chromatography (SEC), Differential Scanning Calorimetry (DSC), Fourier-transform Infrared Spectroscopy (FT-IR) and Scanning Electron Microscopy (SEM) were carried out as outlined in Chapter 2, Section 2.2.2.

Contact angle measurements were carried out on FTA200 equipped with a halogen bulb and a S1640 monochrome camera. The water droplet was automatically delivered to the polymer film using a syringe with a blunt 27 gauge needle. The camera recorded 750 images of the droplet and film over a period of 30 seconds. The contact angle (θ) was calculated by the average of the left and right angles. The reported contact angle measurements are averages of five repeat measurements with a calculated error of ±2.3 %.

3.2.3 Enzymatic Degradation

Enzymatic degradation tests were carried out as outlined in Chapter 2, Section 2.2.3.

3.2.4 Water Uptake

The % swelling of the PCL-PEG copolymer films in PBS solution (pH = 7.4) were measured by immersing films (10 × 20 × 0.5 mm^3, ~110 mg) in 5 mL PBS solution at 37 °C for 2 days, removing and carefully drying films on tissue paper and weighing. The films were dried in a vacuum oven at 40 °C until a constant weight was obtained. The dry films were weighed and the difference in weight of films before and after drying was divided by the weight of the dried films to give a percentage swelling.

3.2.5 Synthesis of Linear (PCL)-*b*-(PEG)-*b*-(PCL) 3.2 – 3.3 and 3.5

PCL-*b*-PEG-*b*-PCL copolymers **3.2 - 3.3** and **3.5** were synthesised by the ROP of ε-CL catalysed using $SnOct_2$ and using either PEG **3.1** or **3.4** macro-initiator, following the procedure in the literature.[28]

Poly(ethylene glycol) **3.1** (M_n = 600 g mol^{-1}) (3.00 g, 5 mmol), ε-caprolactone (11.41 g, 100 mmol) and $SnOct_2$ catalyst (0.10 g, 0.25 mmol) were added to a Schlenk flask purged with N_2 for 10 min. The reaction mixture was stirred and heated to 120 °C for 24 h under a N_2 atmosphere. The mixture was then cooled, dissolved in dichloromethane (10 mL) and precipitated by the addition of diethyl ether (200 mL) at 0 °C using an ice bath. The white solid was collected and dried under reduced pressure at 40 °C and purified by a further precipitation to give **3.2**.

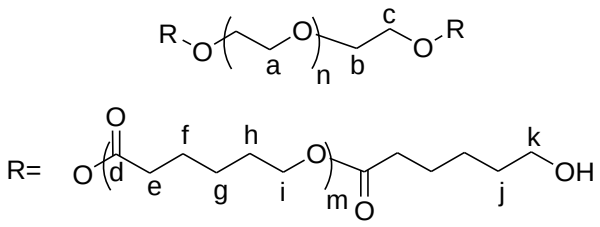

Figure 3.1: Linear PCL-*b*-PEG-*b*-PCL **3.2 – 3.3** and **3.5**

3.2.5.1 $\overline{DP}$ of 10 per arm 3.2

Macro-initiator PEG **3.1** (M_n = 600 g mol^{-1}) and a ratio of 20:1 for ε-CL:PEG was used to give **3.2** (6.88 g, 48% yield). ^{1}H NMR (400 MHz, $CDCl_3$, TMS): (ppm) δ = 1.34 (m, 50H, H_g), 1.61 (m, 100H, H_f, H_h, H_j), 2.27 (t, *J* = 7.5 Hz, 50H, H_e), 3.61 (m, 46H, H_a, H_k), 3.66 (t, *J* = 4.8 Hz, 4H, H_b), 4.02 (t, *J* = 6.6 Hz, 44H, H_i), 4.19 (t, *J* = 4.7 Hz, 4H, H_c). ^{13}C NMR (100 MHz, $CDCl_3$, TMS): (ppm) δ = 24.6 (f), 25.6 (g), 28.4 (h), 32.4 (j), 34.2 (e), 62.6 (k), 63.5 (c), 64.2 (i), 69.2 (b), 70.6 (a), 173.6 (d). FT-IR: ν_{max} = 2948, 2872 (C-H), 1724 (C=O), 1370, 1242, 1176 (C-O), 1048 cm^{-1}. SEC: M_n = 4.79 x 10^3 g mol^{-1}, M_w = 5.43 x 10^3 g mol^{-1}, Đ = 1.13. The ^{1}H, ^{13}C NMR and FT-IR spectra are in good agreement with the literature. [28]

3.2.5.2 $\overline{DP}$ of 50 per arm 3.3

Macro-initiator PEG **3.1** (M_n = 600 g mol^{-1}) and ratio of 100:1 for ε-CL:PEG was used to give **3.3** (31.36 g, 99% yield). ^{1}H NMR (400 MHz, $CDCl_3$, TMS): (ppm) δ = 1.33 (m, 180H, H_g), 1.60 (m, 360H, H_f, H_h, H_j), 2.24 (t, *J* = 7.6 Hz, 180H, H_e), 3.59 (m, 52H, H_a, H_k), 3.64 (t, *J* = 4.8 Hz, 4H, H_b), 3.99 (t, *J* = 6.7 Hz, 180H, H_i), 4.17 (t, *J* = 4.8 Hz, 4H,

H_c). ^{13}C NMR (100 MHz, $CDCl_3$, TMS): (ppm) δ = 24.6 (f), 25.6 (g), 28.4 (h), 32.3 (j), 34.1 (e), 62.5 (k), 63.4 (c), 64.1 (i), 69.1 (b), 70.6 (a), 173.5 (d). FT-IR: ν_{max} = 2949, 2870 (C-H), 1722 (C=O), 1366, 1239, 1179 (C-O), 1047 cm^{-1}. SEC: M_n = 1.05 x 10^4 g mol^{-1}, M_w = 1.18 x 10^4 g mol^{-1}, Đ = 1.13. The ^1H, ^{13}C NMR and FT-IR spectra are in good agreement with the literature. [28]

3.2.5.3 $\overline{DP}$ of 40 per arm 3.5

Macro-initiator PEG **3.4** (M_n = 3350 g mol^{-1}) and a ratio of 80:1 for ε-CL:PEG was used to give **3.5** (14.82 g, 99% yield). ^1H NMR (400 MHz, $CDCl_3$, TMS): (ppm) δ = 1.34 (m, 182H, H_g), 1.61 (m, 358H, H_f, H_h, H_j), 2.27 (t, 177H, *J* = 7.4 Hz, H_e), 3.60 (m, 304H, H_a, H_b, H_k), 4.02 (t, *J* = 6.7, 174H, H_i), 4.18 (t, 4H, *J* = 4.8 Hz, H_c). ^{13}C NMR (400 MHz, $CDCl_3$, TMS): (ppm) δ = 24.6 (f), 25.6 (g), 28.4 (h), 32.4 (j), 34.2 (e), 62.6 (k), 63.5 (c), 64.2 (i), 69.2 (b), 70.6 (a), 173.6 (d). T_m = 54 - 60 °C. FT-IR: ν_{max} = 2948, 2870 (C-H), 1722 (C=O), 1366, 1239, 1180 (C-O), 1047, 962 cm^{-1}. SEC: M_n = 1.24 × 10^4 g mol^{-1}, M_w = 1.63 × 10^4 g mol^{-1}, Đ = 1.31. The ^1H, ^{13}C NMR and FT-IR spectra are in good agreement with the literature. [28]

3.2.6 Synthesis of Four-arm Star $(PCL)_2$-*b*-(PEG)-*b*-$(PCL)_2$ 3.10 - 3.12

Four-arm star copolymers **3.10 - 3.12** with a central hydrophilic PEG **3.4** unit and four hydrophobic PCL arms were synthesised in a four step synthetic route, outlined below.

3.2.6.1 Synthesis of Isopropylidene-2,2'-bis(methoxyl) Propionic Acid 3.7

Hydroxyl-protected bisMPA **3.7** was synthesised following the procedure used in the literature.[29]

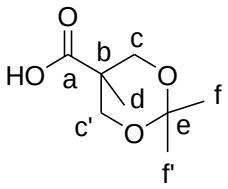

Figure 3.2: Isopropylidene-2,2'-bis(methoxyl) propionic acid **3.7**

Bis-HMPA **3.6** (20.0 g, 149 mmol), 2,2'-dimethoxypropane (27.2 g, 261 mmol) and *p*-toluenesulfonic acid monohydrate (1.42 g, 7.5 mmol) were dissolved in acetone (100 mL) and stirred at ambient temperature for 2 h. The reaction mixture was neutralised by the addition of NaOH methanol solution (0.32 g in 10 mL) and the solvent removed under reduced pressure. The product was dissolved in DCM (100 mL) and extracted twice with

distilled water (2 x 20 mL). The organic phase was collected and dried over $MgSO_4$, filtered and the solvent was removed under reduced pressure at 40 °C to yield a white crystalline product **3.7** (19.72 g, 76% yield). ^{1}H NMR (400 MHz, $CDCl_3$, TMS): (ppm) δ = 1.20 (s, 3H, H_d), 1.40 (s, 3H, H_f), 1.43 (s, 3H, $H_{f'}$), 3.65 (d, *J* = 11.6 Hz, 2H, H_c), 4.18 (d, *J* = 11.6 Hz, 2H, $H_{c'}$), 10.60-11.20 (bs, 1H, -COO*H*). ^{13} C NMR (400 MHz, $CDCl_3$, TMS): (ppm) δ = 18.6 (d), 22.3 (f), 25.1 (f'), 41.9 (b), 65.9 (c), 98.4 (e), 180.4 (a). FT-IR: ν_{max} = 2996 (C-H), 1718 (COOH), 1456, 1380, 1252 (C-O), 1070, 824, 716 cm^{-1}. ASAP Mass Spectrometry: $[M+H]^+$ 175.097 $C_8H_{14}O_4$. The ^{1}H NMR spectrum is in good agreement with the literature. No additional analyses was reported in the literature. [29]

3.2.6.2 Synthesis of Novel Hydroxyl-Protected PEG Macro-initiator 3.8

The synthesis of novel hydroxyl-protected PEG macro-initiator **3.8** was based on the method used in the literature, outlined below.[29]

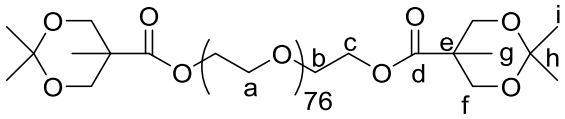

Figure 3.3: Hydroxyl-protected PEG macro-initiator **3.8**

Poly(ethylene glycol) **3.4** (M_n = 3350 g mol^{-1}) (26.8 g, 8 mmol), isopropylidene-2,2'-bis(methoxyl) propionic acid **3.7** (3.48 g, 20 mmol), N,N'-dicyclohexylcarbodiimide (DCC) (5.28 g, 25.6 mmol), DMAP (0.59 g, 4.8 mmol) and DCM (400 mL) were added to a round bottomed flask and the mixture was stirred at ambient temperature for 28 h. The reaction mixture was filtered to remove insoluble 1,3-dicyclohexylurea and then reduced to 10 mL and precipitated into diethyl ether (200 mL). The product was purified by a further precipitation from DCM into diethyl ether. The solid product was collected *via* filtration and dried under reduced pressure at 40 °C to give **3.8**. (29.0 g, 98% yield) ^{1}H NMR (400 MHz, $CDCl_3$, TMS): (ppm) δ = 1.21 (s, 6H, H_g), 1.38 (s, 6H, H_i), 1.42 (s, 6H, $H_{i'}$), 3.64 (m, 323H, H_a, H_b), 3.69 (m, 5H, H_f), 4.19 (d, J = 11.8 Hz, 4H, $H_{f'}$), 4.29 (m, 4H, H_c). ^{13}C NMR (400 MHz, $CDCl_3$, TMS): (ppm) δ = 18.6 (g), 23.0 (i'), 24.2 (i), 41.7 (e), 63.8 (c), 65.8 (f'), 68.9 (f), 70.4 (a), 97.9 (h), 174.0 (d). FT-IR: ν_{max} = 2884 (C-H), 1734 (C=O), 1466, 1340, 1102 (C-O), 960 cm^{-1}.

3.2.6.3 Synthesis of Novel Tetra-hydroxyl PEG Macro-initiator 3.9

The synthesis of novel tetra-hydroxyl PEG macro-initiator **3.9** was based on the method used in the literature.[29]

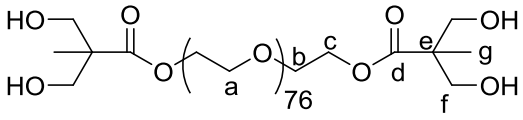

Figure 3.4: Tetra-hydroxyl PEG macro-initiator **3.9**

Hydroxyl-protected poly(ethylene glycol) macro-initiator **3.8** (10 g, 27.71 mmol) from the previous step was dissolved in methanol (100 mL) and then $HCl_{(aq)}$ (10 mL, 0.1M) was added to the mixture and stirred at ambient temperature for 6 h. Upon the completion of the reaction, the solvent was removed under reduced pressure and the solid product was dissolved in DCM (100 mL) and dried over anhydrous $MgSO_4$. The reaction mixture was filtered, concentrated to 5 mL under reduced pressure and precipitated in diethyl ether. The solid product was collected and dried under reduced pressure to give **3.9**. (8.64 g, 88% yield) ^{1}H NMR (400 MHz, $CDCl_3$, TMS): (ppm) δ = 1.08 (s, 6H, H_g), 2.77 (bs, 11H, OH), 3.60 (m, 348H, H_a), 3.67-3.80 (m, 17H, H_b, H_f), 4.28 (m, 4H, H_c). ^{13}C NMR (400 MHz, $CDCl_3$, TMS): (ppm) δ = 17.2 (g), 49.7 (e), 63.4 (c), 67.4 (f), 68.8 (b), 70.6 (a), 175.7 (d). FT-IR: ν_{max} = 3490 (O-H), 2888 (C-H), 1737 (C=O), 1467, 1342, 1104 (C-O), 959 cm^{-1}. SEC: $M_n = 7.35 \times 10^3$ g mol^{-1}, $M_w = 9.09 \times 10^3$ g mol^{-1}, Đ = 1.24.

3.2.6.4 Synthesis of Novel Four-arm Star $(PCL)_2$-*b*-(PEG)-*b*-$(PCL)_2$ 3.10 – 3.12

A series of novel four-arm star copolymers **3.10 – 3.12**, $(PCL)_2$-PEG-$(PCL)_2$, were synthesised based on the method outlined below.

Tetra-hydroxyl PEG macro-initiator **3.9**, $(OH)_2$-PEG-$(OH)_2$ (4.50 g, 1.24 mmol), ε-CL (11.36 g, 99.55 mmol) and $SnOct_2$ catalyst (0.10 g, 0.24 mmol) were added to a Schlenk purged with nitrogen for 10 min. The reaction mixture was heated to 120 °C and stirred for 48 h under a nitrogen atmosphere. The mixture was then cooled, dissolved in DCM (10 mL) and diethyl ether (200 mL) was added to precipitate a white solid. The solid was collected *via* filtration and dried under reduced pressure at 40 °C, then further purified by a second precipitation from DCM into diethyl ether.

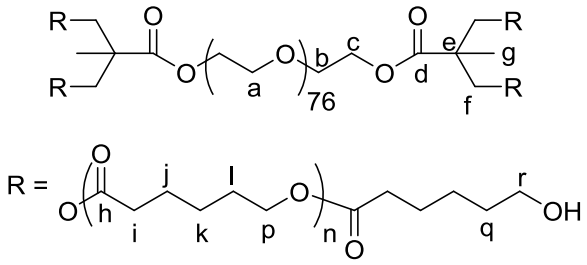

Figure 3.5: Four-arm star $(PCL)_2$-*b*-(PEG)-*b*-$(PCL)_2$ **3.10 - 3.12**

3.2.6.4.1 $\overline{DP}$ of 20 per arm 3.10

(15.33 g, 97%) ^{1}H NMR (400 MHz, $CDCl_3$, TMS): (ppm) δ = 1.21 (s, 6H, H_g) 1.34 (m, 194H, H_k), 1.61 (m, 383H, H_j, H_l, H_q), 2.27 (t, *J* = 7.4 Hz, 196H, H_i), 3.60 (m, 347H, H_a, H_b, H_r), 4.02 (t, *J* = 6.7 Hz, 188H, H_p), 4.16-4.23 (m, 18H, H_c, H_f). ^{13}C NMR (400 MHz, $CDCl_3$, TMS): (ppm) δ = 17.8 (g), 24.6 (j), 25.6 (k), 28.4 (l), 32.4 (q), 34.2 (i), 46.4 (e), 62.6 (r), 63.5 (c), 64.2 (p), 65.2 (f), 68.9 (b), 70.6 (a), 172.9 (d), 173.5 (h). T_m = 50 - 54 °C. FT-IR: ν_{max} = 3498 (O-H), 2938, 2866 (C-H), 1720 (C=O), 1470, 1366, 1292, 1240, 1186, 1108 (C-O), 960 cm^{-1}. SEC: M_n = 1.06 ×10^4 g mol^{-1}, M_w = 1.39 ×10^4 g mol^{-1}, Đ = 1.32.

3.2.6.4.2 $\overline{DP}$ of 50 per arm 3.11

^{1}H NMR (400 MHz, $CDCl_3$, TMS): (ppm) δ = 1.22 (s, 6H, H_g) 1.35 (m, 416H, H_k), 1.62 (m, 832H, H_j, H_l, H_q), 2.28 (t, *J* = 7.6 Hz, 416H, H_i), 3.62 (m, 304H, H_a, H_b, H_r), 4.03 (t, *J* = 6.7 Hz, 416H, H_p), 4.21-4.23 (m, 12H, H_f, H_c). ^{13}C NMR (400 MHz, $CDCl_3$, TMS): (ppm) δ = 24.7 (j), 25.6 (k), 28.4 (l), 32.4 (q), 34.2 (i), 46.3 (e), 62.7 (r), 64.2 (p), 70.7 (a), 173.6 (h). T_m = 52 - 59 °C. FT-IR: ν_{max} = 3544 (OH), 2930, 2860 (C-H), 1722 (C=O), 1466, 1368, 1292, 1240, 1184 (C-O), 1100, 1046, 962 cm^{-1}. SEC: M_n = 1.34 ×10^4 g mol^{-1}, M_w = 1.90 ×10^4 g mol^{-1}, Đ = 1.42.

3.2.6.4.3 $\overline{DP}$ of 100 per arm 3.12

^{1}H NMR (400 MHz, $CDCl_3$, TMS): (ppm) δ = 1.23 (s, 6H, H_g) 1.37 (m, 912H, H_k), 1.64 (m, 1824H, H_j, H_l, H_q), 2.29 (t, *J* = 7.6 Hz, 912H, H_i), 3.63 (m, 304H, H_a, H_b, H_r), 4.05 (t, *J* = 6.7 Hz, 912H, H_p), 4.22 (m 12H, H_f, H_c). ^{13}C NMR (400 MHz, $CDCl_3$, TMS): (ppm) δ = 24.7 (j), 25.6 (k), 28.4 (l), 34.2 (i), 62.7 (r), 64.2 (p), 70.6 (a), 173.6 (h). T_m = 53 - 60 °C. FT-IR: ν_{max} = 3540 (OH), 2942, 2864 (C-H), 1720 (C=O), 1470, 1366, 1292, 1238, 1180 (C-O), 1106, 1046, 960 cm^{-1}. SEC: M_n = 1.63 ×10^4 g mol^{-1}, M_w = 2.46 ×10^4 g mol^{-1}, Đ = 1.51.

3.3 Results and Discussion

3.3.1 Linear PCL-*b*-PEG-*b*-PCL 3.2 – 3.3

Triblock copolymers **3.2** and **3.3** were synthesised in the ROP of ε-CL using PEG (M_n = 600 g mol^{-1}) **3.1** and catalysed by $SnOct_2$, Scheme 3.1. The ratio of PEG : ε-CL was varied from 1:20 to 1:100 to produce triblock copolymers **3.2** and **3.3** with a $\overline{DP}_{Th}$ of ten and fifty per arm, respectively.

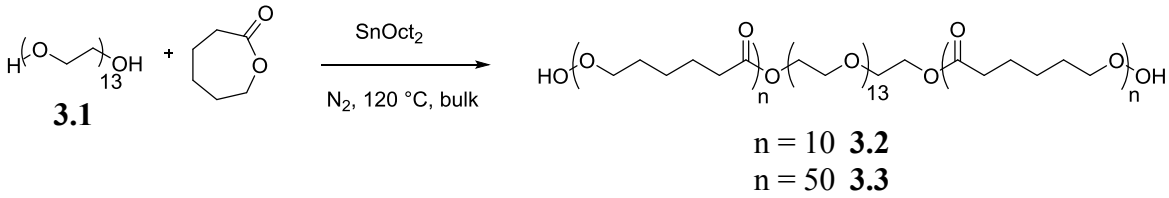

Scheme 3.1: Synthesis of linear PCL-*b*-PEG-*b*-PCL **3.2** and **3.3**

The ^1H NMR spectrum of **3.2**, Figure 3.6, shows the characteristic PCL resonances at 1.34 ppm, 1.61 ppm, 2.27 ppm and 4.02 ppm attributing to the methylene protons **g**, **f/h**, **e** and **i**, respectively. The resonances at 3.61 ppm and 3.66 ppm are attributed to methylene protons **a** and **b** located on the central PEG moiety. The resonance at 4.19 ppm integrated to 4H is attributed to methylene protons **c** on the PEG moiety, neighbouring the ester group. Furthermore, the ^1H – ^1H COSY NMR spectrum of **3.2**, Figure 3.7, shows coupling between neighbouring protons **b** and **c** on the PEG moiety at 3.66 ppm and 4.19 ppm, respectively. Moreover, coupling can be seen between neighbouring protons **j** and **k** on the PCL moiety at 1.61 ppm and 3.61 ppm, respectively. The presence of resonances attributing to protons **b** and **c** neighbouring the ester group, and protons **j** and **k** neighbouring the OH group on the PCL moiety, indicates the successful ROP of ε-CL from the initiating OH groups on the PEG moiety.

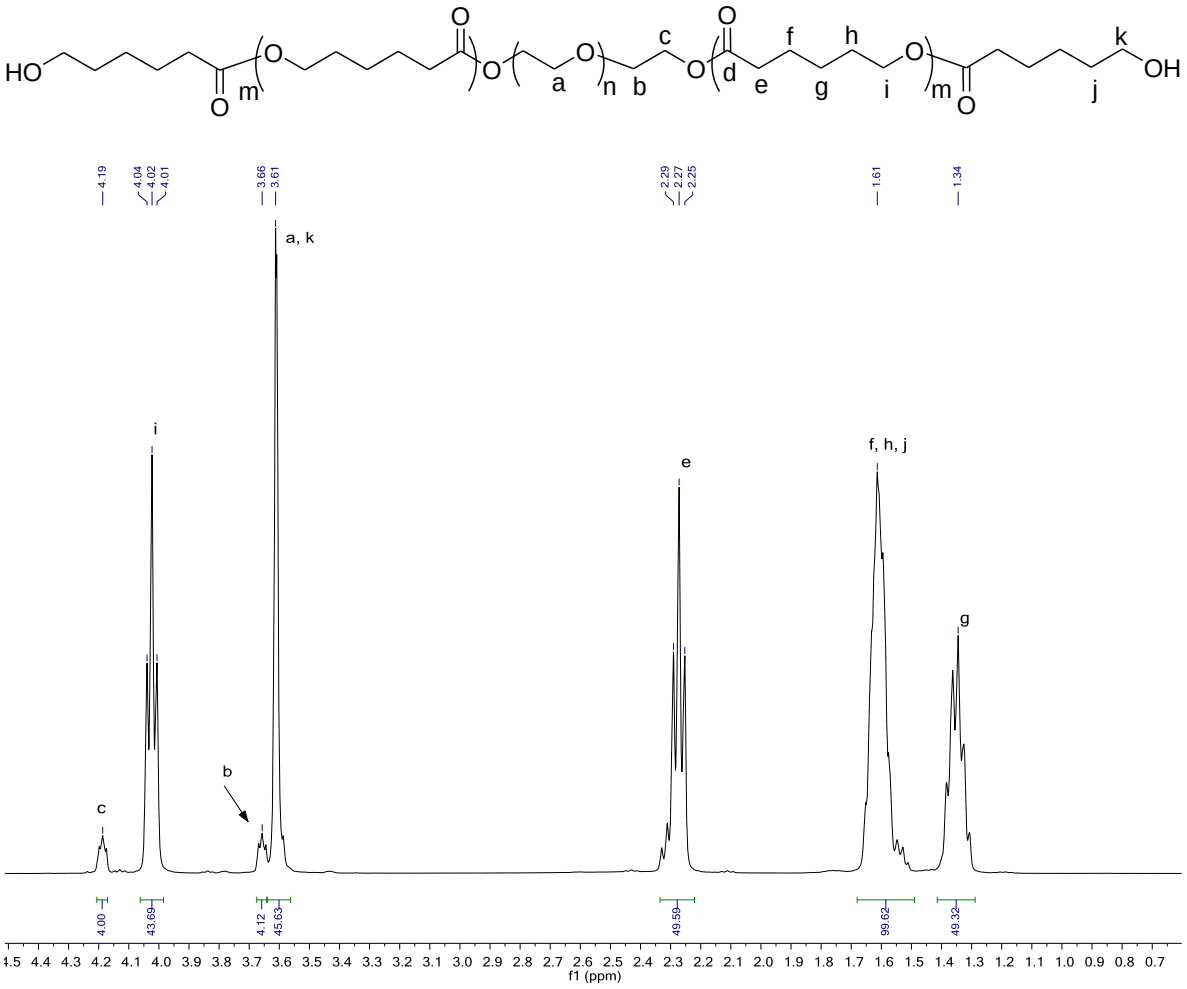

Figure 3.6: 400 MHz ^{1}H NMR spectrum of **3.2** in $CDCl_3$

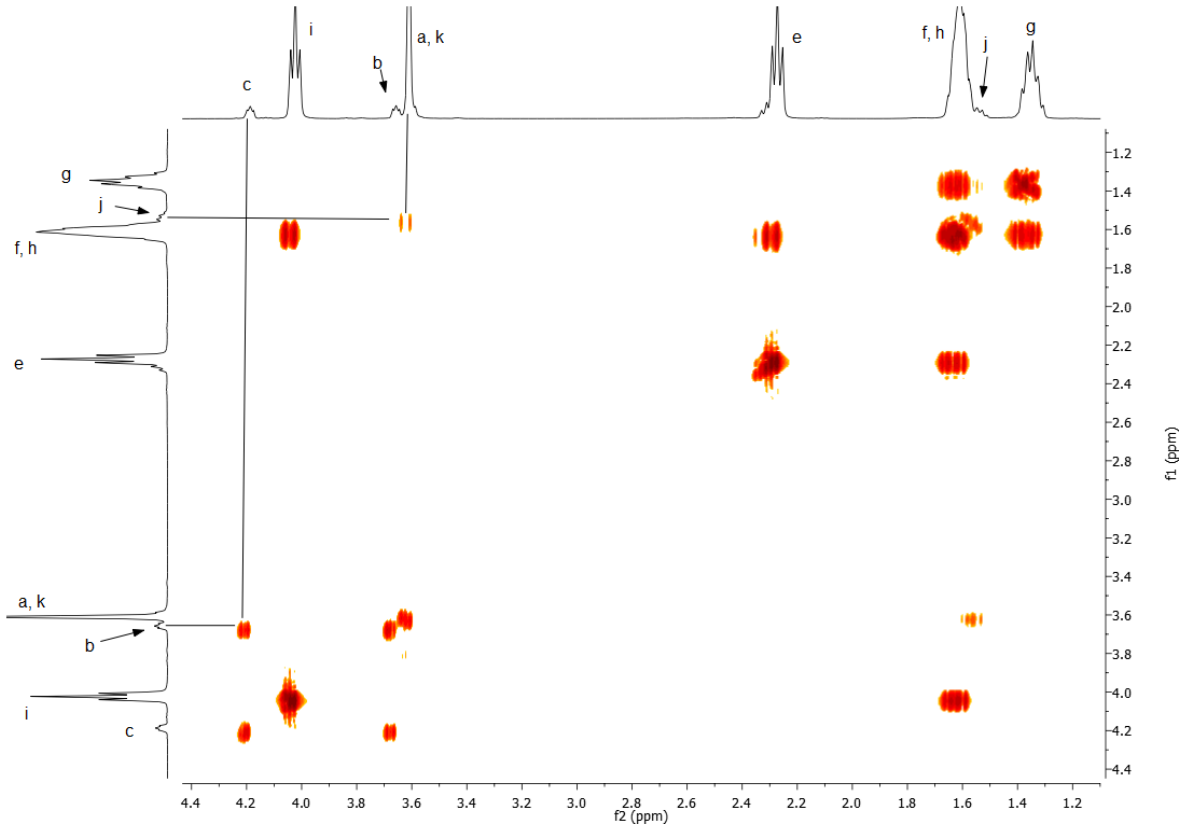

Figure 3.7: ^{1}H - ^{1}H COSY NMR spectrum of **3.2** in $CDCl_3$

The ^{13}C NMR spectrum of **3.2**, Figure 3.8, shows the characteristic PCL resonances at 24.6 ppm, 25.6 ppm, 28.4 ppm, 34.2 ppm and 64.2 ppm, attributing to methylene carbon atoms **f**, **g**, **h**, **e** and **i**, respectively. The downfield resonance at 173.6 ppm is attributed to carbonyl carbon atom **d** on the PCL moiety. The resonances at 32.4 ppm and 62.6 ppm are attributed to methylene carbon atoms **j** and **k** neighbouring the OH group on the PCL moiety, respectively. Furthermore, the resonances at 63.5 ppm, 69.2 ppm and 70.6 ppm are attributed to methylene carbon atoms **c**, **b** and **a** located on the central PEG moiety, respectively.

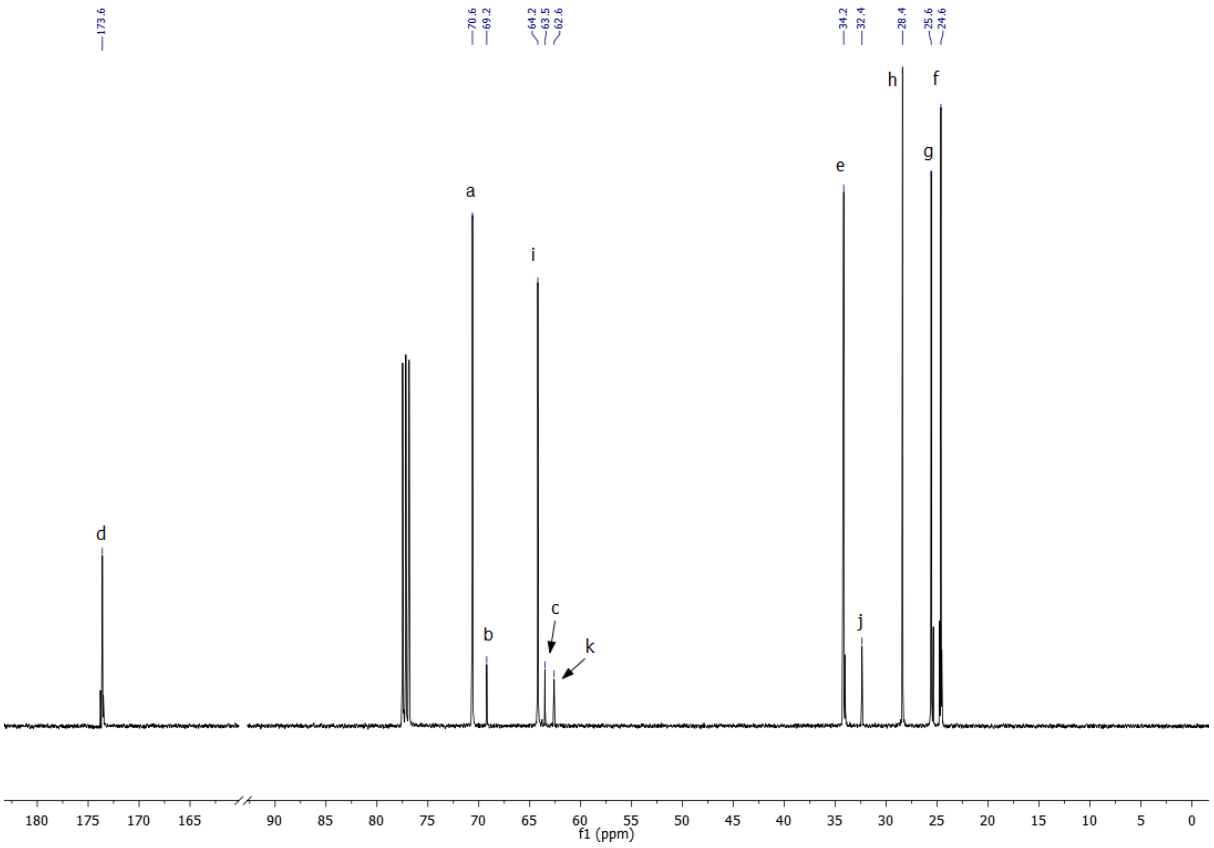

Figure 3.8: 100 MHz ^{13}C NMR spectrum of **3.2** in $CDCl_3$

Linear PCL-*b*-PEG-*b*-PCL **3.5** was synthesised by the ROP of ε-CL using PEG (M_n = 3350 g mol^{-1}) **3.4** macro-initiator and catalysed by $SnOct_2$, Scheme 3.2, to be used as a direct comparison to four-arm star $(PCL)_2$-*b*-(PEG)-*b*-$(PEG)_2$ **3.10 - 3.12**.

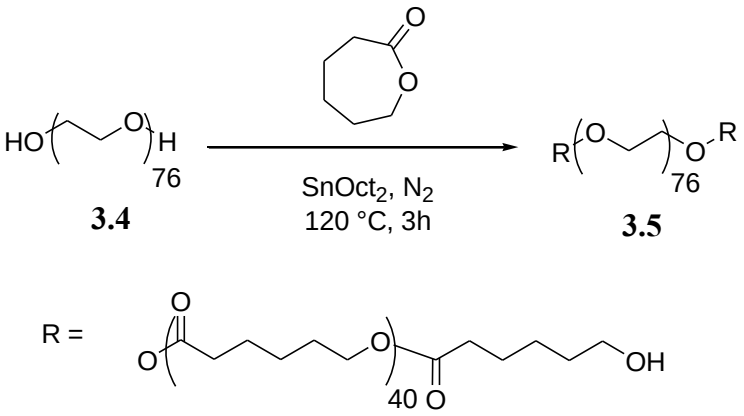

Scheme 3.2: Synthesis of linear PCL-*b*-PEG-*b*-PCL **3.5**

The ^{1}H NMR spectrum of **3.5**, Figure 3.9, shows the characteristic PCL methylene proton resonances at 1.34 ppm, 1.61 ppm, 2.26 ppm and 4.02 ppm, corresponding to **g**, **f**/**h**, **e** and **i**, respectively. Furthermore, the resonance at 3.60 ppm corresponds to methylene protons **a** and **b** located on the PEG moiety.

The degree of polymerisation ($\overline{DP}_{NMR}$) per arm of **3.5** was determined using Equation 3.1, where the integral of protons located on the PCL repeat unit (∫RU) were compared to the integral of protons located on the initiating PEG moiety (∫In). In this case, protons **c** on the PCL repeat unit were compared to protons **a** on the PEG initiator. The $\overline{DP}_{NMR}$ for **3.5** was found to be 44 and in good correlation to the theoretical degree of polymerisation ($\overline{DP}_{Th}$) of 40, determined from the feed ratio.

$$\overline{DP}_{NMR} = \frac{\left(\frac{\int \mathbf{RU}}{n_{H(RU)} \times n_{arms}}\right)}{\left(\frac{\int \mathbf{In}}{n_{H(In)}}\right)}$$

Equation 3.1

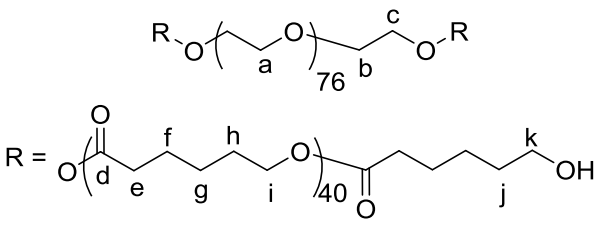

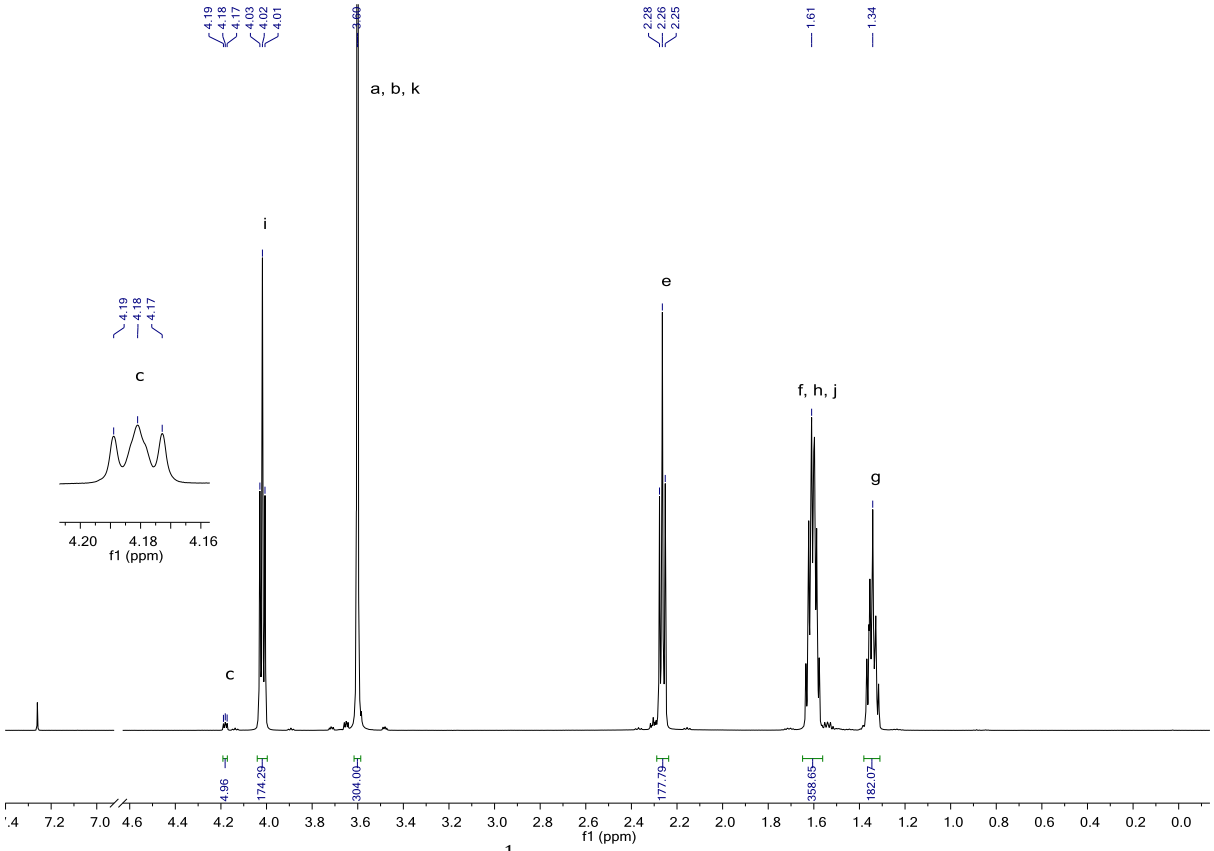

Figure 3.9: 600 MHz ^{1}H NMR spectrum of **3.5** in $CDCl_3$

The triplet resonance at 4.18 ppm and integrating to 4H is assigned to methylene protons **c**, neighbouring the oxygen atom of the ester group. This assignment is supported by the ^{1}H – ^{13}C HMBC spectrum, Figure 3.10, showing the proton resonance **c** at 4.18 ppm couple with neighbouring carbon atom resonances 69.2 ppm and 173.6 ppm, corresponding to **b** and **d**, respectively. The presence of the carbonyl carbon atom **c** in the ester group linking the PEG and PCL moieties, confirms the successful reaction and ROP of ε-CL from both OH groups on the PEG macro-initiator. Moreover, PCL methylene protons **j** and **k** neighbouring the OH group are assigned to resonances 1.61 ppm and 3.60 ppm, respectively. This assignment is supported by the ^{1}H – ^{13}C HMBC spectrum, Figure 3.10, showing methylene proton resonance **j** at 1.61 ppm, coupling with carbon atom resonance **k** at 62.6 ppm. Furthermore, methylene proton resonance **k** at 3.60 ppm can be seen to couple with carbon atom resonance **j**, at 32.4 ppm.

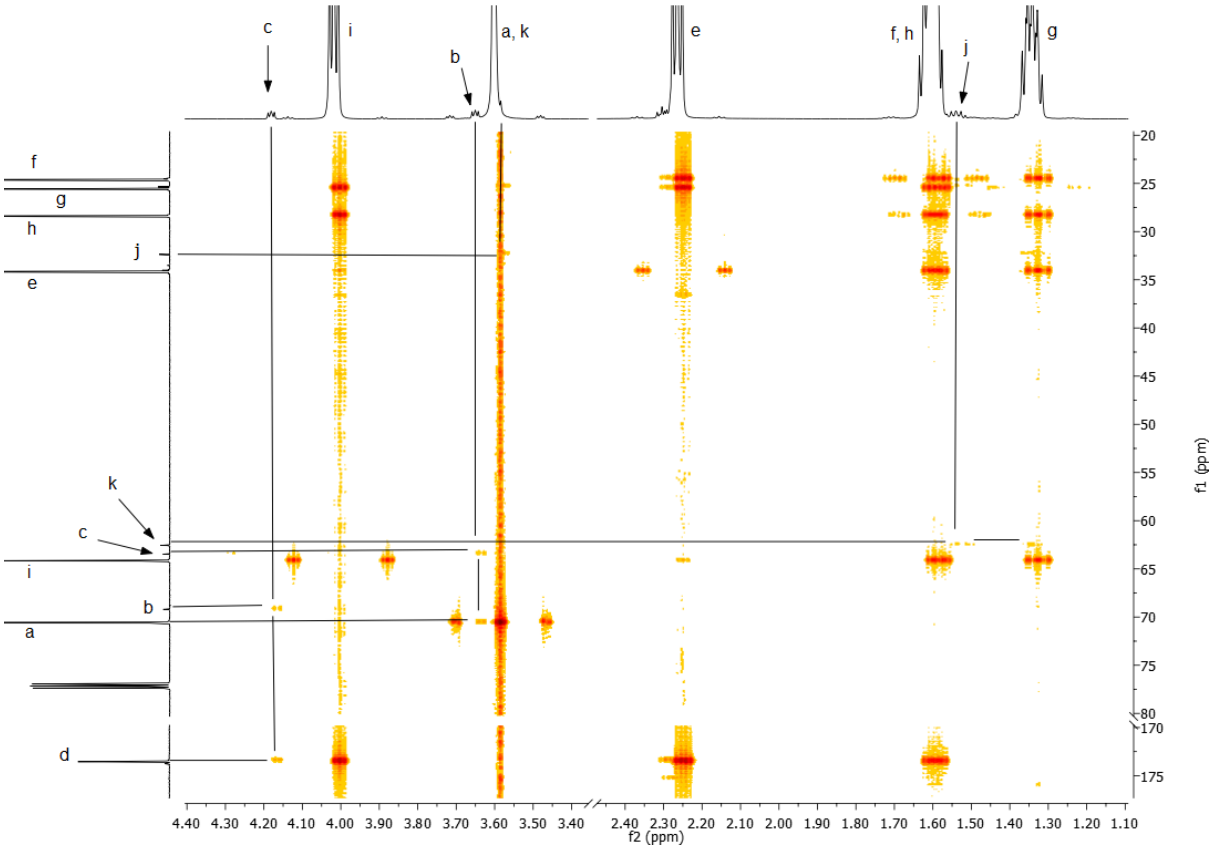

Figure 3.10: ^{1}H - ^{13}C HMBC spectrum of **3.5** in $CDCl_3$

The ^{13}C NMR spectrum of **3.5**, Figure 3.11, shows the characteristic PCL carbon atom resonances 24.6 ppm, 25.6 ppm, 28.4 ppm, 34.2 ppm and 64.2 ppm and 173.6 ppm, corresponding to **f**, **g**, **h**, **e** and **i**, respectively. The downfield resonance at 173.6 ppm is attributed to carbonyl carbon atom **d**. The resonances at 63.5 ppm, 69.2 ppm and 70.6 ppm are assigned to methylene carbon atoms **c**, **b** and **a**, in the PEG moiety, respectively. This assignment is supported by the ^{1}H – ^{13}C HSQC spectrum, Figure 3.12, showing proton resonances **c** and **b** at 4.18 ppm and 3.60 ppm, coupling to carbon atom resonances 63.5 ppm and 69.2 ppm, respectively. Furthermore, PCL carbon atoms **j** and **k** neighbouring the OH group are attributed to the resonances at 32.4 ppm and 62.6 ppm, respectively. These assignments are supported by the ^{1}H – ^{13}C HSQC spectrum of **3.5**, as carbon atom resonances 32.4 ppm and 62.6 ppm couple to proton resonances **j** and **k**, at 1.61 ppm and 3.60 ppm, respectively.

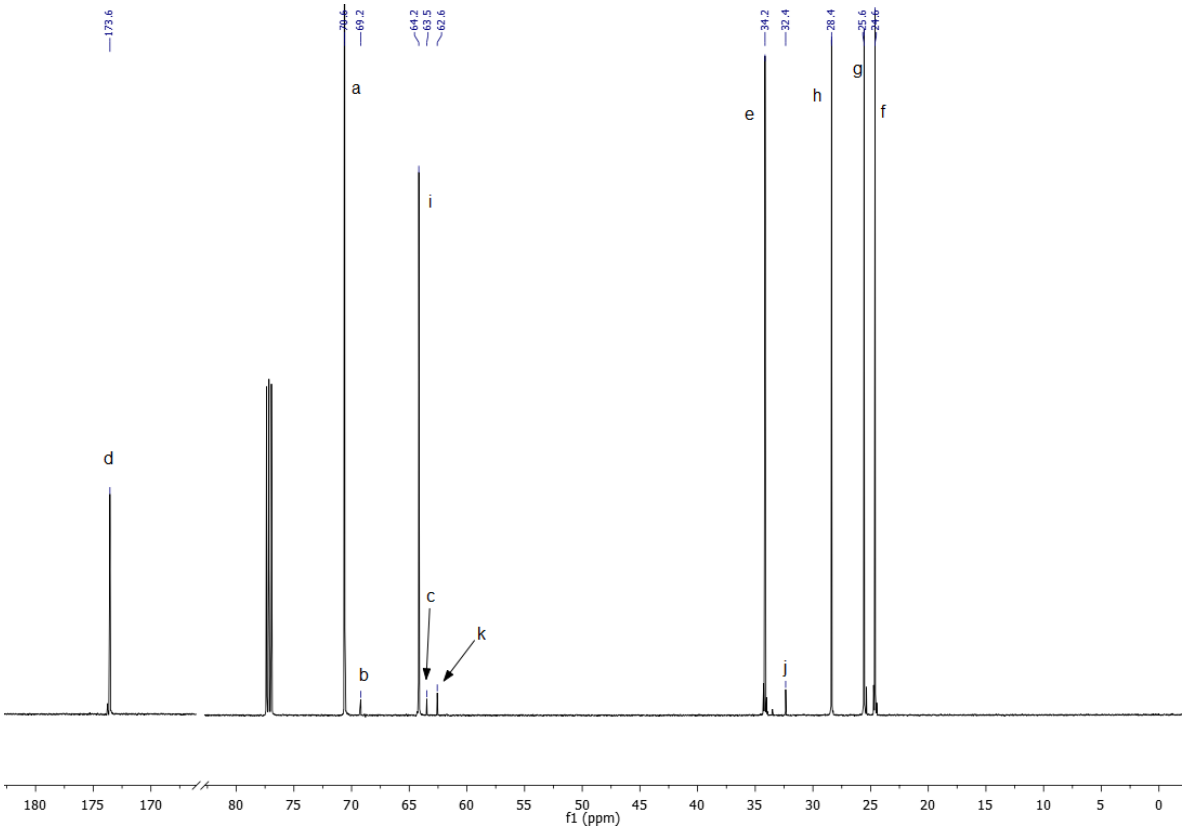

Figure 3.11: 150 MHz ^{13}C NMR spectrum of **3.5** in $CDCl_3$

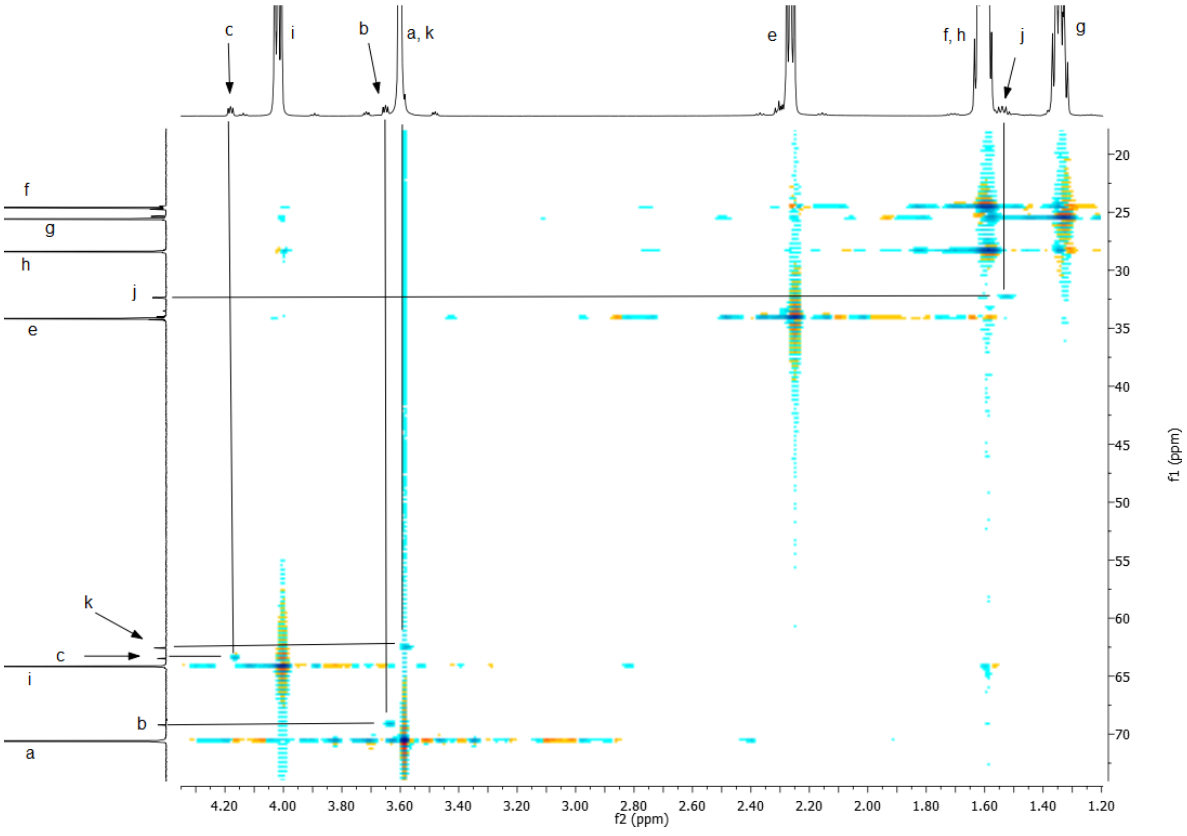

Figure 3.12: 150 MHz ^{1}H - ^{13}C HSQC spectrum of **3.5** in $CDCl_3$

The $\overline{\mathbf{DP}}_{NMR}$ and $\overline{\mathbf{DP}}_{Th}$ of linear copolymer **3.5** of 44 and 40, respectively, are in good correlation indicating a controlled ROP of ε-CL using PEG macro-initiator, Table 3.1. However, a relatively high Đ for **3.5** of 1.49 indicates a polydisperse product. This can be explained due to the disperse PEG starting material with a Đ of 1.77, used in the ROP. Furthermore, it can be noted the M_n^{SEC} of **3.5** at 0.89×10^4 g mol^{-1} is lower than M_n^{NMR} at 1.34×10^4 g mol^{-1} but significantly higher than that of the PEG starting material, showing a M_n^{SEC} of 0.14×10^4 g mol^{-1}. The increase in M_n^{SEC} and decrease in Đ from PEG to **3.5**, indicates a successful and controlled ROP of ε-CL using PEG.

Table 3.1: Molecular weight and Dispersity of linear PCL-*b*-PEG-*b*-PCL **3.5**

Sample	$\overline{DP}_{Th}$	$\overline{DP}_{NMR}$	M_n^{NMR}	M_n^{Th}	M_n^{SEC}	Đ
			$\times 10^{-4}$ / g mol^{-1}			
3.5	40	44	1.34	1.25	0.89	1.49
PEG[†] **3.4**	0	0	-	3.4	0.14	1.77

[†] PEG **3.4** (M_n = 3350 g mol^{-1}) purchased from Sigma Aldrich. The M_n^{NMR} could not be determined as all protons overlap in the ^{1}H NMR spectrum.

The degree of crystallinity (%χ_c) was determined using Equation 3.2 where ΔH_c is the measured enthalpy of crystallisation, determined by DSC. $\Delta H_c{}^*_{PCL}$ and $\Delta H_c{}^*_{PEG}$ are the standard enthalpies of crystallisation for completely crystalline PCL (139.5 J g^{-1}) and PEG (196.8 J g^{-1}).

$$\%Xc = \frac{\Delta Hc}{\%PCL(\Delta Hc^*PCL) + \%PEG(\Delta Hc^*PEG)} \qquad \text{Equation 3.2}$$

The $\%\chi_c$ and thermal analyses of linear copolymer **3.5** are shown in Table 3.2 and compared to that of linear PCL **2.2** (Synthesis outlined in Chapter 2.2.4.1). The incorporation of a PEG unit into PCL, significantly decreases the $\%\chi_c$ (from 71% to 29%) and increases the range of T_m (from 55 - 57 °C to 54 - 60 °C) in linear PCL homopolymer **2.2** and **3.5**, respectively. The same observation has previously been reported for PCL-PEG block copolymer and a PEG copolymer system with poly(1,4-butanediol succinate).[30,31,32]

Table 3.2: Thermal properties of linear PCL **2.2** and linear (PCL)-*b*-(PEG)-*b*-(PCL) **3.5**, determined by DSC

Sample	$\%PEG^{Th}$ content	PEG^{NMR} content	T_c	T_m	ΔH_c	ΔH_m	χ_c
	%		°C		J g^{-1}		%
3.5	27	25	31 - 36	54 - 60	40	40	29
Linear PCL[†] **2.2**	0	0	32 - 38	55 - 57	100	98	71

[†] Values taken from linear PCL **2.2** with a central ethylene glycol initiator unit (Chapter 2, section 2.3.6, Table 2.5)

3.3.2 Four-arm Star $(PCL)_2$-*b*-(PEG)-*b*-$(PCL)_2$] 3.10 – 3.12

A series of novel four-arm star $(PCL)_2$-*b*-(PEG)-*b*-$(PEG)_2$ **3.10 - 3.12** containing a central PEG **3.4** moiety and varying $\overline{DP}_{Th}$ of PCL arms were synthesised in a four step syntheses, outlined in Scheme 3.3. The $\overline{DP}_{Th}$ was 20, 50 and 100, for **3.10**, **3.11** and **3.12**, respectively. The syntheses involved the hydroxyl-protection of the bisMPA **3.6** moiety using acetic anhydride to give **3.7**, followed by the coupling of **3.7** with PEG **3.4** using N,N'-dicyclohexylcarbodiimide (DCC) and 4-dimethylaminopyridine (DMAP), to give **3.8**. Subsequently, the acetal groups on **3.8** were removed under acidic conditions to give **3.9**, followed by the ROP of ε-CL using the tetra-hydroxyl PEG macro-initiator **3.9** and $SnOct_2$ catalyst, to give four-arm star copolymers **3.10 - 3.12**.

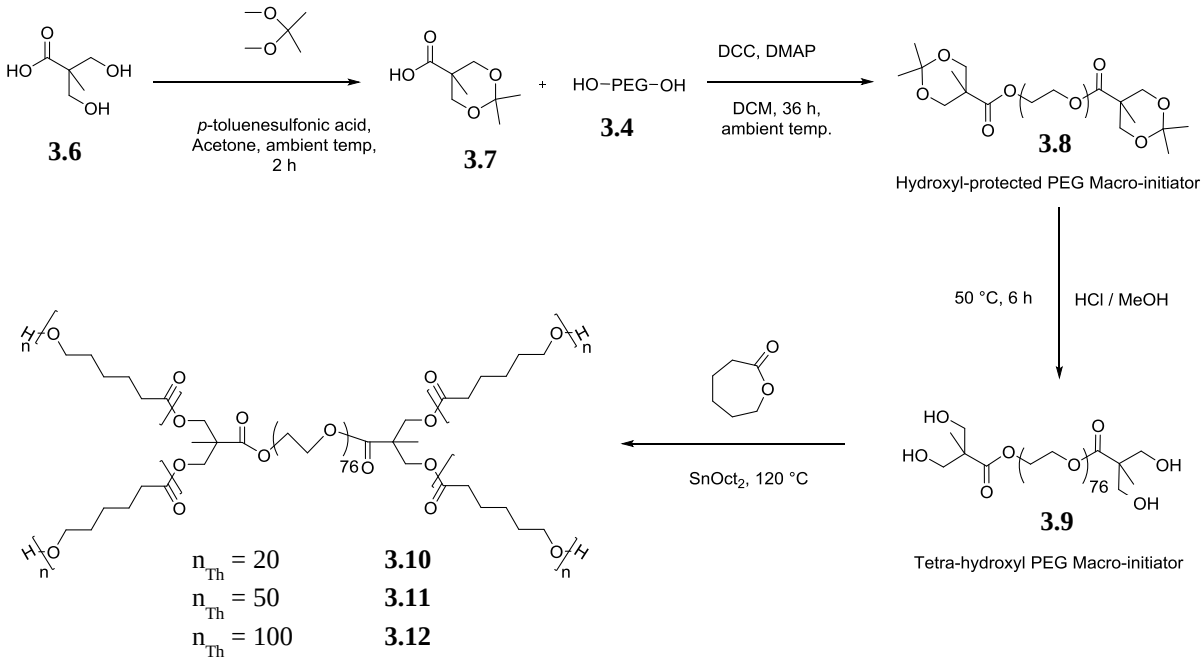

Scheme 3.3: Synthesis of four-arm star $(PCL)_2$-*b*-(PEG)-*b*-$(PCL)_2$ **3.10 – 3.12**

3.3.2.1 Isopropylidene-2,2'-bis(methoxyl) Propionic Acid 3.7

The 1° alcohol groups of the bis-MPA **3.6** moiety were protected with an acetal group, to give **3.7**, Scheme 3.3.

The ^{1}H NMR spectrum of **3.7**, Figure 3.13, is consistent with those in the literature.[29] The disappearance of the broad OH resonance and appearance of resonances at 1.39 ppm and 1.43 ppm attributed to methyl protons **f** and **f'** on the acetal group, indicate the successful 1° alcohol group protection on the bisMPA moiety.

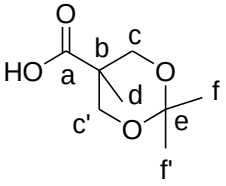

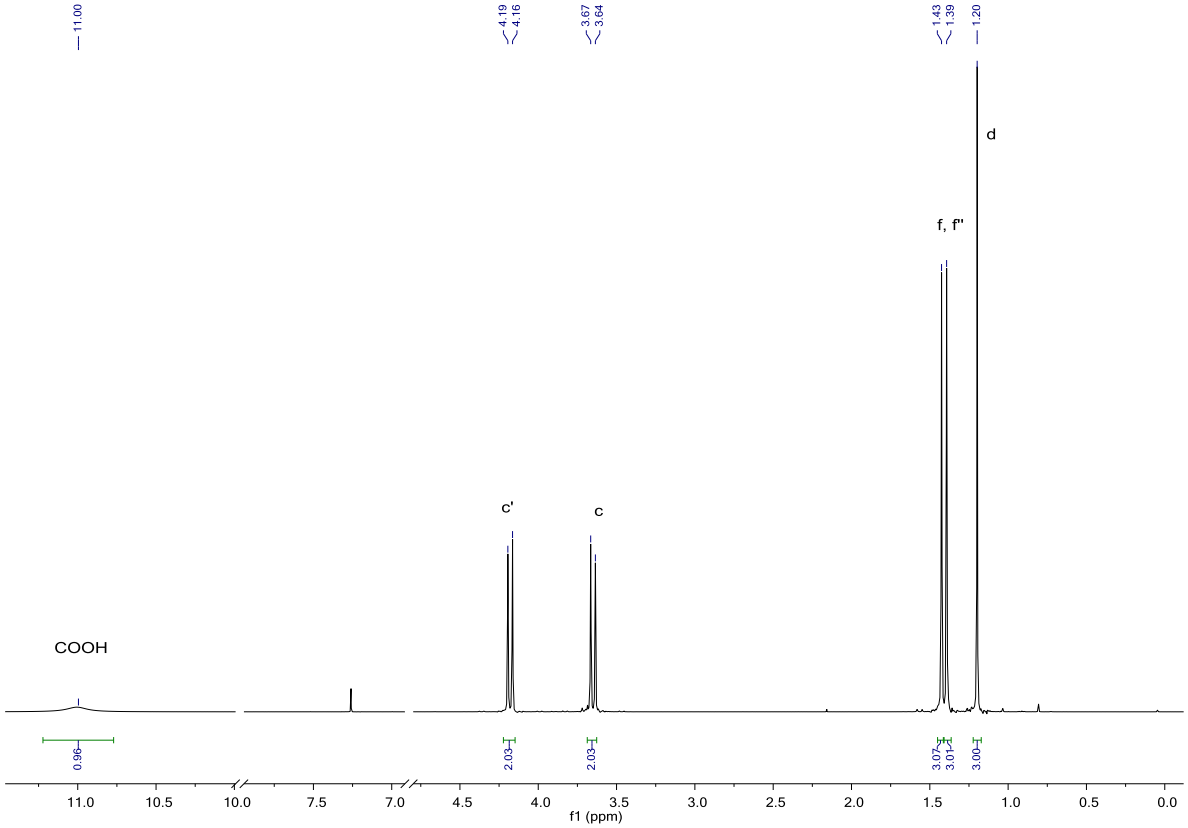

Figure 3.13: 400 MHz ^{1}H NMR spectrum of **3.7** in $CDCl_3$

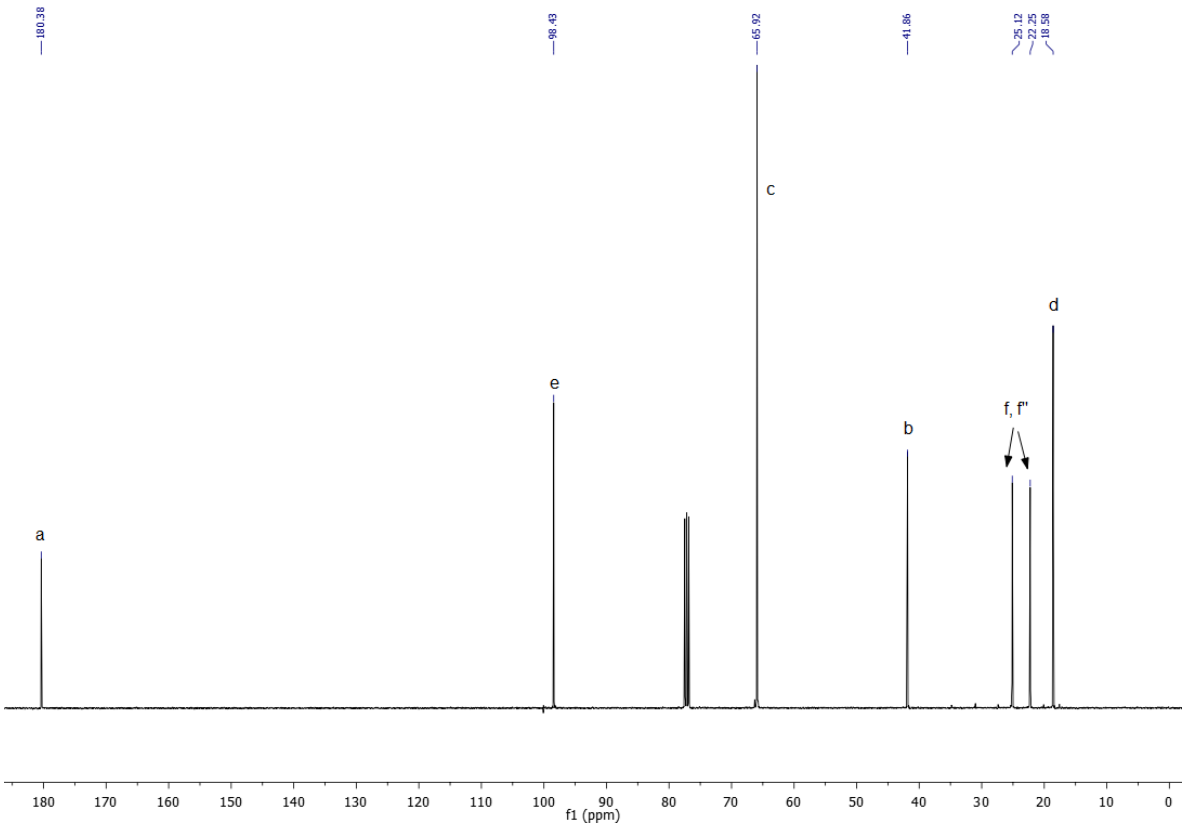

Figure 3.14: 100 MHz ^{13}C NMR spectrum of **3.7** in $CDCl_3$

Furthermore, the ^{13}C NMR spectrum, Figure 3.14, shows the appearance of resonances at 22.3 ppm, 25.1 ppm and 98.4 ppm, correlating to methyl carbon atoms **f**, **f'** and quarternary carbon atom **e**, on the acetal group, respectively. This confirms the complete 1° alcohol protection on the bisMPA moiety.

3.3.2.2 Hydroxyl-Protected PEG Macro-initiator 3.8

Hydroxyl-protected PEG macro-initiator **3.8** was synthesised by the coupling reaction between the hydroxyl-protected bisMPA moiety **3.7** and PEG **3.4**, using DCC and DMAP, Scheme 3.3.

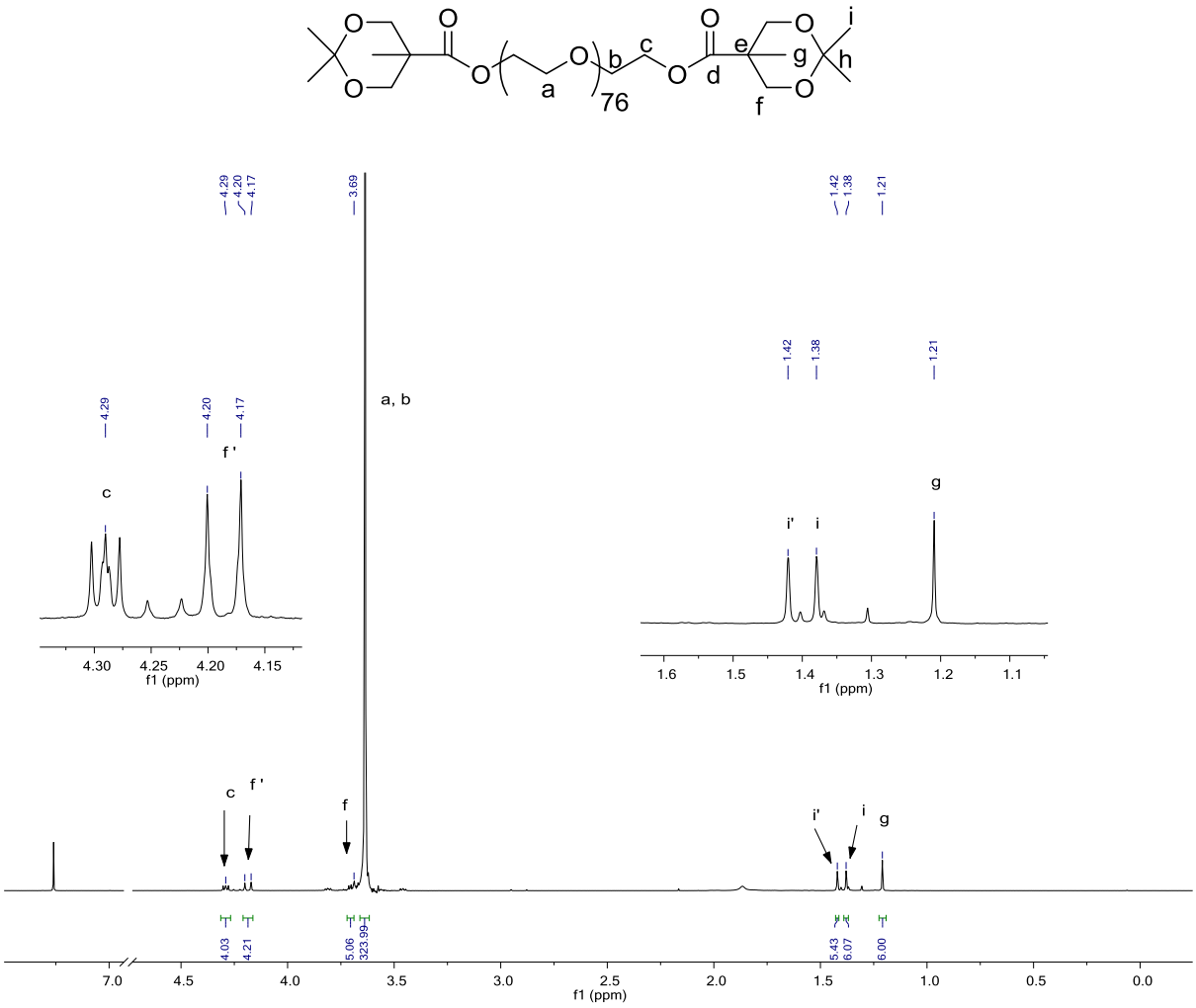

Figure 3.15: 400 MHz ^{1}H NMR spectrum of **3.8** in $CDCl_3$

The ^{1}H NMR spectrum of **3.8**, Figure 3.15, is presented after dialysis in DCM for 3 days in order to remove any unreacted hydroxyl-protected bisMPA moiety **3.7**, as a molar excess of **3.7** was used in the coupling reaction. The large resonance at 3.69 ppm and integrating to 323H, are attributed to methylene protons **a** and **b** on the PEG moiety. Resonances at 1.21 ppm, 1.38 ppm and 1.42 ppm, each integrating to 6H, are attributed to methyl protons **g**, **i** and **i'** located on the hydroxyl-protected bisMPA moiety, **3.7**, respectively. Resonances at 3.69 ppm and 4.18 ppm are attributed to **f** and **f'** methylene protons also located on the bisMPA moiety. Furthermore, the resonance at 4.29 ppm and integrating to 4H, is attributed to methylene protons **c** located on the PEG moiety and neighbouring the oxygen atom of the ester group. The presence of these proton resonances after dialysis indicates a successful coupling reaction between the PEG **3.4** unit and the hydroxyl-protected bisMPA moiety, **3.7**.

FT-IR analysis of **3.8** shows an absorbance at 1734 cm^{-1} attributing to the carbonyl bond in the ester group, confirming the successful coupling reaction of the PEG **3.4** and hydroxyl-protected bis-HMPA **3.7** moieties, Appendix 3.1. Furthermore, the absence of a broad absorbance in the region of 3200 - 3550 cm^{-1} attributing to an OH group, confirms the complete reaction of the PEG **3.4** moiety, containing terminal OH groups.

3.3.2.3 PEG Tetra-hydroxyl Macro-initiator 3.9

Tetra-hydroxyl PEG macro-initiator was synthesised by the removal of the acetal groups in **3.8**, to give **3.9**, Scheme 3.3.

The ^{1}H NMR spectrum of **3.9**, Figure 3.16, shows resonances at 1.08 ppm, integrating to 6H and 3.67 - 3.78 ppm attributed to methyl protons **g** and methylene protons **f** on the bisMPA moiety, respectively. Resonances at 3.59 ppm integrating to 348H, and 4.28 ppm integrating to 4H, are attributed to methylene protons **a** and **c** on the PEG moiety, respectively.

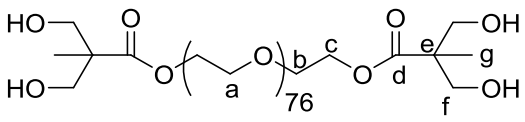

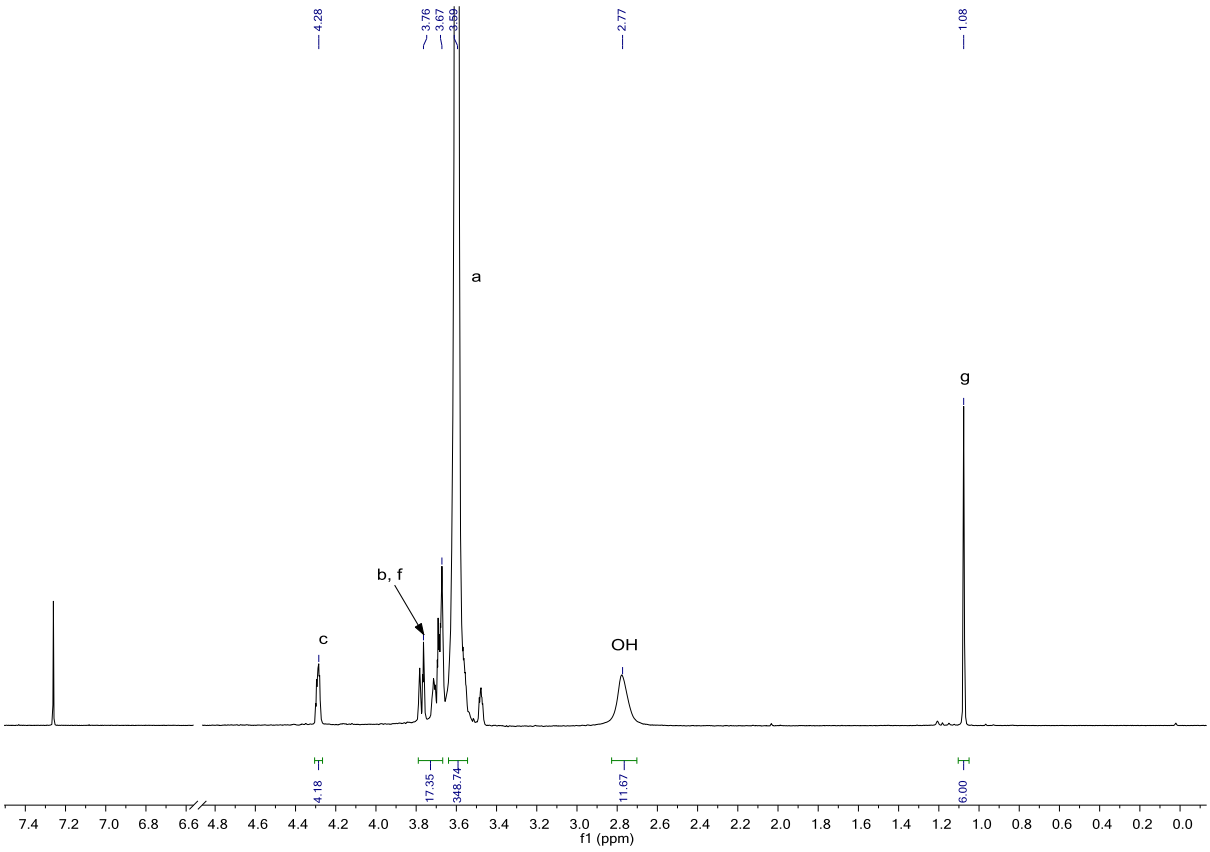

Figure 3.16: 600 MHz ^{1}H NMR spectrum of **3.9** in $CDCl_3$

Furthermore, the $^{1}H - ^{13}C$ HMBC spectrum, Figure 3.17, shows proton resonance **g** at 1.08 ppm, couples with neighbouring carbon atom resonances **e**, **f** and **d** at 49.7 ppm, 67.4 ppm and 175.7 ppm, respectively. Proton resonance **f** at 3.67 – 3.78 ppm can be seen to couple with carbon atom resonances **g**, **e** and **d** at 17.2 ppm, 49.7 ppm and 175.7 ppm, respectively. Moreover, proton resonance **c** at 4.28 ppm is shown to couple to carbon atom resonances **b** and **d**, at 68.8 ppm and 175.7 ppm, respectively. This confirms the ester group was not cleaved during the removal of the acetal moieties under acidic conditions.

However, the integration of 348H for methylene protons **a** on the PEG unit was higher than the expected value of 304H, in respect to the integrations of protons **g** (6H) on the bisMPA moiety and protons **c** (4H), neighbouring the ester group. This indicates a small amount of ester bonds in **3.5** could have been hydrolysed to give the starting material, PEG **3.4**. Purification and separation of PEG **3.4** from **3.5** was not possible as ^{1}H NMR analysis of **3.5** after dialysis in deionised water at ambient temperature, showed an increase in the integration of PEG protons **a**, in respect to bisMPA protons **g**. This was due to further hydrolysis of the ester bonds in de-ionised water.

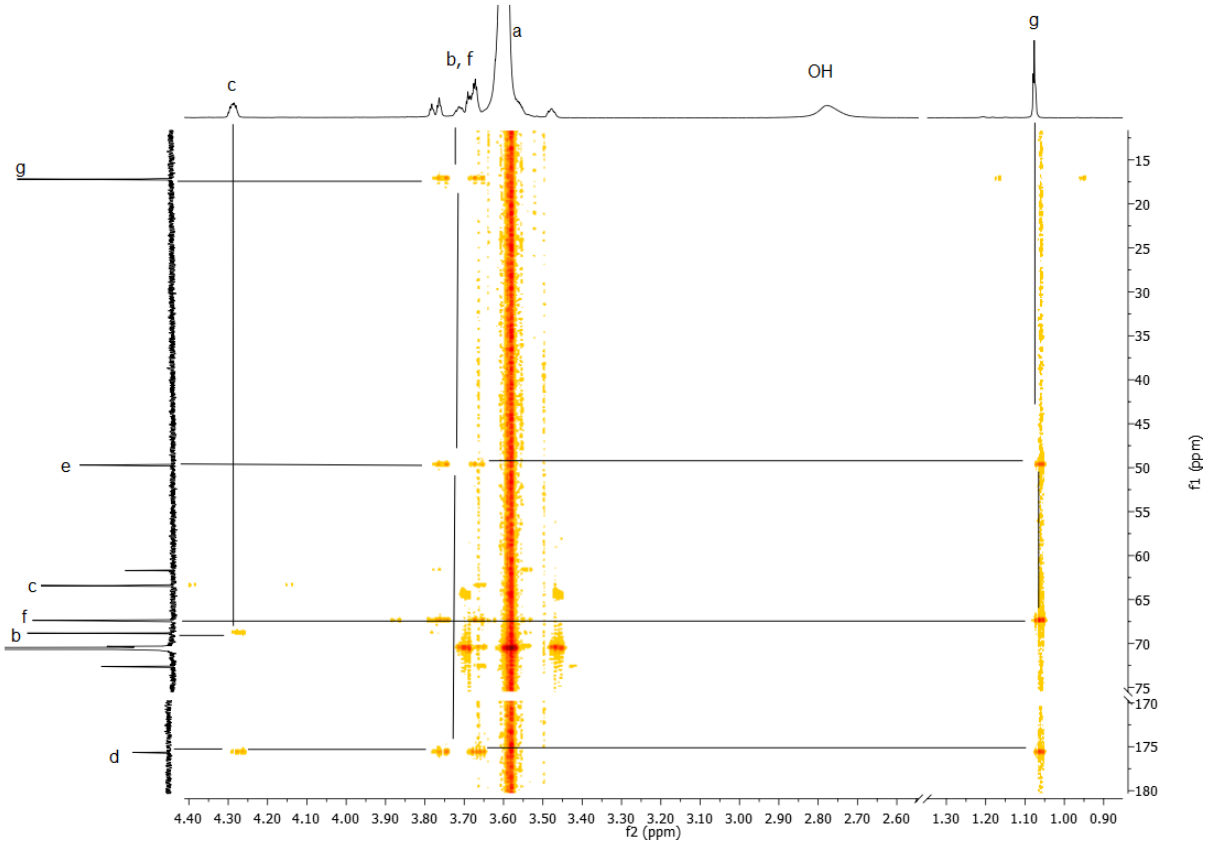

Figure 3.17: ^{1}H - ^{13}C HMBC spectrum of **3.9** in $CDCl_3$

The ^{13}C NMR spectrum of **3.9**, Figure 3.18, shows resonances at 49.7 ppm, 67.4 ppm and 17.2 ppm attributed to the quarternary carbon atom **e**, methylene carbon atom **f** and methyl carbon atom **g** located on the bisMPA moiety, respectively. The ^{1}H – ^{13}C HSQC spectrum, Figure 3.19, confirms these assignments, as quarternary carbon atom **e** at 49.7 ppm does not couple with any protons. Furthermore, carbon atom resonances 67.4 ppm and 17.2 ppm can be seen to couple with proton resonances **f** and **g** at 3.67 – 3.78 ppm and 1.08 ppm, respectively.

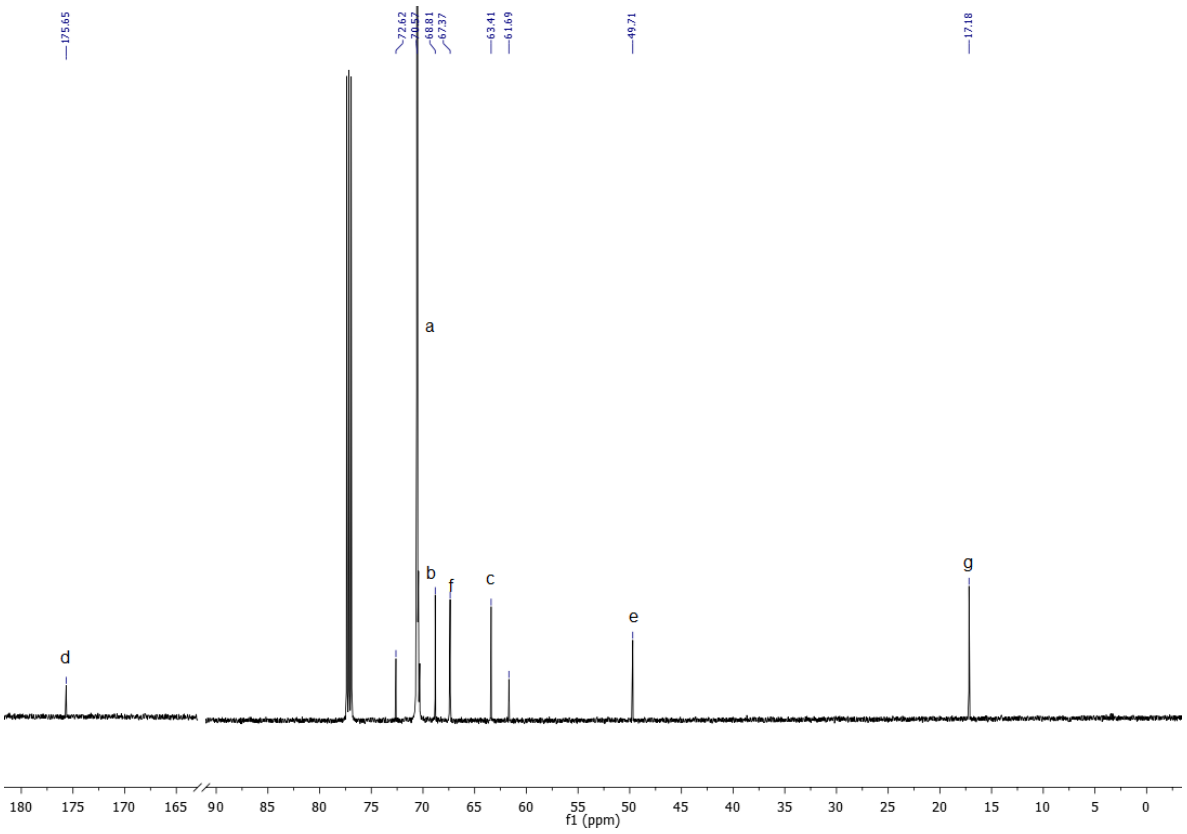

Figure 3.18: 150 MHz ^{13}C NMR spectrum of **3.9** in $CDCl_3$

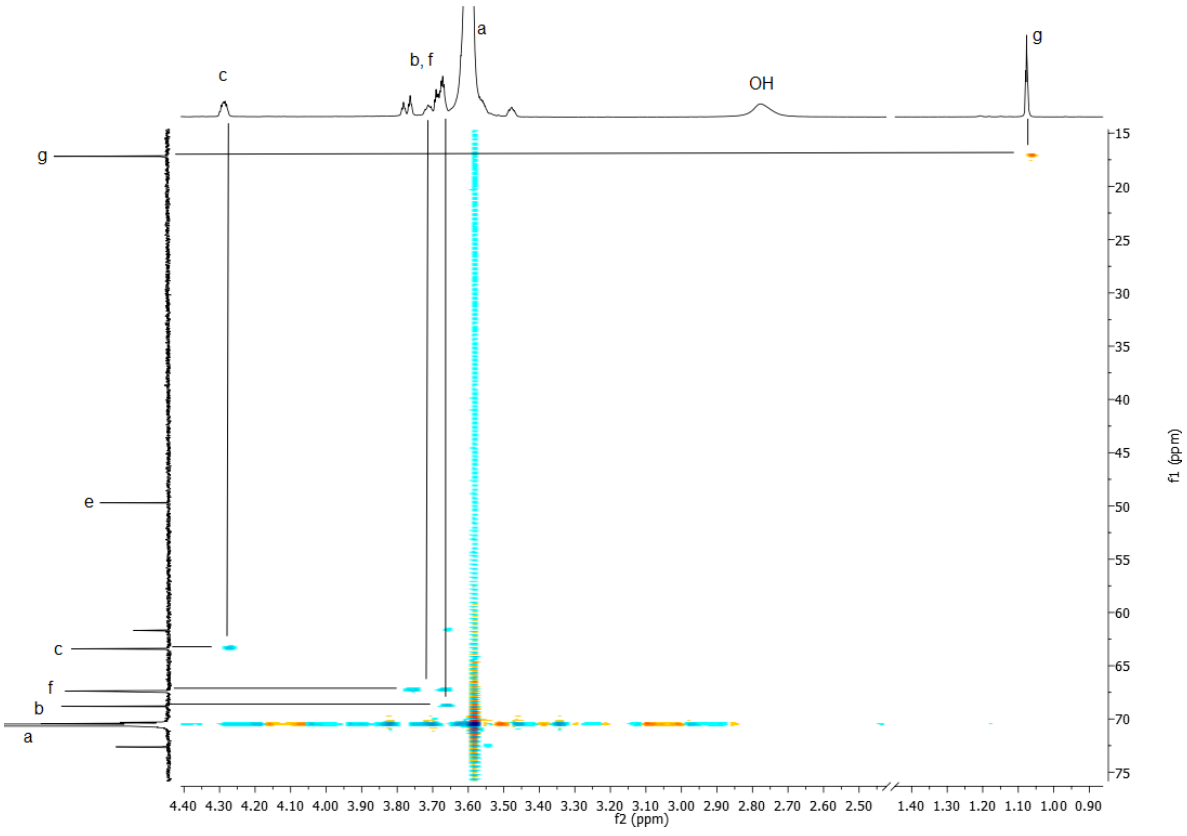

Figure 3.19: ^{1}H - ^{13}C HSQC spectrum of **3.9** in $CDCl_3$

The ^{13}C NMR spectrum, Figure 3.18, shows methylene carbon atom resonances at 70.6 ppm, 68.8 ppm and 63.4 ppm, attributed to **a**, **b** and **c** on the PEG moiety in **3.9**, respectively. The downfield resonance at 175.7 ppm is attributed to carbonyl carbon atom **d** in the ester group. Furthermore, carbonyl carbon atom resonance **d** shifted from 174.0 ppm in the hydroxyl-protected PEG macro-initiator **3.8**, to 175.7 ppm in **3.6**, confirming complete removal of the acetal moieties. Moreover, the presence of carbonyl carbon atom resonance **d** indicates the ester group was not hydrolysed during the acetal removal reaction under acidic conditions. However, it must be noted that unassigned resonances in Figure 3.18, at 61.7 ppm and 72.6 ppm can be attributed to methylene carbon atoms neighbouring the terminal OH in the PEG **3.4** starting material. As seen in the ^{1}H NMR spectrum, Figure 3.16, with the higher than expected integration of methylene PEG protons **a**, this suggests a small amount of ester groups have been hydrolysed during the removal of the acetal moieties, converting a small amount of **3.9** into the PEG **3.4** starting material.

FT-IR analysis of **3.9** shows a broad absorbance at 3490 cm^{-1} attributed to the OH groups on the bisMPA moieties, confirming successful removal of the acetal group, Appendix 3.2. Furthermore, the absorbance at 1737 cm^{-1} attributed to the carbonyl bond in the ester group, confirms this group was not fully hydrolysed during the removal of the acetal groups under acidic conditions.

3.3.2.4 Four-arm Star $(PCL)_2$-*b*-(PEG)-b-$(PCL)_2$ 3.10 – 3.12

A series of novel four-arm star $(PCL)_2$-*b*-(PEG)-*b*-$(PCL)_2$ **3.10 – 3.12** were synthesised in the ROP of ε-CL catalysed by $SnOct_2$ and using tetra-hydroxyl PEG macro-initiator **3.9**, Scheme 3.3. The feed ratios of ε-CL to **3.9** were varied to produce four-arm structures with a central PEG moiety and $\overline{DP}_{Th}$ of 20, 50 and 100 per arm for **3.10**, **3.11** and **3.12**, respectively.

The ^{1}H NMR spectrum of **3.10**, Figure 3.20, shows the characteristic PCL resonances at 1.34 ppm, 1.61 ppm, 2.27 ppm and 4.02 ppm, attributing to methylene protons **k**, **j**/**l**/**q**, **i** and **p**, respectively. Resonances at 3.60 ppm and 4.20 ppm are attributed to methylene protons **a**/**b** and **c** located on the PEG moiety, respectively. Furthermore, resonances at 1.21 ppm integrating to 6H, and 4.20 ppm are attributed to methyl protons **g** and methylene protons **f**, located on the bisMPA moiety, respectively. The presence of proton

resonances attributing to the PEG, bisMPA linkage and PCL moieties, indicate the successful ROP of ε-CL using tetra-hydroxyl macro-initiator **3.9**.

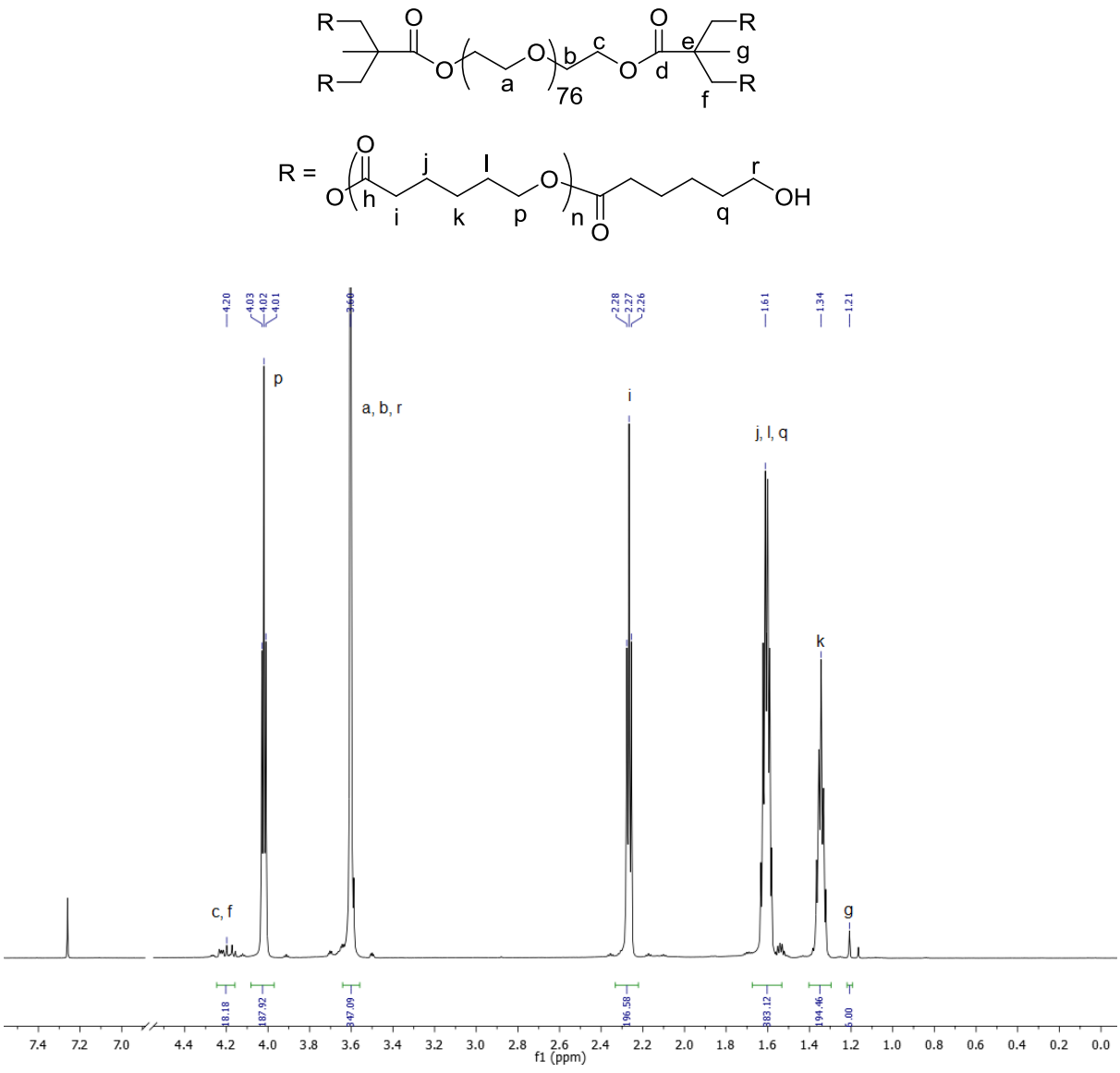

Figure 3.20: 600 MHz ^{1}H NMR spectrum of **3.10** in $CDCl_3$

Due to overlapping resonances, it is not possible to integrate methylene protons **r** in PCL neighbouring the OH group, with initiator bisMPA methyl protons, **g**. This would provide evidence to confirm ROP has occurred from all four initiating OH groups on **3.9**. However, it can be seen that the resonance corresponding to methylene protons **f**, has shifted from 3.67-3.78 ppm in **3.9**, Figure 3.16 in section 3.3.2.3, to 4.20 ppm in **3.10**,

Figure 3.20. This downfield resonance shift is due to methylene protons **f**, changing from neighbouring the oxygen atom in the OH group in **3.9**, to neighbouring the oxygen atom in the ester group, in **3.10**. This proton resonance shift suggests ROP has occurred from all four OH initiating groups on the tetra-hydroxyl PEG macro-initiator **3.9**, indicating that modification has occurred to an indeterminate extent.

The ^{13}C NMR spectrum, Figure 3.21, shows the characteristic PCL resonances at 24.6 ppm, 25.6 ppm, 28.4 ppm, 34.2 ppm and 64.2 ppm, arising from methylene carbon atoms **j**, **k**, **l**, **i** and **p**, respectively. PCL methylene carbon atoms **q** and **r** neighbouring the OH group, can be seen at resonances 32.4 ppm and 62.6 ppm, respectively. This is confirmed by the ^{1}H – ^{13}C HMBC spectrum, Figure 3.22, showing proton resonance **q** at 1.61 ppm coupling to carbon atom resonance **r** at 62.6 ppm.

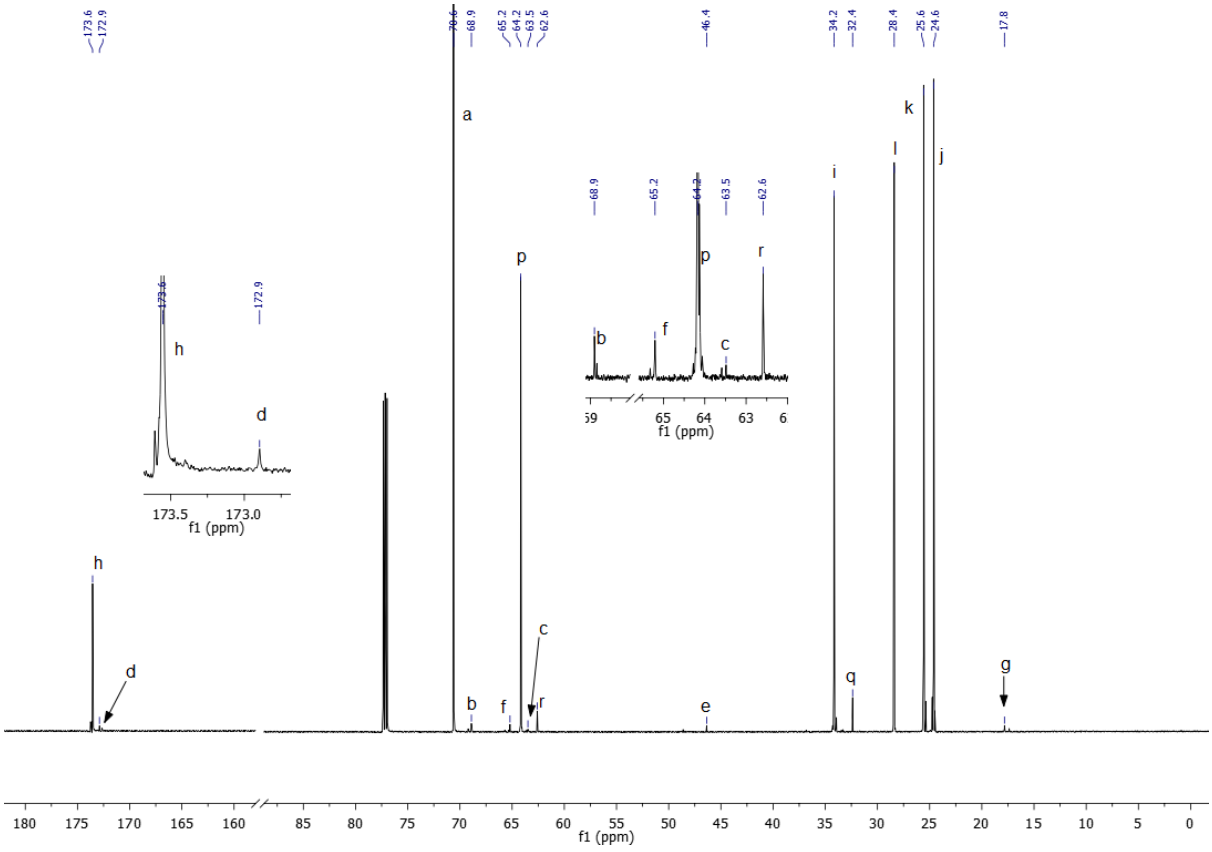

Figure 3.21: 150 MHz ^{13}C NMR spectrum of **3.10** in $CDCl_3$

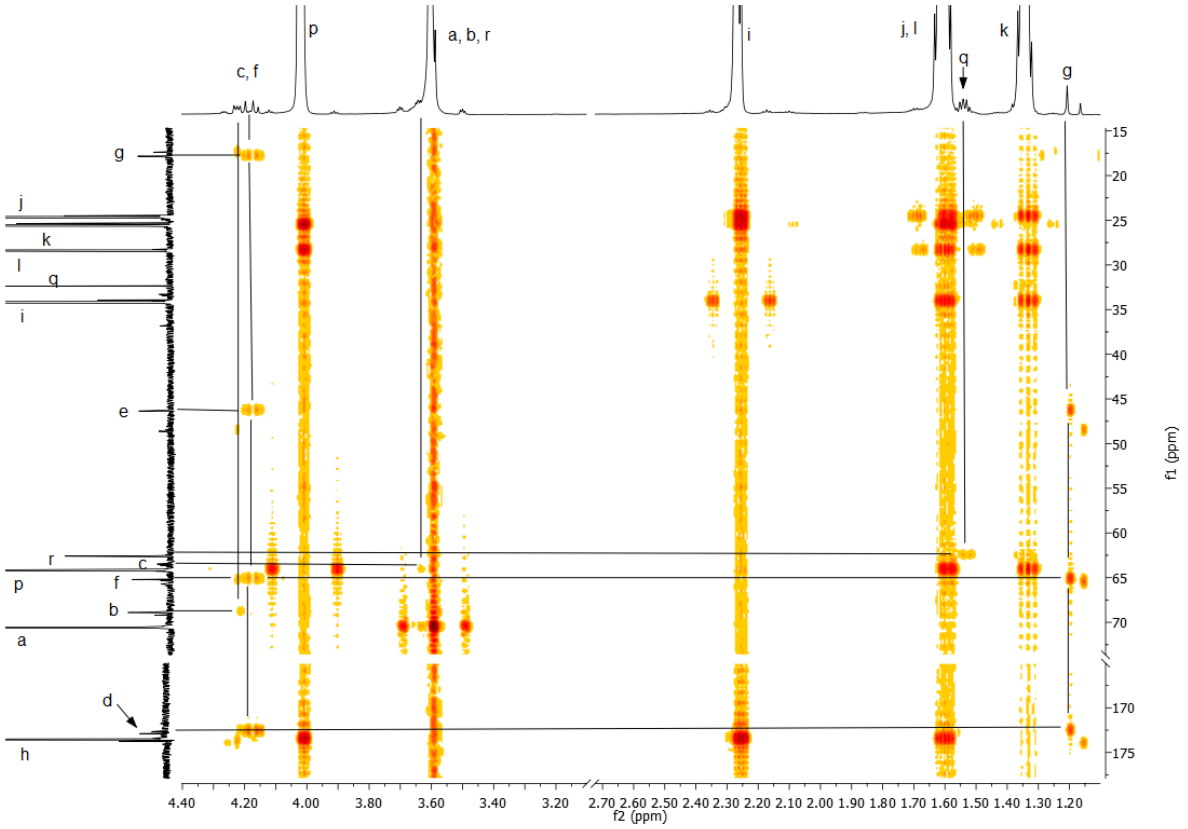

Figure 3.22**:** ^{1}H - ^{13}C HMBC spectrum of **3.10** in $CDCl_3$

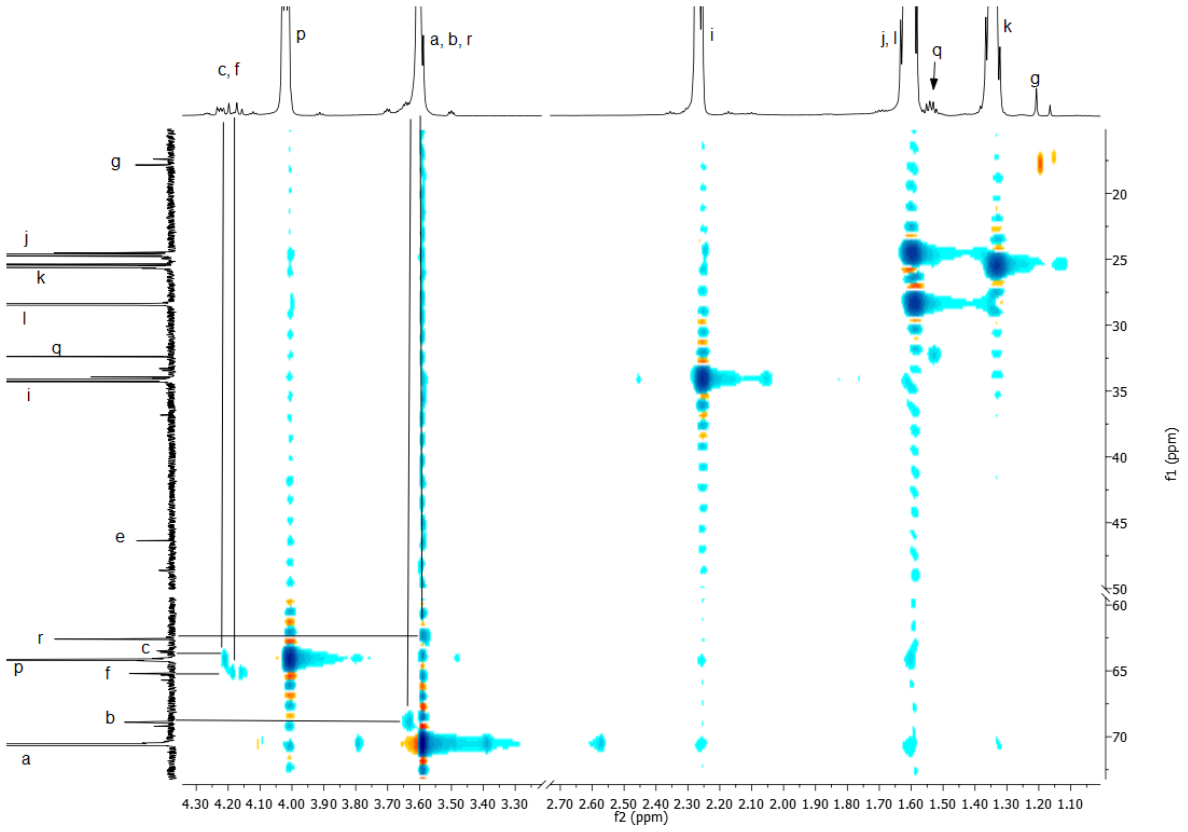

Figure 3.23: ^{1}H - ^{13}C HSQC spectrum of **3.10** in $CDCl_3$

Resonances at 70.6 ppm, 68.9 ppm and 63.5 ppm are attributed to carbon atoms **a**, **b** and **c** on the PEG moiety, respectively. This is supported by the ^{1}H – ^{13}C HSQC spectrum, Figure 3.23, showing carbon atom resonances 70.6 ppm, 68.9 ppm and 63.5 ppm coupling to proton resonances **a**, **b**, **c** at 3.60 ppm, 3.60 ppm and 4.20 ppm, respectively.

The ^{13}C NMR spectrum shows downfield carbonyl carbon atom resonances at 172.9 ppm and 173.6 ppm that are attributed to **d** on the bisMPA-PEG linkage, and **h** in the PCL repeat unit, respectively. This assignment is confirmed in the ^{1}H – ^{13}C HMBC spectrum, Figure 3.22, where carbonyl carbon atom resonance **d** at 172.9 ppm, couples to proton resonances **f** and **g** on the bisMPA moiety, at 4.20 ppm and 1.21 ppm, respectively.

The FT-IR spectrum of **3.10** shows an O-H stretch at 3498 cm^{-1} corresponding to the chain end OH groups in PCL, Appendix 3.3. Furthermore, an intense carbonyl bond absorbance is seen at 1720 cm^{-1} corresponding to the ester groups in the PCL moieties. These absorbances, together with the presence of ether groups at 1108 cm^{-1}, support the successful ROP reaction of ε-CL using PEG macro-initiator **3.9** to give the four-arm star copolymer **3.10**.

Table 3.3: Molecular weights and Đ of PEG **3.4**, tetra-hydroxyl PEG macro-initiator **3.9** and four-arm star copolymers **3.10 – 3.12**, determined by ^{1}H NMR and SEC analyses

Sample	$\overline{DP}_{Th}$	$\overline{DP}_{NMR}$	M_n^{Th}	M_n^{NMR}	M_n^{SEC}	M_w^{SEC}	Đ
			$\times 10^{-4}$ / g mol^{-1}				
†PEG **3.4**	0	0	0.34	-	0.14	0.25	1.77
3.9	0	0	0.37	0.42	0.74	0.91	1.24
3.10	20	24	1.28	1.46	1.06	1.39	1.32
3.11	50	52	2.65	2.74	1.34	1.90	1.42
3.12	100	114	4.93	5.57	1.63	2.46	1.51

† M_n^{NMR} for PEG **3.4** could not be accurately determined due to overlapping resonances in the ^{1}H NMR spectrum

There is good correlation in star copolymers **3.10 - 3.12** for $\overline{DP}_{Th}$ of 20, 50 and 100, and $\overline{DP}_{NMR}$ of 24, 52 and 114, respectively, Table 3.3. However, poor correlation is seen in

3.10 - 3.12 for M_n^{SEC} of 1.06 × 10^4 g mol^{-1}, 1.34 × 10^4 g mol^{-1} and 1.63 × 10^4 g mol^{-1} with M_n^{NMR} values of 1.46 × 10^4 g mol^{-1}, 2.74 × 10^4 g mol^{-1} and 5.57× 10^4 g mol^{-1}, respectively. This is due to the denser star copolymer architecture, exhibiting a different hydrodynamic volume to the linear polymer used as a calibration standard in SEC.

A Đ of 1.24 is found for the tetra-hydroxyl PEG macro-initiator **3.9**. This is believed to be due to PEG exhibiting a Đ of 1.77 which is also responsible for the high Đ of 1.32, 1.42 and 1.51, seen in star copolymers **3.10 - 3.12**, incorporating the central core PEG initiator, respectively. Moreover, an increase in Đ from 1.32 to 1.51 can be seen with an increase in the $\overline{DP}_{NMR}$ from 24 to 114 in star copolymers **3.10 - 3.12**. This can be explained by the decrease in polymer chain mobility as the ROP proceeds in bulk conditions, and the reaction mixture increases in viscosity. The viscosity is greatly increased in the higher molecular weight polymers with higher $\overline{DP}$, leading to a higher Đ and indicating control of ROP decreases with increasing $\overline{DP}$.

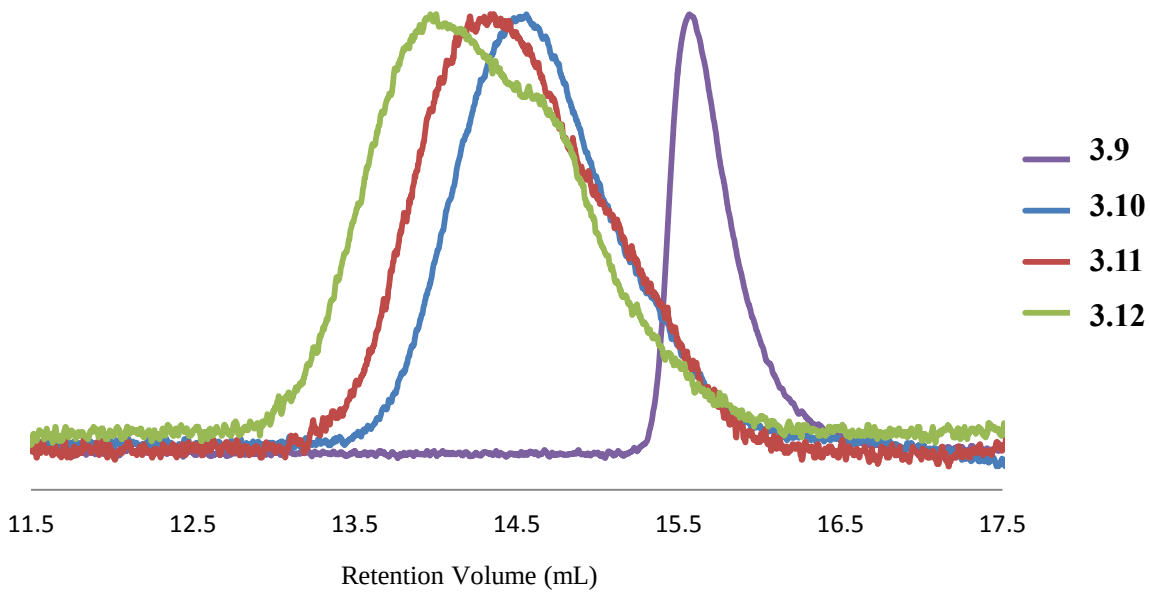

Figure 3.24: Normalised SEC chromatograms of linear tetra-hydroxyl PEG macro-initiator **3.9** precursor to the series of four-arm star copolymers **3.10 - 3.12**

The SEC chromatograms for the tetra-hydroxyl PEG macro-initiator **3.9** and four-arm star copolymers **3.10 - 3.12**, are shown in Figure 3.24. It can be noted that a lower molecular weight shoulder is seen for linear PEG precursor **3.9** as well as star copolymers **3.10 - 3.12** and this is the most pronounced in the highest molecular weight star copolymer **3.12**. The observed lower molecular weight shoulder in star copolymers **3.10 - 3.12** can be explained firstly by using polydisperse PEG **3.4** in the synthesis and hence precursor **3.9** with a Đ of 1.24. Furthermore, the lack of control in the ROP of ε-CL onto multi-hydroxyl initiators may have given a range of $\overline{DP}$ for each arm, therefore, increasing the Đ.

Table 3.4: Thermal properties and $\%\chi_c$ of linear triblock copolymer PCL-*b*-PEG-*b*-PCL **3.5** and four-arm star copolymers **3.10 - 3.12**, determined by DSC analyses at 10 °C min^{-1}

Sample	PEG^{Th}	PEG^{NMR}	T_c	T_m	ΔH_c	ΔH_m	χ_c
	%		°C		J g^{-1}		%
3.5	27	27	31 - 36	54 - 60	40	40	29
3.10	26	23	27 - 32	50 - 54	18	26	12
3.11	13	12	33 - 38	52 - 59	24	36	16
3.12	7	6	31 - 38	53 - 60	47	68	33

The $\%\chi_c$ and thermal properties were determined by DSC analyses for star copolymers **3.10 - 3.12** and compared to linear copolymer **3.5**, Table 3.4. The T_c shows a small increase from 31 - 36 °C to 31 - 38 °C with a decrease in amorphous $\%PEG^{NMR}$ content from 27% to 6% in copolymers **3.5** to **3.10 - 3.12**, respectively. The same observation has been made for PCL-PEG block copolymers and poly[(1,4-butanediol succinate)-*co*-(ethylene glycol)] systems.[32,31] Similarly, T_m is seen to increase from 50 - 54 °C to 53 - 60 °C with a decrease in $\%PEG^{NMR}$ content from 23% to 6% in copolymers **3.10 - 3.12**, respectively. This has been observed in the literature with PCL-*b*-PEG-*b*-PCL triblock copolymer systems.[33,34]

ΔH_c and ΔH_m are both seen to increase from 18 J g^{-1} to 47 J g^{-1} and 26 to 68 J g^{-1} with a decrease in $\%PEG^{NMR}$ content from 23% to 6% in star copolymers **3.10** to **3.12**. This can be explained by the increase in $\%\chi_c$ from 12% to 33% with a decrease in amorphous $\%PEG^{NMR}$ content from 23% to 6% and an increase in $\overline{DP}_{NMR}$ from 24 to 114, in star copolymers **3.10** to **3.12**. The increase in crystalline PCL content and decrease in amorphous PEG content in star copolymers **3.10 - 3.12** causes an overall increase in the $\%\chi_c$ of the copolymer.

Linear copolymer **3.5**, shows a significantly higher $\%\chi_c$ than star copolymer **3.10,** 29% and 12%, despite having a similar $\%PEG^{NMR}$ content of 27% and 26%, respectively. This is due to the increased mobility of polymer chains in linear copolymer **3.5**, in comparison to the PCL chains attached to a central core PEG unit in star copolymer **3.10**. The increased mobility in **3.5** allows the polymers chains to align themselves in a more ordered crystalline arrangement, therefore, increasing the $\%\chi_c$.

3.3.4 Contact Angle

The hydrophilic nature of copolymer films **3.5** and **3.10 - 3.12** was determined *via* contact angle analysis, and compared to that of star PCL homopolymer, Figure 3.25. It can be seen that star PCL is very hydrophobic, showing the largest initial contact angle of 86° with negligible decrease after 30 seconds to 83°, Figure 3.25(e). On the other hand, the initial contact angle is seen to increase in star copolymers **3.10 - 3.12** from 63° to 76°, as the $\%PEG^{NMR}$ content decreases from 26% to 7%, Figures 3.25(b-d).

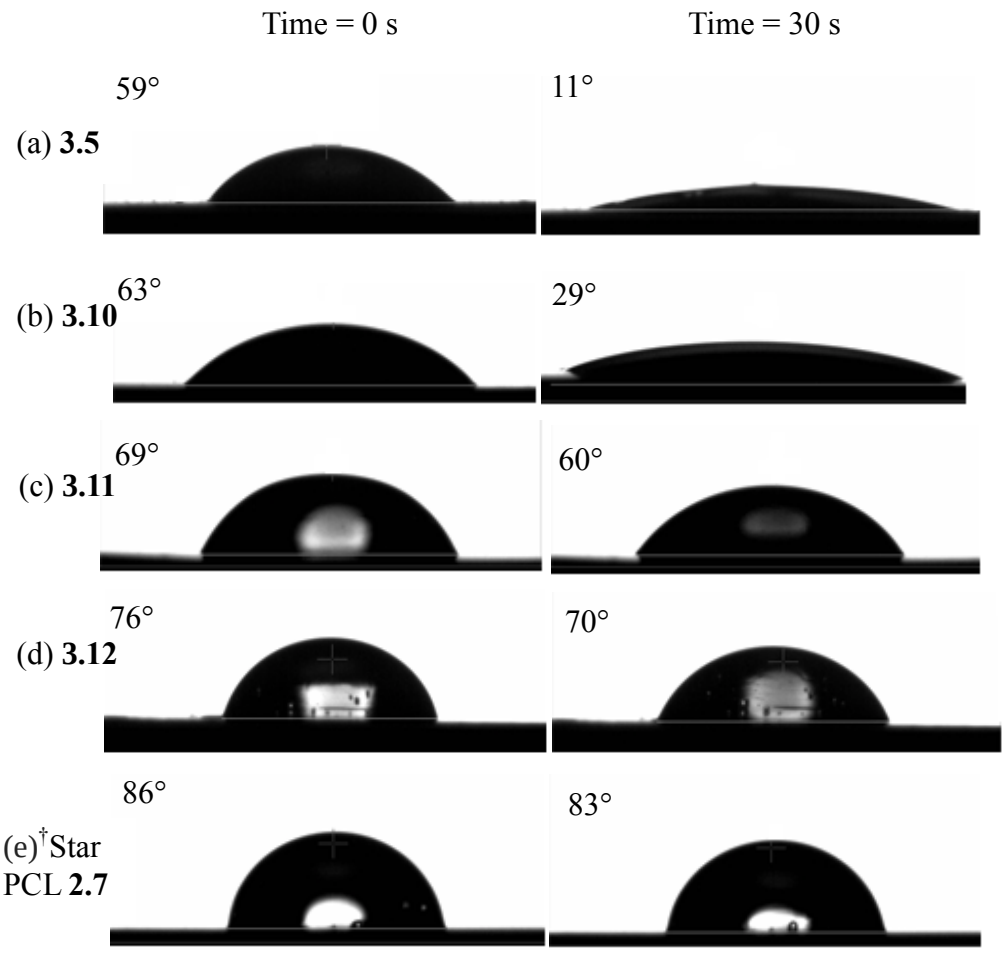

Figure 3.25: Contact Angle at time = 0 s and time = 30 s of (a) linear copolymer **3.5**; (b) star copolymer **3.10**; (c) star copolymer **3.11**; (d) star copolymer **3.12** and (e) †Star PCL **2.7**. The reported contact angle is an average of the left and right contact angle and an average of five repeat measurements. The calculated error for the reported contact angles is ± 2.3%

†Star PCL **2.7** synthesised in Chapter 2 Section 2.2.4.2.4

The change in contact angle as a function of time for star PCL, linear copolymer **3.5** and **3.10 - 3.12**, is presented as a graph, Figure 3.26. Minimal change in contact angle over 30 s is seen for star PCL and star copolymers **3.11 - 3.12** containing 0%, 13% and 7% PEG^{NMR} content, respectively. However, star copolymer **3.10** and linear copolymer **3.5** with 23% and 27% PEG^{NMR} content, respectively, show a significant decrease in contact angle

within the first few seconds. The lowest initial contact angle at 59° as well as the fastest decrease in contact angle is seen for linear copolymer **3.5**, as the hydrophilic PEG unit is less shielded by the two PCL arms, compared to the four PCL arm structures, **3.10 - 3.12**. Furthermore, a clear trend of the decrease in the rate of wetting can be seen from **3.10 - 3.12** to star PCL, with a decrease in the % PEG^{NMR} content from 23% to 0%.

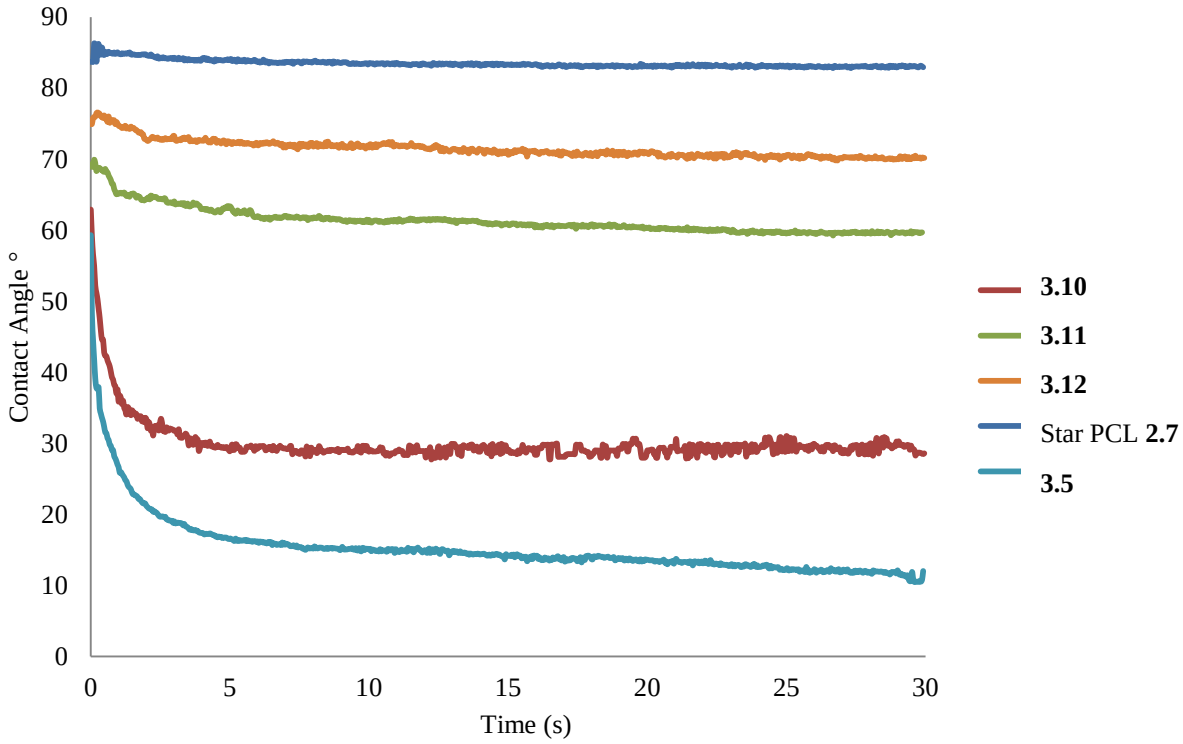

Figure 3.26: Change in Contact Angle over 30 s for films of †star PCL **2.7**, linear triblock copolymer **3.5** and four-arm star copolymers **3.10 - 3.12**. The reported contact angle is an average of the left and right contact angle and an average of five repeat measurements.

†Star PCL **2.7** synthesised in Chapter 2 Section 2.2.4.2.4

3.3.5 Water Uptake

The %water uptake (%WU) of linear copolymer **3.5** and star copolymers **3.10 - 3.12** were measured to determine their hydrophilic nature and the degree of swelling in the polymer films, Table 3.5. Furthermore, the %WU of star PCL was measured and used as a comparison. The %WU can be seen to decrease from 33 to 3% with decreasing $\%PEG^{NMR}$ content from 26 to 7% in star copolymers **3.10 - 3.12**. The highest %WU of 39% was seen with linear copolymer **3.5**, with a similar $\%PEG^{NMR}$ content to **3.10** of 27%, indicating there is a higher degree of swelling in linear copolymer structures compared to a four-arm star copolymer structure. This can be explained by the increased shielding of the hydrophilic PEG moiety by four hydrophobic PCL arms in **3.10 - 3.12**, compared to only two PCL arms in linear **3.5**. Moreover, star PCL showed no %WU, confirming the hydrophobic nature of PCL and that the incorporation of PEG imparts hydrophilicity to the polymer. These results support the contact angle measurements obtained for star copolymer **3.10 - 3.12** and star PCL, Figure 3.25 Section 3.3.4. It is anticipated that the degree of swelling experienced by the polymer films with %WU will significantly affect the enzymatic degradation results.

Table 3.5: %WU of polymer films for star PCL **2.7**, linear triblock copolymer **3.5** and four-arm star copolymers **3.10 - 3.12** in PBS solution (pH 7.4) at 37 °C after 2 days

Sample	% WU	$\%PEG^{NMR}$
3.5	36	27
3.10	33	26
3.11	10	13
3.12	3	7
†Star PCL **2.7**	0	0

†Star PCL **2.7** synthesised in Chapter 2 Section 2.2.4.2.4

3.3.6 Enzymatic Degradation of Copolymers containing a Hydrophilic PEG Moiety

The % mass loss as a function of time for linear copolymer **3.5** and star copolymer **3.10**, containing 27% and 26% PEG^{NMR} content, respectively, after 6 days of enzymatic degradation is presented in Figure 3.27. It can be seen that linear copolymer **3.5** degraded at a faster rate, >97% mass loss in 4 days, than star copolymer **3.10**, >99% mass loss in 6 days, despite having similar PEG^{NMR} content. This indicates a linear copolymer structure, PCL-*b*-PEG-*b*-PCL, has a higher rate of enzymatic degradation than a four-arm star copolymer structure $(PCL)_2$-*b*-PEG-*b*-$(PCL)_2$. This can be explained by the greater hydrophilicity, higher degree of swelling in water and greater polymer chain mobility experienced in linear copolymer **3.5** in comparison to star copolymer **3.10**. These attributes increase the likelihood of *pseudomonas cepacia* enzyme to access and hydrolyse the ester groups contained in the PCL moiety and therefore, increase the rate of enzymatic degradation.

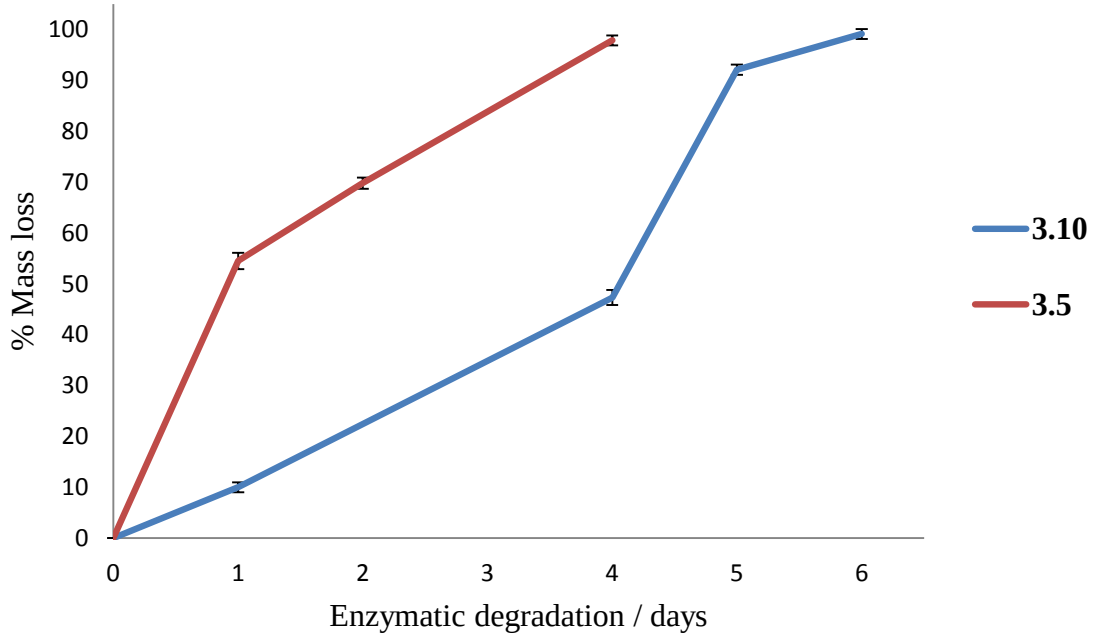

Figure 3.27: % Mass loss of linear triblock copolymer **3.5** and four-arm star copolymer **3.10** over 6 days of enzymatic degradation using *pseudomonas cepacia* lipase in PBS solution (pH 7.4) at 37 °C. The reported % mass losses are the averages of three repeat measurements and % error bars shown.

The % mass losses of star copolymers **3.10 - 3.12** are compared with that of star PCL and linear copolymer **3.5** over 15 days of enzymatic degradation, Figure 3.28. Star PCL exhibits the slowest degradation rate of >94% mass loss in 15 days of enzymatic degradation, in comparison to all copolymers containing a hydrophilic PEG moiety, **3.5** and **3.10 - 3.12**. This indicates the incorporation of a central PEG moiety into a linear or star PCL structure greatly increases the rate of enzymatic degradation. It can be seen that star copolymers **3.10 - 3.12** degrade at a similar rate of >92% mass loss in 6-7 days. However, the degradation of star copolymer **3.12** proceeds at a slightly slower rate than **3.10** and **3.11** due to a combination of increased hydrophobicity, M_n, $\overline{DP}$ and $\%\chi_c$.

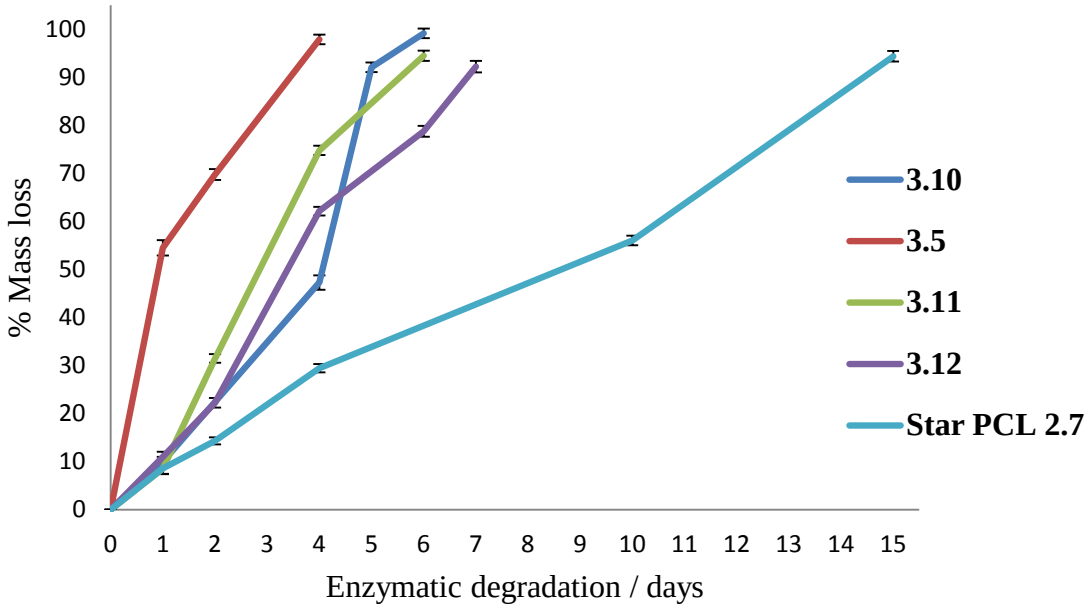

Figure 3.28: % Mass loss of linear triblock copolymer **3.5**, four arm star copolymers **3.10 - 3.12** and [†]star PCL **2.7** as a function of time (days) of enzymatic degradation using *pseudomonas cepacia* lipase in PBS solution (pH 7.4) at 37 °C. The % mass losses are an average of three repeat measurements and % error bars shown.

[†]Star PCL **2.7** synthesised in Chapter 2 Section 2.2.4.2.4

The thermal properties of polymers **3.5, 3.10 - 3.12** and star PCL were measured before and after enzymatic degradation at several time intervals, Table 3.6. Example DSC thermograms for star copolymer **3.12** after 1, 2, 4 and 6 days of enzymatic degradation using *pseudomonas cepacia* lipase can be found in Appendices 3.3 – 3.6. Table 3.6 shows a significant increase in $\%\chi_c$ after 1 or 2 days of enzymatic degradation can be seen for **3.5, 3.10 - 3.12** and star PCL. This has been observed in the literature with the hydrolytic degradation of polyglycolide, polylactide and poly[(lactide)-*co*-(glycolide)] in PBS solution (pH = 7.4) at 37 °C.[35] This can be explained by the enzyme firstly degrading the amorphous regions of the polymer film, increasing the overall crystallinity of the polymer. Furthermore, the $\%\chi_c$ will be increased by the removal of the water-soluble PEG moiety due to cleavage of the PCL arms, as well as the formation of shorter PCL fragments leading to less chain entanglement.

A slight increase in T_c for star PCL, **3.5** and **3.10 - 3.12** supports the increase in $\%\chi_c$ observed during enzymatic degradation. The T_m for polymers **3.5, 3.10 - 3.12** and star PCL **2.7** generally remained unchanged during enzymatic degradation. These results are consistent with previously reported data of the enzymatic degradation of linear PCL using *pseudomonas cepacia* lipase.[27]

Table 3.6: Thermal properties and $\%\chi_c$ of polymer films linear triblock copolymer **3.5**, four-arm star copolymers **3.10 - 3.12** and star PCL **2.7** before and after enzymatic degradation with *pseudomonas cepacia* lipase in PBS solution (pH 7.4) at 37 °C, determined using DSC at 10 °C min^{-1}

Sample	PEG	Time	Mass Loss	ΔH_m	ΔH_c	χ_c	T_m	T_c
	%	days	%	J g^{-1}		%	°C	
3.10	28	0	-	26	18	12	50 - 54	27 - 32
		1	10.0	64	44	29	53 - 60	31 - 36
		4	47.3	43	40	26	49 – 55	29 - 34
		5	92.1	41	41	26	50 - 58	28 - 34
		6	99.1	-	-	-	-	-
3.11	14	0	-	36	24	16	52 - 59	33 - 38
		1	8.6	88	60	41	50 - 60	33 - 38
		2	31.5	58	60	41	51 - 56	33 - 37
		4	74.8	72	71	48	51 - 55	32 - 38
		6	94.4	51	50	34	51 - 55	33 - 38
3.12	6	0	-	68	47	33	53 - 60	31 - 38
		1	11.0	66	70	46	53 - 59	32 - 38
		2	22.3	61	61	43	54 - 60	32 - 39
		4	62.1	48	53	34	53 - 59	32 - 38
		6	78.8	71	73	50	52 - 57	34 - 39
†Star PCL **2.7**	0	0	-	90	101	73	53 - 58	29 - 35
		1	8.6	36	41	29	54 – 59	30 - 34
		2	14.3	42	48	34	54 – 58	30 - 34
		4	29.5	10	11	8	55 – 57	31 - 35
		15	94.3	4	5	3	54 - 56	31 - 35
3.5	27	0	-	40	40	26	54 - 60	31 - 36
		2	69.8	52	51	33	54 - 60	33 - 36
		4	97.8	-	-	-	-	-

†Star PCL **2.7** synthesised in Chapter 2 Section 2.2.4.2.4

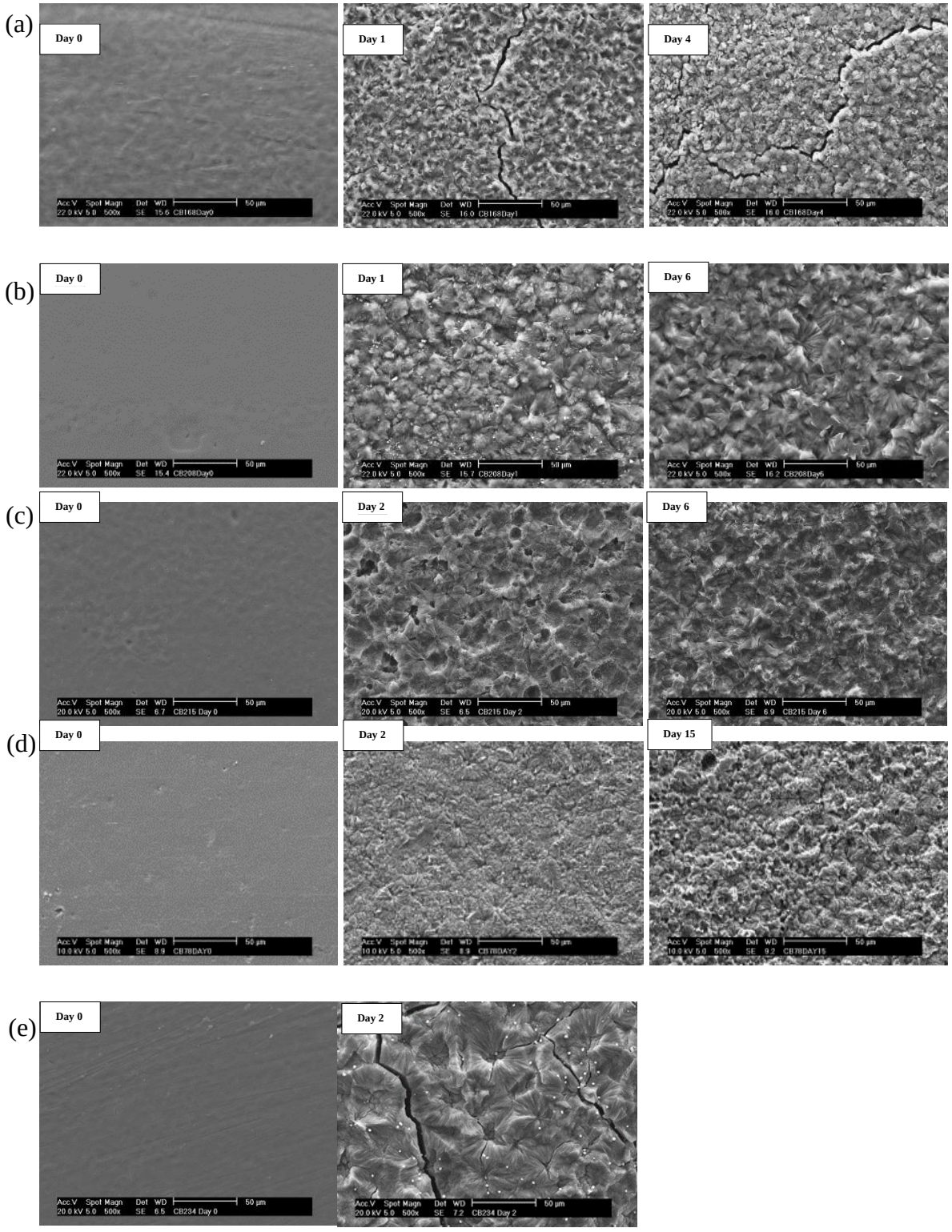

Figure 3.29: SEM micrographs of polymer films before and after enzymatic degradation using *pseudomonas cepacia* lipase on selected days (a) four-arm star copolymer **3.10** with a $\overline{\mathbf{DP}}_{\mathrm{Th}}$ of 20 per arm, at day 0, 1 and 4, (b) four-arm star copolymer **3.11** with a $\overline{\mathbf{DP}}_{\mathrm{Th}}$ of 50 per arm at day 0, 1 and 6, (c) four-arm star copolymer **3.12** with a $\overline{\mathbf{DP}}_{\mathrm{Th}}$ of 100 per arm

at day 0, 2 and 6, (d) †star PCL **2.7** at day 0, 2 and 15, (e) linear triblock copolymer **3.5** at day 0 and 2. The scale bar of the SEM micrographs is 50 μm.

†Star PCL **2.7** synthesised in Chapter 2 Section 2.2.4.2.4

The surface morphologies of the polymer films were analysed with SEM before and after enzymatic degradation using *pseudomonas cepacia* lipase. Figure 3.29 shows the SEM micrographs for polymer films **3.10 - 3.12**, **3.5** and star PCL **2.7** before degradation (day 0) and at various days throughout the degradation period. Enzymatic degradation occurred over the whole surface of the film and significant erosion and was observed after only 1 day. Significant surface pitting and erosion can be seen for four-arm star copolymers **3.10 - 3.12** (Figure 3.29a-c) and linear copolymer **3.5** (Figure 3.29e) after 1-2 days of enzymatic degradation. In comparison, star PCL **2.7** (Figure 3.29d) shows a lesser extent of surface pitting and erosion after 2 days of enzymatic degradation.

Crystal spherulite structures can be seen after 1-2 days of enzymatic degradation, particularly for linear copolymer **3.5**, Figure 3.29e. Similar crystalline structures have been observed in the literature with the enzymatic degradation of several PCL-based polymer samples.[36,37,33,34] This supports the general increase of $\%\chi_c$ seen in the first 2 days of enzymatic degradation, Table 3.6. This can be explained by degradation primarily occurring in amorphous regions meaning the $\%\chi_c$ of the polymer increases within the first 2 days followed by a decrease as the crystalline areas are subsequently degraded.

Large fissures can be seen in the SEM micrographs for the degraded polymer films of **3.10** (Figure 3.29a) and **3.5** (Figure 3.29e). This could be due to high water uptake and swelling of the polymer films during the enzymatic degradation period, followed by drying under reduced pressure to a constant weight. These fissures are only seen in copolymers **3.5** and **3.10** with the highest %PEG content of 27-28%, compared to star PCL **2.7** and copolymers **3.11 - 3.12**, with a lower 0-14% PEG content.

3.4 Conclusions

A series of novel four-arm star copolymers **3.10 – 3.12** containing a central PEG moiety and PCL arms bridged with a bisMPA moiety, were synthesised in a four-step synthesis with a $\overline{DP}_{Th}$ of 20, 50 and 100 ε-CL units per arm. Linear copolymer **3.5** PCL-*b*-PEG-*b*-PCL containing a central PEG moiety and two PCL arms was synthesised as a structural comparison, by the ROP of ε-CL catalysed by $SnOct_2$ and using PEG **3.4** as an macro-initiator.

The four-step synthesis involved the hydroxyl-protection of bisMPA **3.6** using acetic anhydride, followed by a coupling of **3.7** with PEG **3.4** using DCC and DMAP to produce hydroxyl-protected PEG macro-initiator **3.8**. The acetal groups were subsequently removed under acidic conditions to give tetra-hydroxyl PEG macro-initiator **3.9** and used in the ROP of ε-CL to give novel four-arm star copolymers **3.10 – 3.12**. All products were obtained in good yields and fully characterised using NMR analyses. It must be noted a small amount of ester bonds in the tetra-hydroxyl PEG macro-initiator **3.9** were hydrolysed during the acidic acetal removal to give PEG diol **3.4**. This impurity could not be easily removed due to the similar chemical nature of PEG **3.4** and the tetra-hydroxyl PEG macro-initiator **3.9**.

The novel four-arm star copolymers **3.10 - 3.12** showed good control in the ROP of ε-CL as the $\overline{DP}_{NMR}$ were in good correlation with $\overline{DP}_{Th}$. However, Đ from 1.32 to 1.51 and small lower molecular weight shoulders are seen in the SEC chromatograms of the four-arm star copolymers. This is due to using a polydisperse PEG macro-initiator **3.9**. Contact angle and %WU analyses confirmed that as %PEG content decreased from 28% to 6%, the hydrophilic nature of the copolymers decreased. This is expected based on the hydrophilic nature of PEG.

The enzymatic degradation of the linear **3.5** and star copolymers **3.10 – 3.12** was investigated using *pseudomonas cepacia* lipase over 7 days and compared to star PCL homopolymer. The linear copolymer **3.5** exhibited the fastest rate of degradation, due to greater polymer chain mobility and comparatively high hydrophilic %PEG content. There is an increased shielding of the hydrophilic central PEG unit from the four hydrophobic PCL arms in the star structures, leading to a slower degradation rate.

The novel star copolymers **3.10 – 3.12** showed similar enzymatic degradation rates (>90% mass loss within 7 days) however, the degradation rates were notably faster than star PCL

homopolymer **2.7** (>90% mass loss in 15 days). This indicates the incorporation of a central hydrophilic PEG moiety into a star PCL structure, increases the overall hydrophilic nature and hence the enzymatic degradation rate.

DSC and SEM analyses confirm enzymatic degradation and show an increase in $\%\chi_c$ during the first stages of degradation. This is due to enzymes preferentially degrading the amorphous regions of PCL as well as the production of shorter polymer chains during degradation, leading to an overall increase in $\%\chi_c$.

3.5 References

(1) Geng, Y.; Discher, D. E. *J. Am. Chem. Soc.* **2005**, *127*, 12780.
(2) Gref, R.; Minamitake, Y.; Peracchia, M.; Trubetskoy, V.; Torchilin, V.; Langer, R. *Science* **1994**, *263*, 1600.
(3) Kumari, A.; Yadav, S. K.; Yadav, S. C. *Colloids Surf. B: Biointerfaces* **2010**, *75*, 1.
(4) Nuyken, O.; Pask, S. *Polymers* **2013**, *5*, 361.
(5) Guillaume, S. M. *Eur. Polym. J.* **2013**, *49*, 768.
(6) Ghoroghchian, P. P.; Li, G.; Levine, D. H.; Davis, K. P.; Bates, F. S.; Hammer, D. A.; Therien, M. J. *Macromolecules* **2006**, *39*, 1673.
(7) Lu, D. D.; Yuan, J. C.; Li, H.; Lei, Z.-Q. *J. Polym. Sci. Part A: Polym. Chem.* **2008**, *46*, 3802.
(8) Li, S.; Garreau, H.; Pauvert, B.; McGrath, J.; Toniolo, A.; Vert, M. *Biomacromolecules* **2002**, *3*, 525.
(9) He, F. L., S.; Vert, M.; Zhuo, R. *Polymer* **2003**, *44*, 5145.
(10) Goodwin, A. P.; Lam, S. S.; Fréchet, J. M. J. *J. Am. Chem. Soc.* **2007**, *129*, 6994.
(11) Walter, M. V.; Malkoch, M. *Chem. Soc. Rev.* **2012**, *41*, 4593.
(12) Nederberg, F.; Appel, E.; Tan, J. P. K.; Kim, S. H.; Fukushima, K.; Sly, J.; Miller, R. D.; Waymouth, R. M.; Yang, Y. Y.; Hedrick, J. L. *Biomacromolecules* **2009**, *10*, 1460.
(13) Bensaid, F.; Thillaye du Boullay, O.; Amgoune, A.; Pradel, C.; Harivardhan Reddy, L.; Didier, E.; Sablé, S.; Louit, G.; Bazile, D.; Bourissou, D. *Biomacromolecules* **2013**, *14*, 1189.
(14) Coulembier, O.; Kiesewetter, M. K.; Mason, A.; Dubois, P.; Hedrick, J. L.; Waymouth, R. M. *Angew. Chem, Int. Ed* **2007**, *46*, 4719.
(15) Ponsart, S.; Coudane, J.; Saulnier, B.; Morgat, J.-L.; Vert, M. *Biomacromolecules* **2001**, *2*, 373.
(16) Gan, Z.; Yu, D.; Zhong, Z.; Liang, Q.; Jing, X. *Polymer* **1999**, *40*, 2859.
(17) Castilla-Cortázar, I.; Más-Estellés, J.; Meseguer-Dueñas, J. M.; Escobar Ivirico, J. L.; Marí, B.; Vidaurre, A. *Polym. Degrad. Stabil.* **2012**, *97*, 1241.
(18) Nerantzaki, M. P., G. Z.; Bikiaris, D. N. *Polym. Degrad. Stabil.* **2014**, *108*, 257.
(19) Lee, C.; Kimura, Y.; Chung, J.-D. *Macromol. Res.* **2008**, *16*, 651.
(20) Fukuzaki, H.; Yoshida, M.; Asano, M.; Kumakura, M.; Mashimo, T.; Yuasa, H.; Imai, K.; Hidetoshi, Y. *Polymer* **1990**, *31*, 2006.
(21) Mochizuki, M.; Hirano, M.; Kanmuri, Y.; Kudo, K.; Tokiwa, Y. *J. Appl. Polym. Sci.* **1995**, *55*, 289.
(22) Gan, Z.; Liang, Q.; Zhang, J.; Jing, X. *Polym. Degrad. Stabil.* **1997**, *56*, 209.
(23) Li, S. M.; Pignol, M.; Gasc, F.; Vert, M. *Macromolecules* **2004**, *37*, 9798.
(24) Meseguer-Duenas, J. M., Mas-Estelles, J., Castilla-Cortazar, I., Escobar Ivirico, J. L., Vidaurre, A. *J. Mater. Sci. Mater. Med.* **2011**, *22*, 11.
(25) Khatiwala, V. K.; Shekhar, N.; Aggarwal, S.; Mandal, U. K. *J. Polym. Environ.* **2008**, *16*, 61.
(26) Yoshioka, T.; Kamada, F.; Kawazoe, N.; Tateishi, T.; Chen, G. *Polym. Eng. Sci.* **2010**, *50*, 1895.
(27) Sekosan, G.; Vasanthan, N. *J. Polym. Sci. Part B: Polym. Phys.* **2010**, *48*, 202.
(28) Cohn, D.; Stern, T.; Gonzalez, M. F.; Epstein, J. *J. Biomed. Mater. Res.* **2002**, *59*, 273.
(29) Li, Q. B.; Li, F. X.; Jia, L.; Li, Y.; Liu, Y. C.; Yu, J. Y.; Fang, Q.; Cao, A. M. *Biomacromolecules* **2006**, *7*, 2377.

(30) (a) Gan, Z.; Jiang, B.; Zhang, J. *J. Appl. Polym. Sci.* **1996**, *59*, 961(b) Bogdanov, B., Vidts, A., Van Den Buicke, A., Verbeeck, R., Schacht, E. *Polymer* **1998**, *39*, 1631.
(31) Nagata, M.; Kiyotsukuri, T.; Takeuchi, S.; Tsutsumi, N.; Sakai, W. *Polym. Int.* **1997**, *42*, 33.
(32) Bogdanov, B., Vidts, A., Van Den Buicke, A., Verbeeck, R., Schacht, E. *Polymer* **1998**, *39*, 1631.
(33) Bogdanov, B.; Vidts, A.; Schacht, E.; Berghmans, H. *Macromolecules* **1999**, *32*, 726.
(34) Shiomi, T.; Imai, K.; Takenaka, K.; Takeshita, H.; Hayashi, H.; Tezuka, Y. *Polymer* **2001**, *42*, 3233.
(35) You, Y.; Min, B.-M.; Lee, S. J.; Lee, T. S.; Park, W. H. *J. Appl. Polym. Sci.* **2005**, *95*, 193.
(36) Marten, E.; Müller, R.-J.; Deckwer, W.-D. *Polym. Degrad. Stabil.* **2003**, *80*, 485.
(37) Mochizuki, M.; Hirano, M.; Kanmuri, Y.; Kudo, K.; Tokiwa, Y. *J. Appl. Polym. Sci.* **1995**, *55*, 289.

4.1 Introduction

Cyclodextrins (CD) are naturally occurring, biodegradable and biocompatible cyclic oligosaccharides composed of six to eight linked glucose units in α-, β- and γ-CD respectively, Figure 4.1, and obtained from the enzymatic degradation of starch.[1] They have an extensive range of applications from use in food,[2] cosmetics,[3] pharmaceuticals and environmental science.[4]

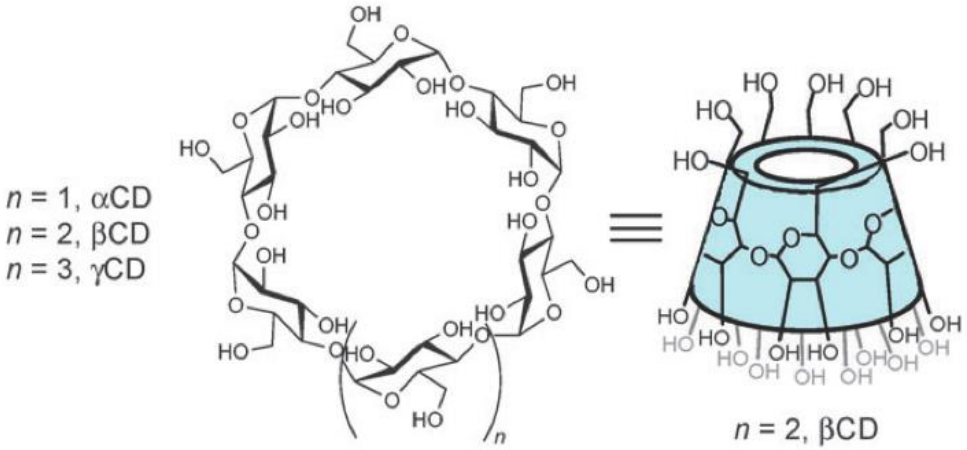

4.1

Figure 4.1: General structure of β-cyclodextrin **4.1**[1]

CD's are commonly used in drug-delivery and controlled drug release systems due to their basket-shaped topology. The OH groups orient to the outer space, and methine protons orient to the inner cavity, imparting an amphiphilic character of a hydrophilic outer part and a hydrophobic inner cavity. It is these properties that have been exploited by increasing the permeability of poorly soluble hydrophobic drug molecules into cell membranes through the formation of a drug-CD inclusion complex.

CD's have been used as a cross-linker in the reaction with diisocyanates in the direct synthesis of polyurethanes (PUs).[4,5] Moreover, it has been reported that β-CD **4.1** has been used in polymer blends to enhance biodegradation of PUs without affecting mechanical properties.[6] It was found that after degradation, the PU blended with β-CD **4.1** showed increased surface erosion and a decrease in molecular weight, compared to the PU control. However, no evidence of an even distribution of β-CD **4.1** throughout the PU blend was provided. Furthermore, only one blended sample was tested after 2 months of soil burial with no repeat measurements taken, giving no indication of the rate of degradation or indication of experimental error.

Gou *et al*. reported the synthesis of amphiphilic $A_{14}B_7$ miktoarm star copolymer containing a central β-CD moiety with fourteen poly(ε-caprolactone) (PCL) arms and seven poly(ethylene glycol) (PEG) arms.[7] The synthesis involved the protection of the seven 1° OH groups on the β-CD moiety using TBDMS-Cl. The fourteen 2° OH groups on the β-CD moiety were then used to initiate the ROP of ε-CL, catalysed by $SnOct_2$. The TBDMS groups were removed using $BF_3.Et_2O$ followed by a "click" reaction with azide-functionalised β-CD star PCL and alkyne terminated PEG, to produce $A_{14}B_7$ miktoarm star copolymers. However, it is difficult to accurately determine the $\overline{DP}$ per arm and to confirm ROP has occurred from all fourteen 2° OH groups on the β-CD moiety, due to very weak methine proton resonances on the β-CD moiety.

The 4-dimethylaminopyridine (DMAP) catalysed ROP of lactide using β-CD **4.1** as an initiator in bulk conditions, has been reported to produce a twenty-one-arm star PCL with a central β-CD moiety.[8] However, the only evidence that ROP had occurred from all twenty-one 1° and 2° OH groups on the β-CD initiator, is the disappearance of the broad and weak 6-O*H*, 3-O*H* and 2-O*H* resonances in the ^{1}H NMR spectrum. Furthermore, no increase in molecular weight has been reported using SEC analysis or change in thermal properties using DSC analysis.

Shen *et al*. reported the synthesis of a seven-arm star PLA with a central β-CD moiety by the ROP of lactide in DMF using the seven 1° OH groups on the β-CD moiety.[9] It was suggested the reaction did not require an additional catalyst and that ROP occurred from the 1° OH groups due to a resonance shift for C-6 from 59.96 ppm to 64.76 ppm in the ^{13}C NMR spectrum. Moreover, no resonance shifts were seen for C-2 and C-3 positions next to the 2° OH groups.

This chapter reports the synthesis and enzymatic degradation of seven-arm star PCL with a β-CD core **4.5**. The four-step syntheses has been characterised using NMR, SEC, FT-IR, contact angle and % water uptake. The enzymatic degradation using *pseudomonas cepacia* lipase was monitored with % mass loss and DSC to determine changes in thermal properties and $\%\chi_c$.

4.2 Experimental

4.2.1 Materials

ε-Caprolactone (ε-CL), tin (II) octoate ($SnOct_2$), *tert*-butylchlorodimethylsilane (TBDMS-Cl), acetic anhydride, boron trifluoride diethyl etherate ($BF_3.Et_2O$), dry pyridine, *pseudomonas cepacia* lipase and phosphate buffer saline salts (pH = 7.4) were purchased from Sigma Aldrich and used as received unless stated otherwise. β-Cyclodextrin **4.1** was purchased from Wacker Chemical Corporation. ε–CL was distilled over CaH_2 under reduced pressure prior to use. All other dry solvents were obtained from Durham Chemistry Department Solvent Purification System (SPS). All solvents were analytical grade and used without any purification. The NMR solvent used was deuterated chloroform ($CDCl_3$) purchased from Apollo Scientific.

4.2.2 Characterisation Techniques

^{1}H and ^{13}C Nuclear magnetic resonance (NMR) spectra, Size Exclusion Chromatography (SEC), Differential Scanning Calorimetry (DSC) and Fourier-transform Infrared Spectroscopy (FT-IR) were carried out using the methods outlined in Chapter 2, Section 2.2.2.

Contact angle measurements were carried out using to the method outlined in Chapter 3, Section 3.2.2.

4.2.3 Enzymatic Degradation

Enzymatic degradation tests were carried out using the method outlined in Chapter 2, Section 2.2.3.

4.2.4 Water Uptake

Water Uptake (%WU) measurements were carried out using the method outlined in Chapter 3, Section 3.2.4.

4.2.5 Synthesis of Seven-arm Star PCL with 2,3-acetyl-β–CD core 4.5

Seven-arm star PCL with a β-CD core **4.5** was synthesised following a 4-step synthetic method originally outlined by Gou *et al*.[10]

4.2.5.1 Synthesis of 6-(*tert*-butyldimethylsilyl)-β-CD 4.2

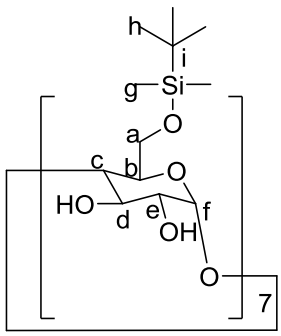

Figure 4.2: 6-(*tert*-butyldimethylsilyl)-β-CD **4.2**

β-CD **4.1** (2.00 g, 2.06 mmol) was dissolved in dry pyridine (30 mL) under vigorous stirring and cooled to 0 °C in an ice bath. TBDMS-Cl (10.87 g, 72.1 mmol) in dry pyridine (50 mL) was added drop-wise to the solution over 1 h and stirred at 0 °C for a further 1 h. The solution was warmed to ambient temperature and stirred for 18 h. After the given reaction time, the solvent was removed under reduced pressure to give a white solid. The product was dissolved in DCM (100 mL) and washed with $KHSO_4$ (80 mL, 1M) followed by saturated NaCl solution (80 mL). The DCM layer was dried over $MgSO_4$, filtered and the solvent was removed under reduced pressure. The white powder was recrystallized from ethyl acetate and hexane to give **4.2** (0.75 g, 19% yield). ^{1}H NMR (400 MHz, $CDCl_3$, TMS): (ppm) δ = 0.02 (s, 21H, $H_{g'}$), 0.04 (s, 21H, H_g), 0.87 (s, 63H, H_h), 3.56 (m, 7H, $H_{a\text{-}1}$), 3.63 (m, 14H, H_e, H_b), 3.71 (d, *J* = 10.8 Hz, 7H, H_d), 3.90 (d, *J* = 20.9 Hz, 7H, $H_{a\text{-}2}$), 4.02 (m, 7H, H_c), 4.89 (d, *J* = 3.2 Hz, 7H, H_f). ^{13}C NMR (100 MHz, $CDCl_3$, TMS): (ppm) δ = -5.1 (g'), -4.9 (g), 18.4 (h), 26.1 (i), 61.8, 72.7, 73.7, 81.8, 102.2, 127.4 (a-f). FT-IR: ν_{max} = 3320 (O-H), 2932 (C-H), 1154 (C-O), 1032 (Si-O), 834 (Si-C) cm^{-1}. The ^{1}H NMR data is in agreement with the literature.[10] Reported MS for $C_{84}H_{168}O_{35}Si_7$: m/z = 1958 $(M+Na)^+$. No additional analyses were reported.

4.2.5.2 Synthesis of 6-(*tert*-butyldimethylsilyl)-2,3-acetyl-β-CD 4.3

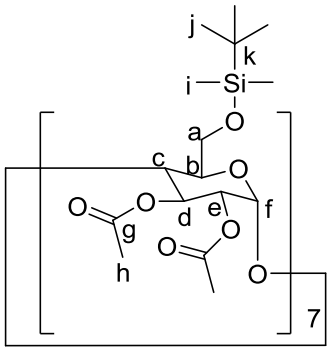

Figure 4.3: 6-(*tert*-butyldimethylsilyl)-2,3-acetyl-β-CD **4.3**

A solution of 6-(*tert*-butyldimethylsilyl)-β-CD **4.2** (0.70 g, 0.36 mmol) and acetic anhydride (3.78 mL) in dry pyridine (10 mL) was stirred under N_2 atmosphere at 70 °C for 12 h. Pyridine was removed under reduced pressure and the residue was dissolved in ethyl acetate (20 mL) and washed successively with 5% $HCl_{(aq)}$ and water (20 mL). The organic layer was dried over $MgSO_4$, filtered and concentrated to 5 mL. Upon addition of hexane the product was precipitated, filtered and dried under reduced pressure at 40 °C until a constant weight was obtained to give a yellow powder **4.3** (0.72 g, 99% yield). ^{1}H NMR (400 MHz, $CDCl_3$, TMS): (ppm) δ = 0.04 (s, 21H, H_i), 0.04 (s, 21H, $H_{i'}$), 0.88 (s, 63H, H_j), 2.06 (s, 21H, H_h), 2.06 (s, 21H, $H_{h'}$), 3.72 (d, *J* = 11.6 Hz, 7H, H_a), 3.87 (m, 14H, H_b, H_f), 4.03 (d, *J* = 10.4 Hz, 7H, $H_{a'}$), 4.70 (dd, *J* = 3.6 Hz,10.0 Hz, 7H, H_d), 5.16 (d, *J* = 3.6 Hz, 7H, H_c), 5.34 (dd, *J* = 8.2 Hz, 9.9 Hz, 7H, H_e). ^{13}C NMR (100 MHz, $CDCl_3$, TMS): (ppm) δ = -5.2 (i), -4.9 (i'), 18.4 (k), 20.9 (h), 21.1 (h'), 25.9 (j), 62.0 (a), 71.5 (d), 71.7 (e), 72.0 (f), 75.4, (b), 96.6 (c), 169.6 (g), 170.9 (g'). FT-IR: ν_{max} = 2938, 2860 (C-H), 1742 (C=O), 1366, 1232 (C-O), 1032 (Si-O), 826 (Si-C) cm^{-1}. The ^{1}H NMR data is in agreement with the literature.[10] Reported MS for $C_{112}H_{196}O_{49}Si_7$: m/z = 2546 $(M+Na)^+$. No additional analyses were reported.

4.2.5.3 Synthesis of 2,3-acetyl-β-CD 4.4

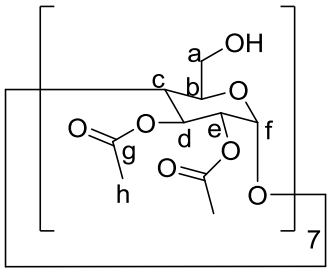

Figure 4.4: 2,3-acetyl-β-CD **4.4**

$BF_3{\cdot}Et_2O$ (0.3 mL, 2.4 mmol) in dry dichloromethane (DCM) (6 mL) was added drop-wise to a stirred solution of 6-(*tert*-butyldimethylsiyl)-2,3-acetyl-β-CD **4.3** (0.61 g, 0.3 mmol) in dry DCM (25 mL). The reaction mixture was stirred for 12 h under a N_2 atmosphere and ambient temperature, then washed successively with $NaHCO_{3(aq)}$ (100 mL, 1 M) and water. The organic phase was dried over $MgSO_4$, filtered and dried under reduced pressure until a constant weight. The white crude product was recrystallised from chloroform ($CHCl_3$) and hexane to yield **4.4** as a white powder (0.19 g, 37% yield). ^{1}H NMR (400 MHz, $CDCl_3$, TMS): δ = 2.00 (m, 41H, H_h), 3.40-5.27 (m, 49H, H_a, $H_{a'}$ H_b, H_c, H_d, H_e, H_f). ^{13}C NMR (100 MHz, $CDCl_3$, TMS): (ppm) δ = 20.9 (h), 20.9 (h'), 60.3, 61.3, 70.8, 71.1, 72.4, 96.7 (a-f), 169.5 (g), 170.9 (g'). FT-IR: ν_{max} = 3408 (OH), 2936 (C-H), 1744 (C=O), 1366, 1216 (C-O) cm^{-1}. The ^{1}H NMR data is in agreement with the literature.[10] Reported MS for $C_{70}H_{98}O49$: m/z = 1746 $(M+Na)^+$. No additional analyses were reported.

4.2.5.4 Synthesis of Seven-arm Star PCL with 2,3-acetyl-β-CD core 4.5

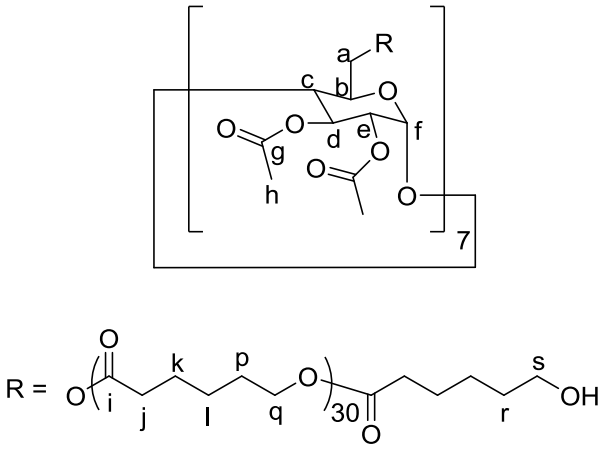

Figure 4.5: Seven-arm star PCL with β-CD core **4.5**

2,3-acetyl-β-CD **4.4** (0.10 g, 0.06 mmol) was added to an oven dried ampule followed by a magnetic stirrer and ε-CL (1.39 g, 12.18 mmol). Once dissolved, the ampule was exhausted and refilled with N_2 three times. $SnOct_2$ in dry toluene (0.09 g in 0.5 mL) was added to the mixture and subsequently heated to 120 °C for 3 h. Upon completion, the mixture was cooled, dissolved in THF and precipitated into excess methanol at 0 °C and dried under reduced pressure until a constant weight was obtained. The product was purified by precipitating a further two times from THF into methanol at 0 °C using an ice bath and collected as a white powder **4.5** (1.47 g, 99% yield). ^{1}H NMR (400 MHz, $CDCl_3$, TMS): δ = 1.36 (m, 336H, H_l), 1.62 (m, 653H, H_k, H_p, H_r), 2.06 (m, 42H, H_h), 2.27 (m, 330H, H_j), 3.61 (m, 15H, H_s), 4.03 (t, 325H, H_q), 4.30-5.30 (m, 49H, H_{a-f}). ^{13}C NMR (100 MHz, $CDCl_3$, TMS): (ppm) δ = 20.9 (h), 24.7 (k), 25.6 (l), 28.4 (p), 32.4 (r), 34.2 (j), 62.6 (s), 64.2 (q), 173.6 (i). T_m = 48 - 53 °C. FT-IR: ν_{max} = 2951, 2871 (C-H), 1723 (C=O), 1366, 1295, 1240 (C-O), 1048 cm^{-1}. The ^{1}H NMR data is in agreement with the literature.[10] No FT-IR data was reported.

4.3 Results and Discussion

4.3.1 Seven-arm Star PCL with 2,3-acetyl-β–CD core 4.5

Seven-arm star PCL with β-CD core **4.5** was synthesised in a four-step reaction, Scheme 4.1. It was not possible to perform a direct ROP of ε-CL using the OH groups of the β-CD **4.1** moiety, due to the insolubility of β-CD **4.1** in ε-CL or common organic solvents. As reported in the literature, a multi-step synthetic approach was needed to acetylate the 2° OH groups on the β-CD **4.1** moiety and thus increase the solubility of β-CD **4.1** in common organic solvents.[10] This was achieved by protecting the seven 1° OH groups on the β-CD **4.1** moiety using TBDMS-Cl to give **4.2**. The fourteen 2° OH groups on the β-CD **4.2** moiety were then acetylated using acetic anhydride to give **4.3**. Thirdly, the TBDMS moieties in **4.3** were removed to give seven 1° OH groups on the β-CD moiety **4.4**. The final synthetic step involved the ROP of ε-CL from the seven 1° OH groups on the β-CD moiety **4.4**, to give **4.5**.

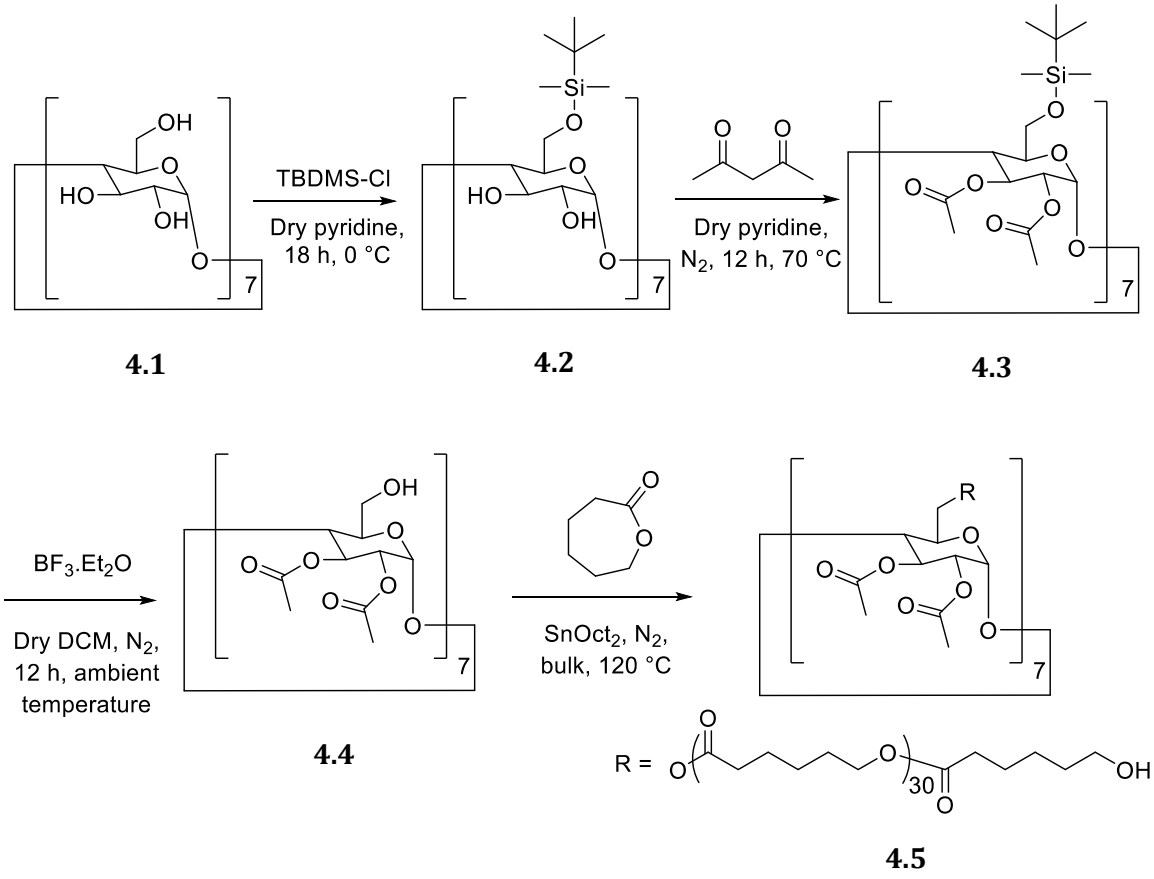

4.1 **4.2** **4.3**

4.4

4.5

Scheme 4.1: Four-step synthetic route to give seven-arm star PCL with β-CD core **4.5**

4.3.1.1 6-(tert-butyldimethylsilyl)-β-CD 4.2

The seven 1° OH groups on the β-CD **4.1** moiety were protected using TBDMS-Cl to give **4.2**, Scheme 4.1. The ^{1}H NMR spectrum of **4.2**, Figure 4.6, shows singlet resonances 0.02 ppm and 0.04 ppm, each integrating to 21H attributing to the methyl protons **g** on the TBDMS moiety. The singlet resonance at 0.87 ppm integrating to 63H is attributed to methyl protons **h** on the TBDMS moiety. The presence of the resonances attributing to protons on the TBDMS moiety indicates the successful protection of the 1° OH groups on the β-CD moiety. The methine protons located on the β-CD ring unit **b**, **c**, **d**, **e** and **f** are assigned to 3.63 ppm, 4.02 ppm, 3.71 ppm, 3.63 ppm and 4.89 ppm, respectively. Furthermore, methylene protons **a**-1 and **a**-2 located on the β-CD moiety are assigned to the resonances at 3.56 ppm and 3.90 ppm. In this case, two resonances are seen due to the axial and equatorial conformations of the protons.

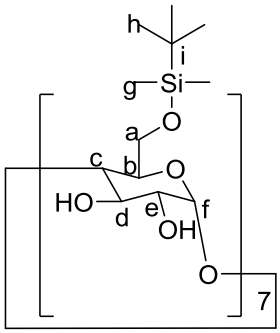

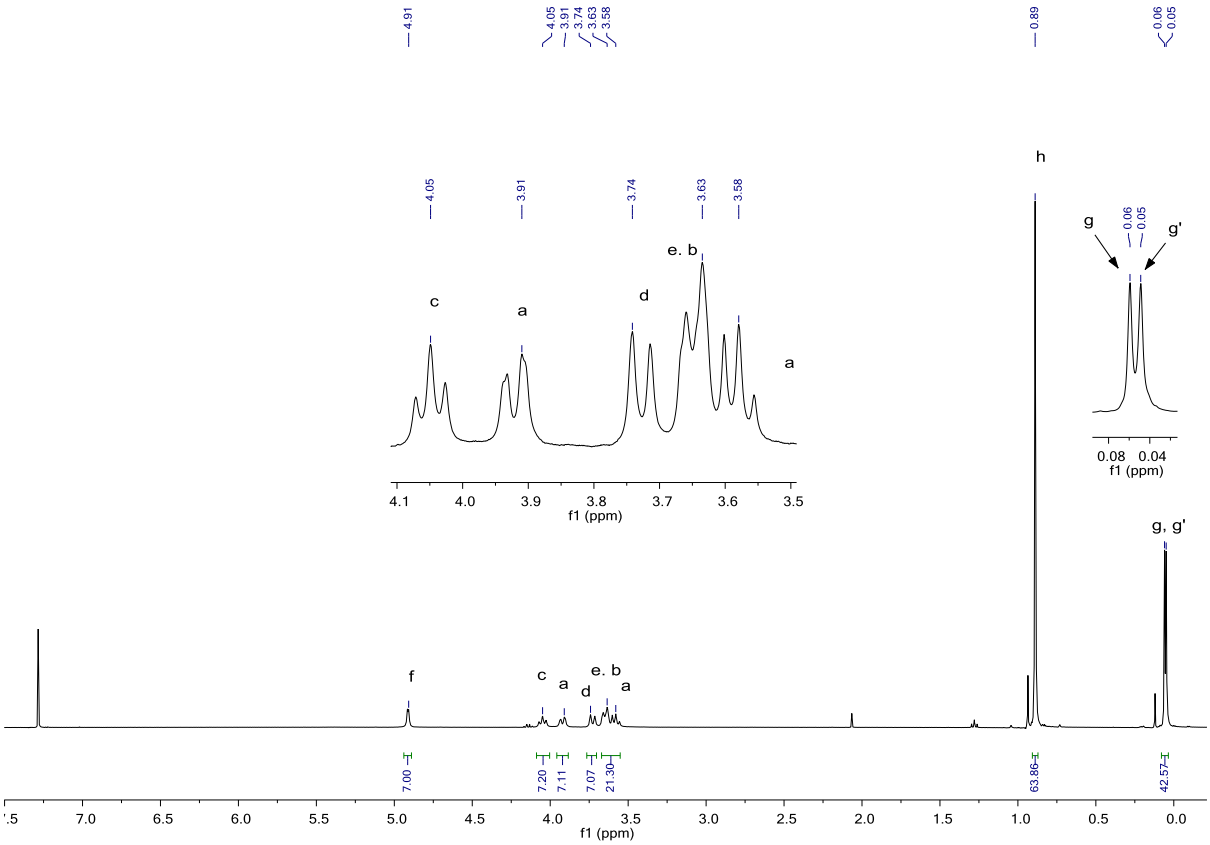

Figure 4.6: 400 MHz ^{1}H NMR spectrum of **4.2** in $CDCl_3$

The ^{13}C NMR spectrum of **4.2**, Appendix 4.1, shows resonances at -5.1 ppm, -4.9 ppm, 18.4 ppm and 26.1 ppm, attributing to carbon atoms **g'**, **g**, **h** and **i**, located on the TBDMS moiety, respectively. Furthermore, the FT-IR spectrum of **4.2**, Appendix 4.2, shows absorbances at 1032 cm^{-1} and 834 cm^{-1} attributing to Si-O and Si-C bonds, respectively. This confirms the successful reaction of TBDMS-Cl and β-CD and the protection of the 1° OH groups on the β-CD moiety.

4.3.1.2 6-(*tert*-butyldimethylsilyl)-2,3-acetyl-β-CD 4.3

The fourteen 2° OH groups on the β-CD moiety in **4.2** were acetylated using acetic anhydride to give **4.3**, Scheme 4.1. The ^{1}H NMR spectrum of **4.3**, Figure 4.7, shows overlapping singlet resonances at 0.04 ppm integrating to a total of 42H, attributing to methyl protons **i** on the TBDMS moiety. Furthermore, the singlet resonance at 0.88 ppm, integrating to 63H, is attributed to methyl protons **j** on the TSDMS moiety. The two singlet resonances at 2.05 ppm, each integrating to 21H, are attributed to methyl protons

h on the acetyl moiety, indicating the successful reaction of acetic anhydride and the 2° OH groups on the β-CD moiety. Resonances at 3.72 ppm, 3.87 ppm, 4.04 ppm, 4.70 ppm, 5.16 ppm and 5.34 ppm, are assigned to protons **a**-1, **b**/**f**, **a**-2, **d, c** and **e** on the β-CD moiety, respectively.

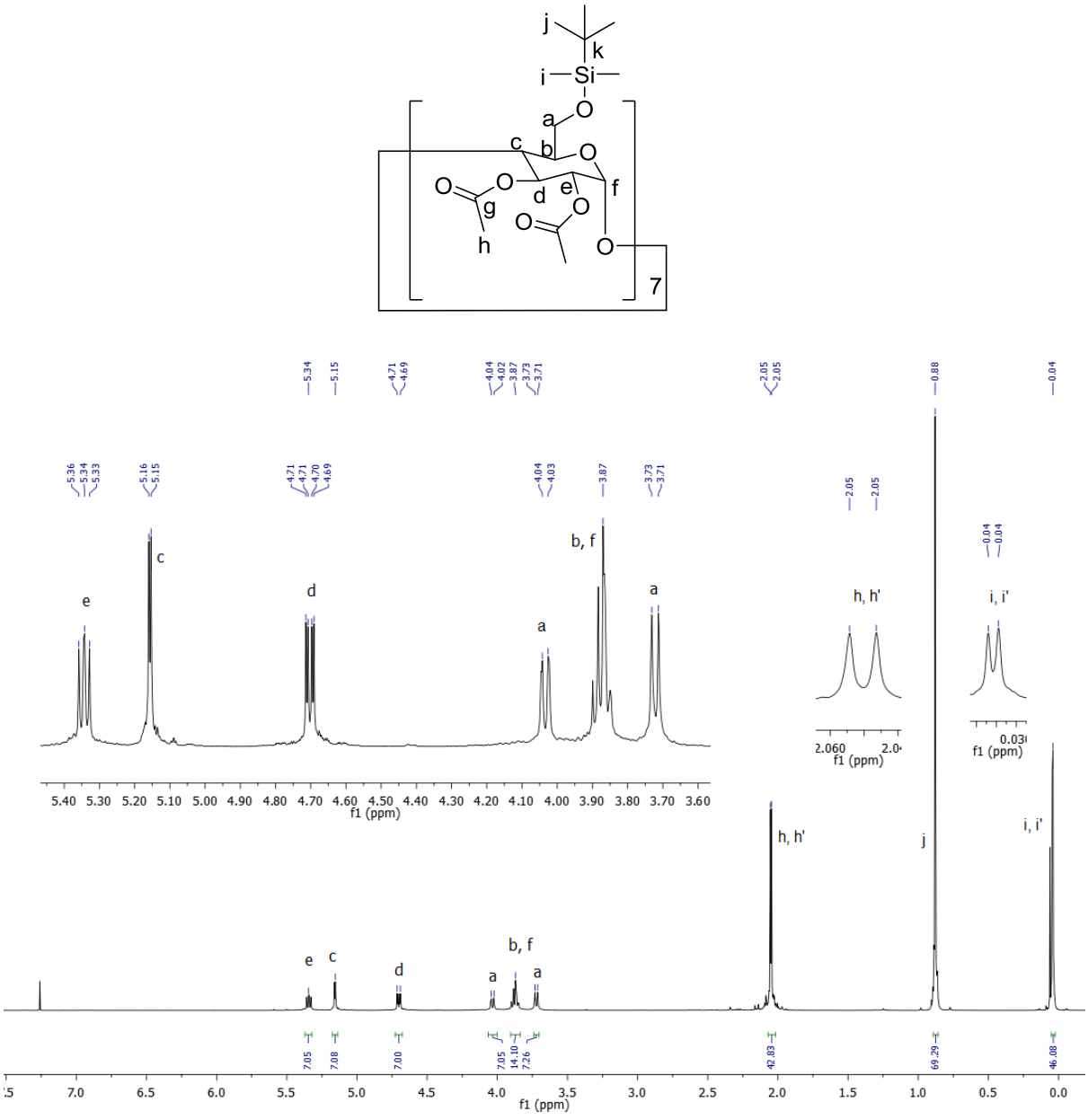

Figure 4.7: 600 MHz ^{1}H NMR spectrum of **4.3** in $CDCl_3$

The ^{13}C NMR spectrum of **4.3**, Figure 4.8, shows resonances at -5.1 ppm, -4.9 ppm, 18.4 ppm and 28.0 ppm, attributing to carbon atoms **i'**, **i**, **k** and **j**, located on the TBDMS moiety, respectively. The resonances at 20.9 ppm, 21.1 ppm, 169.6 ppm and 170.9 ppm are attributed to **h'**, **h g'** and **g**, located on the acetyl moiety, respectively, confirming the successful reaction of acetic anhydride and the 2° OH groups on the β-CD moiety. Furthermore, resonances at 62.0 ppm, 71.4 ppm, 71.7 ppm, 72.0 ppm, 75.4 ppm and 96.6 ppm are attributed to carbon atoms **a**, **d**, **e**, **f**, **b** and **c**, located on the β-CD moiety.

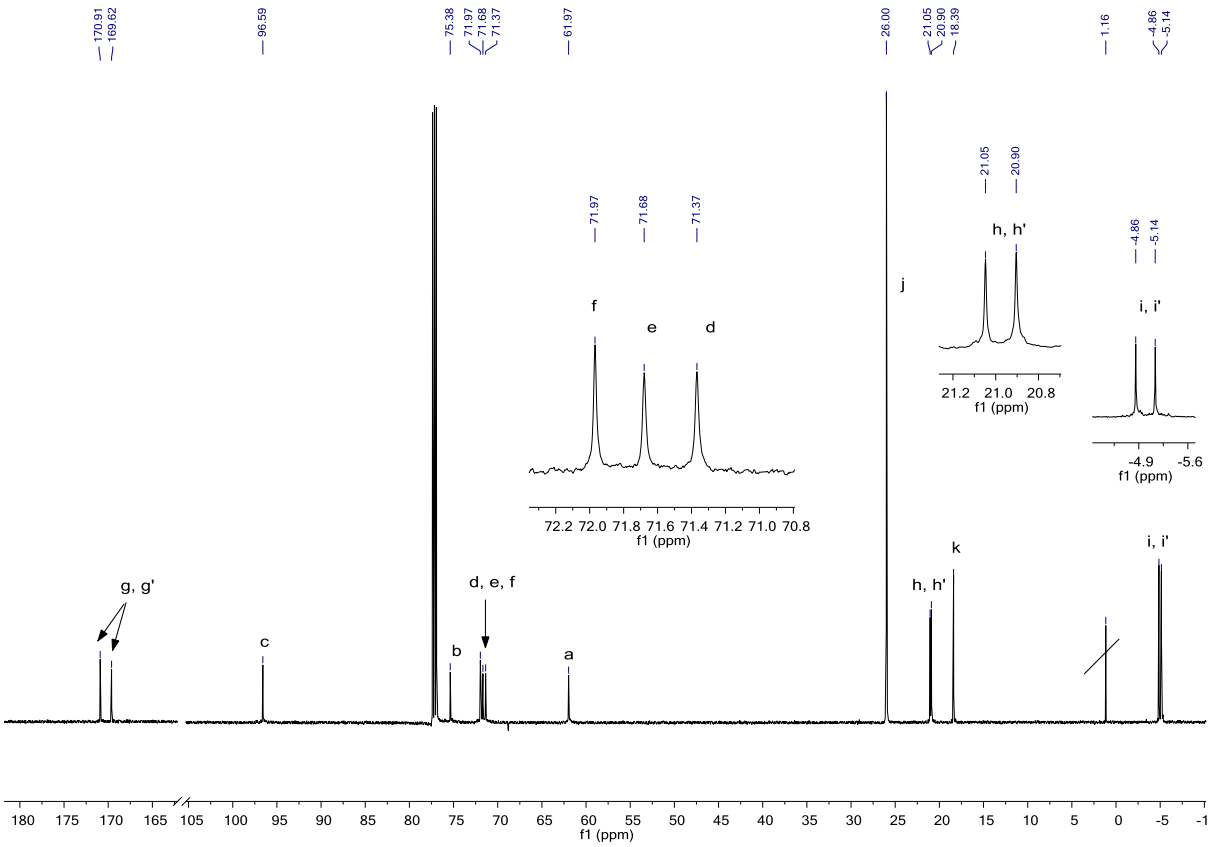

Figure 4.8: 150 MHz ^{13}C NMR spectrum of **4.3** in $CDCl_3$

The ^{1}H – ^{13}C HSQC spectrum of **4.3**, Figure 4.9, shows the correlation between protons **a**-1 and **a**-2 at 3.72 ppm and 4.04 ppm with carbon atom **a** at 62.0 ppm, respectively. Furthermore, the ^{1}H – ^{13}C HMBC spectrum of **4.3**, Figure 4.10, shows protons **a** at 3.72

ppm neighbouring carbon atoms **b** and **e** at 75.4 ppm and 71.7 ppm, respectively. The ^{1}H – ^{13}C HSQC spectrum of **4.3** shows protons **b** and **f** at 3.87 ppm are correlated to carbon atoms **b** and **f** at 75.4 ppm and 72.0 ppm, respectively. Furthermore, the ^{1}H – ^{13}C HMBC spectrum shows protons **b** and **f** at 3.87 ppm to be neighbouring carbon atoms **a**, **e** and **c** at 62.0 ppm, 71.7 ppm and 96.6 ppm, respectively. The ^{1}H – ^{13}C HSQC spectrum of **4.3**, shows protons **d**, **c** and **e** at 4.70 ppm, 5.16 ppm and 5.34 ppm correlate to carbon atoms **d**, **c** and **e** at 71.4 ppm, 96.6 ppm and 71.7 ppm, respectively. The ^{1}H – ^{13}C HMBC spectrum of **4.3**, shows protons **d** at 4.70 ppm neighbouring carbon atoms **e**, **b**, **g'** and **c** at 71.7 ppm, 75.4 ppm, 169.6 ppm and 96.6 ppm, respectively. Protons **c** at 5.16 ppm are shown to neighbour carbon atoms **b**, **d** and **e** at 75.4 ppm, 71.4 ppm and 71.7 ppm, respectively. Moreover, protons **e** at 5.34 ppm are shown to neighbour carbon atoms **d**, **b** and **g** at 71.4 ppm, 75.4 ppm and 170.9 ppm, respectively.

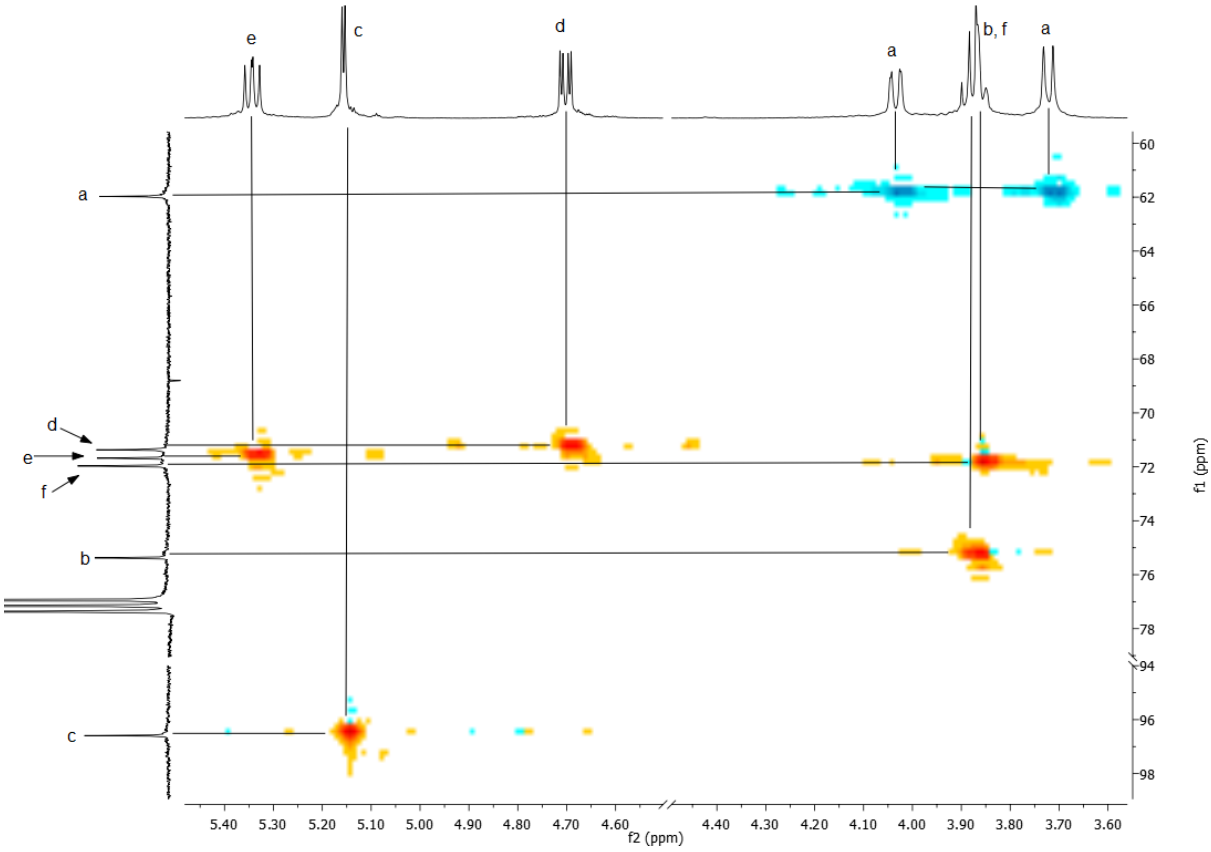

Figure 4.9: ^{1}H - ^{13}C HSQC spectrum of **4.3** in $CDCl_3$

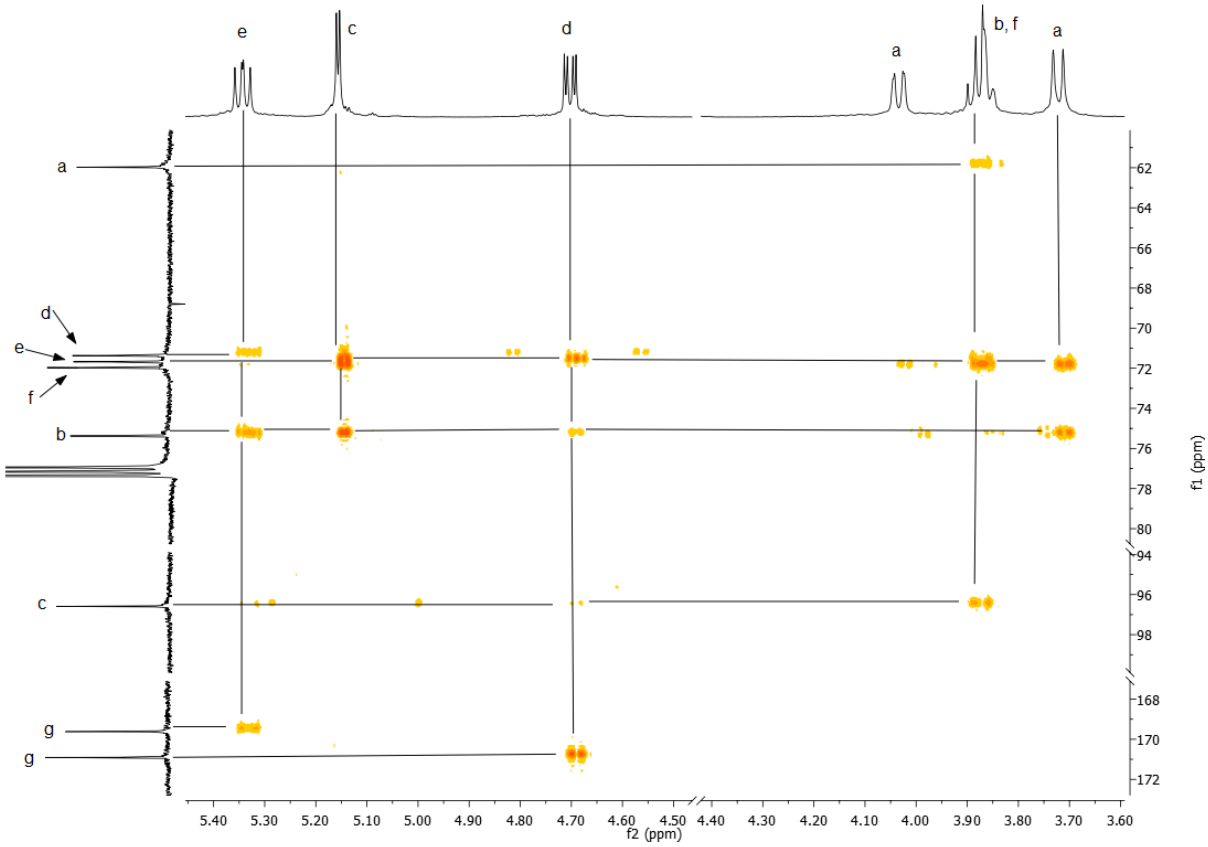

Figure 4.10: ^{1}H - ^{13}C HMBC spectrum of **4.3** in $CDCl_3$

The FT-IR spectrum of **4.3**, Appendix 4.2, shows an absorbance at 1725 cm^{-1} attributed to the C=O group on the acetyl moiety. Furthermore, the disappearance of the absorbance at 3294 cm^{-1} that is seen in **4.2** attributing to the OH group, cannot be seen in the FT-IR spectrum of **4.3**, confirming the OH groups on the β-CD moiety have been fully protected.

4.3.1.3 2,3-acetyl-β-CD 4.4

The TBDMS moieties in **4.3** were removed to give seven 1° OH groups in β-CD **4.4**. The ^{1}H NMR spectrum of **4.4**, Figure 4.11, shows overlapping resonances at 2.00 ppm, integrated together to 41H, attributing to methyl protons **h** on the acetyl group. Methylene protons **a** and methine protons **b**, **c**, **d**, **e** and **f** located on the β-CD moiety are assigned to resonances at 3.49-5.30 ppm. The disappearance of resonances at 0.04 ppm and 0.88 ppm attributing to the methyl protons located on the TBDMS moiety in **4.3**, Figure 4.7, indicates the successful removal of the TBDMS moieties.

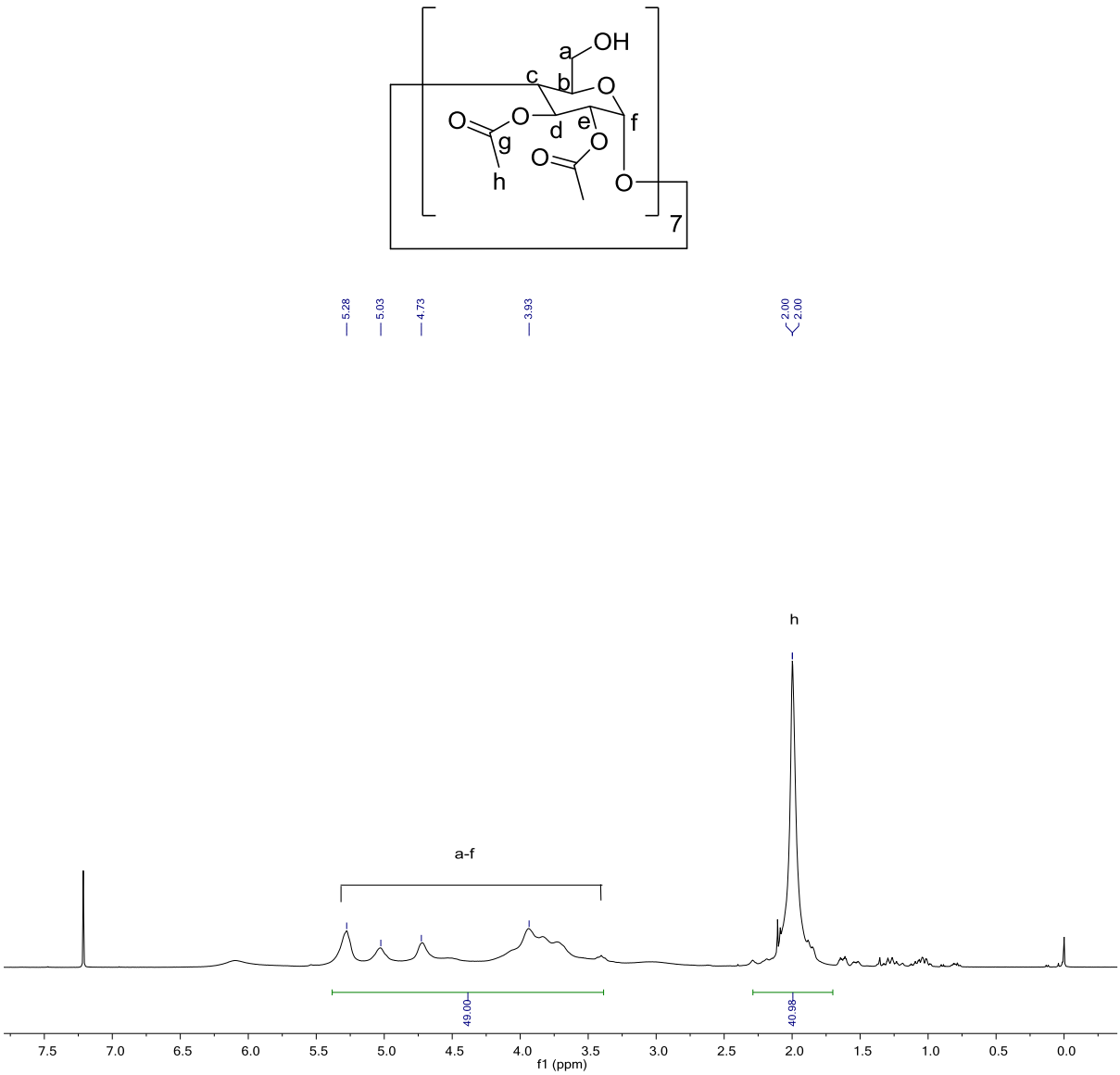

Figure 4.11: 600 MHz ^{1}H NMR spectrum of **4.4** in $CDCl_3$

The ^{13}C NMR spectrum of **4.4**, Figure 4.12, shows overlapped singlet resonances at 20.9 ppm attributed to methyl carbon atoms **h'** and **h** located on the acetyl moiety, respectively. The downfield resonances at 169.5 ppm and 170.9 ppm are attributed to carbonyl carbon atoms **g'** and **g** also located on the acetyl moiety, respectively. The resonances at 61.3 ppm, 70.8-72.4 ppm and 96.7 ppm are attributed to carbon atoms **a**, **b-e** and **f**, located on the β-CD moiety, respectively. Furthermore, the disappearance of resonances -5.1 ppm, -4.9 ppm, 18.4 ppm and 28.0 ppm attributing to the carbons atoms located on the TBDMS moiety in **4.3**, Figure 4.8, confirm the successful removal of the TBDMS moiety.

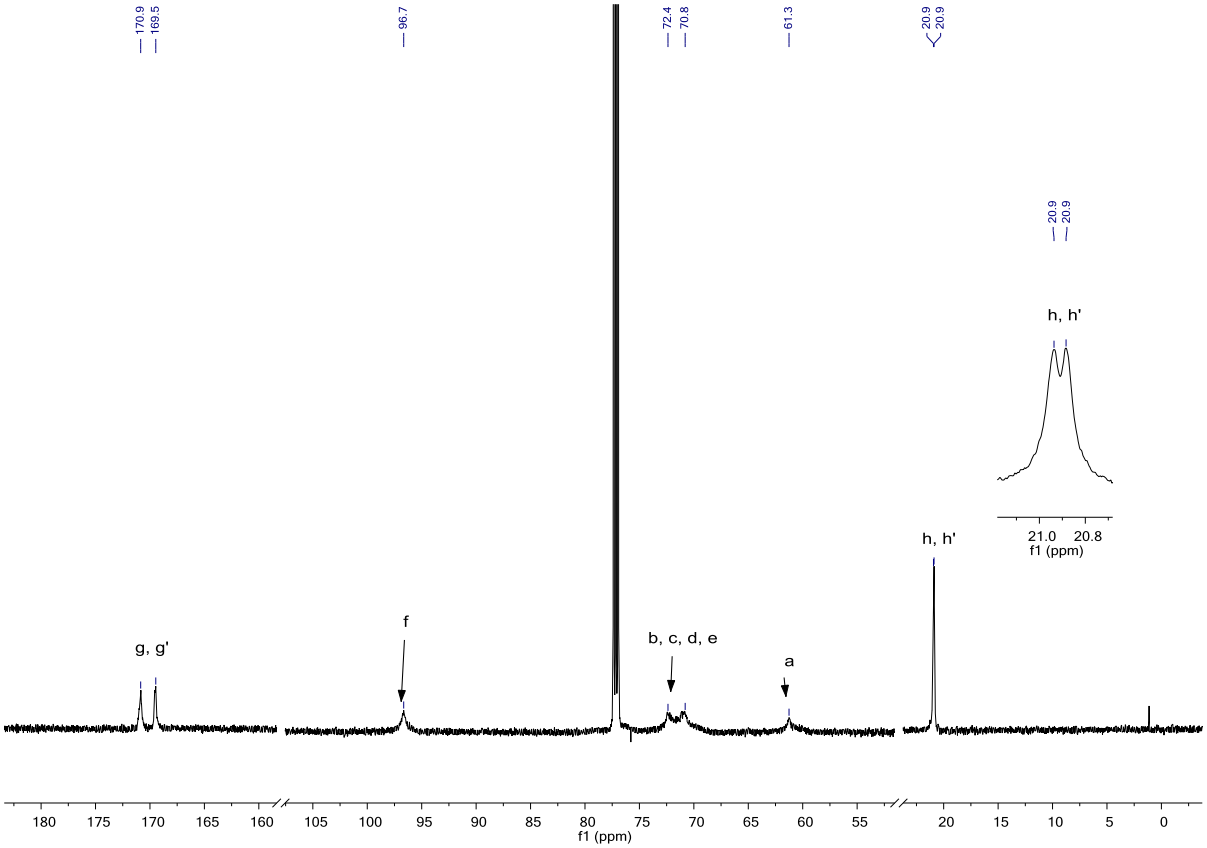

Figure 4.12: 150 MHz ^{13}C NMR spectrum of **4.4** in $CDCl_3$

The FT-IR spectrum of **4.4**, Appendix 4.2, shows an absorbance at 1743 cm^{-1} attributing to the C=O group in the acetyl moiety, confirming the presence of acetylated alcohols. Furthermore, the appearance of a broad absorbance at 3330 cm^{-1} attributing to an OH group indicates the TBDMS moieties were successfully removed to give 1° OH groups on the β-CD moiety, as it has been seen in NMR, discussed earlier. Moreover, the disappearance of absorbances seen in **4.2** and **4.3** at 1032 cm^{-1} and 834 cm^{-1} attributing to Si-O and Si-C, respectively, indicate the successful removal of the TBDMS moiety.

4.3.1.4 Seven arm Star PCL with β-CD core 4.5

Acetylated β-CD **4.4** containing seven 1° OH groups was used as an initiator in the ROP of ε-CL catalysed by $SnOct_2$, to give seven-arm star PCL with a β-CD core, **4.5**, Scheme 4.1. The ^{1}H NMR spectrum of **4.5**, Figure 4.13, shows the characteristic PCL resonances at 1.36 ppm, 1.62 ppm, 2.27 ppm and 4.03 ppm corresponding to methylene protons **l**, **k/p**, **j** and **q**, respectively. Methylene protons **r** and **s** located near to the OH group on the PCL moiety are attributed to resonances at 1.62 ppm and 3.61 ppm, respectively. Moreover, the resonance at 3.61 ppm attributing to protons **s** neighbouring the OH is integrated to 15H and in good correlation to the theoretical value of 14H. The small error can be explained as a result of a high signal to noise ratio. The integration of ≈ 14H indicates that ROP of ε-CL has occurred from all seven initiating OH groups on the β-CD moiety. The resonance at 2.06 ppm integrating to 42H is attributed to methyl protons **h** located on the acetyl moiety. Furthermore the weak resonances at 4.29-5.40 ppm are attributed to protons **a-f** on the β-CD moiety.

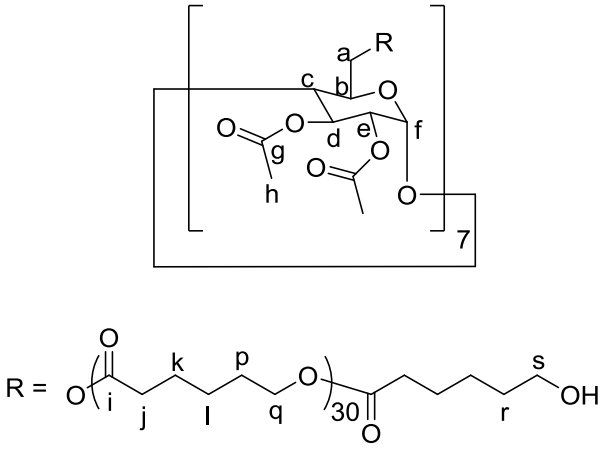

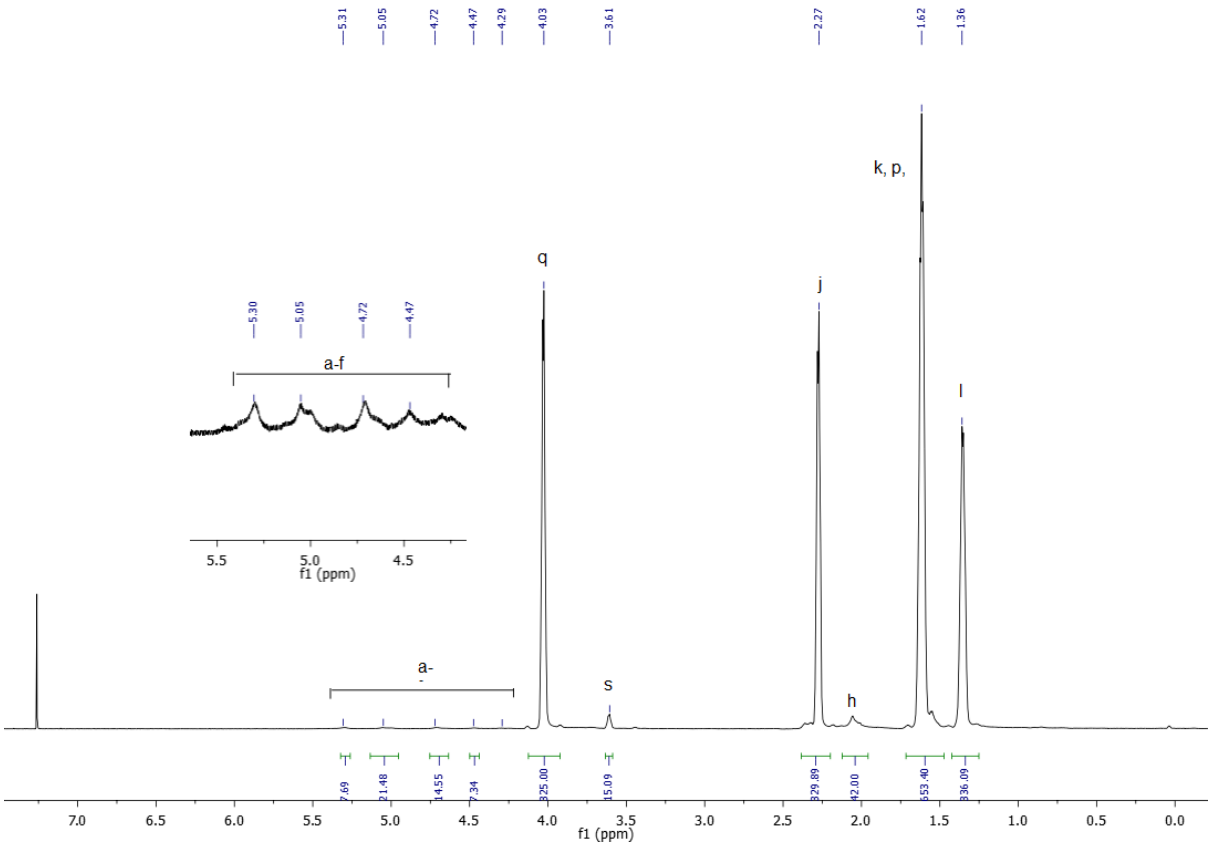

Figure 4.13: 600 MHz ^{1}H NMR spectrum of **4.5** in $CDCl_3$

The ^{13}C NMR spectrum of **4.5**, Figure 4.14, shows the characteristic PCL resonances at 24.7 ppm, 25.6 ppm, 28.4 ppm, 34.2 ppm and 64.2 ppm, attributing to methylene carbon atoms **k**, **l**, **p**, **j** and **q**, respectively. Furthermore, the downfield resonance at 173.6 ppm is attributed to carbonyl carbon atom **i** on the PCL moiety. The resonances at 32.4 ppm and 62.6 ppm are attributed to methylene carbon atoms **r** and **s** located near to the OH group on the PCL moiety, respectively. The resonance at 20.9 ppm is attributed to the methyl carbon atom **h** on the acetyl moiety. It should be noted that the resonances corresponding to carbon atoms located on the β-CD moiety cannot be detected due to weak signals.

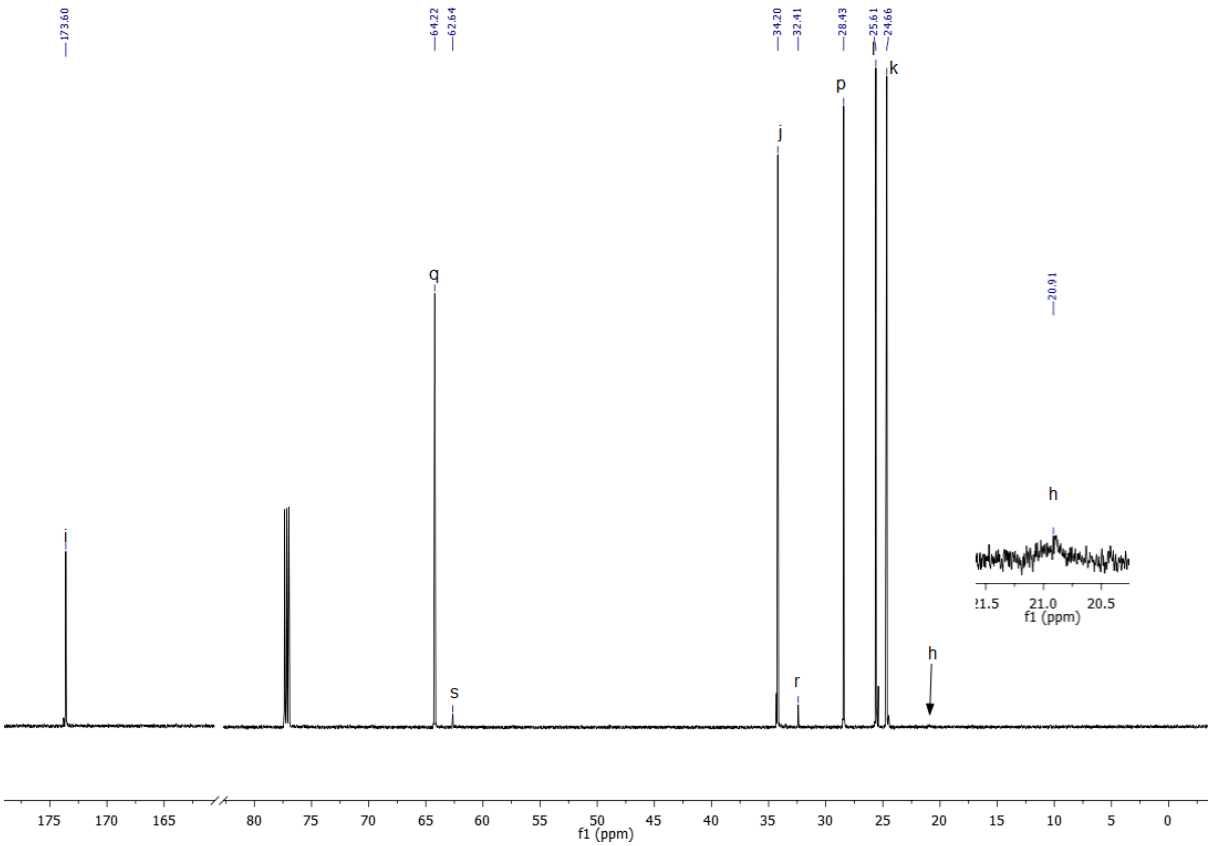

Figure 4.14: 150 MHz ^{13}C NMR spectrum of **4.5** in $CDCl_3$

The ^{1}H – ^{13}C HSQC NMR spectrum of **4.5**, Figure 4.15, shows that protons **h** at 2.06 ppm are correlated to carbon atom **h** at 20.9 ppm. Furthermore, the ^{1}H – ^{13}C HMBC NMR spectrum of **4.5**, Figure 4.16, show that protons **h** at 2.06 ppm are neighbouring carbonyl carbon atom **g** at 172.4 ppm. The ^{1}H – ^{13}C HSQC NMR spectrum shows protons **r** and **s** on the PCL moiety at 1.62 ppm and 3.61 ppm, are correlated to carbon atoms **r** and **s** at 32.4 ppm and 62.6 ppm, respectively. Moreover, the ^{1}H – ^{13}C HMBC NMR spectrum confirms protons **r** at 1.62 ppm are neighbouring carbon atom **s** at 62.6 ppm, and protons **s** at 3.61 ppm are neighbouring carbon atom **r** at 32.4 ppm.

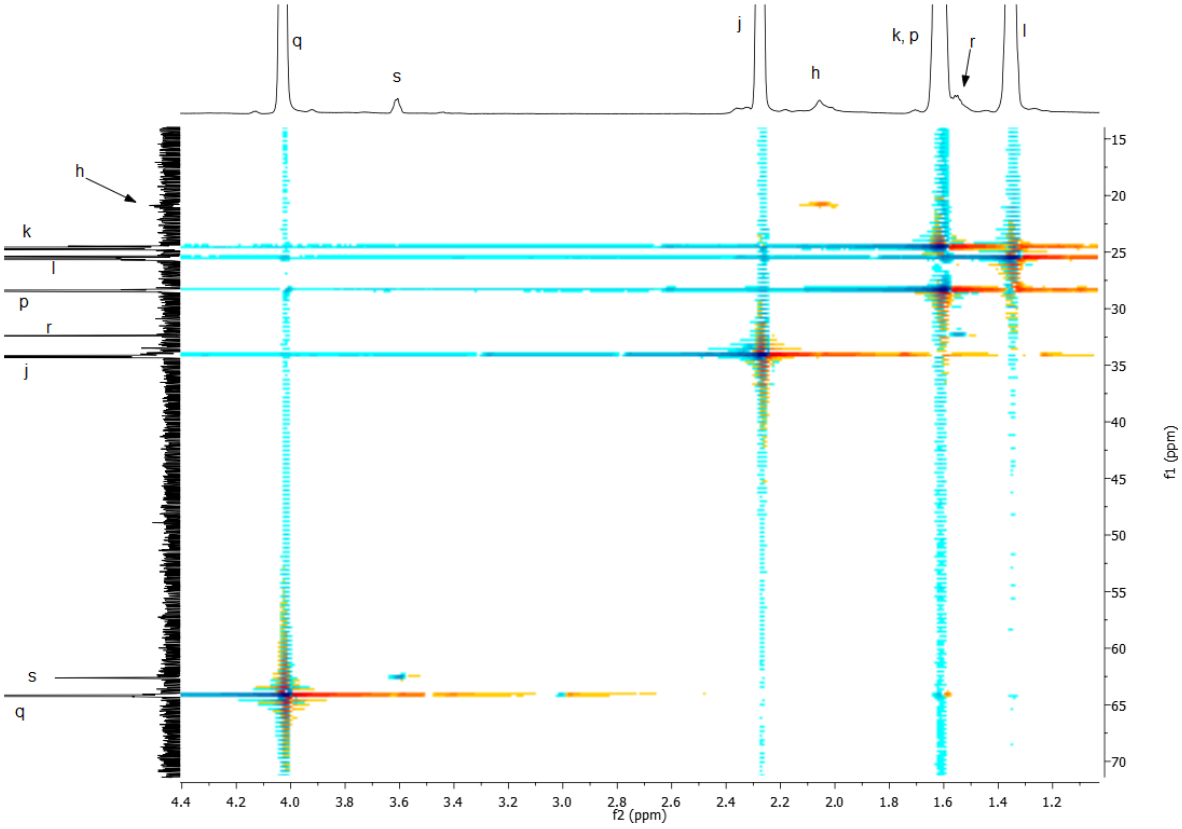

Figure 4.15: ^{1}H - ^{13}C HSQC spectrum of **4.5** in $CDCl_3$

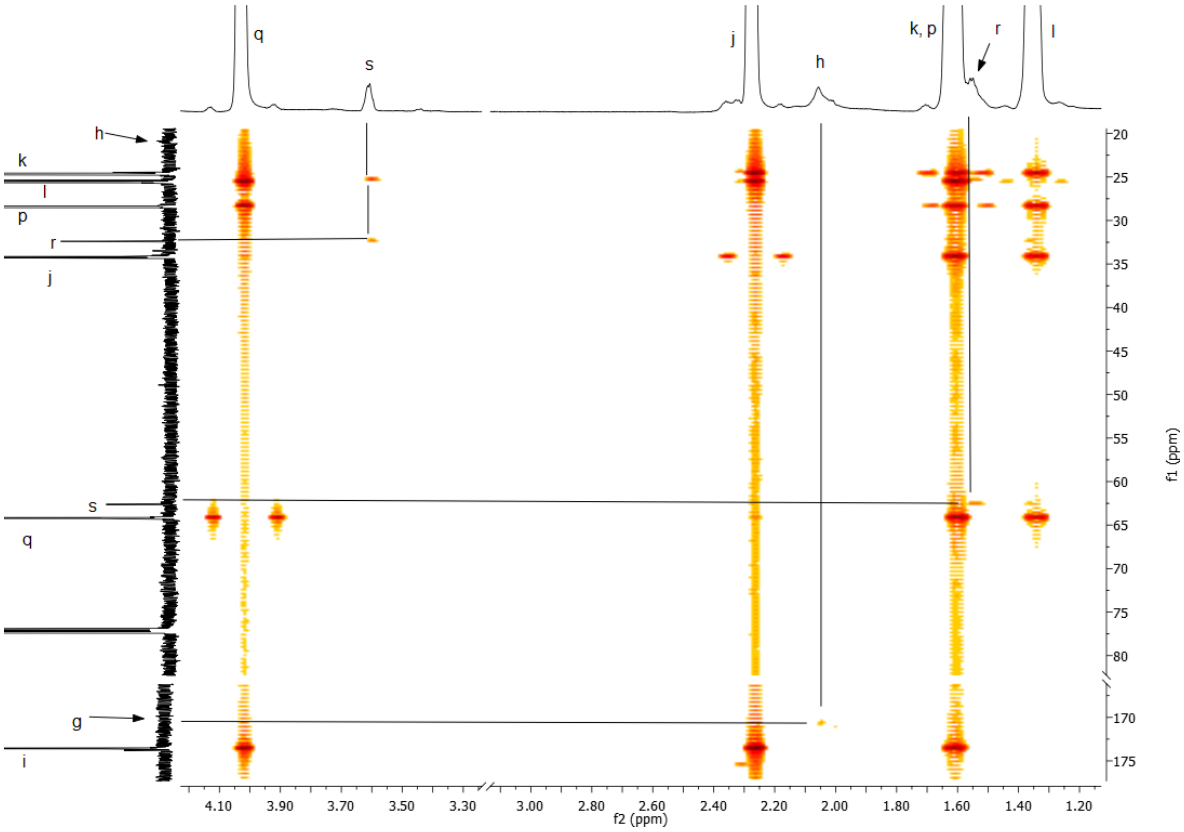

Figure 4.16: ^{1}H - ^{13}C HMBC spectrum of **4.5** in $CDCl_3$

The molecular weights and Đ for seven-hydroxyl β-CD initiator **4.4** and seven-arm star PCL with β-CD core **4.5** are shown in Table 4.1. A significant increase is seen in molecular weight from **4.4** to **4.5** determined by NMR and SEC analyses (M_n^{NMR} and M_n^{SEC}) from 0.17×10^4 g mol^{-1} to 2.97×10^4 g mol^{-1} and from 0.11×10^4 g mol^{-1} to 1.15×10^4 g mol^{-1}, respectively. The M_n^{SEC} of **4.5** at 1.15×10^4 g mol^{-1} is lower than the M_n^{Th} at 2.01×10^4 g mol^{-1} and M_n^{NMR} at 2.97×10^4 g mol^{-1}. This lower value than expected can be explained due to the seven-arm star structure having a different hydrodynamic volume than the linear polymer used as a calibration standard in SEC analyses.

Table 4.1: Molecular weights and Đ for acetylated β-CD with seven 1° OH groups **4.4** and seven-arm star PCL with a β-CD core **4.5**

Sample	$\overline{DP}_{NMR}$	M_n^{Th}	M_n^{NMR}	M_n^{SEC}	Đ
		× 10^{-4} g mol^{-1}			
4.4	0	0.17	0.17	0.11	1.03
4.5	23	2.01	2.97	1.15	2.20

An increase in M_n from **4.4** to **4.5**, can clearly be seen in the SEC chromatograms, Figure 4.17, indicating the successful ROP of ε-CL from the seven 1° OH groups on the β-CD initiator **4.4**. Furthermore, the Đ increases significantly from 1.03 to 2.20 for **4.4** to **4.5**, respectively, and a low molecular weight shoulder is clearly visible in the SEC chromatogram of **4.5**. The high Đ of **4.5** can be explained due to the nature of the ROP of ε-CL in bulk conditions occurring from seven initiating OH groups on one central β-CD moiety. As the ROP of ε-CL proceeds, the reaction mixture becomes increasingly viscous, restricting PCL chain mobility and therefore, decreasing the access of ε-CL monomer to the initiating end groups of PCL chain.

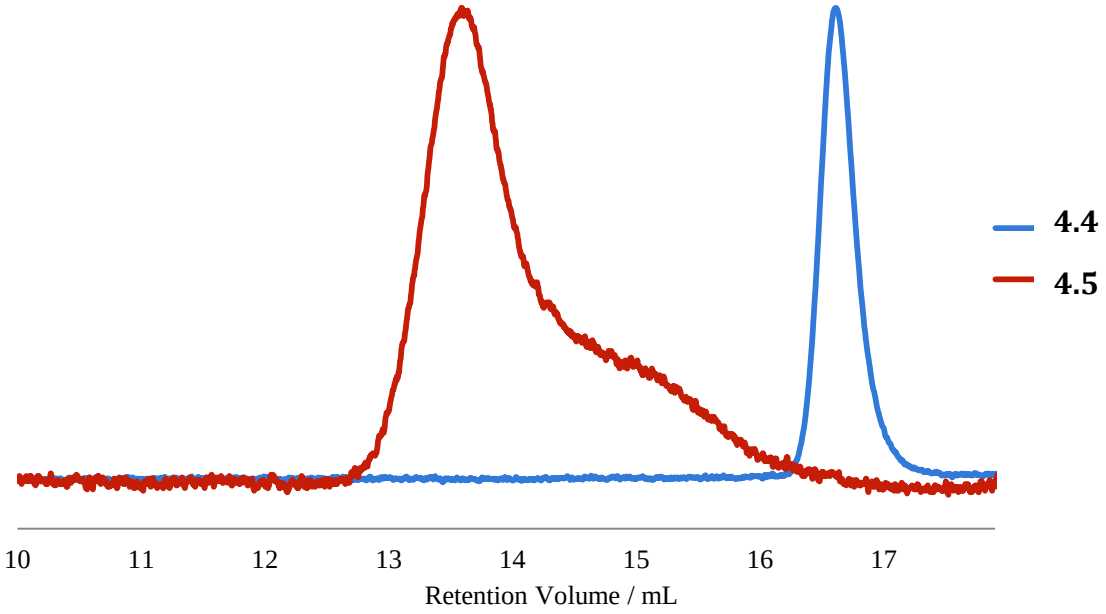

Figure 4.17: Normalised SEC chromatograms of acetylated β-CD with seven 1° OH groups **4.4** and seven arm star PCL with a β-CD core **4.5**

4.3.2 Contact Angle

The contact angle for seven-arm star PCL with β-CD core **4.5** was measured and compared to that of six-arm star PCL with dipentaerythritol core and a $\overline{DP}_{NMR}$ of 67 per arm **2.7**, prepared in Chapter 2, Section 2.2.4.2.4, Figure 4.18. It can be seen that **4.5** showed a lower initial contact angle of 76° than that of star PCL **2.7** at 86°, indicating the incorporation of a central β-CD moiety in star PCL imparts a small degree of hydrophilicity, Figure 4.19. Furthermore, a small decrease in contact angle from 86° to 83° is seen after 30 s in star PCL **2.7**, whereas negligible decrease is seen in β-CD centered star PCL **4.5**. This indicates the film surface of **4.5** has a very poor wettability, due to the relatively dense structure from the seven hydrophobic PCL arms.

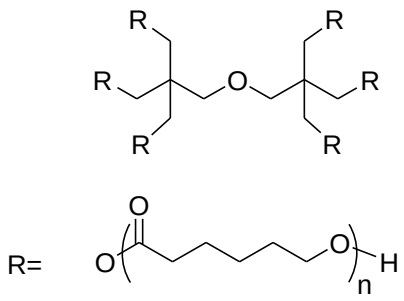

Figure 4.18: Star PCL **2.7** prepared in Chapter 2.2.4.2.4

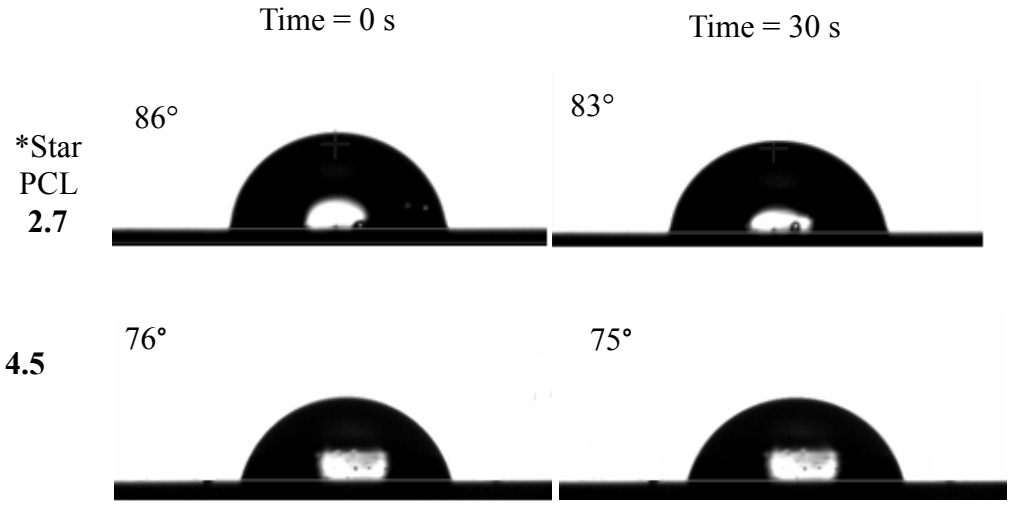

Figure 4.19: Contact angle for star PCL **2.7** and seven-arm star PCL with a β-CD core **4.5** at time = 0 s and time = 30 s. The reported contact angle is an average of the left and right contact angles and an average of five repeat measurements. The calculated error for the reported contact angles is ± 2.3%

*Star PCL **2.7** synthesised in Chapter 2, Section 2.2.4.2.4

4.3.3 Water Uptake

The % water uptake (%WU) for star PCL with β-CD core **4.5** was measured to determine the hydrophilic nature and the degree of swelling of the polymer film in water, Table 4.2. The %WU for six-arm star PCL with dipentaerythritol core **2.7** was also measured and used as a comparison to **4.5**. Star PCL with β-CD core **4.5** with a 9% β-CD content, exhibited a very low water uptake of 2%. The complete functionalisation of all OH groups on the β-CD moiety in **4.5** will decrease the hydrophilic nature and hence water solubility. The results of %WU for star PCL **2.7** and **4.5** indicate the incorporation of a β-CD moiety imparts a small degree of hydrophilicity. This could be due to the presence of free unreacted OH groups on the β-CD moiety.

Table 4.2: %WU of polymer films for star PCL **2.7** and seven-arm star PCL with a β-CD core **4.5** in PBS solution (pH 7.4) at 37 °C after 2 days

Sample	% WU	% β-CD content
*Star PCL **2.7**	0	0
4.5	2	9

*Star PCL **2.7** synthesised in Chapter 2, Section 2.2.4.2.4

4.3.4 Enzymatic Degradation of Seven-arm Star PCL with β-CD core 4.5

The mass loss of seven-arm star PCL with β-CD core **4.5** compared to six-arm star PCL with dipentaerythritol core **2.7** is presented as a function of enzymatic degradation time, Figure 4.20. It can be seen that the six-arm star PCL **2.7** has a faster rate of degradation, 94% mass loss in 15 days, than **4.5**, 7% mass loss in 20 days. This could be attributed to increased structural density and increased PCL chain entanglement in **4.5** as a higher number of PCL arms are attached to a core unit. The low wettability of **4.5** suggests the poor penetration of water and enzymes into the bulk of the polymer to access the hydrolysable ester groups on the PCL moieties.

The low rate of enzymatic degradation of **4.5** could be explained by the formation of an inclusion complex or threading with the central β-CD moiety and either the *pseudomonas cepacia* lipase enzyme or degraded PCL fragments. Studies have shown the formation of non-covalent inclusion complexes of hydrophobic molecules or hydrophobic polyesters such as PCL with the hydrophobic inner cavity of a β-CD moiety.[11,12] Therefore, the formation of an inclusion complex would significantly slow down the rate of enzymatic degradation.

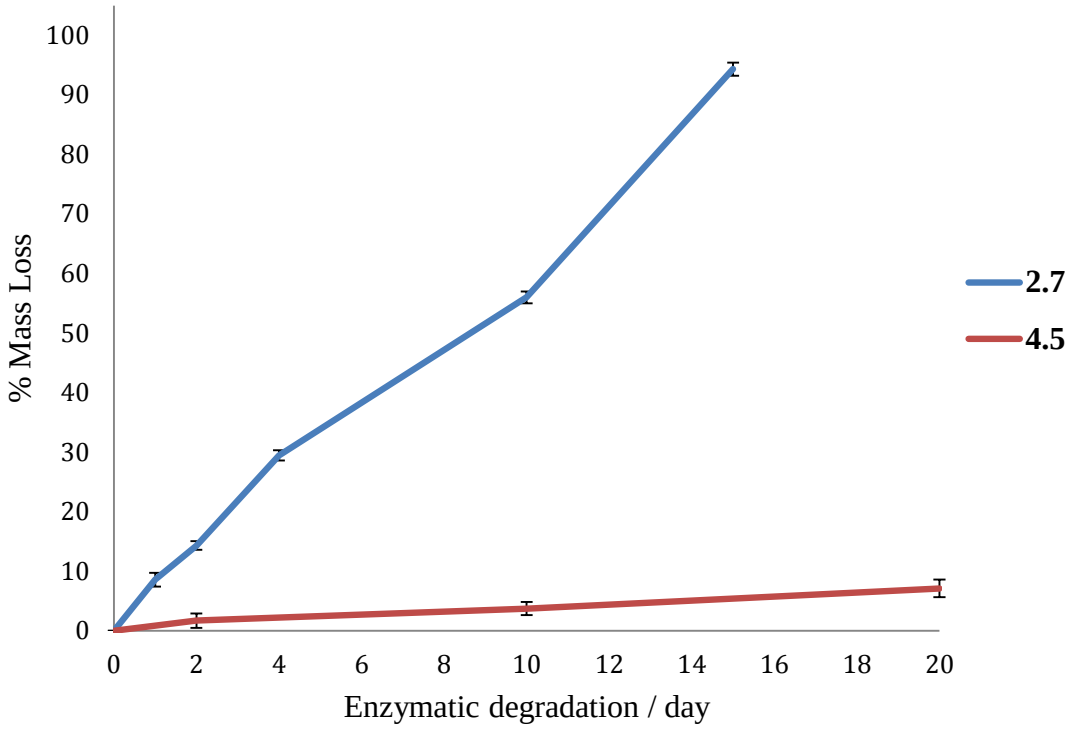

Figure 4.20: % Mass loss of seven-arm star PCL with a β-CD core **4.5** and star PCL **2.7** over 20 days of enzymatic degradation using *pseudomonas cepacia* lipase in PBS solution (pH 7.4) at 37 °C. The % mass losses are averages of three repeat sample measurements and % error bars shown.

The thermal properties of **4.5** and star PCL **2.7** were measured using DSC analyses before and after enzymatic degradation using *pseudomonas cepacia* lipase at several time intervals, Table 4.3. Interestingly, the degree of crytallinity (%χ_c) of **4.5** before enzymatic

degradation was only 16% compared to 73% seen in star PCL **2.7**. This could be due to increased chain entanglement in **4.5**, in comparison to the six-arm star PCL **2.7**. Furthermore, the highly crystalline nature of β-CD is decreased through disruption to the hydrogen bonds due to the functionalization of all OH groups in **4.5**.

Table 4.3: Thermal properties and $\%\chi_c$ of polymer films seven-arm star PCL with a β-CD cpre **4.5** and star PCL **2.7** before and after enzymatic degradation with *pseudomonas cepacia* lipase in a PBS solution (pH 7.4) at 37 °C, determined by DSC at 10 °C min^{-1}

Sample	β-CD	Enzymatic degradation	Mass Loss	ΔH_m	ΔH_c	T_m	T_c	χ_c
	%	days	%	J g^{-1}		°C		%
Star PCL **2.7**	0	0	-	90	101	53 - 58	29 - 35	73
		1	8.6	36	41	54 - 59	30 - 34	29
		2	14.3	42	48	54 - 58	30 - 34	34
		4	29.5	10	11	55 - 57	31 - 35	8
		15	94.3	4	5	54 - 56	31 - 35	3
4.5	9	0	-	23	22	48 - 53	27 - 33	16
		2	1.7	51	52	49 - 55	26 - 32	38
		10	3.7	13	14	48 - 54	28 - 33	10
		20	7.1	102	104	48 - 53	24 - 29	74

It can be seen that **4.5** shows an initial increase in $\%\chi_c$ from 16% to 38 % after 2 days of enzymatic degradation. This can be explained by the enzyme preferentially degrading the amorphous regions in the polymer film and therefore, increasing the overall $\%\chi_c$ of the polymer. Furthermore, the $\%\chi_c$ will be expected to increase upon the formation of shorter,

more crystalline PCL fragments during enzymatic degradation, leading to less chain entanglement. The $\%\chi_c$ of **4.5** is then seen to decrease from 38% to 10% after 2 and 10 days of enzymatic degradation, respectively. This can be explained due to the enzyme then degrading the more crystalline areas in the polymer film and therefore, decreasing the overall $\%\chi_c$ of the polymer. This is supported by the literature, generally showing an initial increase in $\%\chi_c$ during the first stages of enzymatic degradation of polyesters, followed by a decrease in $\%\chi_c$ in the latter stages of enzymatic degradation.[13] However, the $\%\chi_c$ is seen to significantly increase from 10% to 74% after 10 and 20 days of enzymatic degradation, respectively. This could be explained by the formation of inclusion complexes of degraded crystalline PCL fragments inside the β-CD inner cavity. This increase in $\%\chi_c$ significantly decreases the rate of enzymatic degradation, as the enzymes and water have restricted access to the hydrolysable ester groups on the PCL moiety.

The melting temperature (T_m) and crystallisation temperature (T_c) of **4.5** and star PCL **2.7** generally remained unchanged during enzymatic degradation. This is consistent with previously reported data in the enzymatic degradation of polyesters.[14] On the other hand, the enthalpy of melting (ΔH_m) was seen to significantly decrease from 90 J g^{-1} to 4 J g^{-1} in star PCL **2.7**, and significantly increase from 23 J g^{-1} to 102 J g^{-1} in **4.5**. Similarily, the enthalpy of crystallisation (ΔH_c) was seen to significantly decrease from 101 J g^{-1} to 5 J g^{-1} in star PCL **2.7**, and significantly increase from 22 J g^{-1} to 104 J g^{-1} in **4.5**. These results are in line with the relative decreases and increases in $\%\chi_c$ seen in star PCL **2.7** and **4.5**.

4.4 Conclusion

Seven-arm star PCL with a β-CD core **4.5** and $\overline{DP}_{Th}$ of 30 per arm was synthesised in a four-step procedure. Due to the poor solubility of β-CD in ε-CL and common organic solvents, the fourteen 2° OH groups on the β-CD moiety were acetylated using acetic anhydride by firstly protecting the 1° OH groups using TBDMS-Cl. The TBDMS moieties were then removed to give partially acetylated β-CD containing seven 1° OH groups to be used in the ROP of ε-CL in bulk conditions. The products from each step were obtained in good yield and fully characterised using NMR, FT-IR and SEC analyses. Furthermore, contact angle, wettability and %WU were measured for seven-arm star PCL with a β-CD core **4.5** and compared to six-arm star PCL **2.7** with a dipentaerythritol core. The seven-arm star PCL with a β-CD core **4.5** showed increased hydrophilicity with an initial contact angle of 76° compared to star PCL **2.7** with an initial contact angle of 86°, indicating the incorporation of a β-CD moiety imparts a small degree of hydrophilicity. However, seven-arm star PCL with a β-CD core **4.5** exhibited poor wettability as negligible change in contact angle was detected over 30 s, compared to a small decrease seen in star PCL **2.7**. Furthermore, β-CD centered seven-arm star PCL **4.5** showed a very low %WU of 2%, due to the functionalization of all the OH groups in the central β-CD moiety.

The enzymatic degradation of seven-arm star PCL with a β-CD core **4.5** was investigated using *pseudomonas cepacia* lipase and showed a very low rate of enzymatic degradation with 7% mass loss in 20 days, compared to star PCL **2.7** with 94% mass loss in 15 days. This can be explained by the low wettability of seven-arm star PCL with a β-CD core **4.5** and the potential formation of inclusion complexes with the β-CD inner cavity and either the *pseudomonas cepacia* lipase enzyme or degraded PCL fragments. This will restrict mobility and access of the enzyme to the hydrolysable ester groups on the PCL moiety and therefore, decrease the rate of enzymatic degradation.

The changes in thermal properties of seven-arm star PCL with a β-CD core **4.5** throughout enzymatic degradation were monitored using DSC analyses. An initial increase in $\%\chi_c$ from 16% to 38% was seen after 2 days, followed by a decrease to 10% after 10 days, and a significant increase to 74% after 20 days of enzymatic degradation. The initial increase in $\%\chi_c$ could be explained by the preferential enzymatic degradation of the amorphous regions on the polymer film, followed by the subsequent degradation of more crystalline areas, causing a decrease in $\%\chi_c$. The significant increase in $\%\chi_c$ seen

after 20 days of enzymatic degradation could be due to the formation of inclusion complexes with crystalline PCL degradation products and the inner cavity of the β-CD moiety.

4.5 References

(1) Mellet, C. O.; Fernandez, J. M. G.; Benito, J. M. *Chem. Soc. Rev.* **2011**, *40*, 1586.
(2) Astray, G.; Gonzalez-Barreiro, C.; Mejuto, J. C.; Rial-Otero, R.; Simal-Gándara, J. *Food Hydrocoll.* **2009**, *23*, 1631.
(3) Numanoğlu, U.; Şen, T.; Tarimci, N.; Kartal, M.; Koo, O. M. Y.; Önyüksel, H. *AAPS Pharm. Sci. Tech* **2007**, *8*, 34.
(4) Potolinca, V. O.; Oprea, S.; Ciobanu, A.; Lungu, N. C. *J. Optoelectron. Adv. Mater.* **2011**, *13*, 1246.
(5) Zia, F.; Zia, K. M.; Zuber, M.; Kamal, S.; Aslam, N. *Carbohydr. Polym.* **2015**, *134*, 784.
(6) Sreenivasan, K. *Polym. Eng. Sci.* **1996**, *36*, 262.
(7) Gou, P. F.; Zhu, W. P.; Shen, Z. Q. *Biomacromolecules* **2010**, *11*, 934.
(8) Miao, Y.; Rousseau, C.; Mortreux, A.; Martin, P.; Zinck, P. *Polymer* **2011**, *52*, 5018.
(9) Shen, J.; Hao, A.; Du, G.; Zhang, H.; Sun, H. *Carbohydr. Res.* **2008**, *343*, 2517.
(10) Gou, P. F.; Zhu, W. P.; Xu, N.; Shen, Z. Q. *J. Polym. Sci. Pol. Chem.* **2008**, *46*, 6455.
(11) Tonelli, A. E. *Polymer* **2008**, *49*, 1725.
(12) Wenz, G.; Han, B.-H.; Müller, A. *Chem. Rev.* **2006**, *106*, 782.
(13) Khankrua, R.; Pivsa-Art, S.; Hiroyuki, H.; Suttiruengwong, S. *Polym. Degrad. Stabil.* **2014**, *108*, 232.
(14) Sekosan, G.; Vasanthan, N. *J. Polym. Sci. Part B: Polym. Phys.* **2010**, *48*, 202.

5 Synthesis and Degradation Studies of Diisocyanate Prepolymers

5.1 Introduction

Isocyanates are essential components in the synthesis of polyurethanes (PU) and can be di- or multi-functional, containing two or more NCO groups per molecule. The reactivity of the NCO group is determined by the positive character of the carbon atom, which is susceptible to attack from nucleophiles. Aromatic isocyanates show a higher reactivity compared to aliphatic isocyanates as the negative charge on the nitrogen atom can be delocalised in the aromatic ring, see Chapter 1 Section 1.2.5. The choice of isocyanate is dependent on the required physical properties of the PU suitable for its application. For the purpose of this research, aromatic diisocyanates 4,4'-methylenebis(phenyl isocyanate) (MDI) **5.1** and toluene-2,4-diisocyanate (TDI) **5.2**, Figure 5.1, are investigated as they are commonly used in the synthesis of rigid PU foams.

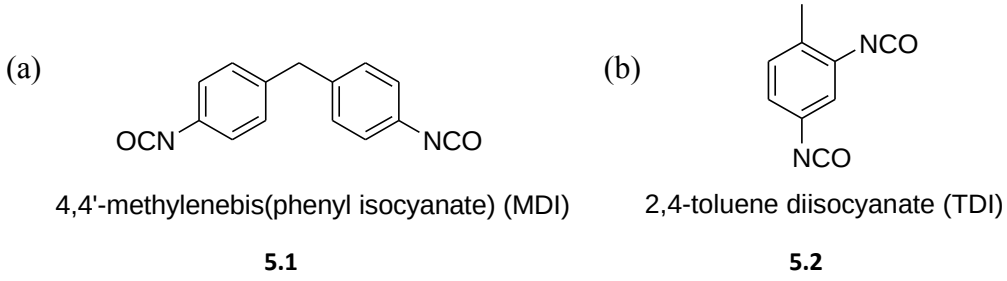

Figure 5.1: Structures of (a) MDI **5.1** and (b) TDI **5.2**

Problems with miscibility of the diisocyanate and polyol components during PU synthesis can lead to phase separation, resulting in incomplete reactions and therefore, poor mechanical properties.[1] This problem is overcome by using a two-step prepolymer synthesis wherein a NCO-terminated prepolymer is synthesised and subsequently reacted with polyols or polyamines to give PU.[2,3] Importantly, this two-step process could increase the rate of biodegradation by the incorporation of a degradable link between the two isocyanate moieties. Furthermore, the two-step process will decrease the number of rigid crystalline aromatic isocyanate regions, as the isocyanate moieties will be spaced apart.

Therefore, polymer chains will show increased mobility and increased access for water and enzymes to degrade the hydrolysable segments in the polymer.

Teng *et al*. reported the synthesis of diisocyanate prepolymers containing a central poly(ε-caprolactone) (PCL) moiety capped with hexamethylene diisocyanate (HDI) moieties.[4] FT-IR and NMR analyses showed the appearance of a urethane group and the presence of NCO groups in the diisocyanate prepolymers. However, no investigation into the degradation characteristics of the diisocyanate prepolymers were undertaken. Similarly, HDI-based diisocyanate prepolymers containing a central PCL moiety have been reported using a ratio of NCO/OH of 2:1.[5] An attempt was made to limit any further reactions of the NCO groups on the prepolymer moiety, by performing the synthesis at a relatively low temperature of 80-85 °C for 1 h. However, no evidence is provided to show if further reactions of the NCO group did or did not occur.

The synthesis of diisocyanate prepolymers were reported by the reaction of PCL diol and diisocyanates MDI, 2,4-TDI, 1,1'-methylenebis(4-isocynaatocyclohexane) (HDMI), or 1,4-phenylene diisocyanate (PDI) in a ratio of 2.07:1 of NCO:OH groups.[6] The prepolymers were then reacted with chain extenders to produce multi-block copolymers. SEC analyses showed significantly higher molecular weights and dispersities (Đ) for copolymers with increasing reaction time. This suggests further reactions of the NCO group and secondary reactions of the urethane group on the diisocyanate prepolymers are taking place. Furthermore, high reaction temperatures used in the diisocyanate prepolymer synthesis with MDI at 170 °C and TDI at 160 °C, is highly likely to increase the possibility of secondary reactions occurring, see Chapter 1 Section 1.2.5.1

The synthesis of environmentally friendly diisocyanate prepolymers have been reported using isophorone diisocyanate and castor oil with an excess of NCO groups to OH groups.[7] The reaction was monitored using FT-IR analyses, showing the appearance of urethane groups, however, no degradation or toxicity tests were undertaken for the diisocyanate prepolymer to confirm the production of harmless degradation products.

This chapter concerns the synthesis of biodegradable diisocyanate prepolymers containing a central PCL or PCL-*b*-PEG-*b*-PCL moiety and capped with either MDI **5.1** or TDI **5.2** moieties. It is believed that prepolymer synthesis, with the incorporation of a biodegradable link between two aromatic isocyanate moieties, will increase the rate of PU biodegradation. This is due to the spacing of large crystalline aromatic groups by a

biodegradable linear moiety. Furthermore, the use of a diisocyanate prepolymer in PU synthesis should decrease the formation of isocyanate-rich domains within the PU structure, which are particularly difficult for enzymes and water to access and degrade. All biodegradable diisocyanate prepolymers were fully characterised using NMR, FT-IR, SEC, % water uptake and contact angle analyses. Enzymatic degradation studies with *pseudomonas cepacia* lipase were monitored using % mass loss and DSC analyses, to determine changes in thermal properties throughout enzymatic degradation.

5.2 Experimental

5.2.1 Materials

ε-Caprolactone (ε-CL), tin (II) ethyl hexanoate ($SnOct_2$), poly(ε-caprolactone) diol (PCL diol) (M_n = 530 g mol^{-1}), toluene-2,4-diisocyanate (TDI) **5.2** and 4,4'-methylenebis(phenyl isocyanate) (MDI) **5.1** were purchased from Sigma Aldrich and used without further purification unless otherwise stated. ε–CL was distilled over CaH_2 under reduced pressure prior to use. All dry solvents were obtained from Durham Chemistry Department Solvent Purification System (SPS). All other solvents were analytical grade and used without any purification. Deuterated chloroform ($CDCl_3$) was purchased from Apollo Scientific.

5.2.2 Characterisation Techniques

^{1}H and ^{13}C Nuclear magnetic resonance (NMR), Fourier transform infra-red spectroscopy (FT-IR), Size Exclusion Chromatography (SEC) and Differential Scanning Calorimetry (DSC) measurements were carried out as described in Chapter 2, Section 2.2.2.

Contact angle measurements were carried out as outlined in Chapter 3, Section 3.2.2.

5.2.3 Enzymatic Degradation

Enzymatic degradation tests were carried out as outlined in Chapter 2, Section 2.2.3.

5.2.4 Water Uptake

The % water uptake (%WU) measurements were carried out as outlined in Chapter 3, Section 3.2.4.

5.2.5 Synthesis of Diisocyanate Prepolymers containing a Central PCL Moiety 5.3 – 5.4

PCL-based diisocyanate prepolymers were synthesised by the reaction of di-hydroxyl linear PCL and two molar equivalents of diisocyanates MDI **5.1** or TDI **5.2** to give a linear diisocyanate prepolymer containing a central PCL moiety **5.3 - 5.4**, following the reported method in the literature.[4]

5.2.5.1 Synthesis of TDI-based Diisocyanate Prepolymer containing a Central PCL moiety 5.3

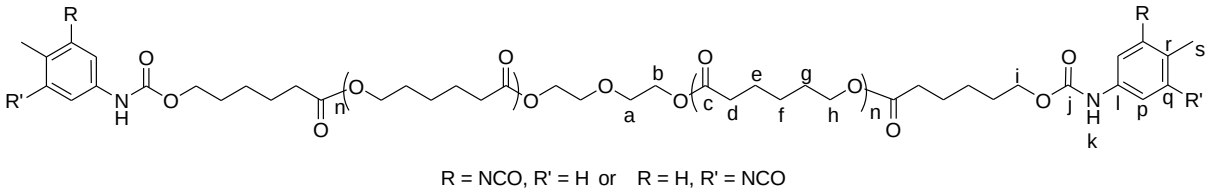

Figure 5.2: TDI-based diisocyanate prepolymer containing a central PCL moiety **5.3**

Poly(ε-caprolactone) diol (M_n = 530 g mol^{-1}) was added to a 3-necked round bottom flask equipped with a mechanical stirrer and heated at 120 °C for 2 h under reduced pressure. The flask was cooled to 100 °C and toluene-2,4-diisocyanate (4.93 g, 28.3 mmol) was added under a flow of N_2 and stirred for 1 h to give a clear, colourless, viscous liquid **5.1**. ^{1}H NMR (600 MHz, $CDCl_3$, TMS): (ppm) δ = 1.34 (m, 10H, H_f), 1.61 (m, 20H, H_e, H_g), 2.21 (s, 10H, H_s), 2.27 (m, 10H, H_d), 3.66 (m, 4H, H_a), 4.02 (m, 6H, H_h), 4.10 (t, *J* = 6.4 Hz, 4H, H_i), 4.19 (m, 4H, H_b), 4.26 (m, 2H, H_k), 7.03-7.22 (m, 8H, H_q, H_p). ^{13}C NMR (150 MHz, $CDCl_3$, TMS): (ppm) δ = 17.6 (s), 24.6 (e), 25.5 (f), 28.3 (g), 34.1 (d), 63.3 (b), 64.1 (h), 65.1 (i), 69.1 (a), 127.4 (r), 130.6 (q), 132.6 (t), 137.0 (l), 153.6 (j), 173.6 (c). FT-IR: ν_{max} = 3342 (N-H), 2948, 2864 (C-H), 2260 (N=C), 1728 (C=O), 1594 (Aromatic C=C), 1530 (C-N), 1218, 1066, 818 cm^{-1}. SEC: M_n = 1.44 x 10^3 g mol^{-1}, M_w = 1.77 x 10^3 g mol^{-1}, Đ = 1.22. The ^{1}H, ^{13}C NMR and FT-IR data are in agreement with that reported in the literature.[4]

5.2.5.2 Synthesis of MDI-based Diisocyanate Prepolymer containing a Central PCL moiety 5.4

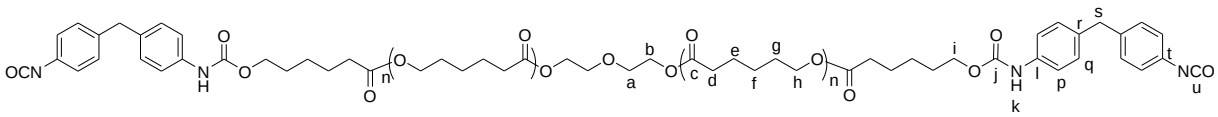

Figure 5.3: MDI-based diisocyanate prepolymer containing a central PCL moiety **5.4**

Poly(ε-caprolactone) diol (M_n = 530 g mol^{-1}) was added to a 3-necked round bottom flask equipped with a mechanical stirrer and heated at 120 °C for 2 h under reduced pressure. The flask was cooled to 80 °C under a N_2 atmosphere and 4,4'-methylenebis(phenyl isocyanate) (7.08 g, 28.30 mmol) was added. The reaction mixture was stirred at 80 °C for

30 min under a flow of N_2 to give a clear, colourless, viscous liquid **5.4**. ^{1}H NMR (600 MHz, $CDCl_3$, TMS): (ppm) δ = 1.37 (m, 10H, H_f), 1.63 (m, 19H, H_e, H_g), 2.29 (m, 10H, H_d), 3.68 (m, 4H, H_a), 3.87 (m, 4H, H_s), 4.06 (t, *J* = 6.4 Hz, 6H, H_h), 4.12 (m, 4H, H_i), 4.21 (t, *J* = 4.6 Hz, 4H, H_b), 4.28 (bs, 2H, H_k), 6.98 (m, 2H, H_p), 7.07 (m, 6H, H_q), 7.29 (m, 3H, H_q). ^{13}C NMR (150 MHz, $CDCl_3$, TMS): (ppm) δ = 24.6 (e), 25.5 (f), 28.4 (g), 34.2 (d), 40.7 (s), 63.4 (b), 64.2 (h), 65.0 (i), 69.1 (a), 118.9 (q), 124.7 (p), 129.4, (q) 130.0 (q), 131.3 (t), 136.0 (r), 139.0 (l), 153.8 (j), 173.7 (c). FT-IR: ν_{max} = 3332 (N-H), 2944, 2866 (C-H), 2256 (N=C), 1718 (C=O), 1598 (Aromatic C=C), 1526 (C-N), 1412, 1218, 1066, 818 cm^{-1}. SEC: M_n = 3.17 x 10^3 g mol^{-1}, M_w = 4.66 x 10^3 g mol^{-1}, Đ = 1.47. The ^{1}H, ^{13}C NMR and FT-IR data are in agreement with that reported in the literature.[4]

5.2.6 Synthesis of TDI-based Diisocyanate Prepolymer containing a Central PCL-*b*-PEG-*b*-PCL moiety with a $\overline{DP}$ of 50 per arm 5.5

Diisocyanate prepolymers with a central PCL-*b*-PEG-*b*-PCL moiety were synthesised based on the method reported in the literature.[4] Di-hydroxyl PCL-*b*-PEG-*b*-PCL **3.3** was reacted with two molar equivalents of either MDI **5.1** or TDI **5.2** to give linear diisocyanate prepolymers **5.5**, **5.6** and **5.7**.

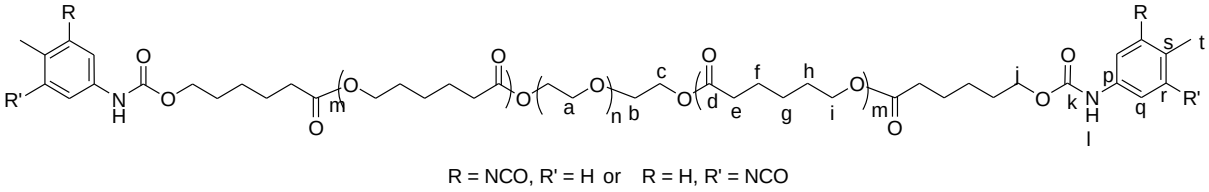

Figure 5.4: TDI-based Diisocyanate Prepolymer containing a central PCL-*b*-PEG-*b*-PCL moiety with a $\overline{DP}$ of 50 per arm **5.5**

Poly[(ε-caprolactone)-*b*-(ethylene glycol)-*b*-(ε-caprolactone)] **3.3** with a $\overline{DP}$ of fifty per arm (synthesis outlined in Chapter 3 Section 3.2.5.2) (3.00 g, 0.64 mmol) was added to a 3-necked round bottom flask equipped with a mechanical stirrer and heated at 120 °C for 2 h under reduced pressure. The flask was cooled to 100 °C and toluene-2,4-diisocyanate **5.2** (0.22 g, 1.28 mmol) was added under a flow of N_2 and stirred for 1 h to give a clear, colourless, viscous liquid **5.5**. ^{1}H NMR (400 MHz, $CDCl_3$, TMS): (ppm) δ = 1.34 (m, 133H, H_g), 1.59 (m, 259H, H_f, H_h), 2.14 (s, 7H, H_q), 2.26 (t, *J* = 7.1 Hz, 123H, H_e), 3.59 (m, 52H, H_a), 3.64 (m, 4H, H_b), 4.00 (t, *J* = 6.1 Hz, 122H, H_i), 4.10 (m, 5H, H_j), 4.17 (m,

4H, H_c), 6.87-7.23 (m, 8H, H_q, H_r). ^{13}C NMR (100 MHz, $CDCl_3$, TMS): (ppm) δ = 17.0 (t), 24.6 (f), 25.6 (g), 28.4 (h), 34.1 (e), 63.5 (c), 64.2 (i), 64.9 (j), 69.2 (b), 70.6 (a), 130.7 (r), 136.2 (p), 153.7 (k), 173.5 (d). FT-IR: ν_{max} = 3360 (N-H), 2946, 2868 (C-H), 2360 (N=C), 1724 (C=O), 1538 (C-N), 1364, 1236, 1164 cm^{-1}. SEC: $M_n = 0.99 \times 10^4$ g mol^{-1}, $M_w = 0.13 \times 10^4$ g mol^{-1}, Đ = 1.29. The ^{1}H, ^{13}C NMR and FT-IR data are in agreement with that reported in the literature.[4]

5.2.7 Synthesis of MDI-based Diisocyanate Prepolymer with a Central PCL-*b*-PEG-*b*-PCL moiety and a $\overline{DP}$ of 50 per arm 5.6

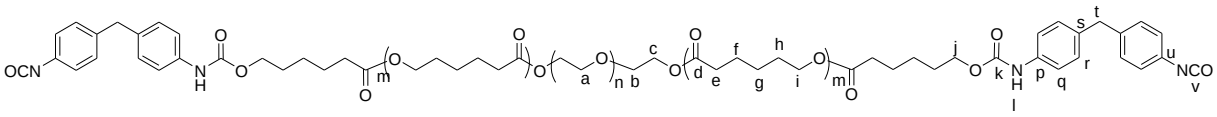

Figure 5.5: MDI-based diisocyanate prepolymer containing a central PCL-*b*-PEG-*b*-PCL moiety with a $\overline{DP}$ of 50 per arm **5.6**

Poly[(ε-caprolactone)-*b*-(ethylene glycol)-*b*-(ε-caprolactone)] **3.3** with a $\overline{DP}$ of fifty per arm (synthesis outlined in Chapter 3 Section 3.2.5.2) (3.00 g, 0.64 mmol) was added to a 3-necked round bottom flask equipped with a mechanical stirrer and heated at 120 °C for 2 h under reduced pressure. The flask was cooled to 80 °C under a N_2 atmosphere and 4,4'-methylenebis(phenyl isocyanate) **5.1** (0.32 g, 1.28 mmol) was added. The reaction mixture was stirred at 80 °C for 30 min under a flow of N_2 to give a clear, colourless, viscous liquid **5.6**. ^{1}H NMR (400 MHz, $CDCl_3$, TMS): (ppm) δ = 1.34 (m, 180H, H_g), 1.61 (m, 360H, H_f, H_h), 2.27 (t, *J* = 7.4 Hz, 180H, H_e), 3.60 (m, 52H, H_a, H_b), 3.86 (m, 4H, H_t), 4.02 (t, *J* = 6.6 Hz, 180H, H_i), 4.10 (t, *J* = 6.3 Hz, 4H, H_j), 4.17 (t, *J* = 4.7 Hz, 4H, H_c), 6.98 (m, 8H, H_q), 7.06 (m, 4H, H_r), 7.26 (m, 4H, H_r). ^{13}C NMR (100 MHz, $CDCl_3$, TMS): (ppm) δ = 24.6 (f), 25.6 (g), 28.4 (h), 34.2 (e), 40.6 (t), 63.5 (c), 64.2 (i), 65.0 (j), 69.2 (b), 70.6 (a), 129.4 (r), 138.4 (s), 153.7 (k), 173.6 (d). FT-IR: ν_{max} = 3358 (N-H), 2946, 2866 (C-H), 2264 (N=C), 1720 (C=O), 1532 (C-N), 1366, 1240, 1172 cm^{-1}. SEC: $M_n = 1.52 \times 10^4$ g mol^{-1}, $M_w = 2.16 \times 10^4$ g mol^{-1}, Đ = 1.42. The ^{1}H, ^{13}C NMR and FT-IR data are in agreement with that reported in the literature.[4]

5.2.8 Synthesis of MDI-based Diisocyanate Prepolymer with a Central PCL-*b*-PEG-*b*-PCL moiety and a $\overline{DP}$ of 10 per arm 5.7

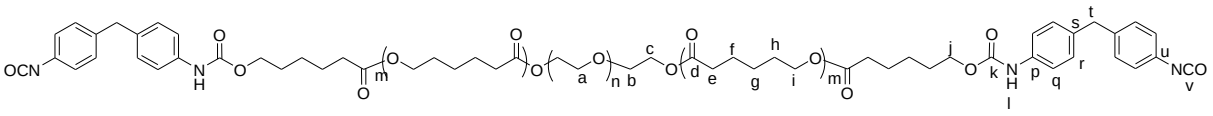

Figure 5.6: MDI-based diisocyanate prepolymer using a central PCL-*b*-PEG-*b*-PCL moiety with a $\overline{\mathbf{DP}}$ of 10 per arm **5**.**7**

Poly[(ε-caprolactone)-*b*-(ethylene glycol)-*b*-(ε-caprolactone)] **3.2** with a $\overline{DP}$ of ten per arm (synthesis outlined in Chapter 3 Section 3.2.5.1) (3.00 g, 1.04 mmol) was added to a 3-necked round bottom flask equipped with a mechanical stirrer and heated at 120 °C for 2 h under reduced pressure. The flask was cooled to 80 °C under a N_2 atmosphere and 4,4'-methylenebis(phenyl isocyanate) **5.1** (0.52 g, 2.08 mmol) was added. The reaction mixture was stirred at 80 °C for 30 min under a flow of N_2 to give a clear, colourless, viscous liquid **5.7**. ^{1}H NMR (400 MHz, $CDCl_3$, TMS): (ppm) δ = 1.35 (m, 60H, H_g), 1.62 (m, 120H, H_f, H_h), 2.27 (t, *J* = 7.4 Hz, 60H, H_e), 3.61 (m, 52H, H_a), 3.65 (m, 4H, H_b), 3.84 (m, 4H, H_t), 4.03 (t, *J* = 6.6 Hz, 60H, H_i), 4.10 (t, *J* = 6.5 Hz, 4H, H_j), 4.18 (t, *J* = 4.6 Hz, 4H, H_c), 6.87 (m, 8H, H_q), 7.05 (m, 4H, H_r), 7.26 (m, 4H, H_r). ^{13}C NMR (400 MHz, $CDCl_3$, TMS): (ppm) δ = 24.6 (e), 25.5 (f), 28.3 (g), 34.1 (d), 40.5 (s), 63.5 (b), 64.1 (f), 65.0 (i), 70.5 (a), 129.4 (q), 136.1 (r), 153.8 (j), 173.5 (c). FT-IR: ν_{max} = 2946, 2866 (C-H), 2260 (C=N), 1722 (C=O), 1536 (Aromatic C=C), 1238, 1170 (C-O) cm^{-1}. SEC: M_n = 1.01 x 10^4 g mol^{-1}, M_w = 1.48 x 10^4 g mol^{-1}, Đ = 1.46. The ^{1}H, ^{13}C NMR and FT-IR data are in agreement with that reported in the literature.[4]

5.3 Results and Discussion

5.3.1 Diisocyanate Prepolymers containing a Central PCL moiety 5.3 – 5.4

Diisocyanate prepolymers containing a central PCL moiety **5.3** and **5.4** were synthesised by the reaction of PCL diol and two molar equivalents of either TDI **5.2** or MDI **5.1** respectively, Scheme 5.1.

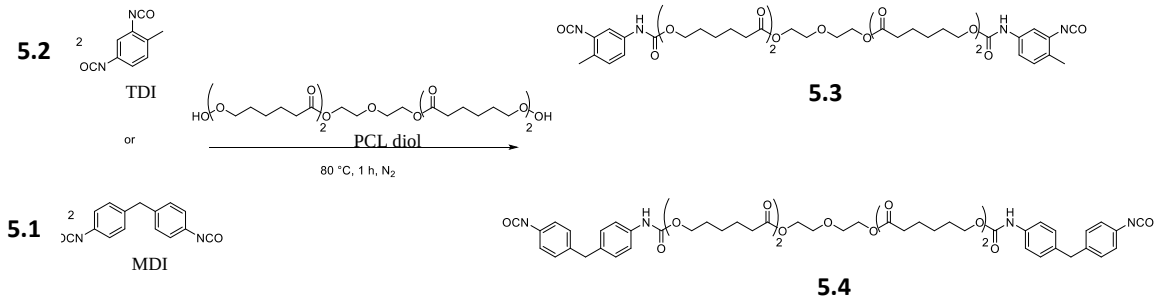

Scheme 5.1: Synthesis of diisocyanate prepolymers **5.3** and **5.4** containing a central PCL moiety

5.3.1.1 TDI-based Diisocyanate Prepolymer containing a Central PCL moiety 5.3

The ^{1}H NMR spectrum of **5.3**, Figure 5.7, shows the characteristic PCL resonances at 1.34 ppm, 1.61 ppm, 2.27 ppm and 4.02 ppm, attributing to methylene protons **f**, **e**/**g**, **d** and **h,** respectively. The resonances attributed to PCL methylene protons **i** neighbouring the urethane bond at 4.10 ppm, are shifted downfield to the resonance attributing to PCL methylene protons **h** neighbouring the ester bond at 4.02 ppm. This indicates the successful reaction of the NCO group on the TDI moiety and OH group on the PCL moiety. Moreover, the appearance of the resonance at 4.26 ppm attributing to the N-H proton **k**, indicates the successful reaction of the NCO and OH groups to give a urethane group. Resonances at 3.66 ppm and 4.19 ppm are attributed to the central ethylene protons **a** and **b** in the PCL diol moiety, respectively. The sharp singlet resonance at 2.21 ppm is attributed to methyl protons **s** on the TDI moiety. Furthermore, resonances at 7.03-7.20 ppm are attributed to aromatic methine protons **p** and **q** on the TDI moiety. The high integration of 4H and 4H for aromatic protons **p** and **q**, respectively, could indicate further reactions of the NCO group on the TDI moiety, or the urethane groups in **5.3**.

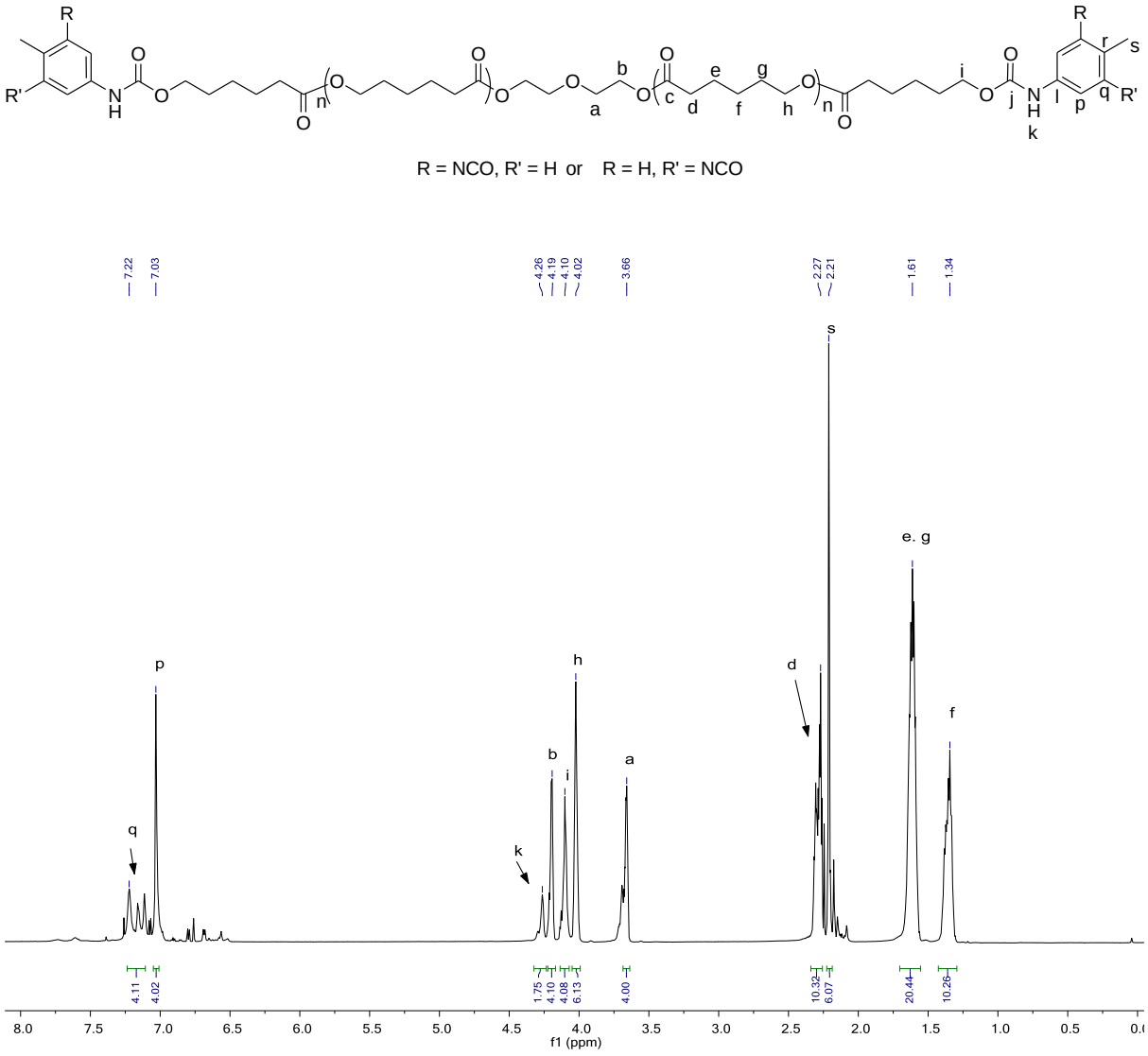

Figure 5.7: 600 MHz ^{1}H NMR spectrum of **5.3** in $CDCl_3$

The ^{13}C NMR spectrum of **5.3**, Figure 5.8, shows the characteristic PCL resonances at 24.5 ppm, 25.5 ppm, 28.3 ppm, 34.1 ppm and 64.1 ppm, attributed to methylene carbon atoms **e**, **f**, **g**, **d** and **h**, respectively. The downfield resonance at 173.6 ppm is attributed to carbonyl carbon atom **c** on the PCL moiety. The resonances at 63.3 ppm and 69.0 ppm are attributed to carbon atoms **b** and **a** located on the central ethylene moiety, respectively. The ^{1}H – ^{13}C HSQC spectrum of **5.3**, Figure 5.9, shows carbon atoms **b** and **a** at 63.3 ppm and 69.0 ppm correlate to protons **b** and **a**, at 4.19 ppm and 3.66 ppm, respectively. Furthermore, the ^{1}H – ^{13}C HMBC spectrum of **5.3**, Figure 5.10 shows protons **b** and **a** at 4.19 ppm and 3.66 ppm are neighbouring carbon atoms **a** and **b** at 69.0 ppm and 63.3 ppm, respectively.

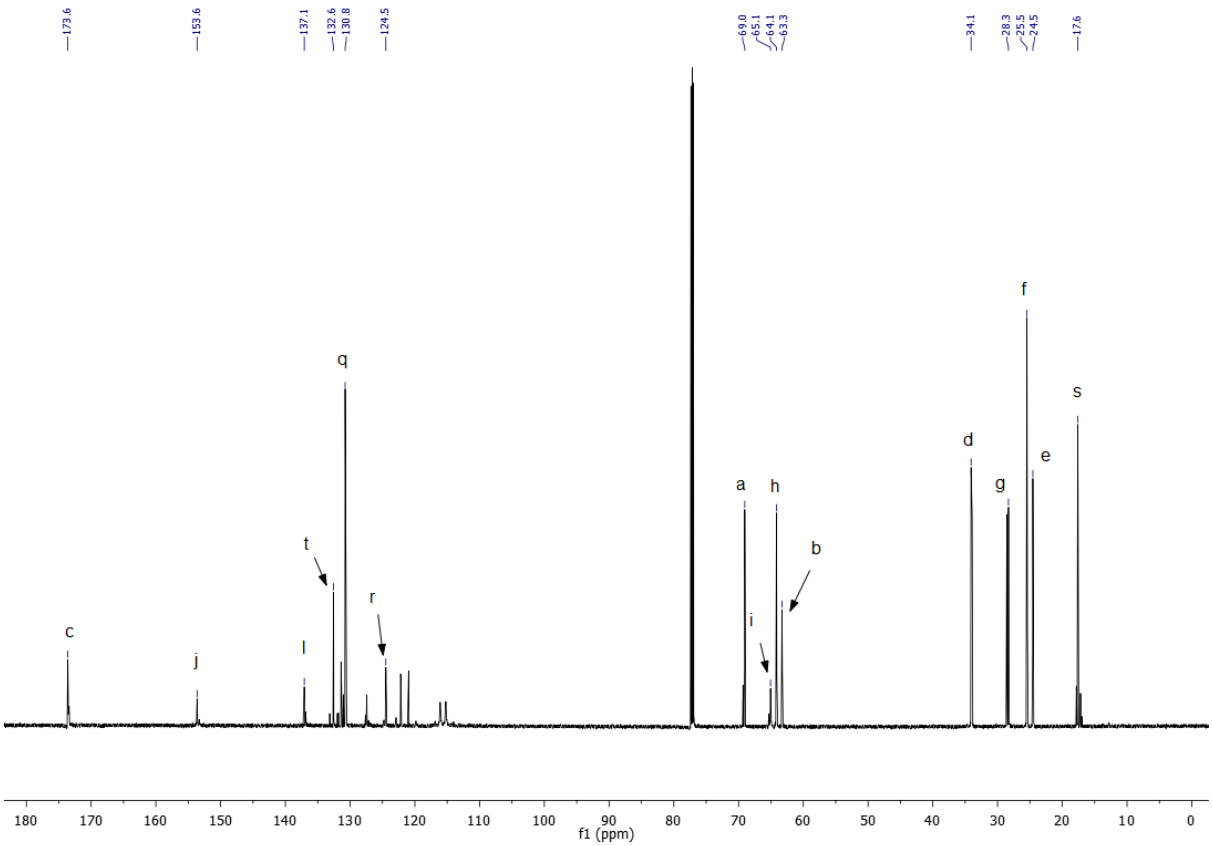

Figure 5.8: 150 MHz ^{13}C NMR spectrum of **5.3** in $CDCl_3$

The resonances at 65.1 ppm and 153.6 ppm are attributed to methylene carbon atom **i** neighbouring the urethane group on the PCL moiety, and carbonyl carbon atom **j** in the urethane group, respectively. The ^{1}H – ^{13}C HSQC spectrum of **5.3**, Figure 5.9, shows carbon atom **i** at 65.1 ppm correlate to protons **i** at 4.10 ppm. Furthermore, the ^{1}H – ^{13}C HMBC spectrum of **5.3**, Figure 5.10, shows PCL protons **i** at 4.10 ppm neighbouring carbonyl carbon atom **j** at 153.6 ppm in the urethane group. This confirms the reaction between the OH group on the PCL moiety and NCO group on the TDI moiety to form a urethane group.

The resonance at 17.6 ppm is attributed to the methyl carbon atom **s** on the TDI moiety. Furthermore, the resonances at 124.5 ppm, 130.8 ppm and 137.1 ppm are attributed to carbon atoms **r**, **q** and **l** on the aromatic ring of the TDI moiety. ^{1}H – ^{13}C HSQC spectrum of **5.3** shows the correlation between carbon atom **s** at 17.6 ppm and protons **s** at 2.21 ppm, confirming this assignment. Moreover, ^{1}H – ^{13}C HMBC spectrum of **5.3** show protons **s** at 2.21 ppm are neighbouring aromatic carbon atoms at 127.4-133.0 ppm on the TDI moiety.

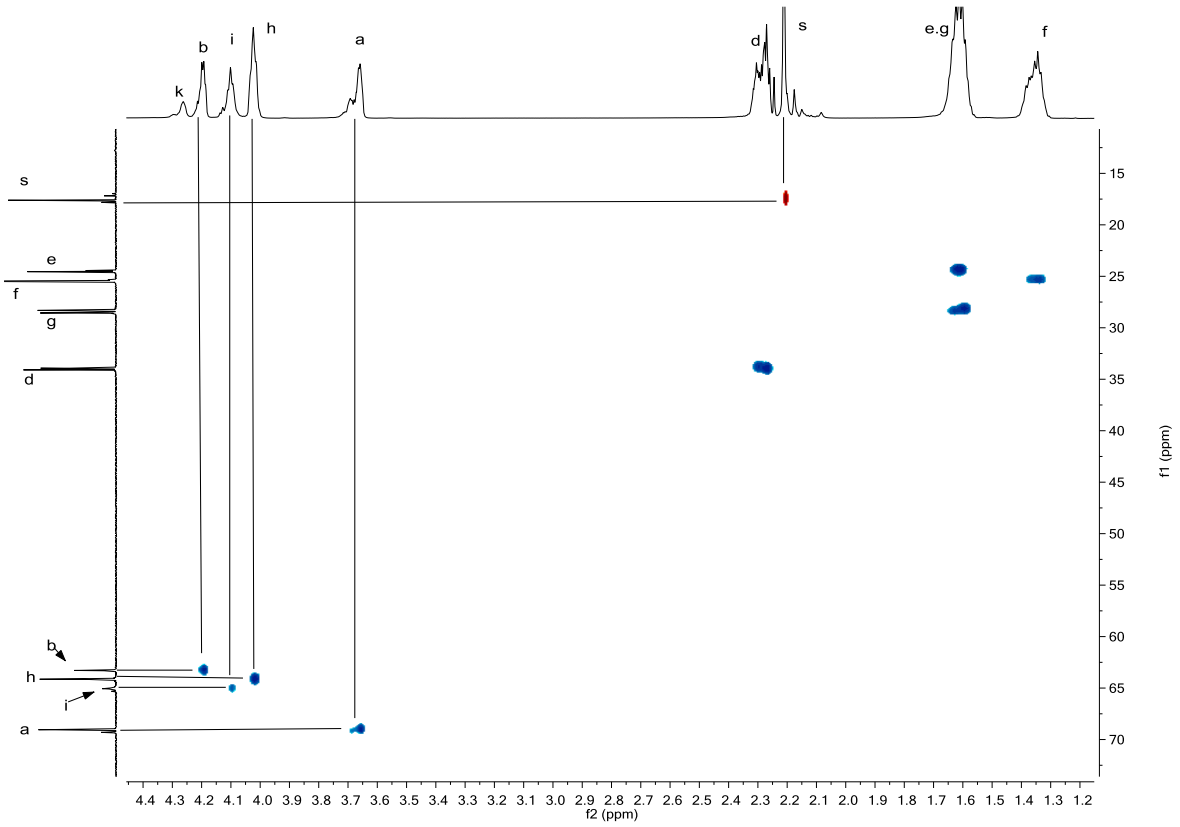

Figure 5.9: ^{1}H – ^{13}C HSQC spectrum of **5.3** in $CDCl_3$

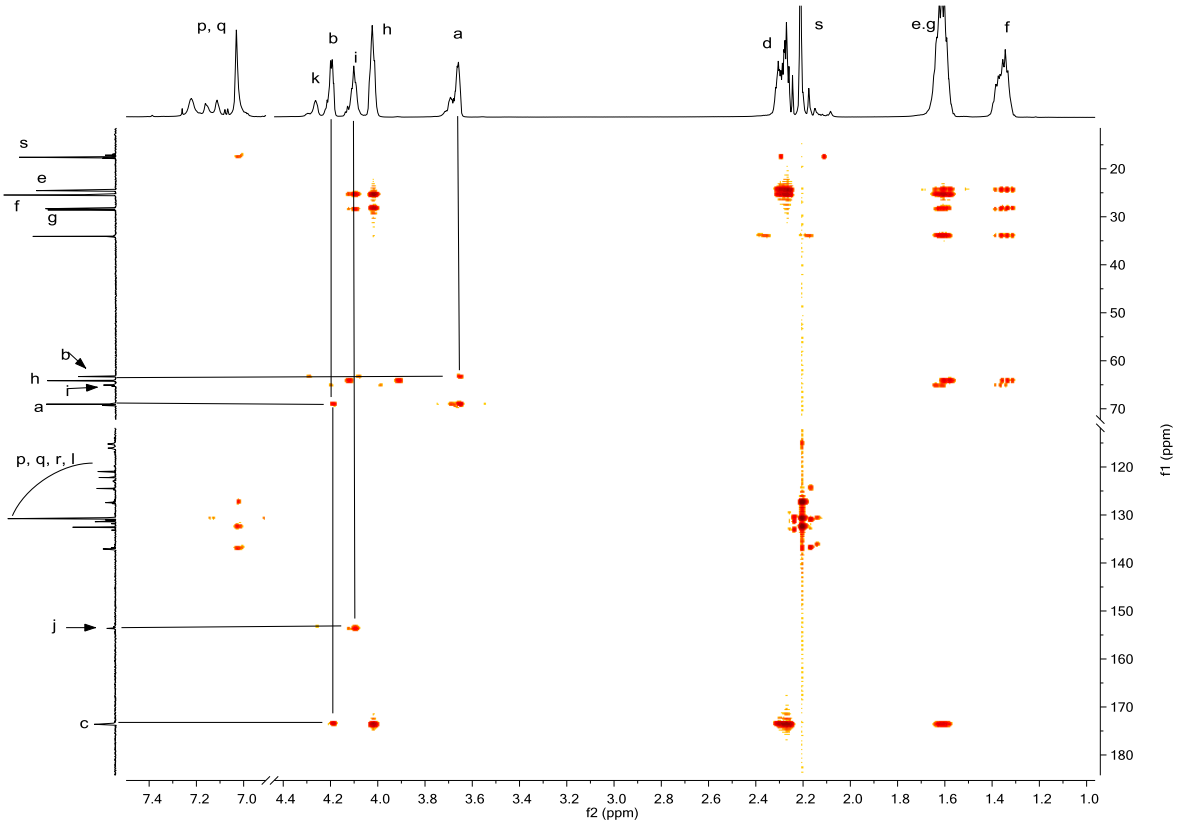

Figure 5.10: ^{1}H – ^{13}C HMBC spectrum of **5.3** in $CDCl_3$

5.3.1.2 MDI-based Diisocyanate Prepolymer containing a Central PCL moiety 5.4

The ^{1}H NMR spectrum of **5.4**, Figure 5.11, shows the characteristic PCL resonances at 1.37 ppm, 1.63 ppm, 2.29 ppm and 4.06 ppm, attributing to methylene protons **f**, **e**/**g**, **d** and **h**, respectively. The resonances at 3.68 ppm and 4.21 ppm are attributed to protons **a** and **b** on the central ethylene moiety, respectively. The broad resonance at 4.28 ppm is attributed to the N-H proton on the urethane bond, indicating the successful reaction of the NCO groups on the MDI moiety and OH groups on the PCL moiety. Furthermore, the resonance at 4.12 ppm is attributed to the methylene protons **i** on the PCL moiety neighbouring the urethane group, supporting the successful reaction between the PCL and MDI moieties. The resonance at 3.87 ppm is attributed to methylene protons **s** on the MDI moiety. Moreover, downfield resonances at 6.98-7.29 ppm are attributed the aromatic methine protons **p** and **q** on the MDI moiety.

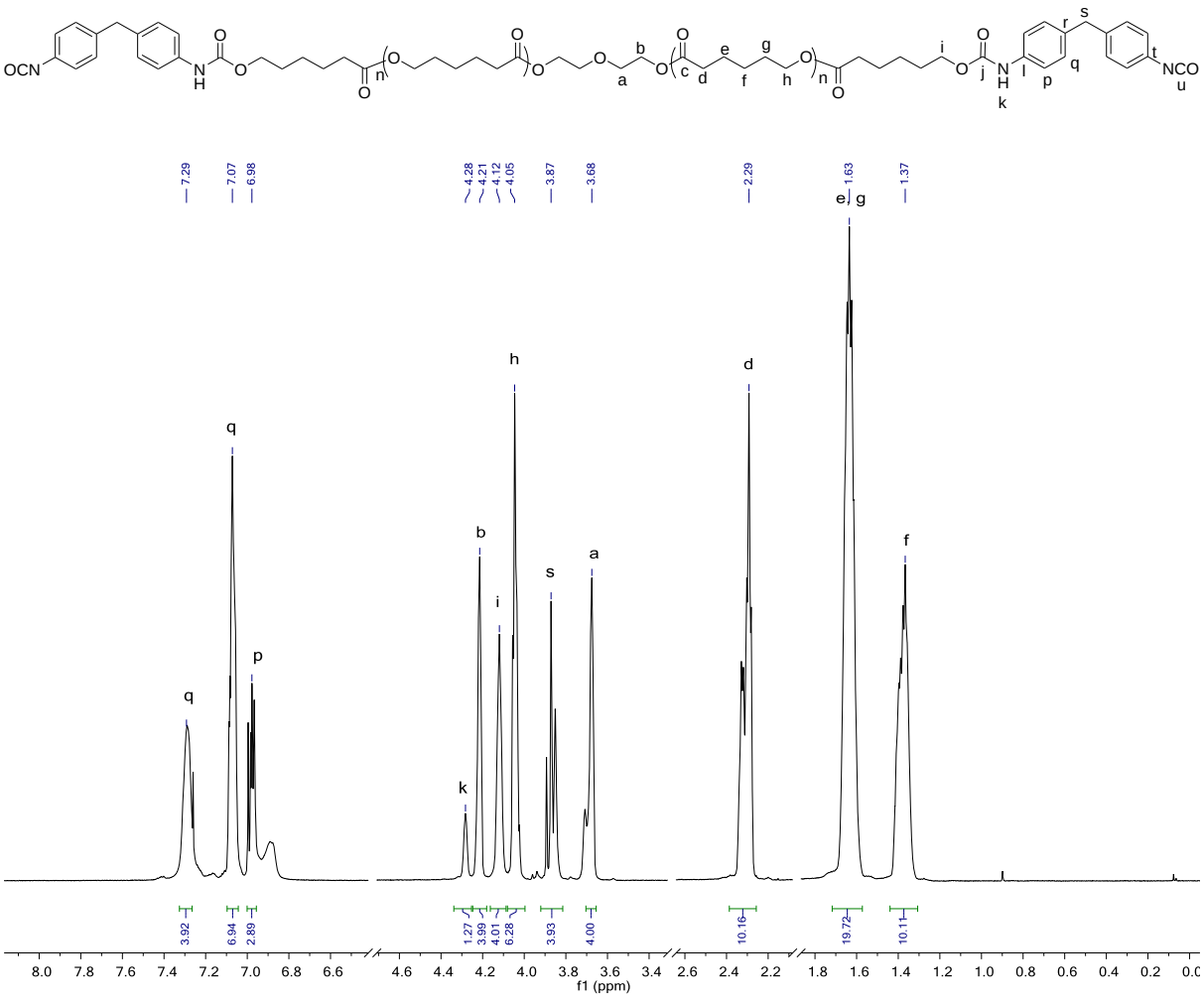

Figure 5.11: 600 MHz ^{1}H NMR spectrum of **5.4** in $CDCl_3$

The ^{13}C NMR spectrum of **5.4**, Figure 5.12, shows the characteristic PCL resonances at 24.6 ppm, 25.5 ppm, 28.4 ppm, 34.2 ppm and 64.2 ppm, attributing to methylene protons **e**, **f**, **g**, **d** and **h**, respectively. The downfield resonance at 173.7 ppm is attributed to the carbonyl carbon atom **c** on the PCL moiety. The resonances at 63.4 ppm and 69.1 ppm are attributed to protons **b** and **a** on the central ethylene moiety, respectively. The ^{1}H – ^{13}C HSQC spectrum of **5.4**, Figure 5.13, confirms this assignment by showing carbon atoms **b** and **a** at 63.4 ppm and 69.1 ppm correlate to protons **b** and **a** at 4.21 ppm and 3.68 ppm, respectively. Furthermore, the ^{1}H – ^{13}C HMBC spectrum of **5.4**, Figure 5.14, shows protons **b** at 4.21 ppm are neighbouring carbon atoms **a** and **c** at 69.1 ppm and 173.7 ppm, respectively.

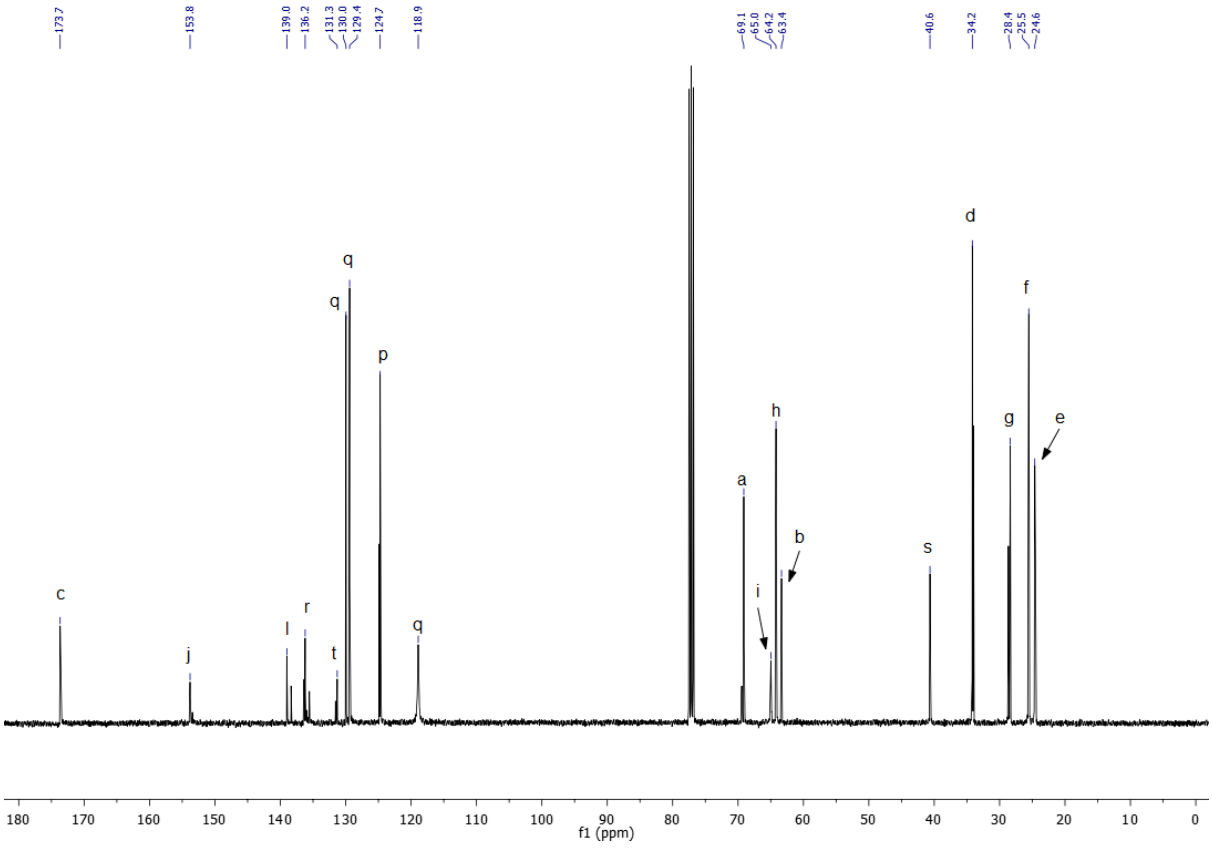

Figure 5.12: 150 MHz ^{13}C NMR spectrum of **5.4** in $CDCl_3$

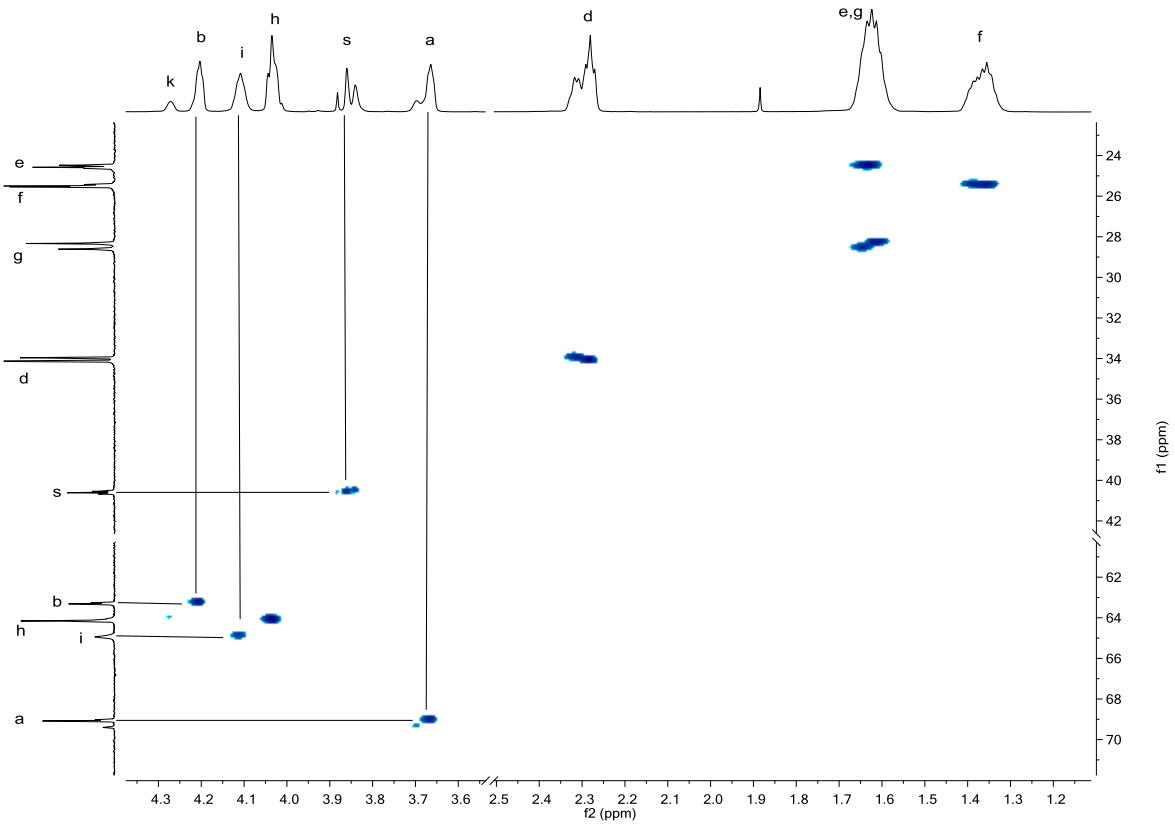

Figure 5.13: ^{1}H – ^{13}C HSQC spectrum of **5.4** in $CDCl_3$

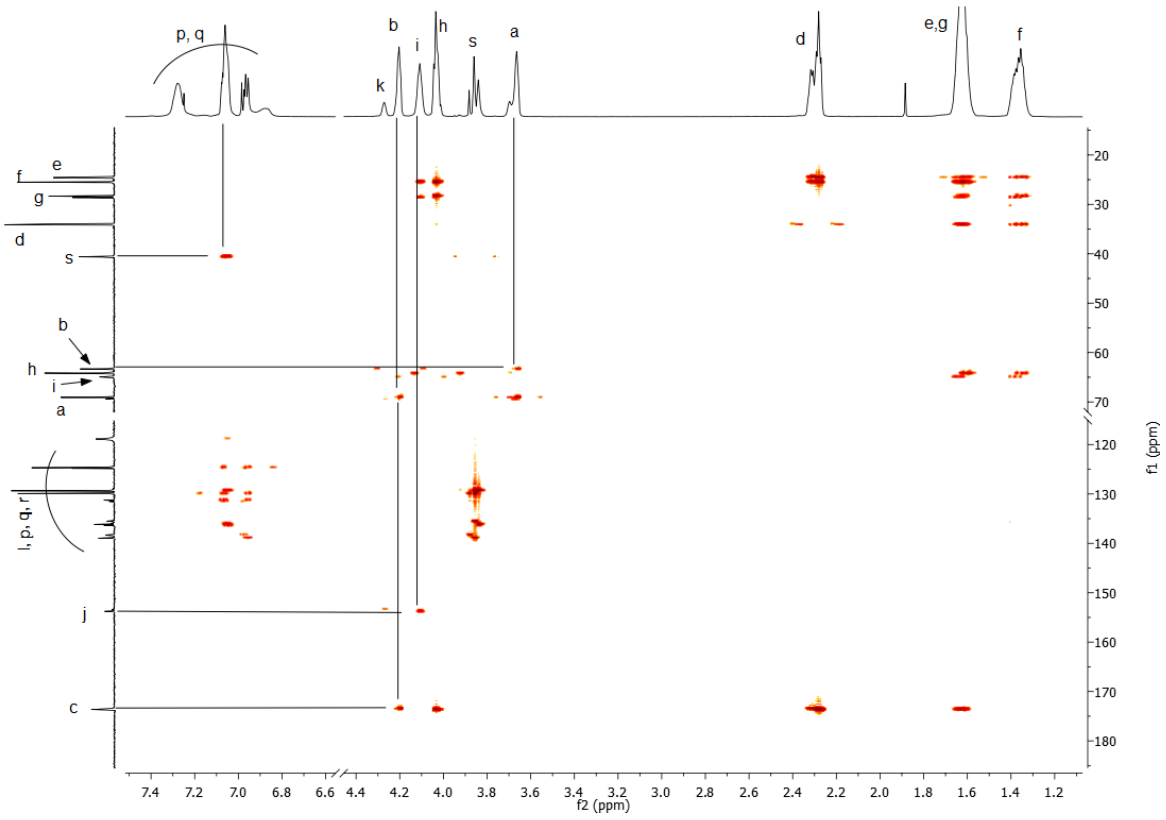

Figure 5.14: ^{1}H – ^{13}C HMBC spectrum of **5.4** in $CDCl_3$

The resonances at 65.0 ppm and 153.8 ppm are attributed to methylene carbon atom **i** on the PCL moiety neighbouring the urethane group, and carbonyl carbon atom **j** in the urethane group, respectively. The ^{1}H – ^{13}C HSQC spectrum of **5.4**, confirms this assignment showing carbon atom **i** at 65.0 ppm correlate to protons **i** at 4.12 ppm. Furthermore, the ^{1}H – ^{13}C HMBC spectrum of **5.4** shows protons **i** at 4.12 ppm are neighbouring carbonyl carbon atom **j** at 153.8 ppm. This indicates the successful reaction between the NCO group on the MDI moiety and the OH group on the PCL moiety to give a urethane group. The ^{1}H – ^{13}C HSQC spectrum of **5.4** shows the resonance at 40.6 ppm is attributed to methylene carbon atom **s** on the MDI moiety, as they correlate to **s** protons at 3.87 ppm. Furthermore, resonances at 118.9 ppm, 124.7 ppm, 129.4 ppm, 130.0 ppm, 131.3 ppm, 136.2 ppm and 139.0 ppm are attributed to aromatic carbon atoms on the MDI moiety.

The FT-IR spectrum of diisocyanate **5.4**, Figure 5.15(c), shows the disappearance of the broad absorbance attributed to the O-H bond at 3490 cm^{-1}, seen in PCL-diol, Figure 5.15(a). This indicates the OH groups in the PCL diol moiety have completely reacted with the NCO groups on the MDI **5.1** moiety. Furthermore, the appearance of absorbances at 3332 cm^{-1} and 1526 cm^{-1} in **5.4** are attributed to N-H and C-N bonds, respectively. This suggests the NCO groups on the MDI **5.1** moiety have reacted with the OH groups on the PCL moiety to give urethane groups. However, the C-N absorbance is also seen in the FT-IR spectrum of MDI **5.1**, Figure 5.15(b), indicating the starting material was impure and a small degree of NCO groups on the MDI moiety had reacted, prior to the synthesis of **5.4**. The reactions could have involved the trimerisation of MDI **5.1**, see Chapter 1 Section 1.2.5.1, or the reaction between the NCO groups and a nucleophile, such as water in the atmosphere. The decreased number of available NCO groups and the possible production of isocyanurate trimers could lead to cross-linking in the synthesis of diisocyanate prepolymers. The absorbance at 2256 cm^{-1} in **5.4** can be attributed to C=N bonds in the NCO group on the MDI moiety. This confirms the presence of NCO groups in the diisocyanate prepolymer.

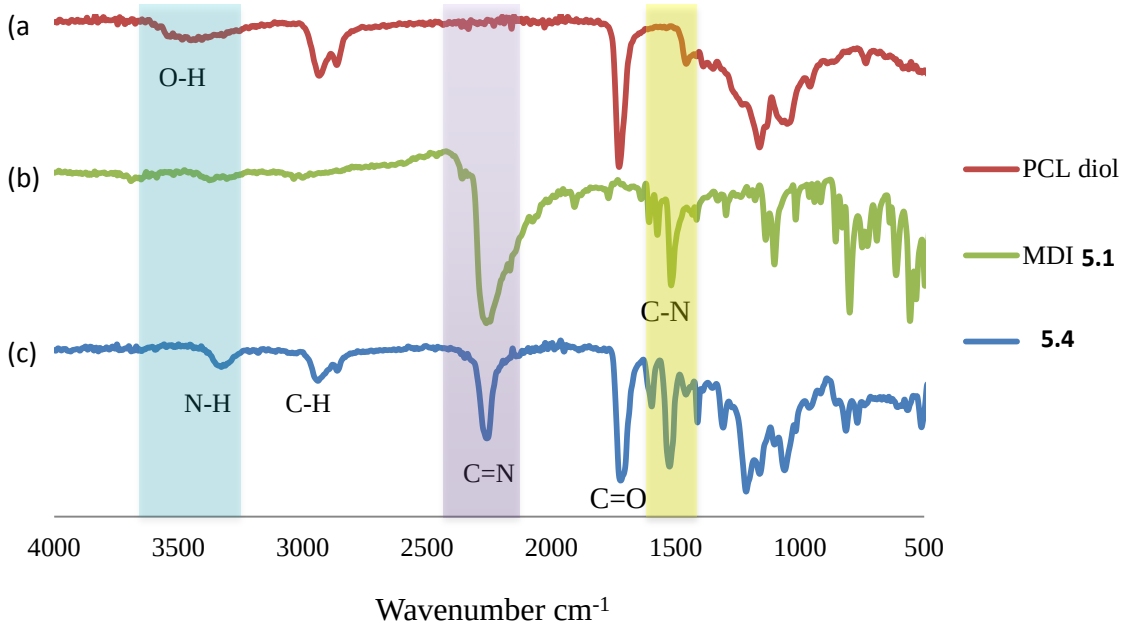

Figure 5.15: FT-IR spectra of (a) PCL diol, (b) MDI **5.1** and (c) MDI-PCL-MDI diisocyanate prepolymer **5.4**

The molecular weights of diisocyanate prepolymers **5.3** and **5.4** determined by SEC analyses (M_n^{SEC}) of 1.44 × 10^3 g mol^{-1} and 3.17 × 10^3 g mol^{-1} are higher than the theoretical molecular weights (M_n^{Th}) of 0.90 × 10^3 g mol^{-1} and 1.05 × 10^3 g mol^{-1}, respectively, Table 5.1. This could be due to additional reactions of NCO groups in diisocyanate prepolymers **5.3** and **5.4** with another OH group on the PCL-diol moiety, giving polymers with significantly higher M_n. It can be seen that the extent of this additional reaction is greater in the prepolymer containing the MDI moiety **5.4**, showing a significantly higher M_n^{SEC} than expected as well as a high Đ of 1.47. However, the prepolymer containing the TDI moiety **5.3** exhibits a lower Đ of 1.22, suggesting a lower likelihood of additional reactions. This can be explained due to the more hindered position of the NCO group neighbouring a methyl group on the TDI moiety in **5.3**, compared to the *para* NCO groups on the MDI moiety in **5.4**.

Table 5.1: Molecular weights and Đ of diisocyanate prepolymers containing a central PCL moiety **5.3** and **5.4**

Sample	Structure	M_n^{Th}	M_n^{SEC}	Đ
		$\times 10^{-3}$ g mol^{-1}		
5.3	TDI-PCL-TDI	0.90	1.44	1.22
5.4	MDI-PCL-MDI	1.05	3.17	1.47

The SEC chromatogram of diisocyanate prepolymer containing the MDI moiety **5.4**, Figure 5.16, shows a significant lower molecular weight shoulder compared to diisocyanate prepolymer containing the TDI moiety **5.3**. This supports the hypothesis of significant additional and secondary reactions of the NCO groups seen with the diisocyanate prepolymer containing the MDI moiety.

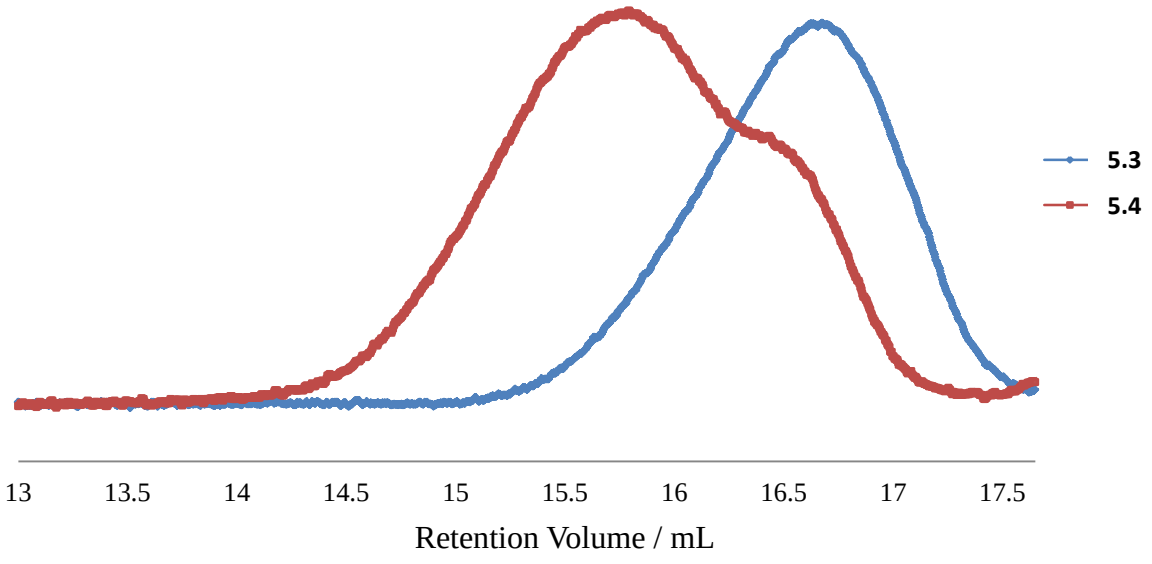

Figure 5.16: Overlayed normalised SEC chromatograms of diisocyanate prepolymers containing a central PCL moiety capped with TDI **5.3** and MDI **5.4**

5.3.2 Diisocyanate Prepolymers containing a Central PCL-*b*-PEG-*b*-PCL moiety 5.5 - 5.7

Diisocyanate prepolymers containing a central PCL-*b*-PEG-*b*-PCL moiety with a $\overline{DP}_{Th}$ of fifty per arm, were synthesised by the reaction of di-hydroxyl PCL-*b*-PEG-*b*-PCL **3.3** (Chapter 3, Section 3.2.5.2) and two molar equivalents of either TDI **5.2** or MDI **5.1** to give diisocyanate prepolymers **5.5** and **5.6** respectively, Scheme 5.2.

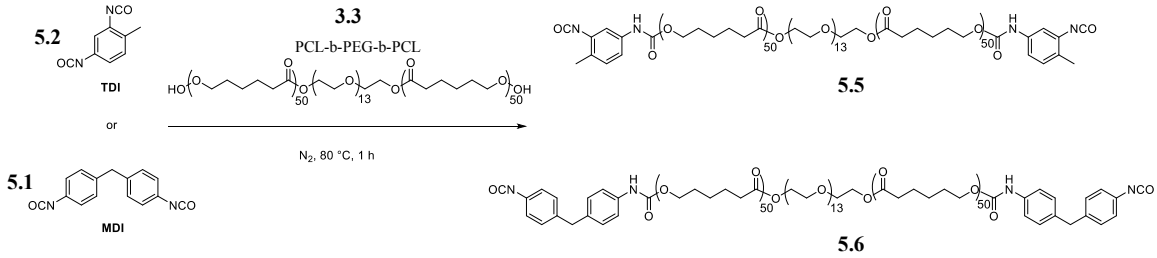

Scheme 5.2: Synthesis of diisocyanate prepolymers containing a central PCL-PEG-PCL moiety and capped with TDI **5.5** and MDI **5.6**

The ^{1}H NMR spectrum of **5.5**, Figure 5.17, shows the characteristic PCL resonances at 1.34 ppm, 1.59 ppm, 2.26 ppm and 4.01 ppm, attributing to methylene protons **g**, **f**/**h**, **e** and **i**, respectively. The resonances at 3.59 ppm, 3.64 ppm and 4.17 ppm are attributed to methylene protons **a**, **b** and **c** on the central PEG moiety, respectively. The resonance at 4.10 ppm is attributed to methylene protons **j** next to the urethane group on the PCL moiety. This indicates the successful reaction of the OH group on the PCL moiety and the NCO group on the TDI moiety. Furthermore, the resonances at 2.14 ppm and 6.87-7.23 ppm are attributed to methyl protons **t** and aromatic methine protons **q**-**r**, respectively.

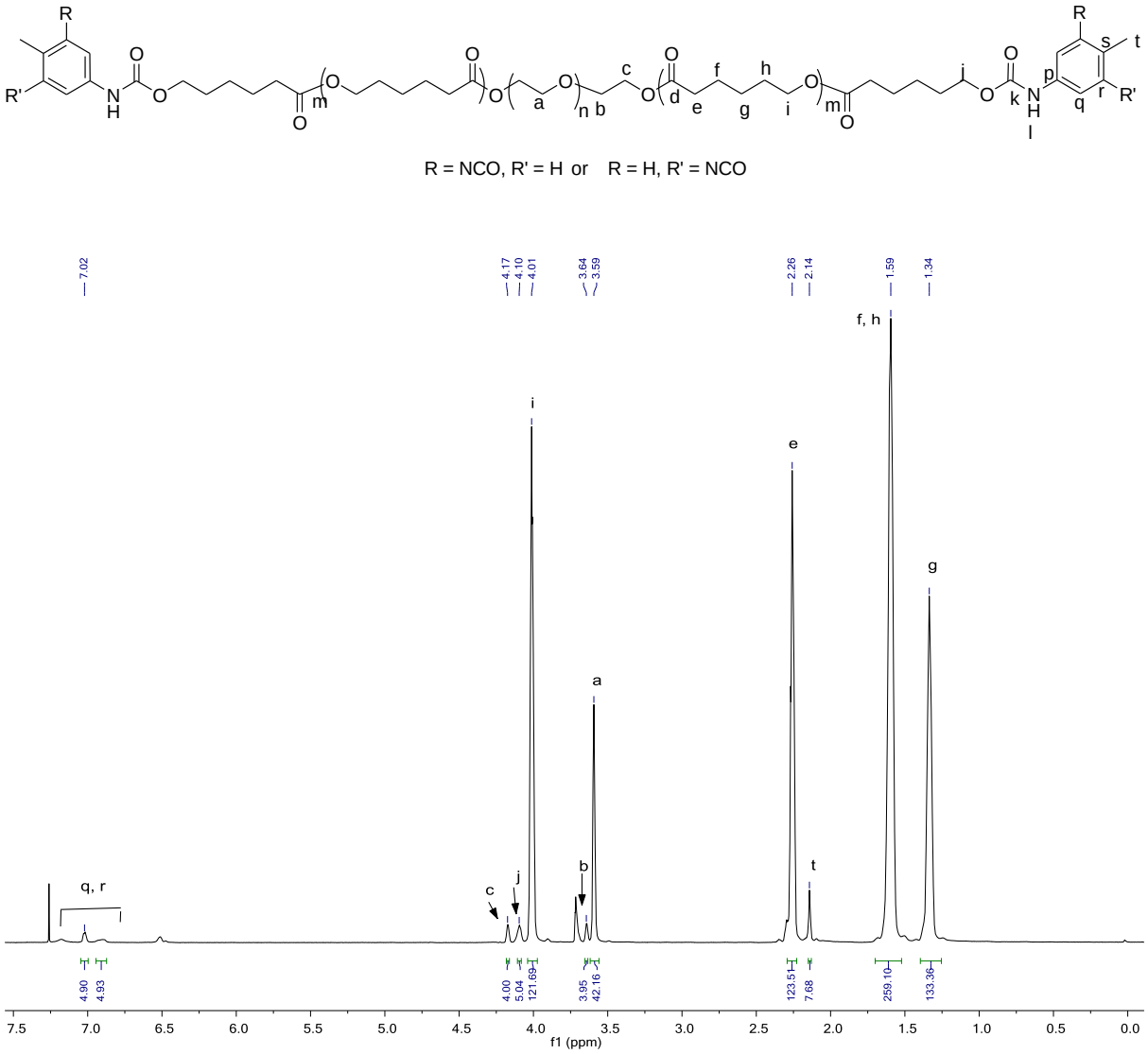

Figure 5.17: 400 MHz ^{1}H NMR spectrum of **5.5** in $CDCl_3$

The ^{13}C NMR spectrum of **5.5**, Figure 5.18, shows the characteristic PCL resonances at 24.6 ppm, 25.5 ppm, 28.4 ppm, 34.1 ppm and 64.1 ppm, attributing to methylene carbon atoms **f**, **g**, **h**, **e** and **i**, respectively. The downfield resonance at 173.5 ppm is attributed to carbonyl carbon atom **d** on the PCL moiety. The resonances at 61.5 ppm, 69.2 ppm and 70.6 ppm are attributed to methylene carbon atoms **c**, **b** and **a** on the central PEG moiety, respectively. The resonances at 64.9 ppm and 153.7 ppm are attributed to methylene carbon atom **j** next to the urethane group on the PCL moiety, and carbonyl carbon atom **k** in the urethane group, respectively. This confirms the successful reaction of the OH group on the PCL moiety and the NCO group on the TDI moiety to give a urethane group.

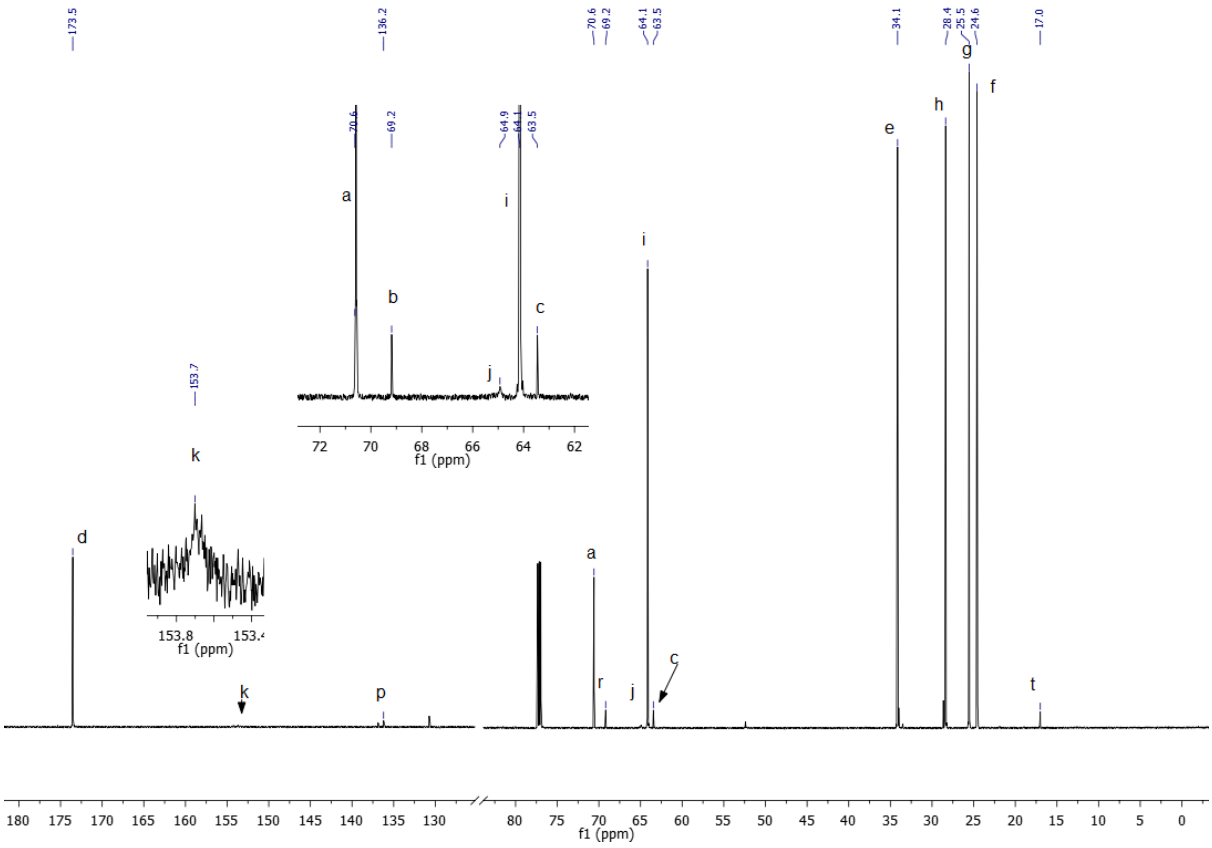

Figure 5.18: 100 MHz ^{13}C NMR spectrum of **5.5** in $CDCl_3$

The ^{1}H NMR spectrum of **5.6**, Appendix 5.1, shows the characteristic resonances for the protons in the PCL, PEG and MDI moieties, including the resonance at 4.10 ppm attributed to methylene protons **j** next to the urethane group on the PCL moiety. This indicates the successful reaction of the OH groups on the PCL moiety and the NCO groups on the MDI moiety. The ^{13}C NMR spectrum of **5.6**, Appendix 5.2, shows the characteristic resonances for carbon atoms in the PCL, PEG and MDI moieties. Furthermore, the resonances at 65.0 ppm and 153.8 ppm, are attributed to methylene carbon atom **j** neighbouring the urethane group, and carbonyl carbon atom **k** in the urethane group, respectively. This confirms the successful reaction of the OH group on the PCL moiety and NCO group on the MDI moiety, to give a urethane group.

The SEC chromatograms of PCL-*b*-PEG-*b*-PCL **3.3** with a $\overline{DP}$ of fifty per arm (Chapter 3 Section 3.2.5.2), used in the synthesis of MDI-based diisocyanate prepolymer **5.6**, are shown in Figure 5.19. The SEC chromatogram of **5.6** appears broader and shifted to the left, showing an increase in M_n from 1.05×10^4 g mol^{-1} to 1.52×10^4 g mol^{-1} and increase

in Đ from 1.13 to 1.42, from PCL-*b*-PEG-*b*-PCL **3.3** to **5.6**, respectively. This significant increase in M_n and Đ from PCL-*b*-PEG-*b*-PCL **3.3** to **5.6** upon the addition of two MDI moieties, clearly shows additional reactions are taking place with the NCO groups on the diisocyanate prepolymer **5.6**.

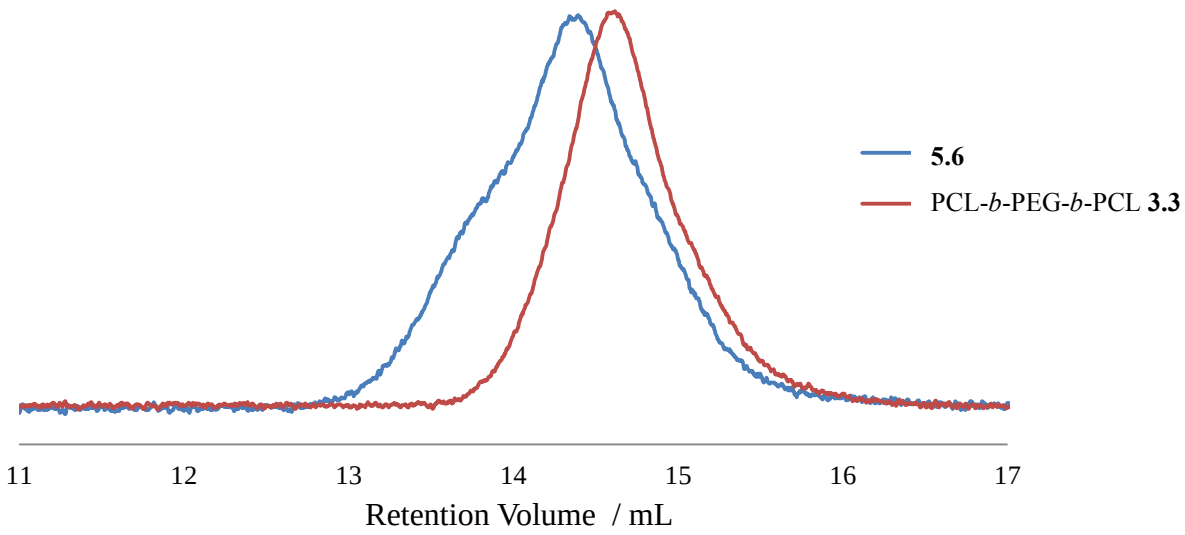

Figure 5.19: Overlayed SEC chromatograms of triblock copolymer PCL-*b*-PEG-*b*-PCL **3.3** and MDI capped triblock copolymer MDI-PCL-*b*-PEG-*b*-PCL-MDI **5.6**

The FT-IR spectrum of diisocyanate prepolymer **5.6**, Figure 5.20(c), shows absorbances at 2264 cm^{-1} and 1720 cm^{-1}, attributing to the C=N bond in the NCO group on the MDI moiety and the C=O bond in the PCL moiety, respectively. The presence of the NCO groups confirm that the diisocyanate prepolymer contains reactive end-groups. The absorbance at 1532 cm^{-1} is attributed to the C-N bond in the urethane group, indicating the successful reaction between the NCO group on the MDI moiety and an OH group. However, as discussed in Section 5.3.1.2, the C-N absorbance at 1532 cm^{-1} is also seen in the FT-IR spectrum of MDI, Figure 5.20(b), indicating the starting material was impure and a small degree of NCO groups on the MDI moiety had reacted, prior to the synthesis of **5.6**.

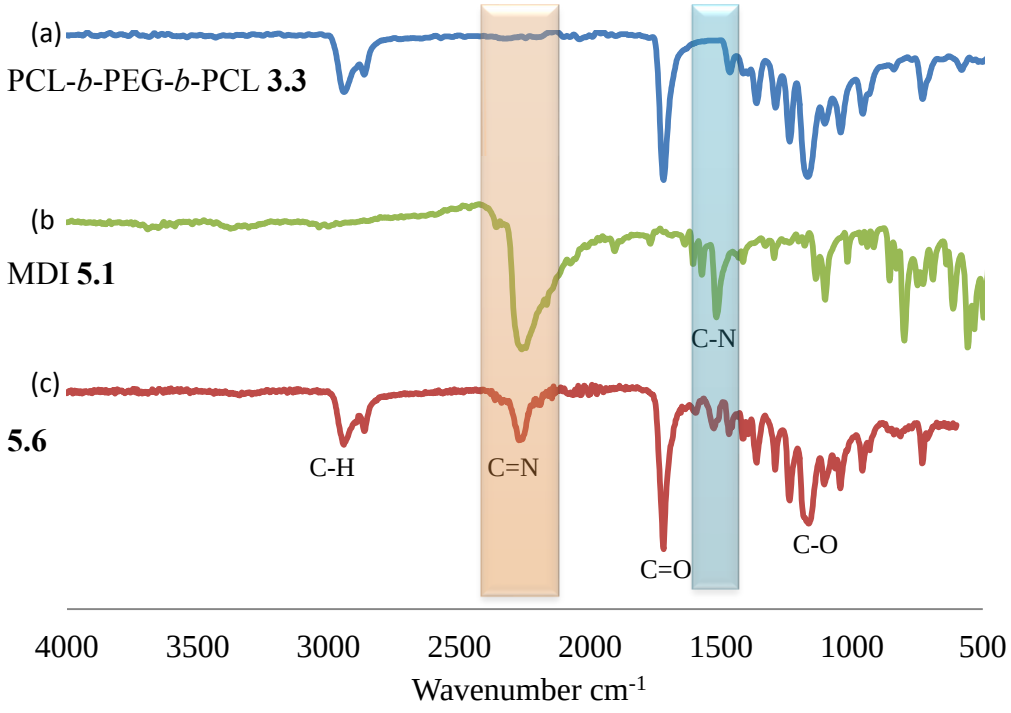

Figure 5.20: FT-IR spectra of (a) PCL-*b*-PEG-*b*-PCL **3.3**, (b) MDI **5.1** and (c) MDI-capped triblock copolymer MDI-PCL-*b*-PEG-*b*-PCL-MDI **5.6**

The SEC chromatograms of diisocyanate prepolymers containing a central PCL-*b*-PEG-*b*-PCL moiety with a $\overline{DP}_{Th}$ of fifty per arm capped with either TDI **5.2** to give prepolymer **5.5** or capped with MDI **5.1** to give prepolymer **5.6**, are shown in Figure 5.21. It can be clearly seen that the SEC chromatogram for the diisocyanate prepolymer containing the MDI moiety **5.6** is significantly broader and shifted to the left of the diisocyanate prepolymer containing the TDI moiety **5.5**. An increase from **5.5** to **5.6** in M_n^{SEC} from 0.99 × 10^4 g mol^{-1} to 1.52 × 10^4 g mol^{-1} and Đ from 1.29 to 1.42, respectively, clearly shows significant further reactions occurring, and to a greater extent in the diisocyanate prepolymer containing the MDI moieties.

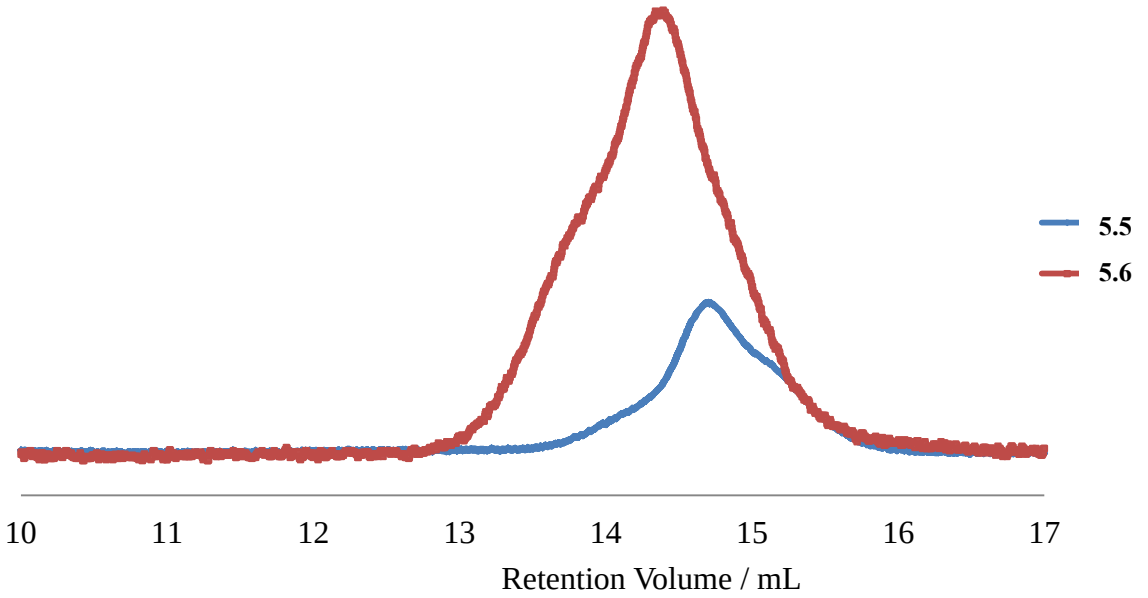

Figure 5.21: Overlayed normalised SEC chromatograms of diisocyanate prepolymers containing a central PCL-*b*-PEG-*b*-PCL moiety capped with either TDI **5.5** or MDI **5.6**

As a direct comparison to **5.6**, a diisocyanate prepolymer with a central PCL-*b*-PEG-*b*-PCL moiety with a $\overline{DP}_{Th}$ of ten per arm, was synthesised by the reaction of di-hydroxyl PCL-*b*-PEG-*b*-PCL **3.2** (Chapter 3, Section 3.2.5.1) and two molar equivalents of MDI, to give **5.7**, Scheme 5.3.

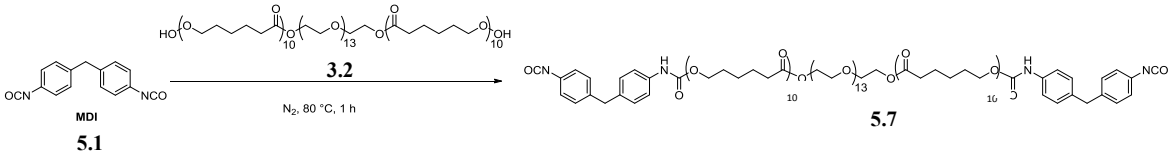

Scheme 5.3: Synthesis of MDI-capped diisocyanate prepolymer, MDI-PCL-*b*-PEG-*b*-PCL, with a $\overline{\mathbf{DP}}_{Th}$ of ten per arm **5.7**

The ^{1}H NMR spectrum of **5.7**, Appendix 5.3, shows the characteristic resonances attributing to protons in the PCL, PEG and MDI moieties, including the resonance at 4.10 ppm attributed to methylene protons **j** next to the urethane group on the PCL moiety.

Furthermore, the ^{13}C NMR spectrum of **5.7**, Appendix 5.4, shows resonances at 65.0 ppm and 153.8 ppm attributed to carbon atom **j** next to the urethane group on the PCL moiety, and carbonyl carbon atom **k** in the urethane group, respectively. This confirms the successful reaction between the OH groups on the PCL moiety and the NCO groups on the MDI moiety to give a urethane group.

The SEC chromatogram of MDI-based diisocyanate prepolymer containing a central PCL-*b*-PEG-*b*-PCL moiety with a $\overline{DP}$ of ten per arm **5.7**, Figure 5.22, shows an M_n^{SEC} of 1.01×10^4 g mol^{-1} with a lower molecular weight shoulder. It can be seen that the M_n^{SEC} is significantly higher than the expected M_n^{Th} of 0.34×10^4 g mol^{-1}, Table 5.2. This phenomenon is evident in diisocyanate prepolymers **5.5** and **5.6** (Table 5.2), and **5.3** and **5.4** (Table 5.1), due to additional reactions of the NCO groups on the diisocyanate prepolymer with OH groups on the PCL moieties. Furthermore, secondary reactions of the urethane group and an NCO group could result in the formation of allophonate and substituted biureate group, producing cross-linking, see Chapter 1 Section 1.2.5.1. These additional reactions result in diisocyanate prepolymers with significantly higher M_n and Đ than expected.

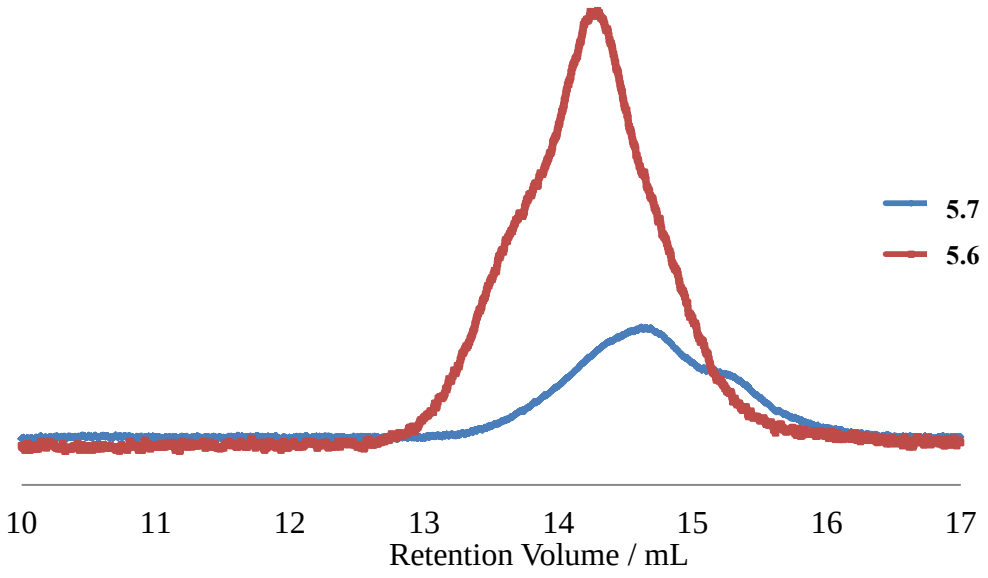

Figure 5.22: Overlayed normalised SEC chromatograms of diisocyanate prepolymers MDI-PCL-*b*-PEG-*b*-PCL-MDI with a $\overline{\mathbf{DP}}_{\mathbf{Th}}$ of fifty per arm **5.6** and a $\overline{\mathbf{DP}}_{\mathbf{Th}}$ of ten per arm **5.7**

Table 5.2: Molecular weights and Đ of diisocyanate prepolymers **5.5 – 5.7** containing a central PCL-*b*-PEG-*b*-PCL moiety

Sample	Structure	$\overline{DP}$ arm (PCL)	M_n^{Th}	M_n^{SEC}	Đ
			$\times 10^{-4}$ g mol^{-1}		
5.5	TDI-PCL-PEG-PCL-TDI	50	1.23	0.99	1.29
5.6	MDI-PCL-PEG-PCL-MDI	50	1.25	1.52	1.42
5.7	MDI-PCL-PEG-PCL-MDI	10	0.34	1.01	1.46

The thermal properties and $\%\chi_c$ of diisocyanate prepolymers **5.5 – 5.7** are shown in Table 5.3. It can be seen that the melting temperature (T_m) significantly decreases from 53 – 59 °C to 39 – 46 °C with a decrease in $\overline{DP}$ per arm from 50 to 10, in **5.6** and 5.**7**, respectively. The T_m for diisocyanate prepolymer containing the TDI moiety **5.5** at 48 – 55 °C, can be seen to be lower than the diisocyanate prepolymer containing the MDI moiety **5.6** at 53 – 59 °C. This increase could be due to the higher reactivity of MDI producing higher M_n weight diisocyanate prepolymers and hence higher T_m. It could also be due to the presence of a small degree of cross-linking at the reaction temperature with the formation of allophanate and biuret groups. Moreover, the MDI moiety contains two aromatic rings in its structure, imparting rigidity and crystallinity, as opposed to only one aromatic ring in the TDI moiety.

Diisocyanate prepolymers **5.5** and **5.6** show a similar $\%\chi_c$ of about 17%. However, diisocyanate prepolymer **5.7**, containing a central PCL-*b*-PEG-*b*-PCL moiety with a $\overline{DP}$ of ten per arm, showed a significantly lower $\%\chi_c$ of 2%. This could be due to a decreased crystalline PCL content and an increased amorphous PEG content, in comparison to **5.5** and **5.6**.

Table 5.3: Thermal properties of diisocyanate prepolymers **5.5 – 5.7** containing a central PCL-*b*-PEG-*b*-PCL moiety, determined by DSC analyses

Sample	Structure	$\overline{DP}_{arm}$	M_n^{SEC}	T_m	T_c	ΔH_f	ΔH_c	χ_c
			$\times 10^{-4}$ g mol^{-1}	°C		J g^{-1}		%
5.5	TDI-PCL-PEG-PCL-TDI	50	0.99	48 - 55	18 - 24	22	22	16
5.6	MDI-PCL-PEG-PCL-MDI	50	1.52	53 - 59	30 - 36	25	25	17
5.7	MDI-PCL-PEG-PCL-MDI	10	1.01	39 - 46	33 - 38	3	3	2

5.3.3 Contact Angle

The initial contact angles (time = 0 s) for diisocyanate prepolymers **5.6** and **5.7,** Figure 5.23, were identical at 76°. However, **5.7** showed considerably more surface wetting than **5.6**, Figure 5.24, showing contact angles of 29° and 75° after 30 s, respectively. This can be explained by the presence of the central PCL-*b*-PEG-*b*-PCL moieties with a $\overline{DP}$ of 10 and 50 per arm in diisocyanate prepolymers **5.7** and **5.6**, respectively. The decreased content of crystalline and hydrophobic PCL and increased content of amorphous PEG in **5.7**, leads to an increase in surface wetting, in comparison to **5.6**.

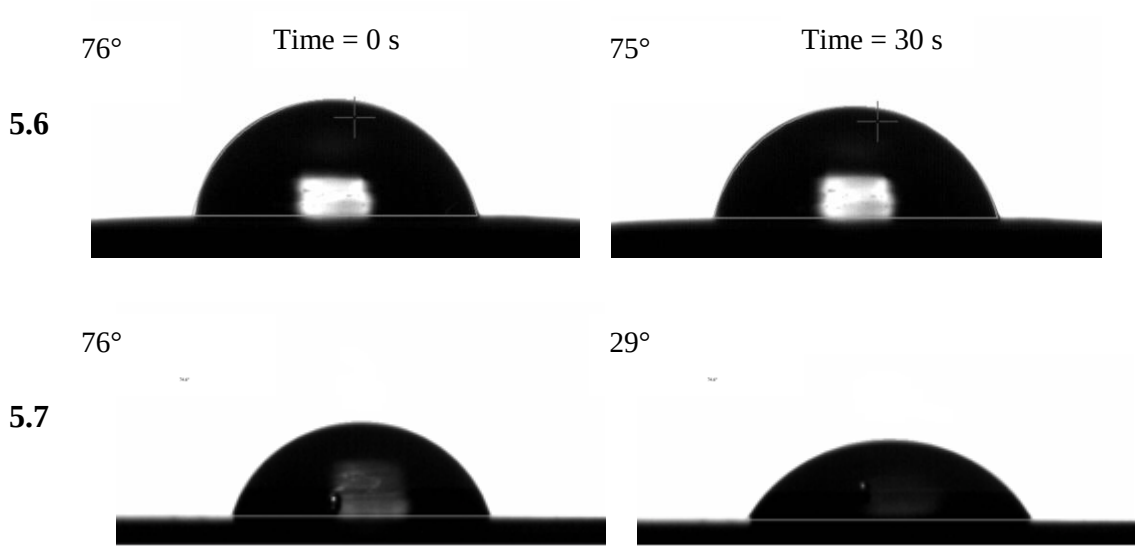

Figure 5.23: Contact angle for diisocyanate prepolymers MDI-PCL-*b*-PEG-*b*-PCL-MDI with a $\overline{\mathbf{DP}}_{Th}$ of fifty per arm **5.6** and a $\overline{\mathbf{DP}}_{Th}$ of ten per arm **5.7**, measured after 0 s and 30 s. Reported contact angles are the averages of the left and right contact angles and the average of five repeat measurements. The calculated error for contact angle analyses was found to be ±2.3%.

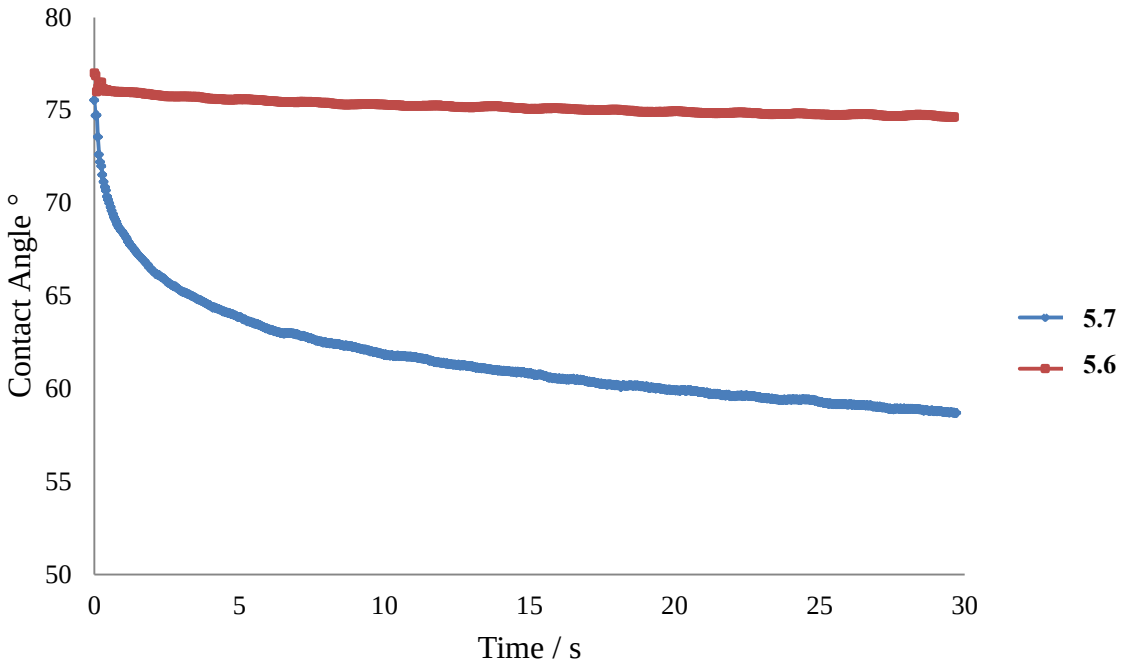

Figure 5.24: Surface wettability of diisocyanate prepolymers MDI-PCL-*b*-PEG-*b*-PCL-MDI with a $\overline{\mathbf{DP}}_{\mathrm{Th}}$ of fifty per arm **5.6** and a $\overline{\mathbf{DP}}_{\mathrm{Th}}$ of ten per arm **5.7** measured by contact angle analysis. Reported contact angles are the averages of the left and right contact angles and the average of five repeat measurements. The calculated error for contact angle analyses was found to be ±2.3%.

5.3.4 Water Uptake

The % water uptake (%WU) and $\%PEG^{NMR}$ content of diisocyanate prepolymers **5.5 – 5.7** are shown in Table 5.4. It can be seen that diisocyanate prepolymers **5.5** and **5.6** with a central PCL-*b*-PEG-*b*-PEG moiety and a $\overline{DP}$ of fifty per arm and capped with TDI and MDI moieties, respectively, have the same %PEG content of 5%, and therefore the same %WU of ~3%. This indicates that the increased hydrophobic aromatic content of MDI compared to TDI has no effect on %WU. Furthermore, it can be seen that an increase in hydrophilic $\%PEG^{NMR}$ content from 5% to 13% causes an increase in the %WU from 2% to 6% in diisocyanate prepolymers **5.6** and **5.7**, respectively.

Table 5.4: %WU for diisocyanate prepolymer films **5.5 – 5.7** containing a central hydrophilic PCL-*b*-PEG-*b*-PCL moiety in PBS solution (pH 7.4) at 30 °C after 2 days

Sample	Structure	$\overline{DP}_{arm}$	% PEG^{NMR} content	% WU
5.5	TDI-PCL-PEG-PCL-TDI	50	5	3
5.6	MDI-PCL-PEG-PCL-MDI	50	5	2
5.7	MDI-PCL-PEG-PCL-MDI	10	13	6

5.3.4 Enzymatic Degradation of Diisocyanate Prepolymers

Diisocyanate prepolymers **5.5 – 5.7** were added to excess methanol to prevent unwanted reactions of the NCO groups and to ensure safe handling during the enzymatic degradation tests. The appearance of a singlet resonance at 3.73 ppm in the ^{1}H NMR spectra corresponding to the methyl protons next to the urethane group, indicate a complete reaction between the NCO groups on either the MDI or TDI moieties and the OH group on the methanol moiety. Furthermore, ^{1}H – ^{13}C HMBC analyses show the methyl protons at 3.73 ppm neighbour a urethane group, confirming the complete reaction of NCO groups on the diisocyanate prepolymers to give a urethane group. Moreover, FT-IR spectra show the disappearance of the C=N absorbance at 2260-2360 cm^{-1}, confirming the complete reaction of the NCO functionality.

It must be noted that TDI and MDI-based diisocyanate prepolymers **5.3** and **5.4** containing a central PCL moiety, could not be subjected to enzymatic degradation using methods outlined in Section 5.2.3. The diisocyanate prepolymers **5.3** and **5.4** are viscous liquids and therefore could not be pressed into discs.

The rates of enzymatic degradation of diisocyanate prepolymers **5.5 – 5.7**, are presented as %mass loss as a function of time, Figure 5.25. It can be clearly seen that diisocyanate prepolymer **5.5** containing TDI moieties, degrades at a significantly faster rate of 100% mass loss in 4 days than the MDI-based prepolymers **5.6** and **5.7** with 23% and 79% mass in 40 and 10 days, respectively. This could partly be explained by the decreased aromatic content of TDI. It is expected that increasing the aromatic content in the prepolymers will increase the hydrophobic nature therefore, decrease the rate of enzymatic degradation. On

the other hand, SEC analyses (Figure 5.21 in Section 5.3.2) have indicated further reactions of the NCO group, significantly in the diisocyanate prepolymers containing the MDI moiety. This observed increase in M_n and the possibility of cross-linking decreases polymer chain mobility. Therefore it restricts the ability of enzymes to access the hydrolysable ester groups in the PCL moiety, decreasing the rate of enzymatic degradation.

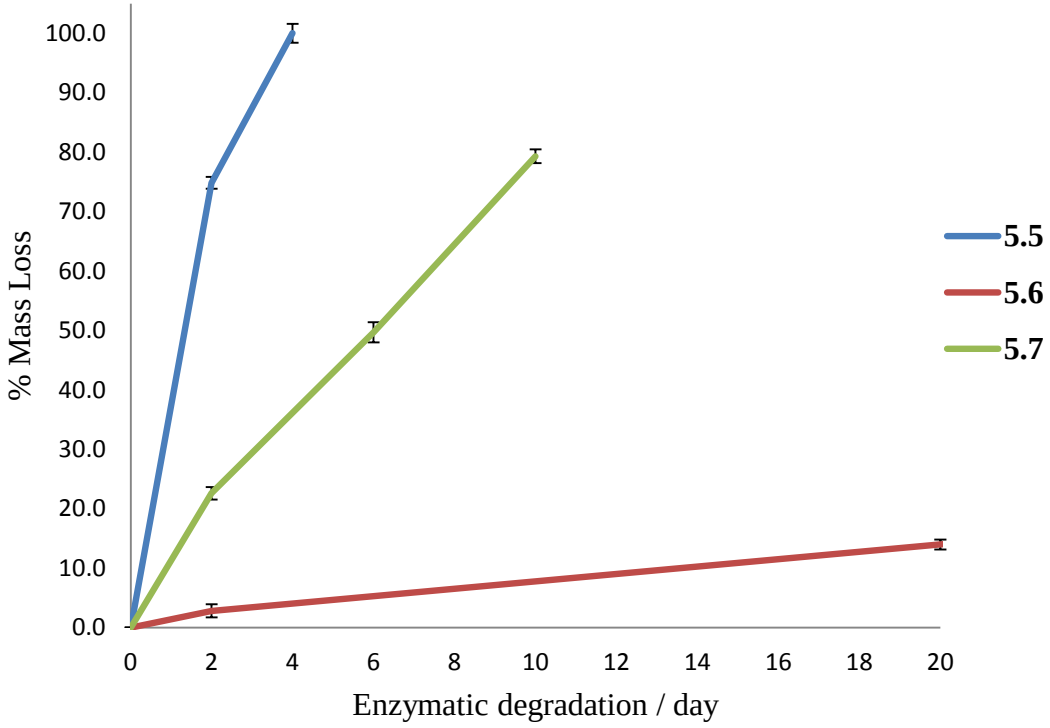

Figure 5.25: % Mass loss of diisocyanate prepolymer discs; TDI-PCL-PEG-PCL-TDI with a $\overline{\mathbf{DP}}_{\mathbf{Th}}$ of fifty per arm **5.5,** MDI-PCL-PEG-PCL-MDI with a $\overline{\mathbf{DP}}_{\mathbf{Th}}$ of fifty per arm **5.6,** and MDI-PCL-PEG-PCL-MDI with a $\overline{\mathbf{DP}}_{\mathbf{Th}}$ of ten per arm **5.7**. The mass loss was measured over 40 days of enzymatic degradation using *pseudomonas cepacia* lipase in PBS solution (pH 7.4). The % mass losses are an average of three repeat sample measurements and % error bars shown.

It can be seen that the MDI-based diisocyanate prepolymer **5.7** with a central PCL-*b*-PEG-*b*-PEG moiety and a $\overline{DP}$ of ten per arm, degrades at a significantly faster rate of 79% mass loss in 10 days than MDI-based **5.6** with a $\overline{DP}$ of fifty per arm of 23% mass loss in 40 days. This could be due to the combination of decreased M_n, decreased hydrophobic crystalline PCL content and increased amorphous PEG content in **5.7**. The increased mobility of polymer chains in **5.7** gives increased ability for the enzyme to penetrate into the bulk of the polymer, to hydrolyse the ester groups on the PCL moiety therefore, increasing the rate of enzymatic degradation. It can be seen that TDI-based prepolymer **5.5** exhibits almost 100% mass loss after 4 days compared to MDI-based prepolymer **5.6** of 23% after 40 days. This can be explained in terms of cross-linking side reactions known to be associated with the presence of MDI.

The changes in thermal properties of diisocyanate prepolymers **5.5 – 5.7** were monitored throughout enzymatic degradation using DSC analyses, Table 5.5. It must be noted that some of the DSC data obtained for **5.7** were unclear and values could not be confirmed. Diisocyanate prepolymers **5.5** and **5.6** show a decrease in $\%\chi_c$ of 16% to 8% and 17% to 7% after 2 days of enzymatic degradation, respectively. This could be explained by the decrease of crystalline PCL content through mass loss during enzymatic degradation. However, **5.6** subsequently shows a large increase in $\%\chi_c$ from 7% to 28% after 2 and 20 days of enzymatic degradation. This could be due to the increased crystalline aromatic MDI content, as the PCL moiety is degraded and removed. Moreover, the production of shorter polymer chains during enzymatic degradation, leads to greater chain mobility and ability to align into a more crystalline structure. Furthermore, as the more amorphous regions of the PCL moiety are preferentially degraded, the overall $\%\chi_c$ of the polymer will increase.

A minimal decrease in T_m and T_c is seen for diisocyanate prepolymers **5.5 – 5.6** due to the overall decrease in M_n, throughout enzymatic degradation.

Table 5.5: Thermal analyses for diisocyanate prepolymers; TDI-PCL-PEG-PCL-TDI with a $\overline{\mathbf{DP}}_{\mathbf{Th}}$ of fifty per arm **5.5,** MDI-PCL-PEG-PCL-MDI with a $\overline{\mathbf{DP}}_{\mathbf{Th}}$ of fifty per arm **5.6,** and MDI-PCL-PEG-PCL-MDI with a $\overline{\mathbf{DP}}_{\mathbf{Th}}$ of ten per arm **5.7** during enzymatic degradation using *pseudomonas cepacia* lipase in PBS solution (pH 7.4).

Sample	Enzymatic Degradation	Mass Loss	T_m	T_c	ΔH_c	ΔH_f	χ_c
	Day	%	°C		J g^{-1}		%
5.5	0	-	48 - 55	18 - 24	22.2	21.7	16
	2	75	48 - 54	19 - 23	11.7	11.9	8
	4	100	-	-	-	-	-
5.6	0	-	53 - 59	30 - 36	24.6	25.0	17
	2	3	52 - 57	30 - 36	9.49	9.58	7
	20	14	53 - 58	30 - 35	39.4	39.2	28
	40	23	54 - 59	29 - 35	39.8	40.2	28
5.7	0	-	39 - 46	33 - 38	2.50	2.77	2
	2	23	35 - 43	-	-	5.01	-
	6	50	36 - 42	-	-	9.96	-
	10	79	-	-	-	-	-

5.4 Conclusion

Biodegradable diisocyanate prepolymers containing a central PCL moiety **5.3 – 5.4** were synthesised by the reaction of PCL diol with two molar equivalents of either MDI **5.1** or TDI **5.2**. Furthermore, a central hydrophilic PEG moiety was incorporated into the biodegradable diisocyanate prepolymers by the reaction of a triblock copolymer PCL-*b*-PEG-*b*-PEG **3.2** and **3.3** with a $\overline{DP}$ of 10 or 50 respectively, (Chapter 3) and capped with either MDI **5.1** or TDI **5.2**. The diisocyanate prepolymers **5.3 – 5.7** were fully characterised using NMR, SEC and FT-IR analyses, showing the successful reaction of the NCO and OH groups to form a urethane group. Furthermore, FT-IR showed the presence of C=N bonds in the diisocyanate prepolymers attributing to the NCO group, required for the synthesis of PU, discussed in Chapter 6. The SEC analyses showed the biodegradable diisocyanate prepolymers exhibited a higher M_n than expected, particularly in those containing the MDI moiety, due to additional and secondary reactions of the NCO group on the diisocyanate prepolymers.

The hydrophilic nature of the MDI-based diisocyanate prepolymers containing a central PCL-*b*-PEG-*b*-PEG moiety with a $\overline{DP}$ of 10 (**5.7**) and 50 (**5.6**) per arm, was determined by contact angle, surface wetting and %WU analyses. Significantly increased wetting over 30 s, decreased contact angle and increased %WU were seen for the diisocyanate prepolymer **5.7** with the lower $\overline{DP}$ of 10 per arm, due to the decreased hydrophobic PCL content and increased hydrophilic PEG content.

The enzymatic degradation using *pseudomonas cepacia* lipase of diisocyanate prepolymers **5.5 – 5.7** containing a central PCL-*b*-PEG-*b*-PEG moiety and either MDI or TDI moieties, was monitored using % mass loss and DSC analyses. The fastest rate of degradation was seen for the TDI-based diisocyanate prepolymer **5.5** with a $\overline{DP}$ of 50 per arm of 100% mass loss in 4 days. This could be due to decreased crystalline and hydrophobic aromatic content in comparison to the MDI-based diisocyanate prepolymers **5.6 – 5.7**. Furthermore, the light cross-linking reactions with the NCO group led to a significant increase in M_n and therefore, decreased the rate of enzymatic degradation. MDI-based diisocyanate prepolymer **5.7** with a $\overline{DP}$ of 10 per arm, degraded at a significantly faster rate at 79% mass loss in 10 days, than diisocyanate prepolymer **5.6** with a $\overline{DP}$ of 50 per arm, of 23% mass loss in 40 days of enzymatic degradation. This is due to the lower M_n polymer exhibiting increased chain mobility and therefore increased ability for the enzyme to

penetrate the bulk of the polymer and access the hydrolysable ester groups on the PCL moiety. Furthermore, the MDI-based diisocyanate prepolymer **5.7** with a $\overline{DP}$ of 10 per arm contains a decreased content of hydrophobic PCL and increased content of hydrophilic PEG in comparison to the MDI-based diisocyanate prepolymer **5.6** with a $\overline{DP}$ of 50 per arm. The overall increase in hydrophilic nature and surface wettability of diisocyanate prepolymer **5.7** will increase the mobility of the enzymes and water through the bulk of the polymer and access to the hydrolysable ester groups, therefore increasing the rate of enzymatic degradation.

5.5 References

(1) Guelcher, S. A.; Srinivasan, A.; Dumas, J. E.; Didier, J. E.; McBride, S.; Hollinger, J. O. *Biomaterials* **2008**, *29*, 1762.

(2) Bonzani, I. C.; Adhikari, R.; Houshyar, S.; Mayadunne, R.; Gunatillake, P.; Stevens, M. M. *Biomaterials* **2007**, *28*, 423.

(3) Adhikari, R.; Gunatillake, P. A.; Griffiths, I.; Tatai, L.; Wickramaratna, M.; Houshyar, S.; Moore, T.; Mayadunne, R. T. M.; Field, J.; McGee, M.; Carbone, T. *Biomaterials* **2008**, *29*, 3762.

(4) Teng, C.; Yang, K.; Ji, P.; Yu, M. *J. Polym. Sci. Part A: Polym. Chem,* **2004**, *42*, 5045.

(5) Petrova, S. M., S., Mateva, R., Iliev, I. *Chem. Technol. Metall.* **2008**, *43*, 199.

(6) Khan, F.; Valere, S.; Fuhrmann, S.; Arrighi, V.; Bradley, M. *J. Mater. Chem. B* **2013**, *1*, 2590.

(7) Gurunathan, T.; Mohanty, S.; Nayak, S. K. *J. Mater. Sci.* **2014**, *49*, 8016.

6 Synthesis and Degradation Studies of Polyurethanes

6.1 Introduction

The main components in the syntheses of polyurethanes (PUs) are a diisocyanate component containing NCO groups, and a polyol component containing OH groups. The reaction of multi-functional components containing NCO and OH groups results in the formation of urethane groups and a cross-linked PU structure.

There has been extensive research into the degradation of linear PUs, commonly synthesised in a two-step process involving the synthesis of a diisocyanate prepolymer followed by a reaction involving a chain extender.[1,2] Commonly, biodegradable PUs have been synthesised using aliphatic diisocyanates such as lysine diisocyanate (LDI),[3,4] hexamethylene diisocyanate (HDI)[5,2] and 1,4-diisocyanatobutane (BDI)[6]

Hong *et al*. reported a significant increase in the hydrolytic degradation of linear poly(ε-caprolactone) (PCL) based PU with increasing β-butyrolactone (β-BL) content in the polyol component.[7] However, FT-IR analyses were not employed to confirm the complete reaction of NCO groups on the 4,4'-methylenebisphenyl diisocyanate (MDI) moiety, with the OH groups on the linear PCL-*co*-PBL moiety. Furthermore, hydrolytic degradation tests were performed on PU films using a 3% $NaOH_{(aq)}$ solution at 37 °C and 45 °C, and monitored by mass loss. The results showed a significant increase in % mass loss from 10-45% during hydrolytic degradation at 37 °C with PUs containing PCL polyols with 0-12% β-BL content, respectively. It has been suggested that the increase in the rate of hydrolytic degradation of PU with the increase in β-BL content is due to the overall decreased crystallinity of PU, imparted by the polyol moiety containing the random copolymer of ε-CL and β-BL. Moreover, less crystalline aliphatic polyesters including PCL show an increased rate of hydrolytic and enzymatic degradation.[8,9,10,11,12]

It has been reported that the incorporation of a hydrophilic PEG moiety in a linear PCL-based PU has increased hydrolytic degradation by increasing the hydrophilicity and %water uptake of the PU.[3] Furthermore, an increase in PEG content showed a decrease in crystallinity and therefore an increase in hydrolytic degradation. However, the effect of hydrophilic PEG incorporation on the enzymatic degradation rate was not discussed.

There have been limited studies on the enzymatic degradation of cross-linked PUs, particularly in PUs containing aromatic MDI or TDI moieties. This is partly due to reports indicating the generation of aromatic diamines (Discussed in Chapter 1, Section 1.2.5.1) upon PU degradation containing MDI and TDI moieties, producing carcinogenic 4,4-methylene diamine (MDA)[13] and toluene diamine (TDA),[14] respectively.

Barroni *et al.* reported the hydrolytic degradation of cross-linked PU films synthesised using a HDI prepolymer and different compositions of PCL-triol, PEG and glycerol, to give cross-linked PU.[15] The PU films were immersed in simulated body fluid (SBF) buffer (pH = 7.4) for 90 days showing up to 10% mass loss, with the highest degradation seen for the PU containing the highest PCL content. However, the degree of cross-linking in the PUs were not determined. Studies have shown that increasing the number of arms of star polyols used in PU syntheses, increases the cross-linking density and therefore, decreases the rate of hydrolytic degradation.[16] It has been suggested that this is due to restricted chain mobility in PUs as a result of an increased cross-link density, limiting the diffusion of water molecules into the PU film.

It has been proposed that the enzymatic degradation of PU involves the synergistic activity of enzymes hydrolysing the PU chain at random points and at polymer chain-ends with endopolyurethanases and exopolyurethanses, respectively.[17] Furthermore, lipases[18] and esterases[19,20,21] have been shown to significantly increase the rate of PU degradation in comparison to hydrolytic degradation in buffer solution alone. However, the mechanism of enzymatic polymer degradation is still not greatly understood.

Chapter 6 concerns the syntheses and enzymatic degradation of PUs **6.1 – 6.11** using biodegradable polyols **2.7**, **2.14**, **3.10** and **4.5** (synthesised in Chapters 2-4) and either biodegradable diisocyanates **5.3 – 5.6** (synthesised in Chapter 5) or MDI **5.1** or TDI **5.2**. The PUs are characterised by FT-IR, TGA, % water uptake (%WU), % solvent uptake (%SU) and % extracted material (%EM). The enzymatic degradation of PUs using *pseudomonas cepacia* lipase in PBS solution (pH 7.4) were monitored by % mass loss over 30 days. To the best of our knowledge, there has been no systematic study in the synthesis and enzymatic degradation of PUs containing star PCL based polyols and MDI or TDI diisocyanate prepolymers containing a central PCL-*b*-PEG-*b*-PCL moiety.

6.2 Experimental

6.2.1 Materials

Toluene-2,4-diisocyanate (TDI) **5.2**, 4,4-methylenebis(phenyl isocyanate) (MDI) **5.1**, *pseudomonas cepacia* lipase and phosphate buffer saline salts (PBS) (pH = 7.4) were purchased from Sigma Aldrich and used as received. Six-arm star poly(caprolactone) with a central dipentaerythritol moiety and a $\overline{DP}$ of twenty per arm **2.7** (synthesis outlined in Chapter 2, Section 2.2.4.4.2), six-arm star poly[(ε-caprolactone)-*co*-(β-butyrolactone)] with a central dipentaerythritol moiety and a $\overline{DP}$ of seven ε-caprolactone (ε-CL) and three β-butyrolactone (β-BL) per arm **2.14** (synthesis outlined in Chapter 2, Section 2.2.5.2.1), four-arm star poly(ε-caprolactone) with a central poly(ethylene glycol) moiety bridged with 2,2-bis(methyl)propionic acid moieties and a $\overline{DP}$ of twenty per arm **3.10** (synthesis outlined in Chapter 3, Section 3.2.5.2.4), seven-arm star poly(ε-caprolactone) with a central acetylated β-cyclodextrin unit and a $\overline{DP}$ of Thirty per arm **4.5** (synthesis outlined in Chapter 4, Section 4.2.5.4), MDI-based diisocyanate prepolymer containing a central poly(ε-caprolactone) moiety **5.4** (synthesis outlined in Chapter 5, Section 5.2.5.1), TDI-based diisocyanate prepolymer containing a central poly(ε-caprolactone) moiety **5.3** (synthesis outlined in Chapter 5, Section 5.2.5.2), MDI-based diisocyanate prepolymer containing a central poly[(ε-caprolactone)-*b*-(ethylene glycol)-*b*-(ε-caprolactone)] moiety **5.6** (synthesis outlined in Chapter 5, Section 5.2.6.2.1) and TDI-based diisocyanate prepolymer containing a central poly[(ε-caprolactone)-*b*-(ethylene glycol)-*b*-(ε-caprolactone)] moiety **5.5** (synthesis outlined in Chapter 5, Section 5.2.6.2.2) were used without further purification in the synthesis of PU. Dry dichloromethane was obtained from the Durham Solvent Purification System (SPS)

6.2.2 Characterisation Techniques

Fourier-transform Infrared Spectroscopy (FT-IR) was performed on a PerkinElmer 1600 series FT-IR.

Thermogravimetric Analysis (TGA) measurements were collected using a Perkin Elmer Pyris 1 TGA, samples were heated in air or nitrogen (N_2) to 500 °C at a rate of 10 °C min^{-1}.

6.2.3 Enzymatic Degradation

The method used for enzymatic degradation is outlined in Chapter 2, Section 2.2.3. The only exception is that PU samples (100 mg) were cut into small pieces prior to testing.

6.2.4 Water Uptake Measurements

The method used for % water uptake (%WU) is outlined in Chapter 3, Section 3.2.4.

6.2.5 % Solvent Uptake and % Extracted Material Measurements

The % solvent uptake (%SU) of the PU were measured by immersing the PU pieces (100 mg) in toluene (5 mL) at 37 ±1 °C for 2 days. The PU pieces were removed and carefully dried on tissue paper and weighed. The PU pieces were then dried under reduced pressure at 40 °C until a constant weight was obtained. The dry PU pieces were weighed and the difference in weight of PU pieces before and after drying was divided by the weight of the dried PU pieces to give a %SU.

All solvent fractions were collected for each PU and the solvent was removed under reduced pressure to give a solid mass of extracted material. The dried PU extracted materials were weighed and divided by the initial weight of PU to give a % extracted material (%EM).

6.2.6 Synthesis of Polyurethane Foams 6.1 – 6.11

PU foams were synthesised using the following synthetic method.

Six-arm star poly(ε-caprolactone) containing a central dipentaerythritol moiety **2.7** (Synthesis outlined in Chapter 2, Section 2.2.4.4.2) (2.00 g, 0.14 mmol) was added to a round bottomed flask equipped with a mechanical stirrer and purged with N_2. A minimal amount of dichloromethane (DCM) (~3 mL) was added to the flask and stirred using a mechanical stirrer to ensure complete dissolution. 4,4-Methylenebis(phenyl isocyanate) **5.1** (0.11 g, 0.44 mmol) was added to the flask under a N_2 atmosphere and stirred with a mechanical stirrer for 1 min. The mechanical stirrer was removed and the flask was loosely covered with aluminium foil and left overnight (~16 h). The product was collected as a PU

gel which was cut into small pieces and dried under reduced pressure at 40 °C to a constant weight.

The quantities used in the PU formulations were calculated according to the molar ratios of OH groups in the polyol component and predicted NCO groups in the isocyanate component. A ratio of 1:1 for NCO:OH groups was employed unless otherwise specified.

6.2.6.1 Synthesis of PU using Star PCL and MDI 6.1

Six-arm star PCL with a central dipentaerythritol unit and a $\overline{DP}$ of twenty per arm **2.7** (2.00 g, 0.14 mmol) and MDI **5.1** (0.11 g, 0.43 mmol) were used to give cross-linked PU **6.1**. FT-IR (ν max): 3463 (N-H), 2246 and 2868 (C-H), 1722 (C=O), 1603 and 1472 (Aromatic C=C), 1239 (C-N), 1168 (C-O) cm^{-1}. T_d: 311 °C.

6.2.6.2 Synthesis of PU using Star PCL and MDI in a molar ratio of 1.5:1 for OH:NCO 6.2

Six-arm star PCL with a central dipentaerythritol unit and a $\overline{DP}$ of twenty per arm **2.7** (3.00 g, 0.16 mmol) and MDI **5.1** (0.083 g, 0.48 mmol) were used to give cross-linked PU **6.2**. A 1:1.5 molar ratio of NCO:OH functional groups was used. FT-IR (ν max): 3474 (N-H), 2948 and 2871 (C-H), 1723 (C=O), 1601 and 1477 (Aromatic C=C), 1241 (C-N), 1172 (C-O) cm^{-1}. T_d: 331 °C.

6.2.6.3 Synthesis of PU using Star PCL and TDI 6.3

Six-arm star PCL with a central dipentaerythritol unit and a $\overline{DP}$ of Twenty per arm **2.7** (3.00 g, 0.16 mmol) and TDI **5.2** (0.083 g, 0.48 mmol) were used to give cross-linked PU **6.3**. FT-IR (ν max): 3410 (N-H), 2952 and 2873 (C-H), 1724 (C=O), 1608 and 1472 (Aromatic C=C), 1240 (C-N), 1172 (C-O) cm^{-1}. T_d: 318 °C.

6.2.6.4 Synthesis of PU using Star Poly[(ε-CL)-*co*-(β-BL)] and TDI 6.4

Six-arm star (PCL)-*co*-(PBL) with a central dipentaerythritol moiety and a $\overline{DP}$ of seven ε-CL and three β-BL per arm **2.14** (3.00 g, 0.3 mmol) and TDI **5.2** (0.16 g, 0.9 mmol) were used to give cross-linked PU **6.4**. FT-IR (ν max): 3386 (N-H), 2953 and 2874 (C-H), 1723 (C=O), 1610 and 1472 (Aromatic C=C), 1243 (C-N), 1180 (C-O) cm^{-1}. T_d: 274 °C.

6.2.6.5 Synthesis of PU using Star PCL with acetylated β-CD core and TDI 6.5

Seven-arm star PCL containing a central acetylated β-cyclodextrin (β-CD) moiety and a $\overline{DP}$ of thirty per arm **4.5** (2.0 g, 7.69×10^5 mmol) and TDI **5.2** (0.05 g, 2.69×10^4 mmol) were used to give cross-linked PU **6.5**. FT-IR (ν max): 3349 (N-H), 2950 and 2870 (C-H), 1725 (C=O), 1602 and 1472 (Aromatic C=C), 1240 (C-N), 1167 (C-O) cm^{-1}. T_d: 315 °C.

6.2.6.6 Synthesis of PU using Star Poly[(ε-CL)-*co*-(β-BL)] and MDI-based prepolymer containing a central PCL moiety 6.6

Six-arm star (PCL)-*co*-(PBL) with a central dipentaerythritol unit and a $\overline{DP}$ of seven ε-CL and three β-BL per arm **2.14** (2.07 g, 0.31 mmol) and MDI-based diisocyanate prepolymer containing a central PCL moiety **5.4** (0.97 g, 0.94 mmol) were used to give cross-linked PU **6.6**. FT-IR (ν max): 3353 (N-H), 2948 and 2872 (C-H), 2286 (C=N), 1727 (C=O), 1512, 1234 (C-N), 1167 (C-O) cm^{-1}. T_d: 323 °C.

6.2.6.7 Synthesis of PU using Star Poly[(ε-CL)-*co*-(β-CL)] and TDI-based prepolymer containing a central PCL moiety 6.7

Six-arm star (PCL)-*co*-(PBL) with a central dipentaerythritol unit and a $\overline{DP}$ of seven ε-CL and three β-BL per arm **2.14** (2.08 g, 0.32 mmol) and TDI-based diisocyanate prepolymer containing a central PCL moiety **5.3** (0.83 g, 0.95 mmol) were used to give cross-linked PU **6.7**. FT-IR (ν max): 3394 (N-H), 2948 and 2870 (C-H), 1723 (C=O), 1604 and 1472 (Aromatic C=C), 1243 (C-N), 1190 (C-O) cm^{-1}. T_d: 310 °C.

6.2.6.8 Synthesis of PU using Star PCL and MDI-based prepolymer containing a central PCL-*b*-PEG-*b*-PCL moiety 6.8

Six-arm star PCL with central dipentaerythritol unit and a $\overline{DP}$ of twenty per arm **2.7** (2.89 g, 0.21 mmol) and MDI-based diisocyanate prepolymer containing a central PCL-*b*-PEG-*b*-PCL moiety **5.6** (9.95 g, 1.91 mmol) were used to give cross-linked PU **6.8**. FT-IR (ν max): 3394 (N-H), 2499 and 2870 (C-H), 1722 (C=O), 1602 and 1471 (Aromatic C=C), 1244 (C-N), 1190 (C-O) cm^{-1}. T_d: 301 °C.

6.2.6.9 Synthesis of PU using Star PCL and TDI-based prepolymer containing a Central PCL-*b*-PEG -*b*-PCL moiety 6.9

Six-arm star PCL with central dipentaerythritol unit and a $\overline{DP}$ of twenty per arm **2.7** (3.00 g, 0.21 mmol) and TDI-based diisocyanate prepolymer containing a central PCL-*b*-PEG-*b*-PCL moiety **5.5** (8.75 g, 1.75 mmol) were used to give cross-linked PU **6.9**. FT-IR (ν max): 3371 (N-H), 2950 and 2869 (C-H), 1722 (C=O), 1606 and 1472 (Aromatic C=C), 1244 (C-N), 1189 (C-O) cm^{-1}. T_d: 292 °C.

6.2.6.10 Synthesis of PU using Star Poly[(ε-CL)-*co*-(β-BL)] and TDI-based prepolymer containing a central PCL-*b*-PEG-*b*-PCL moiety 6.10

Six-arm star (PCL)-*co*-(PBL) with a central dipentaerythritol unit and a $\overline{DP}$ of seven ε-CL and three β-BL per arm **2.14** (1.50 g, 0.22 mmol) and TDI-based diisocyanate prepolymer containing a central PCL-*b*-PEG-*b*-PCL moiety **5.5** (9.00 g, 1.8 mmol) were used to give cross-linked PU **6.10**. FT-IR (ν max): 3408 (N-H), 2952 and 2871 (C-H), 1719 (C=O), 1619 and 1471 (Aromatic C=C), 1243 (C-N), 1183 (C-O) cm^{-1}. T_d: 304 °C.

6.2.6.11 Synthesis of PU using Star $(PCL)_2$-*b*-PEG-*b*-$(PCL)_2$ and TDI-based prepolymer containing a central PCL-*b*-PEG-*b*-PCL moiety 6.11

Four-arm star PCL with a PEG central unit bridged with 2,2-bis(methyl)propionic acid moieties and a $\overline{DP}$ of twenty per arm **3.10** (3.41 g, 0.28 mmol) and TDI-based diisocyanate prepolymer containing a central PCL-*b*-PEG-*b*-PCL **5.5** (9.00 g, 1.8 mmol) were used to give cross-linked PU **6.11**. FT-IR (ν max): 3412 (N-H), 2952 and 2860 (C-H), 1723 (C=O), 1617 and 1472 (Aromatic C=C), 1242 (C-N), 1179 (C-O) cm^{-1}. T_d: 291 °C.

6.3 Results and Discussion

6.3.1 Polyurethanes 6.1 – 6.11

PUs **6.1 – 6.11** were synthesised by the reaction of a polyol (synthesised in Chapters 2-4) and either a diisocyanate prepolymer moiety (synthesised in Chapter 5) or MDI **5.1** or TDI **5.2** moieties. A molar ratio of 1:1 was used for NCO groups on the diisocyanate moiety to OH groups on the polyol moiety in PUs **6.1** and **6.3 – 6.11**. As a comparison to **6.1**, **6.2** was synthesised with the same reagents but a molar ratio of 1:1.5 for NCO:OH groups. It was expected that the decrease in aromatic isocyanate content in **6.2** would decrease the cross-linking density and decrease the overall crystallinity of PU therefore, increase the rate of enzymatic degradation.

PUs **6.1** and **6.2** were synthesised using six-arm star PCL containing a central dipentaerythritol moiety with a $\overline{DP}$ of twenty per arm **2.7** and MDI **5.1**, using molar ratios of 1:1 and 1:1.5 for NCO:OH groups, respectively, Scheme 6.1. The FT-IR spectra of **6.1** and **6.2**, Appendix 6.1 and 6.2, show weak absorbances at 3463 cm^{-1} and 1242 cm^{-1}, attributing to N-H and C-N stretches in the urethane group, due to a very low MDI content. Furthermore, absorbances can be seen at 1722 cm^{-1} and 1168 cm^{-1}, attributing to C=O and C-O stretches in the PCL moiety. The disappearance of the strong absorbance at 2210-2260 cm^{-1} attributing to the C=N stretch in the NCO group, indicates complete reaction of the NCO group on the MDI moiety and the OH group on the PCL moiety, to give a urethane group.

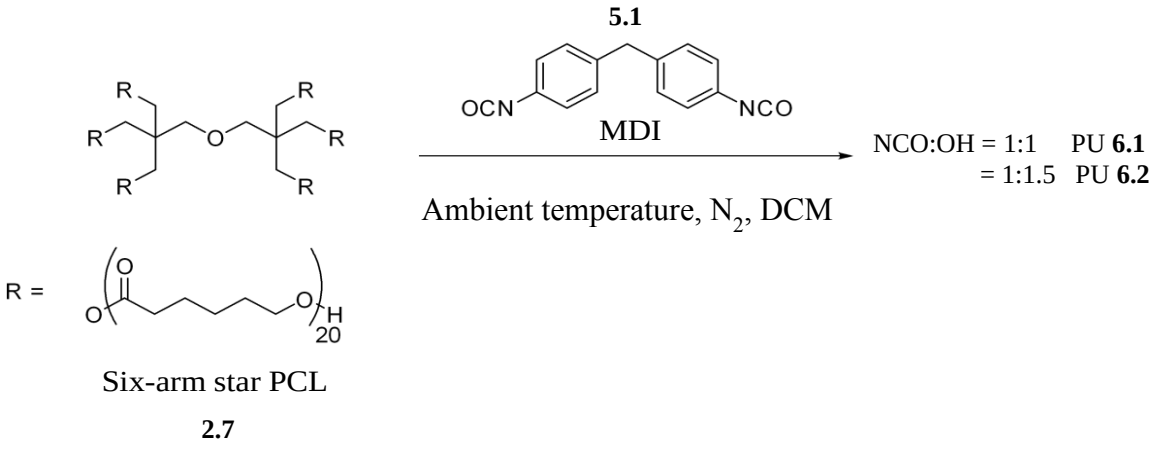

Scheme 6.1: Synthesis of PU **6.1** and **6.2**

PU **6.3** was synthesised by the reaction of TDI **5.2** with six-arm star PCL containing a central dipentaerythritol moiety with a $\overline{DP}$ of twenty per arm **2.7**, Scheme 6.2. The FT-IR spectrum of **6.3**, Appendix 6.3, shows the disappearance of the strong absorbance at 2210-2260 cm^{-1} attributing to the C=N stretch in the NCO group, suggesting complete reaction with the OH groups on the PCL moiety, giving a urethane group. Furthermore, the formation of a urethane group is supported by the weak absorbances at 3410 cm^{-1} and 1240 cm^{-1}, attributing to N-H and C-N stretches, respectively.

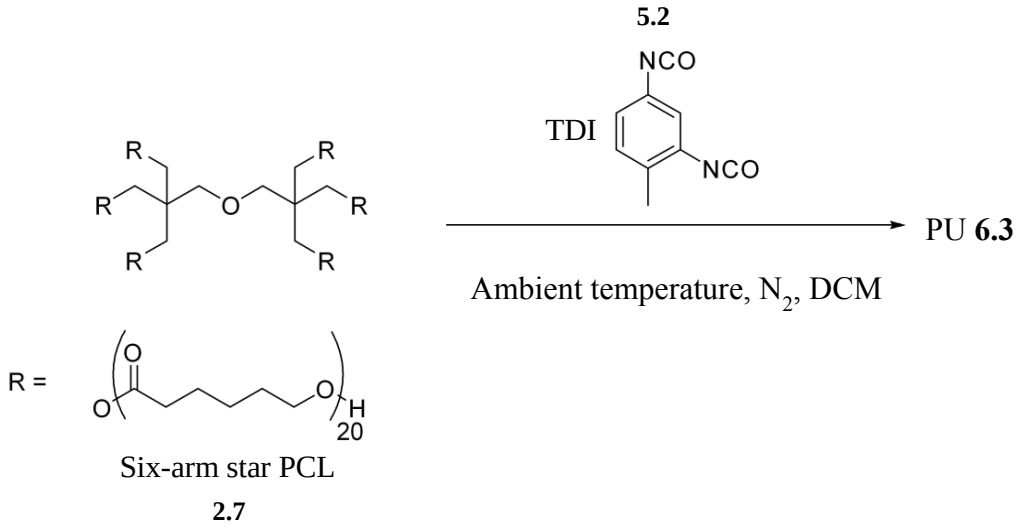

Scheme 6.2: Synthesis of PU **6.3**

PU **6.4** was synthesised by the reaction of TDI **5.2** with six-arm star (PCL)-*co*-(PBL) containing a central dipentaerythritol moiety and a $\overline{\mathbf{DP}}$ of ten per arm with a ratio of 7:3 for ε-CL : β-BL **2.14**, Scheme 6.3. The FT-IR spectrum of **6.4**, Appendix 6.4, shows the disappearance of the strong absorbance at 2210-2260 cm^{-1} attributing to the C=N stretch in the NCO group, indicating the complete reaction of the NCO group with the OH group on the PCL moiety to give a urethane group. Moreover, the formation of a urethane group is supported by the absorbances at 3386 cm^{-1} and 1243 cm^{-1}, attributing to N-H and C-N stretches, respectively.

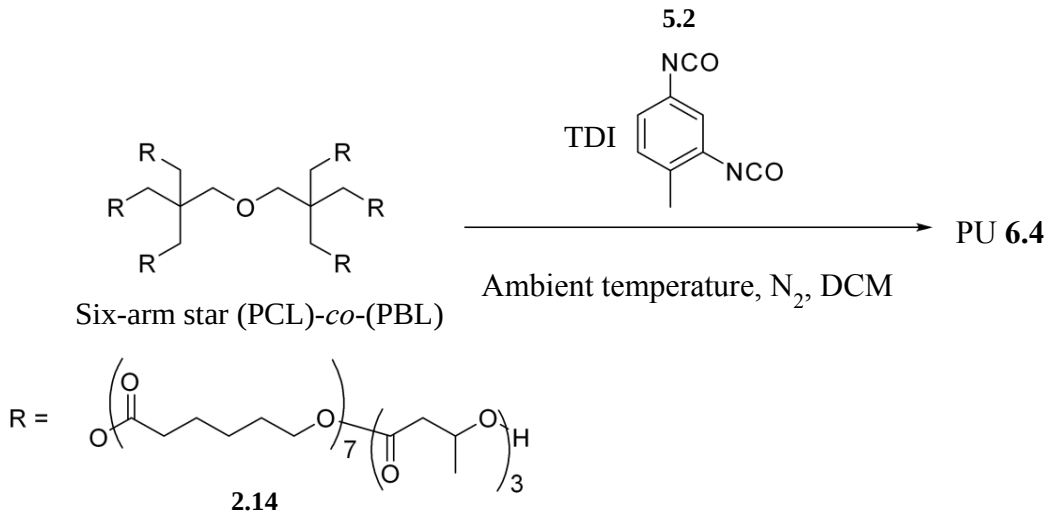

Scheme 6.3: Synthesis of PU **6.4**

PU **6.5** was synthesised by the reaction of TDI **5.2** with seven-arm star PCL containing a central acetylated β-CD moiety with a $\overline{DP}$ of thirty **4.5**, Scheme 6.4. The FT-IR spectrum of **6.5**, Appendix 6.5, shows the disappearance of the strong absorbance at 2210-2260 cm^{-1}, attributing to the C=N stretch in the NCO group, indicating complete reaction of the NCO groups with OH groups, to give a urethane group. Moreover, absorbances at 3349 cm^{-1} and 1240 cm^{-1} attributing to N-H and C-N stretches, respectively, indicate the presence of a urethane group.

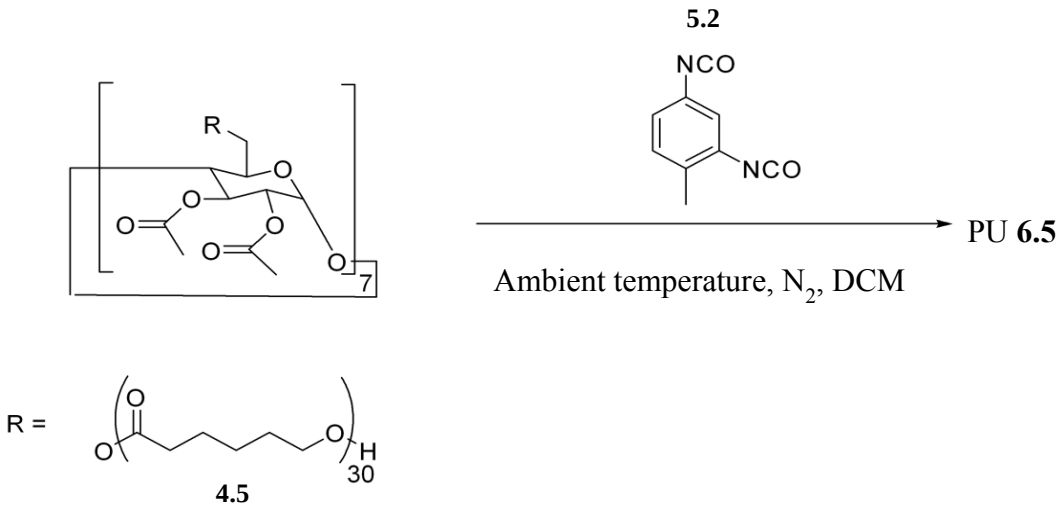

Scheme 6.4: Synthesis of PU **6.5**

PUs **6.6** and **6.7** were synthesised by the reaction of six-arm star (PCL)-*co*-(PBL) with a central dipentaerythritol moiety and a $\overline{DP}$ of ten per arm and a ratio of 7:3 for ε-CL : β-BL **2.14**, with either MDI-based diisocyanate prepolymer **5.4** or TDI-based diisocyanate prepolymer **5.3**, containing a central PCL moiety, respectively, Scheme 6.5.

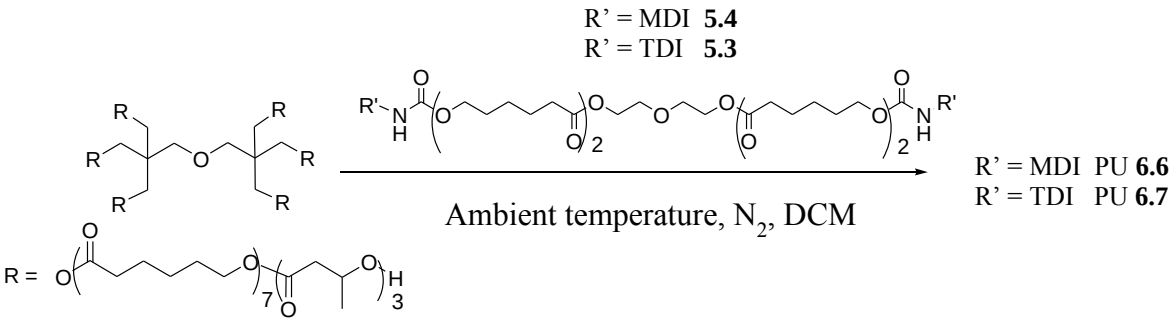

Six-arm star (PCL)-*co*-(PBL)
2.14

Scheme 6.5: Syntheses of PUs **6.6** and **6.7**

The FT-IR spectrum of **6.7**, Figure 6.1, shows the disappearance of the absorbance at 2210-2260 cm^{-1} attributing to the C=N stretch in the NCO group, indicating a complete reaction of the NCO group on the TDI moiety and the OH group on the PCL moiety to give a urethane group. However, the FT-IR spectrum of **6.6** shows a weak absorbance at 2286 cm^{-1} attributing to the C=N stretch in the NCO group. This suggests the incomplete reaction of the NCO groups on the diisocyanate prepolymer **5.4** and OH groups on the PCL **2.14** moiety. This result is unexpected as the higher molecular weights of the MDI diisocyanate prepolymers in comparison to TDI diisocyanate prepolymers, discussed in Chapter 5, indicated that the NCO groups on the MDI moiety were more reactive than on the TDI moiety. One potential explanation could be inefficient physical mixing of the polyol and diisocyanate prepolymer components during the PU synthesis. Furthermore, a potential hypothesis could be the occurrence of a reversible NCO group self-addition reaction. This would form a uretidione group during the MDI prepolymer synthesis and subsequently generating the NCO group in a back reaction, after the synthesis of PU (see Chapter 1, Section1.2.5.1, Scheme 1.7). However, these hypotheses would need confirmation by further investigation and repeat syntheses.

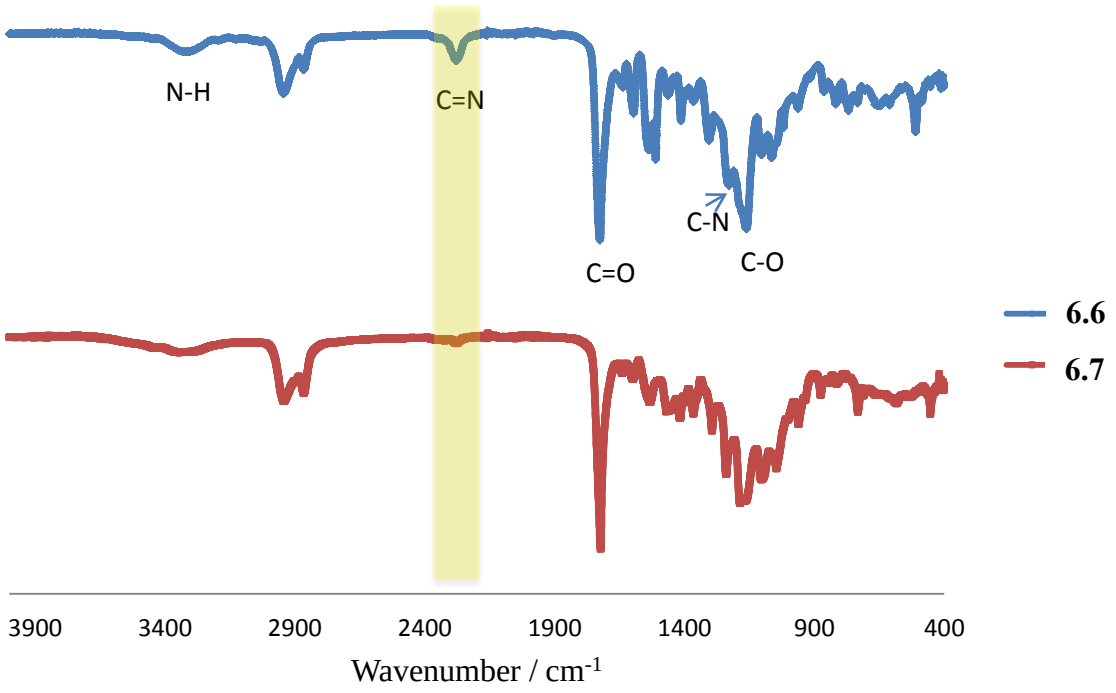

Figure 6.1: FT-IR spectra of PUs containing star poly(CL)-*co*-(BL) polyol **2.14** and either diisocyanate prepolymer TDI-PCL-TDI **5.3** (to give PU **6.6**) or diisocyanate prepolymer MDI-PCL-MDI **5.4** (to give PU **6.7**)

It should be noted that both **6.6** and **6.7** show absorbances in the FT-IR spectra at 3353 cm^{-1} and 3394 cm^{-1}, and at 1234 cm^{-1} and 1243 cm^{-1} attributing to the N-H stretch the C-N stretch in the urethane group, respectively, Figure 6.1. This indicates the successful reaction of a portion of the NCO groups on the diisocyanate prepolymer moiety and OH groups on the polyol moiety.

PU **6.8** was synthesised by the reaction of six-arm star PCL with a $\overline{DP}$ of twenty per arm **2.7** and MDI-based diisocyanate prepolymer containing a central PCL-*b*-PEG-*b*-PCL moiety **5.6**, Scheme 6.6. The FT-IR spectrum of **6.8**, Appendix 6.7, shows the disappearance of the absorbance at 2210-2260 cm^{-1} attributing to the C=N stretch in the NCO group, indicating the complete reaction with the OH groups on the PCL moiety. Moreover, the absorbances attributing to the N-H and C-N stretches in the urethane group can be seen at 3394 cm^{-1} and 1244 cm^{-1}, respectively.

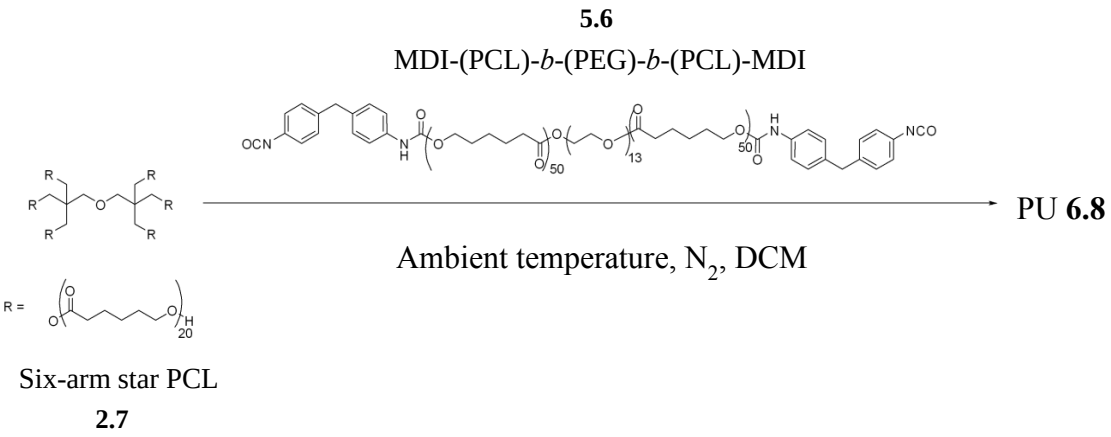

Scheme 6.6: Synthesis of PU **6.8**

PU **6.9** was synthesised by the reaction of six-arm star PCL with a $\overline{DP}$ of twenty per arm **2.7** and TDI-based diisocyanate prepolymer containing a central PCL-*b*-PEG-*b*-PCL moiety **5.5**, Scheme 6.7. The FT-IR spectrum of **6.9**, Appendix 6.8, shows the disappearance of the strong absorbance at 2210-2260 cm^{-1} attributing to the C=N stretch in the NCO group, indicating complete reaction with the OH groups on the PCL moiety. Moreover, the absorbances attributing to the N-H and C-N stretches in the urethane group can be seen at 3371 cm^{-1} and 1244 cm^{-1}, respectively.

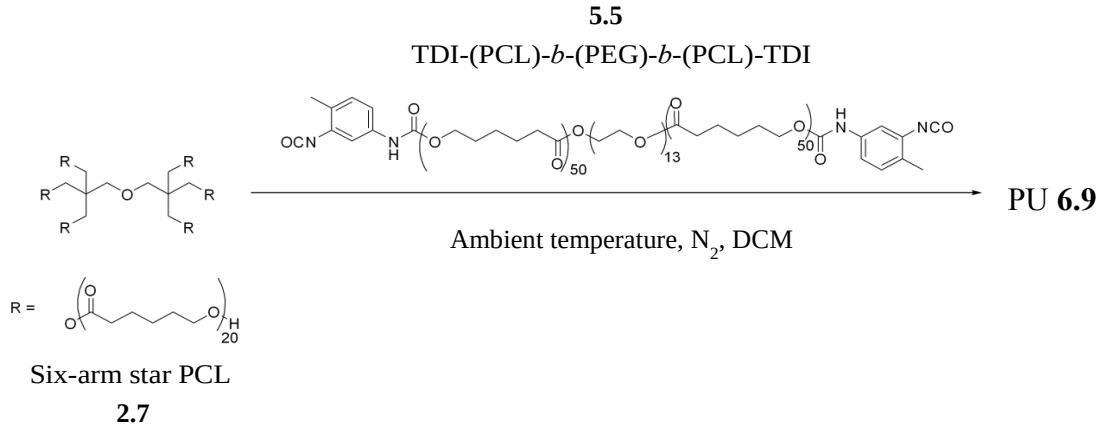

Scheme 6.7: Synthesis of PU **6.9**

PU **6.10** was synthesised by the reaction of six-arm star (PCL)-*co*-(PBL) containing a central dipentaerythritol moiety and a $\overline{DP}$ of ten per arm with a ratio of 7:3 for ε-CL : β-BL **2.14** with TDI-based diisocyanate prepolymer containing a central PCL-*b*-PEG-*b*-PCL moiety **5.5**, Scheme 6.8. The FT-IR spectrum of **6.10**, Appendix 6.9, shows the disappearance of the absorbance at 2210-2260 cm^{-1} attributing to the C=N stretch in the NCO group, indicating complete reaction with the OH groups on the PCL moiety. Moreover, the absorbances attributing to the N-H and C-N stretches in the urethane group can be seen at 3408 cm^{-1} and 1243 cm^{-1}, respectively.

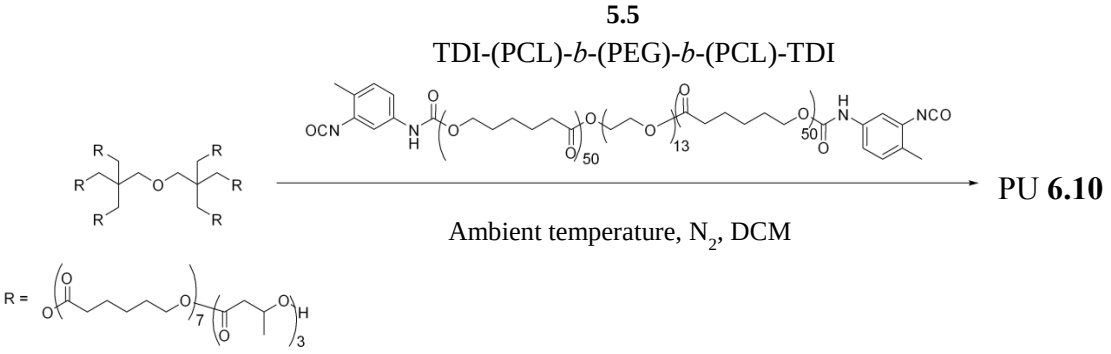

Scheme 6.8: Synthesis of PU **6.10**

PU **6.11** was synthesised by the reaction of four-arm star PCL containing a central PEG moiety with a $\overline{DP}$ of twenty per arm **3.10** and TDI-based diisocyanate prepolymer containing a central PCL-*b*-PEG-*b*-PCL moiety **5.5**, Scheme 6.9. The FT-IR spectrum of **6.11**, Appendix 6.10, shows the disappearance of the absorbance at 2210-2260 cm^{-1} attributing to the C=N stretch in the NCO group, indicating complete reaction with the OH groups on the PCL moiety. Moreover, the absorbances attributing to the N-H and C-N stretches in the urethane group can be seen at 3412 cm^{-1} and 1242 cm^{-1}, respectively.

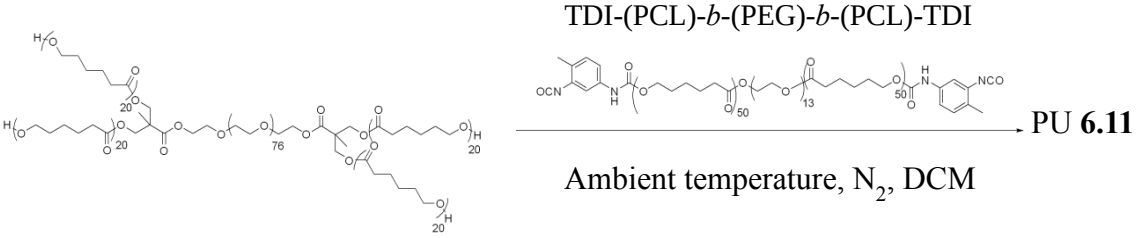

Scheme 6.9: Synthesis of PU **6.11**

The thermal decomposition temperature (T_d) for PUs **6.1 – 6.11** were in the range of 274 - 331 °C, Appendix 6.11. Generally PUs **6.8 – 6.11** containing a PEG moiety showed a lower T_d than PUs **6.1 – 6.7** containing no PEG moiety. Furthermore, PUs **6.1 – 6.2**, **6.6** and **6.8** containing an MDI moiety showed a higher T_d than PUs **6.3 – 6.5**, **6.7** and **6.9 – 6.11** containing a TDI moiety, suggesting a higher degree of cross-linking in the PUs synthesised using an MDI-based diisocyanate. This supports the previous hypothesis of the MDI moiety containing more reactive NCO groups than the TDI moiety. This can be explained by the unhindered NCO groups on the MDI moiety exhibiting a higher reactivity to the sterically hindered NCO groups on the TDI moiety. However, a repeat synthesis would be required to confirm this observation.

6.3.2 Solvent Uptake

The % solvent uptake (%SU) using toluene was measured for PUs **6.1 – 6.11** to evaluate the extent of cross-linking in the samples, Table 6.1. Furthermore, the decanted solvent from each PU extraction was collected, dried under reduced pressure and weighed to determine the % extracted material (%EM). PUs **6.6 – 6.7** showed the lowest %SU of 63% and 58%, with MDI and TDI-based diisocyanate prepolymers containing a central PCL moiety, respectively. These values were significantly lower than PUs **6.1 – 6.5** and **6.8 – 6.11**, showing %SU in the range of 251 – 603%. This could be explained by the polyol component in PUs **6.6 – 6.7** having a lower $\overline{DP}$ of ten per arm compared to PUs **6.1 – 6.3**, **6.5**, **6.8 – 6.9** and **6.11**, containing polyol components with a $\overline{DP}$ of twenty or thirty per arm. Moreover, PUs **6.6 – 6.7** contain a significantly shorter diisocyanate prepolymer

component than PUs **6.8 – 6.11**. This could lead to PUs **6.6 – 6.7** having a denser structure due to a higher degree of cross-linking therefore, showing a lower %SU. Furthermore, this dense structure could explain the unreacted NCO groups in the FT-IR spectrum of **6.6**, Figure 6.1, due to steric hindrance. Interestingly, **6.6** and **6,7** exhibited low %EM of 8% and 4%, respectively, despite **6** having unreacted NCO groups within its structure.

Table 6.1: %SU and %EM for PUs **6.1 – 6.11**

PU	Diisocyanate	Polyol	SU	EM
			%	
6.1	MDI **5.1**	Star PCL **2.7**	350	31
6.2	MDI **5.1**	Star PCL **2.7**	515	10
6.3	TDI **5.2**	Star PCL **2.7**	603	12
6.4	TDI **5.2**	Star Poly(ε-CL)-*co*-(β-BL) **2.14**	295	46
6.5	TDI **5.2**	Star PCL with β-CD core **4.5**	251	10
6.6	MDI-PCL-MDI **5.4**	Star Poly(ε-CL)-*co*-(β-BL) **2.14**	63	8
6.7	TDI-PCL-TDI **5.3**	Star Poly(ε-CL)-*co*-(β-BL) **2.14**	58	4
6.8	MDI-(PCL)-*b*-(PEG)-*b*-(PCL)-MDI **5.6**	Star PCL **2.7**	394	6
6.9	TDI-(PCL)-*b*-(PEG)-*b*-(PCL)-TDI **5.5**	Star PCL **2.7**	359	8
6.10	MDI-(PCL)-*b*-(PEG)-*b*-(PCL)-MDI **5.6**	Star Poly(ε-CL)-*co*-(β-BL) **2.14**	445	35
6.11	MDI-(PCL)-*b*-(PEG)-*b*-(PCL)-MDI **5.6**	Star $(PCL)_2$-*b*-PEG-*b*-$(PCL)_2$ **3.10**	545	10

The large %EM of 46% and 35% seen in **6.4** and **6.10**, respectively, could be attributed to the lower reactivity of the OH groups on the six-arm star (PCL)-*co*-(PBL) **2.14** polyol moiety. The random copolymerisation of the star (PCL)-*co*-(PBL) **2.14** moiety results in a mixture of chain-end OH groups on either a PCL or PBL moiety. The lower reactivity of the 2° OH groups on the star (PCL)-*co*-(PBL) **2.14** moiety could lead to a higher amount of unreacted material. A higher %SU was seen for **6.10** at 445% than **6.4** at 295%, due to the TDI-based diisocyanate prepolymer containing a central PCL-*b*-PEG-*b*-PCL moiety in **6.10** as opposed to a TDI moiety used in the synthesis of **6.4**. The less dense cross-linked network in **6.10**, containing longer and more flexible polymer chains shows a higher %SU than the denser, less flexible cross-linked network in **6.4**. This hypothesis is supported by the low %EM of **6.8** and **6.9** at 6% and 8%, respectively, both containing six-arm star PCL **2.7** and either a MDI-based diisocyanate prepolymer **5.6** or TDI-based diisocyanate prepolymer **5.5** with a central PCL-*b*-PEG-*b*-PCL moiety. Contrastingly, a significantly higher %EM is seen for **6.10** containing a star (PCL)-*co*-(PBL) **2.14** moiety and a TDI based diisocyanate prepolymer with a central PCL-*b*-PEG-*b*-PCL moiety **5.5**. In this case, the higher %EM in **6.10** due to unreacted components could be explained by` the decreased reactivity of the 2° OH groups in the star (PCL)-*co*-(PBL) **2.14** moiety.

PU **6.2** shows a higher %SU of 515% compared to PU **6.1** at 350%, due to an increased polyol content. PU **6.2** was synthesised using a ratio of 1:1.5 for NCO:OH groups as opposed to PU **6.1**, using a ratio of 1:1 for NCO:OH groups. This ratio implies a certain degree of OH groups on the star PCL moiety will be unreacted in **6.2**, giving a partially cross-linked and less dense structure than **6.1**. However, the %EM was 31% and 10% for **6.1** and **6.2**, respectively, indicating a higher proportion of materials were left unreacted in **6.1**. This unexpected result could be explained with the same hypothesis used in the explanation of unreacted NCO groups in PU **6.6**. The denser and more cross-linked structure in **6.1** could restrict polymer chain mobility and decrease access of the OH group on the star PCL moiety to the NCO group on the MDI moiety. This would probably lead to a higher proportion of unreacted material in **6.1** compared to **6.2**.

The high %SU of 545% seen for **6.11** could be due to the presence of the large TDI-based diisocyanate prepolymer containing a central PCL-*b*-PEG-*b*-PCL **5.5** moiety together with the large four-arm star PCL containing a central linear PEG **3.10** moiety. The high $\overline{DP}$ in both diisocyanate prepolymer and polyol components may result in a less dense cross-linked PU structure and therefore, show a higher %SU. Furthermore, the four OH chain

end groups on the large polyol moiety and two NCO chain end groups on the large diisocyanate prepolymer moiety have a low probability of coming into close proximity for a reaction to occur due to their relatively large structures. It is expected that an increase in the $\overline{DP}$ of the star polyol and diisocyanate prepolymer moieties, would show a decrease in the number of reactions and crosslinking between the NCO and OH groups. Therefore, the decrease in cross-linking results in a less dense PU structure and exhibits a relatively high %EM measured at 10% for PU **6.11**.

In general, the %EM was relatively low in the range of 4-12% in all PUs except **6.1**, **6.4** and **6.10** showing %EM of 31%, 46% and 35%, respectively. There is no reasonable hypothesis when considering the chemical structures of the polyol and diisocyanate moieties to explain why specifically PUs **6.1**, **6.4** and **6.10** exhibited a significantly higher %EM than all other PUs. It is possible that problems occurred during the syntheses of these PUs, such as inefficient mixing and the variation in viscosities of the reaction mixtures due to the addition of a minimal amount of solvent.

6.3.3 Water Uptake

The % water uptake (%WU) was measured for PUs **6.1 – 6.11** to determine the relative hydrophilic nature of the cross-linked materials, Table 6.2. The %PEG content and % mass loss over 30 days of enzymatic degradation are included in Table 6.2 to determine the effect of the incorporation of a hydrophilic PEG component in PU on the rate of enzymatic degradation.

It can be seen that PU **6.11** exhibits the highest %WU at 30%, due to the polyol and diisocyanate components containing the highest hydrophilic %PEG content at 16%. PU **6.2** shows a higher %WU than PU **6.1**, both containing the same components of six-arm star PCL and MDI with ratios of 1:1.5 and 1:1 of NCO:OH groups, respectively. The higher %WU in **6.2** could be due to excess of unreacted chain end hydrophilic OH groups, increasing the hydrophilic nature of the PU. This could contribute towards the initial increase in the rate of enzymatic degradation in **6.2** from 0% to 8.8% to 16.8% mass loss, compared to **6.1** from 0% to 8.3% to 13.5% mass loss in days 0 to 10 to 20, respectively.

Table 6.2: %WU for PUs **6.1 – 6.11** with corresponding %PEG content and % mass loss by enzymatic degradation using *pseudomonas cepacia* lipase in PBS solution (pH 7.4).

PU	Diisocyanate	Polyol	WU	PEG	Mass loss %		
			%		Day 10	Day 20	Day 30
6.1	MDI **5.1**	Star PCL **2.7**	6	0	8.3	13.5	18.5
6.2	MDI **5.1**	Star PCL **2.7**	19		8.8	16.8	16.9
6.3	TDI **5.2**	Star PCL **2.7**	22		2.2	5.9	9.2
6.4	TDI **5.2**	Star Poly(ε-CL)-*co*-(β-BL) **2.14**	5		9.1	16.5	16.8
6.5	TDI **5.2**	Star PCL with β-CD core **4.5**	9		0.7	1.9	2.8
6.6	MDI-PCL-MDI **5.4**	Star Poly(ε-CL)-*co*-(β-BL) **2.14**	6		2.8	4.7	5.3
6.7	TDI-PCL-TDI **5.3**	Star Poly(ε-CL)-*co*-(β-BL) **2.14**	10		1.1	1.8	1.8
6.8	MDI-(PCL)-(PEG)-(PCL)-MDI **5.6**	Star PCL **2.7**	7	4	4.9	8.8	12.0
6.9	TDI-(PCL)-(PEG)-(PCL)-TDI **5.5**	Star PCL **2.7**	7	9	2.1	3.2	7.0
6.10	MDI-(PCL)-(PEG)-(PCL)-MDI **5.6**	Star Poly(ε-CL)-*co*-(β-BL) **2.14**	3	10	6.1	10.0	18.0
6.11	MDI-(PCL)-(PEG)-(PCL)-MDI **5.6**	Star $(PCL)_2$-PEG-$(PCL)_2$ **3.10**	30	16	3.8	10.3	15.1

It is evident that PU **6.3** containing a six-arm star PCL **2.7** moiety and TDI **5.2** shows a higher %WU at 22% than PU **6.1** at 6%, containing the same six-arm star PCL **2.7** moiety but with MDI **5.1**. This can be explained by the increased hydrophobic aromatic content in the MDI moiety. Furthermore, the aromatic rings impart rigidity and crystallinity to the PU, therefore decreasing the %WU.

PUs **6.3** and **6.4** contain a six-arm star PCL **2.7** and a six-arm star (PCL)-*co*-(PBL) **2.14** moiety with TDI **5.2**, and show a %WU of 22% and 5%, respectively. This can be explained using the hypothesis of the 2° OH groups on the six-arm star (PCL)-*co*-(PBL) **2.14** moiety having lower reactivity than the 1° OH groups on the six-arm star PCL **2.7** moiety. This leads to partial cross-linking in PU synthesis leaving an increased amount of polyol or diisocyanate components unreacted. This is evident with PU **6.4** showing a %EM of 46%, Table 6.1. Therefore, the incorporation of β-BL into the polyol component, decreases the %WU of the resulting PU. This is supported by the decreased %WU of **6.10** at 3% compared to **6.9** at 7%, containing six-arm star (PCL)-*co*-(PBL) **2.14** moiety and six-arm star PCL **2.7** moiety, respectively, and both containing the TDI-based diisocyanate prepolymer with a central PCL-*b*-PEG-*b*-PCL moiety **5.5**.

6.3.4 Enzymatic degradation of Polyurethanes 6.1 – 6.11

PUs **6.1 – 6.11** were subjected to enzymatic degradation using *pseudomonas cepacia* lipase and monitored using % mass loss. Comparisons are made between selected PUs, dependent on their relative compositions of polyol and diisocyanate component.

6.3.4.1 Polyurethanes with star PCL and either MDI or TDI

PUs **6.1** and **6.3** were synthesised to determine the effect of MDI and TDI on the rate of enzymatic degradation. PUs **6.1** and **6.3** contain the same six-arm star PCL **2.7** with a central dipentaerythritol unit and a $\overline{DP}$ of twenty per arm and either MDI **5.1** or TDI **5.2**, respectively. PU **6.1** can be seen to degrade at a significantly faster rate (18.5% mass loss after 30 days) than **6.3** (9.2% mass loss after 30 days), Figure 6.2. It is expected that a PU containing an MDI moiety will be more crystalline and hydrophobic than a PU containing a TDI moiety due to the two aromatic rings in its chemical structure. This increased crystallinity and hydrophobicity in PU containing the MDI moiety is expected to decrease

the rate of enzymatic degradation, due to the decreased mobility of enzymes and water to access the bulk of the polymer and degrade the hydrolysable ester groups. However, in this case the unexpected increase in the rate of enzymatic degradation seen in PU **6.1**, could be explained by the more reactive NCO groups on the MDI moiety undergoing secondary or self-addition reactions (discussed in Chapter 1, Section 2.5.1). The decreased amount of available NCO groups could result in partially reacted six-arm star PCL **2.7** leading to some unreacted pendant PCL chains in the less dense, lightly cross-linked PU structure. Therefore, enzymes and water will have increased mobility into the bulk of the polymer and increased access to the hydrolysable ester groups on the PCL moieties, particularly to pendant PCL chains.

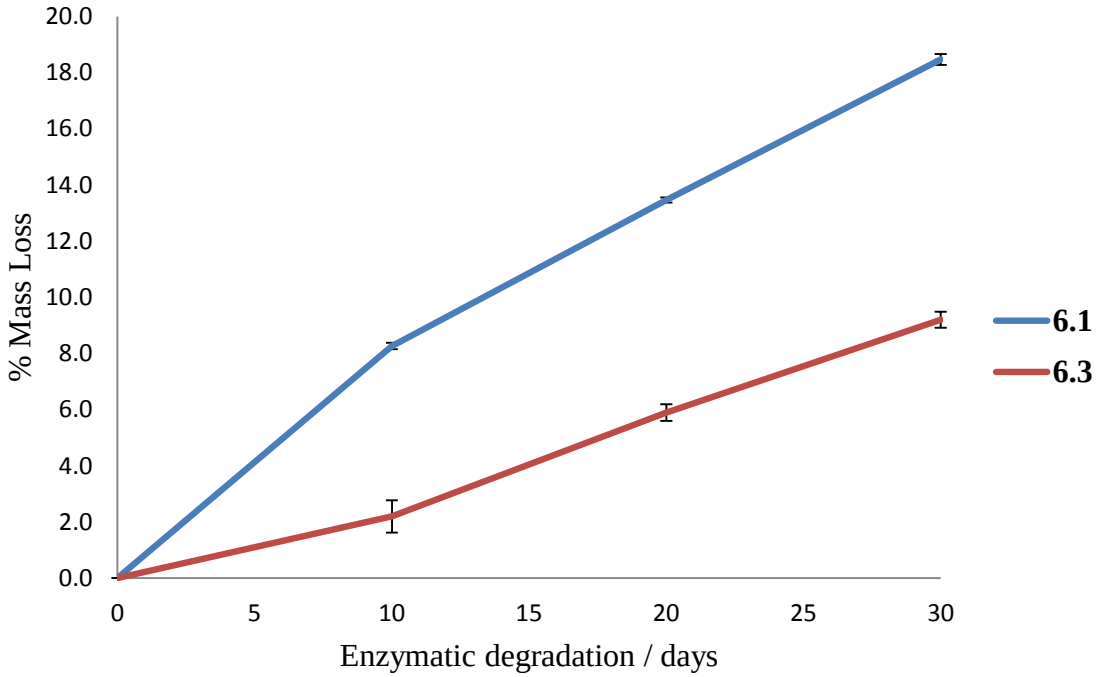

Figure 6.2: % Mass losses for PU **6.1** and **6.3** over 30 days of enzymatic degradation using *pseudomonas cepacia* lipase in PBS solution (pH 7.4). The % mass losses are averages of three repeat sample measurements and the % error bars are shown.

6.3.4.2 Polyurethanes with TDI and various polyols

PUs **6.3** – 6.**5** were synthesised with TDI **5.2** and either six-arm star PCL **2.7**, six-arm star (PCL)-*co*-(PBL) **2.14**, and seven-arm star PCL **4.5** containing a central β-CD moiety, respectively, to determine the effect of the polyol component in PU on the rate of enzymatic degradation. The % mass losses for **6.3 – 6.5** over 30 days of enzymatic degradation are shown in Figure 6.3. PU **6.4** shows the fastest rate of degradation, however the rate significantly decreases after day 20 at 16.5% mass loss to day 30 at 16.8% mass loss. This could be due to preferential degradation occurring initially in the more amorphous areas of the polymer chain containing the PBL moieties. The degradation of amorphous areas in PU would result in an overall increase in crystallinity and therefore, a decrease in the rate of enzymatic degradation. Moreover, PU **6.3** degraded at a slower rate (9.2% mass loss after 30 days) than **6.4**, due to the lower crystallinity of the star (PCL)-*co*-(PBL) **2.14** polyol component, imparted by the random incorporation of the β-BL monomer. The lower crystallinity of star (PCL)-*co*-(PBL) **2.14** polyol (%χ_c of 20%, Chapter 2) used in **6.4**, than star PCL **2.7** (%χ_c of 27%, Chapter 2) used in **6.3**, increases the mobility of the enzyme and water into the bulk of the cross-linked PU. This increases the access to hydrolysable ester groups on the PCL and PBL moieties therefore, increasing the rate of enzymatic degradation.

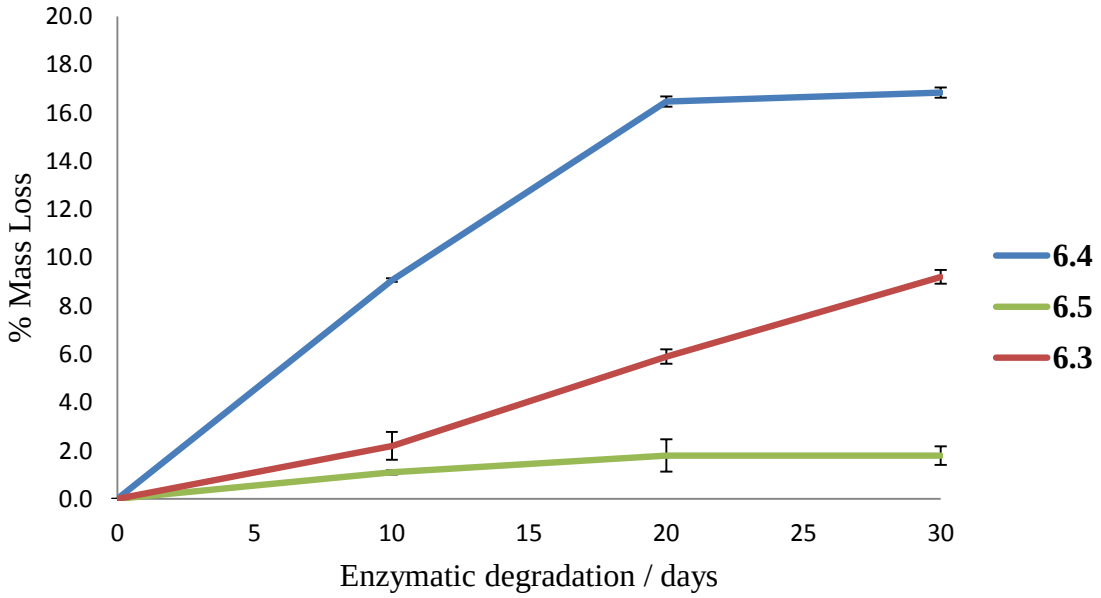

Figure 6.3: % Mass losses of PU **6.3 – 6.5** over 30 days of enzymatic degradation using *pseudomonas cepacia* lipase in PBS solution (pH 7.4). The % mass losses are an average of three repeat sample measurements and the % error bars are shown.

PU **6.5** exhibits the lowest rate of enzymatic degradation at 2.8% mass loss after 30 days. This result was expected as the seven-arm star PCL **4.5** containing a central β-CD moiety exhibited a significantly lower rate of degradation (7% mass loss after 20 days, Chapter 4) than both the six-arm star PCL **2.7** and six-arm star (PCL)-*co*-(PBL) **2.14** polyols (>94% mass loss after 15 days, Chapter 2). The low rate of enzymatic degradation in PU **6.5** could be explained by the seven-arm star PCL **4.5** having a large crystalline β-CD central moiety imparting rigidity to the cross-linked PU structure and therefore, decreasing the mobility and access of enzymes and water to the hydrolysable ester groups. Furthermore, the polyol component in **6.5** contains seven PCL arms, opposed to the six PCL arm polyols incorporated in PUs **6.3** and **6.4** leading to increased cross-linking and therefore, lower enzyme mobility and a decreased rate of degradation. Moreover, the seven-arm star PCL with a central β-CD core has a higher $\overline{DP}$ of thirty per arm **4.5**, compared to **6.3** and **6.4** with a $\overline{DP}$ of ten and twenty per arm, respectively. The longer PCL chains in **6.5** have increased potential to become entangled and further decrease enzyme mobility, as well as increase the hydrophobic nature of the PU therefore, decreasing the rate of enzymatic degradation.

6.3.4.3 Polyurethanes with Star poly[(ε-CL)-*co*-(β-BL)] and diisocyanate prepolymer containing a central PCL moiety and either TDI or MDI

PUs **6.6** and **6.7** were synthesised using a six-arm star poly[(ε-CL)-*co*-(β-BL)] **2.14** polyol component and either an MDI-based diisocyanate prepolymer **5.6** or TDI-based diisocyanate prepolymer **5.5** containing a central PCL moiety, respectively. The % mass loss of **6.6** and **6.7** over 30 days of enzymatic degradation are compared and shown in Figure 6.4. It can be seen that **6.6** and **6.7** both show a gradual decrease in the rate of enzymatic degradation throughout the 30 days, with minimal increase in % mass loss from day 20 to day 30. The same phenomenon was seen in Figure 6.3 for PU **6.4** containing the same six-arm star poly[(ε-CL)-*co*-(β-BL)] **2.14** polyol component, showing the rate of degradation significantly decreased between day 20 and day 30. This supports that the *pseudomonas cepacia* lipase enzyme preferentially degrades the more amorphous regions containing the PBL moieties in the random star copolymer, eventually causing an overall increase the in crystallinity of the PU and therefore, a decrease in enzyme and water mobility.

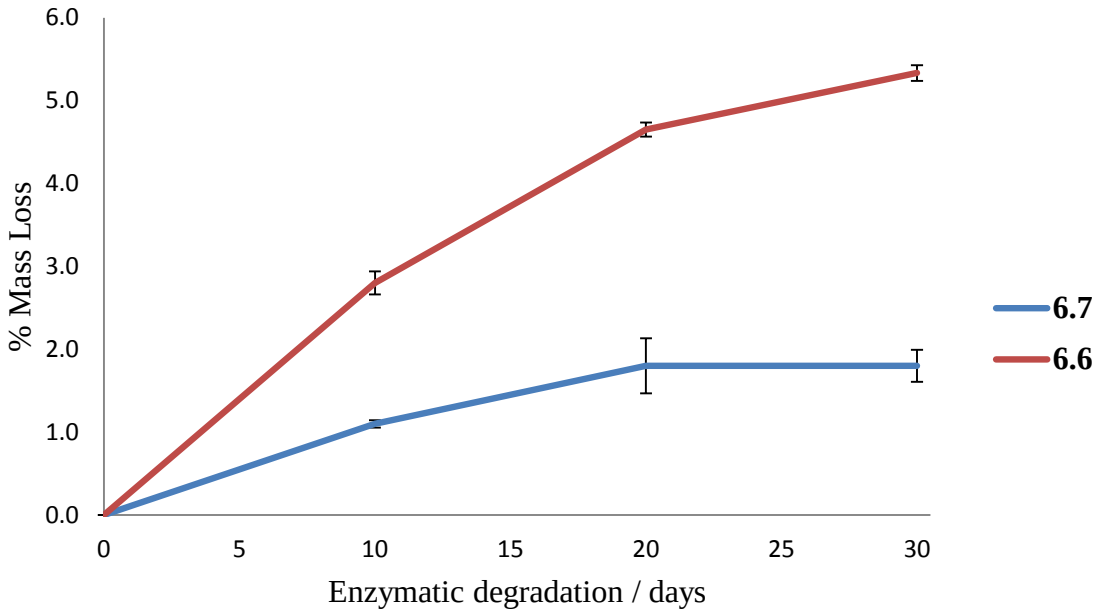

Figure 6.4: % Mass losses of PU **6.6 – 6.7** over 30 days of enzymatic degradation using *pseudomonas cepacia* lipase in PBS solution (pH 7.4). The % mass losses are averages of three repeat sample measurements and % error bars are shown.

PU **6.6** degraded at a faster rate (5.3% mass loss after 30 days) than **6.7** (1.8% mass loss after 30 days), due to the increased reactivity of the NCO groups on the MDI moiety compared to the TDI moiety. This supports the results seen in PUs **6.2** and **6.3** whereby the MDI containing PU **6.1** degraded at a faster rate than the TDI containing PU **6.3**, Figure 6.2.

6.3.4.4 Polyurethanes with Star Poly[(ε-CL)-*co*-(β-BL)] and TDI or TDI-based diisocyanate prepolymers

The % mass loss for TDI-based PUs **6.4**, **6.7** and **6.10** over 30 days of enzymatic degradation are compared in Figure 6.5. PUs **6.4**, **6.7** and **6.10** were synthesised with the same six-arm star poly[(ε-CL)-*co*-(β-BL)] **2.14** polyol and either TDI **5.2**, a TDI-based prepolymer containing a central PCL moiety **5.3**, or a TDI-based prepolymer containing a central PCL-*b*-PEG-*b*-PCL moiety **5.5**, respectively. Diisocyanate prepolymers incorporating a central biodegradable PCL moiety were synthesised with the aim to

increase the rate of enzymatic degradation of the resulting PU, by increasing the spacer length between the non-degradable aromatic isocyanate groups. Furthermore, biodegradable diisocyanate prepolymers containing a central hydrophilic PEG moiety were synthesised with the aim to increase the hydrophilic nature of the resulting PU and therefore, increase the rate of enzymatic degradation of the PCL moieties. It can be seen that **6.10** exhibited the highest % mass loss of 18.0% after 30 days, as opposed to **6.4** (16.8% mass loss after 30 days) and **6.7** (1.8% mass loss after 30 days). Interestingly, PU **6.7** containing the biodegradable TDI-based diisocyanate prepolymer with a central PCL moiety **5.3**, was significantly slower to degrade than PU **6.4**, containing TDI **5.2**. The unexpected slower rate of degradation for **6.7** could possibly be due to an increased hydrophobic PCL content and higher hydrophobic aromatic content as two TDI moieties are present in the TDI-based diisocyanate prepolymer. The incorporation of the hydrophilic PEG moiety into the TDI-based diisocyanate prepolymer used in the synthesis of **6.10**, greatly increased the rate of degradation in comparison to **6.7** containing TDI-based diisocyanate prepolymer with a central PCL moiety. This supports that the incorporation of a central hydrophilic PEG moiety increases the rate of enzymatic degradation.

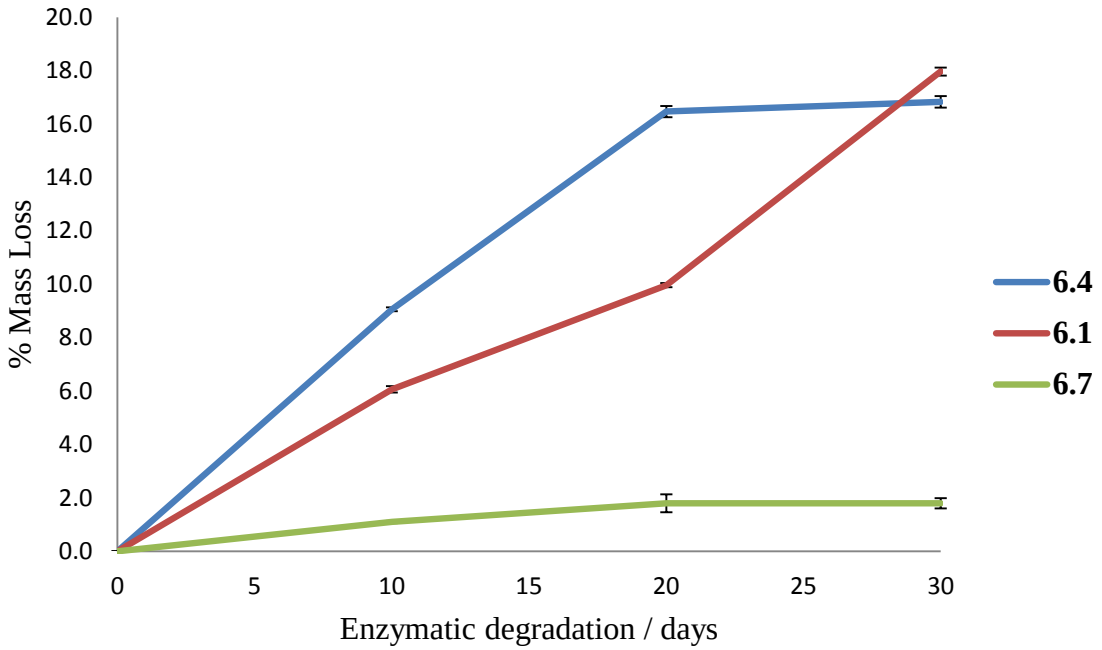

Figure 6.5: % Mass losses of PU **6.4**, **6.7** and **6.10** over 30 days of enzymatic degradation using *pseudomonas cepacia* lipase in PBS solution (pH 7.4). The % mass losses are averages of three repeat sample measurements and the % error bars are shown.

It must be noted that the rate of degradation changed throughout the 30 day enzymatic degradation period. This is particularly noticeable for PU **6.4**, which had the fastest rate of degradation from day 0-20 (16.5% mass loss after 20 days) compared to **6.7** (1.8% mass loss after 20 days) and **6.10** (10.0% mass loss after 20 days). However, the late increase in the rate of enzymatic degradation after day 20 in PU **6.10** suggests there is a slower initial lag phase. This could be due to the water in the degradation media taking time to penetrate into the bulk of the cross-linked PU material and access the hydrophilic PEG moieties. After this initial lag phase, the water and enzymes have greater mobility into the bulk of material therefore, increasing the rate of enzymatic degradation.

6.3.4.5 Polyurethane with Star $(PCL)_2$-*b*-PEG-*b*-$(PCL)_2$ and TDI-based diisocyanate prepolymer containing a central PCL-*b*-PEG-*b*-PCL moiety

Four-arm star PCL with a central PEG moiety **3.10** was synthesised to determine the effect of the incorporation of a hydrophilic PEG moiety into the star PCL polyol component, on the rate of enzymatic degradation of the resulting PU. It can be seen that PU **6.11** containing the four-arm star PCL with a central PEG unit **3.10**, degraded at a faster rate (15.1% mass loss after 30 days) than PU **6.9** (7.0% mass loss after 30 days), containing the six-arm star PCL polyol **2.7**, Figure 6.6. This result was expected as the four-arm star PCL with a central PEG moiety **3.10** showed the fastest rate of degradation (>99% mass loss after 6 days, Chapter 3) compared to star PCL **2.7** (94% mass loss after 15 days, Chapter 2). This suggests the incorporation of a central hydrophilic PEG moiety into the star PCL polyol, increases the rate of enzymatic degradation, due to the increase in mobility of the enzyme and water leading to increased access to the hydrolysable ester groups on the PCL moieties.

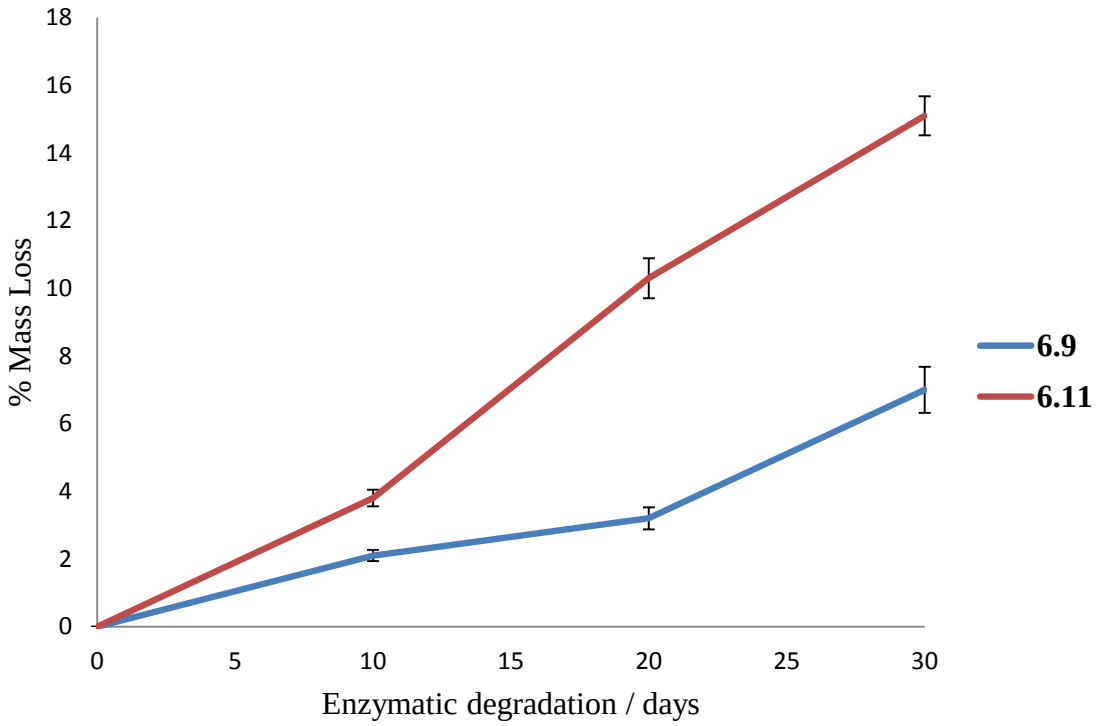

Figure 6.6: % Mass losses of PU **6.9** and **6.11** over 30 days of enzymatic degradation using *pseudomonas cepacia* lipase in PBS solution (pH 7.4). The % mass losses are averages of three repeat sample measurements and % error bars are shown.

The rate of enzymatic degradation in **6.9** and **6.11** can both be seen to generally increase throughout the 30 days of enzymatic degradation. This can be explained by the increasing hydrophilic PEG content throughout enzymatic degradation due to the decrease in PCL content during the process of degradation. The increase in PEG content will increase the mobility of water and enzyme into the bulk of the polymer to access the hydrolysable ester groups on the PCL moiety.

6.3.4.6 Polyurethane with Star PCL and various diisocyanates

PUs **6.8** and **6.9** were synthesised with six-arm star PCL **2.7** and either MDI-based diisocyanate prepolymer **5.6** or TDI-based diisocyanate prepolymer **5.5** containing a central PCL-*b*-PEG-*b*-PCL moiety, respectively, to determine the effect of diisocyanate prepolymer type (MDI-based or TDI-based) on the rate of enzymatic degradation. For comparison, PUs **6.1** and **6.3** were synthesised with the same six-arm star PCL **2.7** and

either MDI **5.1** or TDI **5.2**, respectively, to determine the effect of using a diisocyanate prepolymer containing a central PCL-*b*-PEG-*b*-PCL moiety, Figure 6.7. As previously discussed in Section 6.3.4.1, PU **6.1** containing the MDI moiety degrades at a faster rate of 18.5% mass loss after 30 days, than PU **6.3** containing the TDI moiety, at 9.2% mass loss after 30 days. The same phenomenon can be seen in PU **6.8** containing the MDI-based diisocyanate prepolymer, showing a faster rate of degradation at 12.0% mass loss after 30 days, than PU **6.9** containing the TDI-based diisocyanate prepolymer, at 7.0% mass loss after 30 days.

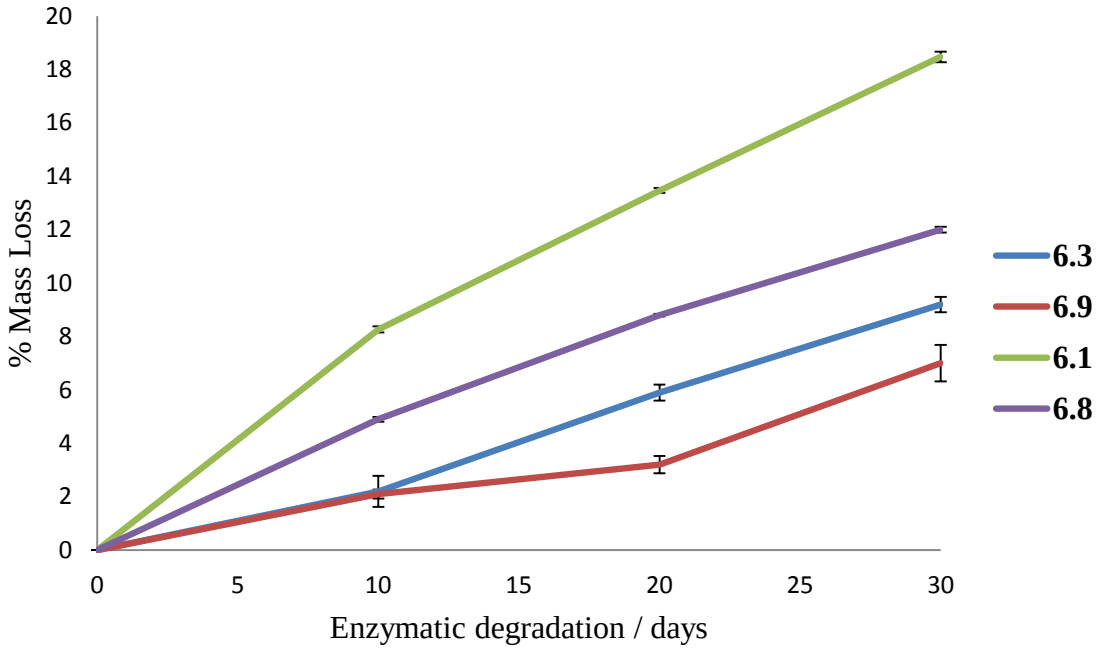

Figure 6.7: % Mass losses of PU **6.1**, **6.3**, **6.8** and **6.9** over 30 days of enzymatic degradation using pseudomonas cepacia lipase in PBS solution (pH 7.4). The % mass losses are averages of three repeat sample measurements and the % error bars are shown.

Both PUs **6.8** and **6.9** containing MDI-based diisocyanate prepolymer **5.6** and TDI-based diisocyanate prepolymers **5.5** exhibit a decreased rate of degradation than the corresponding PUs **6.1** and **6.3**, synthesised with an MDI **5.1** or TDI **5.2** moiety, respectively. This could be explained by the potential secondary and self-addition reactions of the NCO groups during the diisocyanate prepolymer syntheses. This could

lead to longer polymeric chains, increased aromatic content and increased cross-linking therefore, decreasing the rate of enzymatic degradation.

6.3.4.7 Polyurethane with Star PCL and MDI

PU **6.2** was synthesised with six-arm star PCL **2.7** and MDI **5.1** using a molar ratio of 1:1.5 for NCO:OH groups, to determine the effect of isocyanate concentration on the rate of enzymatic degradation. As a comparison, PU **6.1** was synthesised with the same six-arm star PCL **2.7** and MDI **5.1** using a molar ratio of 1:1 for NCO:OH groups.

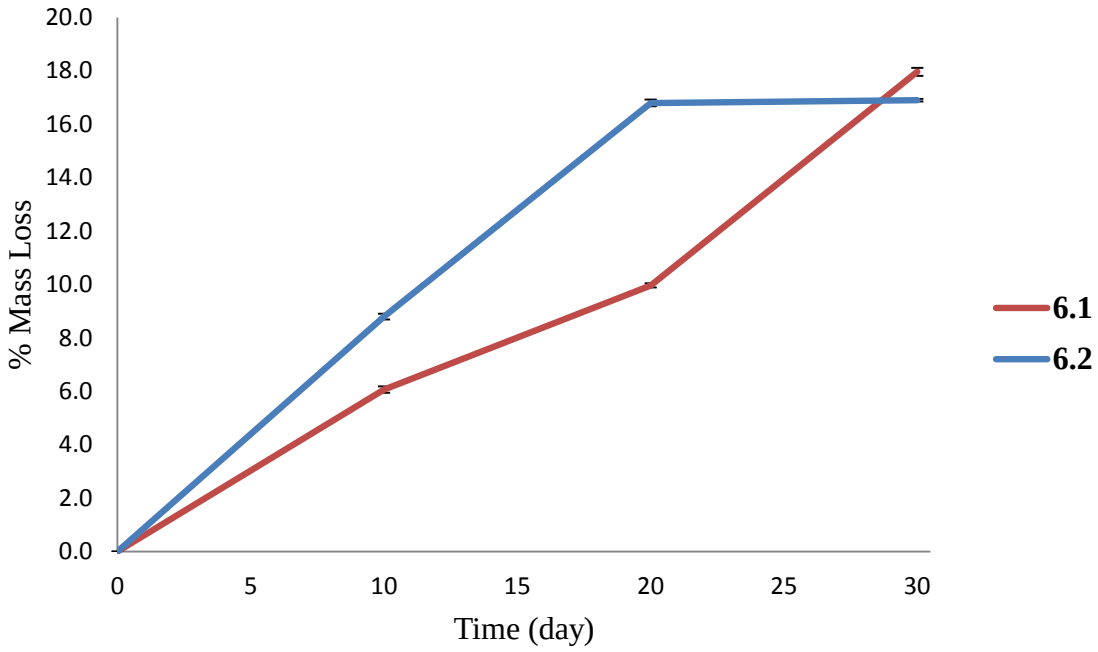

Figure 6.8: % Mass losses of PU **6.1 – 6.2** over 30 days of enzymatic degradation using *pseudomonas cepacia* lipase in PBS solution (pH 7.4). The % mass losses averages of three repeat sample measurements and the % error bars are shown.

It can be seen that PU **6.2** and **6.1** have similar degradation rates during the first 10 days of enzymatic degradation, showing mass losses of 8.8% and 8.3% on day 10, respectively, Figure 6.8. The rate of degradation of **6.2** remains the same from day 10-20 showing a mass loss of 16.8% at day 20, then sharply decreases from day 20-30 showing minimal

change in mass loss to 16.9% at day 30. On the other hand, the rate of degradation in **6.1** shows a small decrease from day 10-30 but proceeds in a linear fashion, giving **6.1** a higher total % mass loss at day 30 of 18.5% than **6.2** at 16.9% mass loss. This suggests the lower MDI content in PU **6.2** initially increases the rate of degradation, however, significantly decreases the rate of degradation after 20 days of enzymatic degradation. This can be explained by the decreased cross-linking density in PU **6.2** with an excess of unreacted OH groups on the star PCL moiety leading to a less dense structure than PU **6.1**. This means the that enzymes and water have increased mobility through a more flexible, less dense and partially cross-linked network therefore, would increase the rate of enzymatic degradation. The sharp decrease in the rate of degradation after 20 days could be explained by the preferential degradation of the more flexible and amorphous pendant PCL chains, leaving a more crystalline and cross-linked structure behind, causing a subsequent decrease in the rate of enzymatic degradation.

6.5 Conclusions

Biodegradable PUs **6.1 – 6.11** were synthesised using biodegradable star PCL based polyols **2.7**, **2.14**, **3.10** and **4.5** (Chapters 2-4) and either biodegradable diisocyanate prepolymers **5.3 – 5.6** (Chapter 5) or MDI **5.1** or TDI **5.2**.

The PUs were characterised using FT-IR, TGA, %WU, %SU and %EM. Generally the FT-IR analyses showed the disappearance of the strong absorbance corresponding to the C=N stretch in the NCO group, suggesting complete reaction with OH groups to give a urethane group. This is supported by the appearance of absorbances attributing to N-H and C-N stretches. The %WU for PUs were measured to determine their relative hydrophilic nature and its effect on the rate of enzymatic degradation. However, there was no clear correlation between the %WU and the rate of enzymatic degradation due to experimental error in %WU. The %SU of the PUs using toluene were measured to indicate the degree of cross-linking and the effect on the rate of enzymatic degradation. In general, PUs containing longer and more flexible diisocyanate prepolymers showed a higher %SU due to the formation of a less dense structure due to a light degree of cross-linking. However, the PUs synthesised using the diisocyanate prepolymers generally showed a lower rate of enzymatic degradation than PUs synthesised with either MDI **5.1** or TDI **5.2**. It is suggested that this is due to secondary and self-addition reactions of the NCO groups during the synthesis of diisocyanate prepolymers. This would increase the extent of aromatic content, M_n and cross-linking in the diisocyanate prepolymers. PUs synthesised using the six-arm star poly[(ε-CL)-*co*-(β-BL)] **2.14** polyol showed a higher %EM than with six-arm star PCL **2.7**, due to the decreased reactivity of the 2° OH groups on the PBL chain-end moieties.

The rate of enzymatic degradation using *pseudomonas cepacia* lipase was monitored using % mass loss after 10, 20 and 30 days. It must be noted that the enzymatic degradation analyses ceased after 30 days due to time restrictions. Therefore, conclusions about the degradation characteristics of PUs are based on the first part of degradation, showing up to 18.5% mass loss after 30 days. The novel investigation of the enzymatic degradation of PUs **6.1 – 6.11** show a much faster rate of degradation than previous studies, showing PUs with up to 10% mass loss after 90 days of hydrolytic degradation in PBS solution (pH 7.4).[15]

In general, PUs synthesised using MDI **5.1** or a MDI-based diisocyanate prepolymer **5.4** or **5.6**, showed an increased rate of degradation in comparison to PUs synthesised using TDI **5.2** or TDI-based diisocyanate prepolymers **5.3** or **5.5**. This is due to the MDI moiety containing less hindered and more reactive NCO groups, with an increased probability of secondary and self-addition reactions. This would decrease the number of NCO groups available in the system to react with the OH groups on the polyol component and hence give a less dense structure. Therefore, the enzymes and water will have increased mobility and increased access to hydrolyse the ester groups on the PCL moieties.

PUs synthesised using six-arm star poly[(ε-CL)-*co*-(β-BL)] **2.14** polyols showed an increased rate of enzymatic degradation compared to PUs synthesised using six-arm star PCL **2.7** polyols. This is due to the decreased reactivity of the 2° OH groups in PBL chain end moieties, giving a less dense PU structure. This is supported by the generally high %EM shown in PUs containing the six-arm star poly[(ε-CL)-*co*-(β-BL)] **2.14** polyol. The unreacted and partially reacted star polyol will have greater polymer chain mobility and therefore, the enzyme and water will have increased access to the hydrolysable ester groups on the PCL and PBL moieties. Furthermore, the lower $\overline{DP}$ of ten per arm in the six-arm star poly[(ε-CL)-*co*-(β-BL)] **2.14** polyol could also increase the rate of enzymatic degradation in comparison to the $\overline{DP}$ of twenty per arm in the six-arm star PCL **2.7** polyol.

PUs synthesised using a seven-arm star PCL containing a central β-CD moiety **4.5** exhibited a very low rate of enzymatic degradation. This could be due to the large central β-CD moiety imparting rigidity to the cross-linked PU structure. Furthermore, there will be a higher degree of cross-linking using a seven-arm polyol in comparison to the six-arm and four-arm polyols, decreasing the mobility and access of enzyme and water into the bulk of the polymer. On the other hand, PUs synthesised using four-arm star PCL **3.10** containing a central hydrophilic PEG moiety, showed a high rate of enzymatic degradation after 30 days. Interestingly, the increased rate of enzymatic degradation over 30 days due to the time required for the water and enzymes to penetrate into the bulk of the material to access the hydrophilic moieties and subsequently hydrolyse the neighbouring PCL moieties.

6.6 References

(1) Domanska, A., Boczkowska, A., *Polym. Degrad. Stabil.* **2014**, *108*, 175.

(2) Cohn, D.; Lando, G.; Sosnik, A.; Garty, S.; Levi, A. *Biomaterials* **2006**, *27*, 1718.

(3) Skarja, G. A.; Woodhouse, K. A. *J. Biomater. Sci.-Polym. Ed.* **2001**, *12*, 851.

(4) Skarja GA, W. K. *J. Appl. Polym. Sc.i* **2000**, *75*, 1522.

(5) He, M.; Chu, C.-C. *Polymer* **2013**, *54*, 4112.

(6) Guan, J. S., M. S.; Beckman, E. J.; Wagner, W. R. *J. Biomed. Mater. Res. Part A* **2002**, *61*, 493.

(7) Hong, J. H.; Jeon, H. J.; Yoo, J. H.; Yu, W.-R.; Youk, J. H. *Polym. Degrad. Stabil.* **2007**, *92*, 1186.

(8) You, Y.; Min, B.-M.; Lee, S. J.; Lee, T. S.; Park, W. H. *J. Appl. Polym. Sci.* **2005**, *95*, 193.

(9) Zong, X.-H.; Wang, Z.-G.; Hsiao, B. S.; Chu, B.; Zhou, J. J.; Jamiolkowski, D. D.; Muse, E.; Dormier, E. *Macromolecules* **1999**, *32*, 8107.

(10) Hurrell, S.; Cameron, R. E. *Biomaterials* **2002**, *23*, 2401.

(11) Fu, B. X.; Hsiao, B. S.; Chen, G.; Zhou, J.; Koyfman, I.; Jamiolkowski, D. D.; Dormier, E. *Polymer* **2002**, *43*, 5527.

(12) Huang, S. J., Roby, M. S. *J. Bioact. Compat. Polym.* **1986**, *1*, 61.

(13) Sendijarevic, V.; Sendijarevic, A.; Sendijarevic, I.; Bailey, R. E.; Pemberton, D.; Reimann, K. A. *Environ. Sci. Technol.* **2004**, *38*, 1066.

(14) Akutsu-Shigeno, Y.; Adachi, Y.; Yamada, C.; Toyoshima, K.; Nomura, N.; Uchiyama, H.; Nakajima-Kambe, T. *Appl. Microbiol. Biotechnol.* **2005**, *70*, 422.

(15) Barrioni, B. R.; de Carvalho, S. M.; Oréfice, R. L.; de Oliveira, A. A. R.; Pereira, M. d. M. *Mater. Sci. and Eng. C* **2015**, *52*, 22.

(16) Yi, J.; Huang, C.; Zhuang, H.; Gong, H.; Zhang, C.; Ren, R.; Ma, Y. *Prog. Org. Coat.* **2015**, *87*, 161.

(17) Wales, D. S., Sagar, B. R. *Mechanistic aspects of polyurethane deterioration* 7th ed.; Elsevier Applied Science, London, 1988.

(18) Brzeska, J.; Heimowska, A.; Sikorska, W.; Jasinska-Walc, L.; Kowalczuk, M.; Rutkowska, M. *Int. J. Polym. Sci.* **2015**.

(19) Santerre, J. P.; Labow, R. S.; Duguay, D. G.; Erfle, D.; Adams, G. A. *J. Biomed. Mater. Res.* **1994**, *28*, 1187.

(20) Tang, Y. W.; Labow, R. S.; Santerre, J. P. *J. Biomed. Mater. Res.* **2001**, *56*, 516.

(21) Akutsu, Y.; Nakajima-Kambe, T.; Nomura, N.; Nakahara, T. *Appl. Environ. Microbiol.* **1998**, *64*, 62.

7.1 Conclusions

This project involved the development of biodegradable rigid PU foams using biodegradable PCL-based polyol and diisocyanate prepolymer components. Aromatic diisocyanates MDI **5.1** and TDI **5.2** were used due to current industrial processes. The synthesised polyols, diisocyanate prepolymers and the resulting PUs were subjected to enzymatic degradation using *Pseudomonas Cepacia* lipase over 30 days and analysed using % mass loss, DSC and SEM.

Four- and six-arm star polyols **2.4 – 2.7, 2.9 – 2.10** and **2.12** were synthesised *via* the ROP of ε-CL catalysed by $SnOct_2$ and using pentaerythritol **2.11**, di(trimethylolpropane) **2.8** and dipentaerythritol **2.3** initiators with a $\overline{DP}$ of 10, 20, 50 and 100 per arm. For comparative analysis, linear PCL **2.2** and linear poly(ε-CL)-*co*-(β-BL) **2.13** were also synthesised in a similar manner using ethylene glycol **2.1** as initiators. Linear PCL **2.2** exhibited significantly faster enzymatic degradation than both star PCL **2.7** and star poly(ε-CL)-*co*-(β-BL) **2.14**. This is due to increased mobility and decreased entanglement of polymer chains in the linear structure. Therefore, enzymes and water have increased access to hydrolysable ester groups.

Star PCL **2.7** and star poly(ε-CL)-*co*-(BL) **2.14** showed similar enzymatic degradation rates of >90% mass loss within 15 days. Generally the $\%\chi_c$ increased within the first few days (0-3 days) of enzymatic degradation and then subsequently decreased. This suggests enzymatic degradation occurs primarily in the amorphous regions of the polymer, therefore increasing the overall $\%\chi_c$ of the polymer. SEM analyses supports this result, showing significant changes in surface morphology such as surface pitting and occurrence of crystal spherulite structures within the first few days of enzymatic degradation.

A series of novel four-arm star PCL **3.10 – 3.12** containing a central PEG moiety bridged with bisMPA linkages were synthesised and fully characterised. The four-step syntheses involved the hydroxyl-protection of bisMPA **3.6** using acetic anhydride, followed by coupling with PEG **3.4** using DCC and DMAP to produce hydroxyl-protected PEG macro-initiator **3.8**. The acetal groups were subsequently removed under acidic conditions to give tetra-hydroxyl PEG macro-initiator **3.9** and used in the ROP of ε-CL to give novel four-

arm star copolymers **3.10 – 3.12**. It must be noted a small amount of ester bonds in the tetra-hydroxyl PEG macro-initiator **3.9** were hydrolysed during the acidic acetal removal to give PEG diol **3.4**. This impurity could not be easily removed due to the similar chemical nature of PEG **3.4** and the tetra-hydroxyl PEG macro-initiator **3.9**. For comparison, linear copolymer PCL-*b*-PEG-*b*-PCL **3.5** was synthesised by the ROP of ε-CL catalysed by $SnOct_2$ and using PEG **3.4** as a macro-initiator. The novel four-arm star copolymers **3.10 – 3.12** showed good control in the ROP of ε-CL as the $\overline{DP}_{NMR}$ were in good correlation with $\overline{DP}_{Th}$. However, Đ from 1.32 to 1.51 and small lower molecular weight shoulders are seen in the SEC chromatograms of the four-arm star copolymers. This is due to using a polydisperse PEG macro-initiator **3.9**. Contact angle and %WU analyses confirmed that as %PEG content decreased from 28% to 6%, the hydrophilic nature of the copolymers decreased. This is expected based on the hydrophilic nature of PEG.

The linear copolymer PCL-*b*-PEG-*b*-PCL **3.5** exhibited the fastest rate of enzymatic degradation, due to greater polymer chain mobility and comparatively high hydrophilic %PEG content. There is an increased shielding of the hydrophilic central PEG unit from the four hydrophobic PCL arms in the star structures **3.10 – 3.12**, leading to a slower degradation rate. The series of novel star copolymers **3.10 – 3.12** showed similar enzymatic degradation rates (>90% mass loss within 7 days) however, the degradation rates were notably faster than star PCL **2.7** (>90% mass loss in 15 days). This indicates the incorporation of a central hydrophilic PEG moiety into a star PCL structure, increases the overall hydrophilic nature and hence the enzymatic degradation rate. DSC and SEM analyses confirm enzymatic degradation and show an increase in $\%\chi_c$ during the first stages of degradation. This is due to enzymes preferentially degrading the amorphous regions of PCL as well as the production of shorter polymer chains during degradation, leading to an overall increase in $\%\chi_c$.

Seven-arm star PCL **4.5** with acetylated β-CD core and a $\overline{DP}_{Th}$ of 30 per arm was synthesised. The four-step synthetic approach involved protecting the 1° OH groups of β-CD **4.1** using TBDMS-Cl to give **4.2**. The 2° OH groups were then acetylated to give **4.3**, using acetic anhydride. The TBDMS moieties were then removed to give partially acetylated β-CD **4.4** containing seven 1° OH groups to be used as an initiator in the ROP

of ε-CL catalysed by $SnOct_2$ to give **4.5**. The products from each step were obtained in good yield and fully characterised. Seven-arm star PCL with a β-CD core **4.5** showed increased hydrophilicity with an initial contact angle of 75.6° compared to star PCL **2.7** with an initial contact angle of 86.3°, indicating the incorporation of a β-CD moiety imparts a small degree of hydrophilicity. However, seven-arm star PCL with a β-CD core **4.5** exhibited poor wettability as negligible change in contact angle was detected over 30 s, compared to a small decrease seen in star PCL **2.7**. Furthermore, seven-arm star PCL with a β-CD core **4.5** showed a very low water uptake of 2%, due to the functionalization of the OH groups in the β-CD moiety.

Seven-arm star PCL with a β-CD core **4.5** showed a very low rate of enzymatic degradation with 7% mass loss in 20 days, compared to star PCL **2.7** with 94% mass loss in 15 days. This can be explained by the low wettability of seven-arm star PCL with a β-CD core **4.5** and the potential formation of inclusion complexes with the β-CD inner cavity and either the lipase enzyme or degraded PCL fragments. This would restrict mobility and access of the enzyme to the hydrolysable ester groups on the PCL moiety and therefore, decrease the rate of enzymatic degradation. An initial increase in $\%\chi_c$ from 16% to 38% was seen after 2 days, followed by a decrease to 10% after 10 days, and a significant increase to 74% after 20 days of enzymatic degradation. The initial increase in $\%\chi_c$ could be explained by the preferential enzymatic degradation of the amorphous regions of the polymer, followed by the degradation of more crystalline areas, causing a decrease in $\%\chi_c$. The significant increase in χ_c to 74% seen after 20 days of enzymatic degradation could be due to the formation of inclusion complexes with crystalline PCL degradation products and the inner cavity of the β-CD moiety.

Diisocyanate prepolymers **5.3** and **5.4** containing a central PCL moiety were synthesised by the reaction of PCL-diol with two molar equivalents of either TDI **5.2** or MDI **5.1**, respectively. Diisocyanate prepolymers **5.5** and **5.6** containing a central PCL-*b*-PEG-*b*-PEG moiety were synthesised by the reaction of PCL-*b*-PEG-*b*-PEG **3.3** having a $\overline{DP}$ of 50 per arm with either TDI **5.2** or MDI **5.1**. Diisocyanate prepolymer **5.7** containing a central PCL-*b*-PEG-*b*-PEG moiety was synthesised by the reaction of PCL-*b*-PEG-*b*-PEG **3.2** having a $\overline{DP}$ of 10 per arm MDI **5.1**. Diisocyanate prepolymers were fully characterised and showed the successful reaction of the NCO and OH groups to form a urethane group.

FT-IR showed the presence of C=N bonds in the diisocyanate prepolymers attributed to the NCO group, as well as C-N and N-H bonds, attributed to the urethane group. SEC showed that diisocyanate prepolymers exhibited a higher M_n than expected, particularly those containing the MDI moiety. This is due to further reactions of the NCO group and the diisocyanate prepolymers, leading to light cross-linking. The hydrophilic nature of MDI-based diisocyanate prepolymers, **5.6** and **5.7** containing a central PCL-*b*-PEG-*b*-PEG moiety, was determined by contact angle, surface wetting and % water uptake (%WU) analyses. Significantly increased wetting over 30 s, decreased contact angle and increased %WU was seen for diisocyanate prepolymer **5.7** with the lower $\overline{DP}$ of 10 per arm. This was due to the decreased hydrophobic PCL content and increased hydrophilic PEG content.

The fastest rate of degradation was seen for TDI-based diisocyanate prepolymer **5.5** having a $\overline{DP}$ of 50 per arm with 100% mass loss in 4 days. This could be due decreased crystalline and hydrophobic aromatic content in comparison to MDI-based diisocyanate prepolymers **5.6 – 5.7**. Furthermore, the light cross-linking reactions with the NCO group led to a significant increase in M_n and therefore, decreased the rate of enzymatic degradation. MDI-based diisocyanate prepolymer **5.7** with a $\overline{DP}$ of 10 per arm, degraded at a significantly faster rate at 79% mass loss in 10 days, than diisocyanate prepolymer **5.6** with a $\overline{DP}$ of 50 per arm, of 23% mass loss in 40 days of enzymatic degradation. This is due to the lower M_n polymer exhibiting increased chain mobility and therefore, increased ability for the enzyme to penetrate the bulk of the polymer and access the hydrolysable ester groups on the PCL moiety. Furthermore, MDI-based diisocyanate prepolymer **5.7** with a $\overline{DP}$ of 10 per arm contains a decreased content of hydrophobic PCL and increased content of hydrophilic PEG in comparison to the MDI-based diisocyanate prepolymer **5.6** with a $\overline{DP}$ of 50 per arm. The overall increase in hydrophilicity of the diisocyanate prepolymer will increase the access of enzymes and water through the bulk of the polymer and therefore increase the rate of enzymatic degradation.

A series of PUs **6.1 – 6.11** were synthesised using biodegradable star PCL-based polyols **2.7**, **2.14**, **3.10** and **4.5** (Chapters 2-4) and either biodegradable diisocyanate prepolymers **5.3 – 5.7** (Chapter 5) or MDI **5.1** or TDI **5.2**. FT-IR showed the disappearance of the C=N bond attributed to the NCO group, suggesting complete reaction with OH groups to give a

urethane group. This was supported by the appearance of absorbances attributing to N-H and C-N bonds. There was no clear correlation between the %WU and the rate of enzymatic degradation, due to experimental error in %WU. Generally, PUs containing longer and more flexible diisocyanate prepolymers showed a higher % solvent uptake (%SU) due to the formation of a less dense structure. However, the PUs synthesised using the diisocyanate prepolymers exhibited a lower rate of enzymatic degradation than PUs synthesised with either MDI **5.1** or TDI **5.2**. This is due to secondary and self-addition reactions of the NCO group during the syntheses of diisocyanate prepolymers. This is believed to increase the extent of aromatic content, M_n and cross-linking in the diisocyanate prepolymers.

The enzymatic degradation analyses ceased after 30 days due to time restrictions. Therefore, conclusions about the degradation characteristics of PUs **6.1 – 6.11** are based on the earlier part of degradation, showing up to 18.5% mass loss after 30 days. In general, PUs synthesised using MDI **5.1** or an MDI-based diisocyanate prepolymer **5.4** and **5.6 – 5.7** showed an increased rate of degradation in comparison to PUs synthesised using TDI **5.2** or TDI-based diisocyanate prepolymers **5.3** and **5.5**. This is due to the MDI moiety containing less hindered and more reactive NCO groups, with an increased probability of secondary and self-addition reactions. This would decrease the number of NCO groups available in the system to react with the OH groups on the polyol component and hence give a less dense structure. Therefore, the enzymes and water will have increased mobility and increased access to hydrolyse the ester groups on the PCL moieties. PUs **6.4**, **6.6 – 6.7** and **6.10** synthesised using star poly[(ε-CL)-*co*-(β-BL)] **2.14** showed an increased rate of enzymatic degradation compared to PUs **6.1 – 6.3** and **6.8 – 6.9** synthesised using star PCL **2.7**. This is due to the decreased reactivity of the 2° OH groups in PBL chain end moieties, giving a less dense PU structure. This is supported by the generally high % extracted material (%EM) shown in PUs **6.4**, **6.6 – 6.7** and **6.10** containing the star poly[(ε-CL)-*co*-(β-BL)] **2.14**. The unreacted and partially reacted star polyol will have greater polymer chain mobility and therefore, the enzyme and water will have increased access to the hydrolysable ester groups on the PCL and PBL moieties.

PU **5.5** synthesised using seven-arm star PCL **4.5** with a β-CD core exhibited a very low rate of enzymatic degradation. This could be due to the large central β-CD moiety imparting rigidity to the PU structure. Furthermore, there will be a higher degree of cross-

linking in the seven-arm polyol in comparison to the six-arm and four-arm polyols. This leads to decreased mobility and access of enzyme and water into the bulk of the polymer. On the other hand, PU **6.11** synthesised using four-arm star PCL **3.10** containing a central hydrophilic PEG moiety, showed a high rate of enzymatic degradation after 30 days. The increased rate of enzymatic degradation over 30 days was due to the time required for the water and enzymes to penetrate into the bulk of the material to access the hydrophilic moieties and subsequently hydrolyse the PCL moieties.

7.2 Future Perspectives

With the successful enzymatic degradation of PUs **6.1 – 6.11** within 30 days, further investigation needs to be carried out on a longer time frame, to achieve a full degradation profile. It would be interesting to compare the degradation characteristics of the polyols, diisocyanate prepolymers and PUs using a range of enzymes. This could provide insight into the degradation mechanism of different enzymes. Furthermore, a representative method of polymer degradation in the natural environment could be investigated, such as sludge testing.[1] This would show the extent of PU degradation in the likely conditions of their application end-use, such as sewage-works.

The method used for enzymatic degradation whereby the media was replaced every 24 h, required sufficiently large solid pieces of polymeric material to effectively collect and transfer. The intended application of the biodegradable PUs require small PU particles; therefore it would be beneficial to use these small particles in degradation tests. This would entail development of a suitable method to collect and analyse the degraded PU particles efficiently. Future investigations into the polyol, diisocyanate prepolymer and PU degradation products could lead to further insight into the degradation mechanism. Moreover, any harmful or toxic degradation products could be identified, such as MDA.

It would be beneficial to perform repeat syntheses and enzymatic degradation of PUs to verify the conclusions made in Chapter 6. Any changes in the mixing of PU components or reaction mixture viscosity during PU syntheses could have significant effects on the degree of cross-linking and hence density of the resulting PU. No clear trend for PUs **6.1 – 6.11** can be seen in the relationship between %EM and %SU. Generally %EM showed between

4-12% with a significantly large range of %SU of 58-603%, Figure 7.1. It can be seen that PUs **6.1**, **6.4** and **6.10** appear as anomalous results. It is possible that this was due to inefficient mixing and the variation in viscosities of the reaction mixtures due to the addition of a minimal amount of solvent. Therefore, the syntheses of **6.1**, **6.4** and **6.10** would need to be repeated to verify these unexpected results. Furthermore, development of a PU scale-up reaction necessary for industry could show the effects of heat transfer on the chemical structure of the PU.

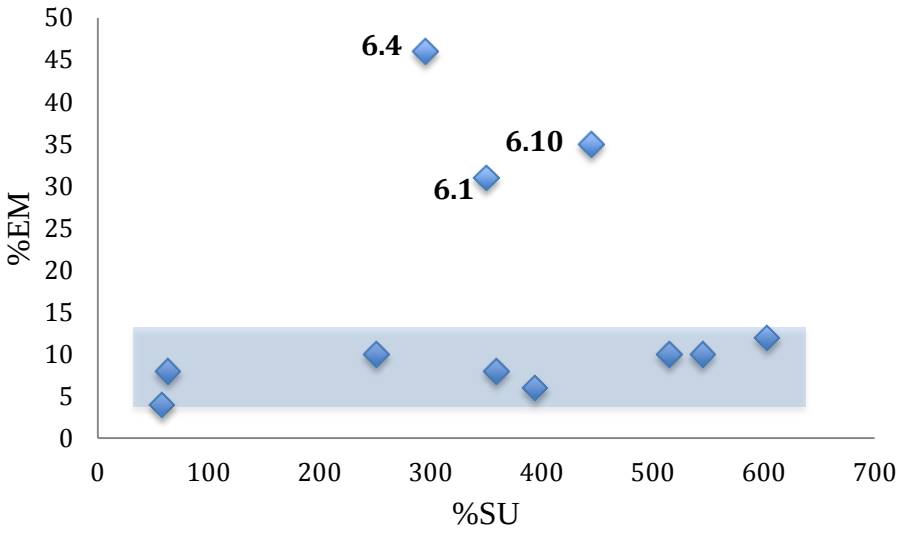

Figure 7.1: Relationship of %EM and %SU in PUs **6.1 – 6.11** (Chapter 6)

Due to time restrictions, only a selection of star PCL-based polyols could be subjected to enzymatic degradation. Furthermore, the method used required heat-pressed polymer discs with the lower M_n polyol discs being too brittle to stay intact during preparation. It would be interesting to investigate the effect of star polyol $\overline{DP}$ per arm and number of arms, on the rate of enzymatic degradation. This would necessitate development of the enzymatic degradation testing method to ensure brittle polymers could be tested.

It would be interesting the synthesise four-arm star poly(ε-CL)-*co*-(β-BL) **7.1** with a central PEG moiety bridged with bisMPA linkages, Figure 7.2. This could be achieved using the four-step synthetic approach outlined in Chapter 3, however the final step would involve the ROP of a mixture of ε-CL and β-BL monomers catalysed by $SnOct_2$. It is anticipated that the incorporation of β-BL would decrease the overall $\%\chi_c$ and therefore, increase the rate of enzymatic degradation.

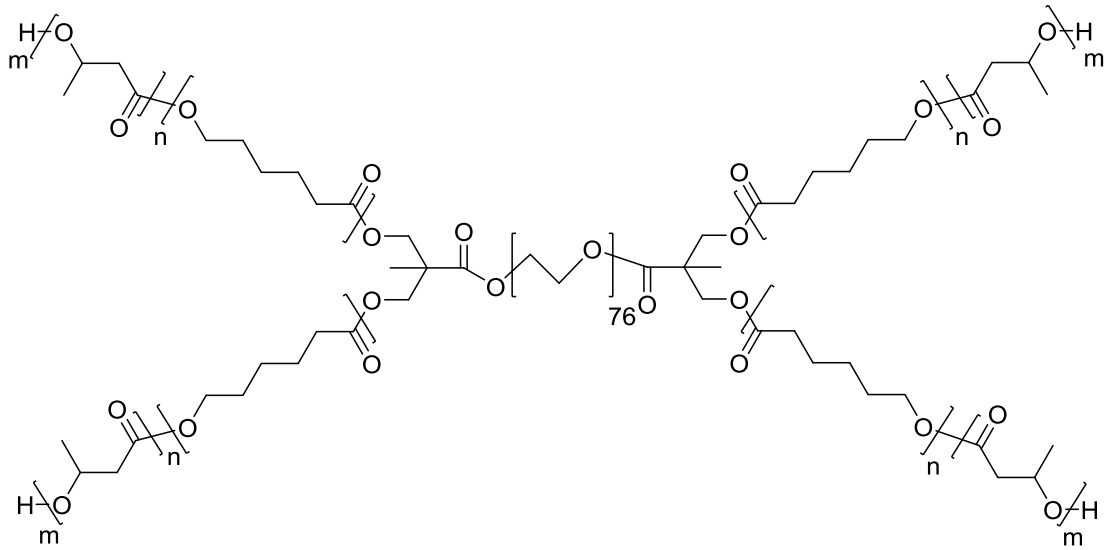

7.1

Figure 7.2: Four-arm star poly[(ε-CL)-*co*-(β-BL)] **7.1** with a central PEG moiety bridged with bisMPA moieties

Investigation into physical properties of the PU materials such as rheology, mechanical strength and hardness testing could give an indication of the degree of cross-linking and density. This information could help explain the degradation behaviour seen for PUs **6.1 – 6.11** in Chapter 6 and assist in the development of future biodegradable PUs.

7.3 References

(1) Juretschko, S., Loy, A., Lehner, A., Wagner, M. *Syst. Appl. Microbio.* **2002**, 84.

Appendices

2.0 Appendices for Chapter 2

2.1 DSC thermogram of star PCL 2.6

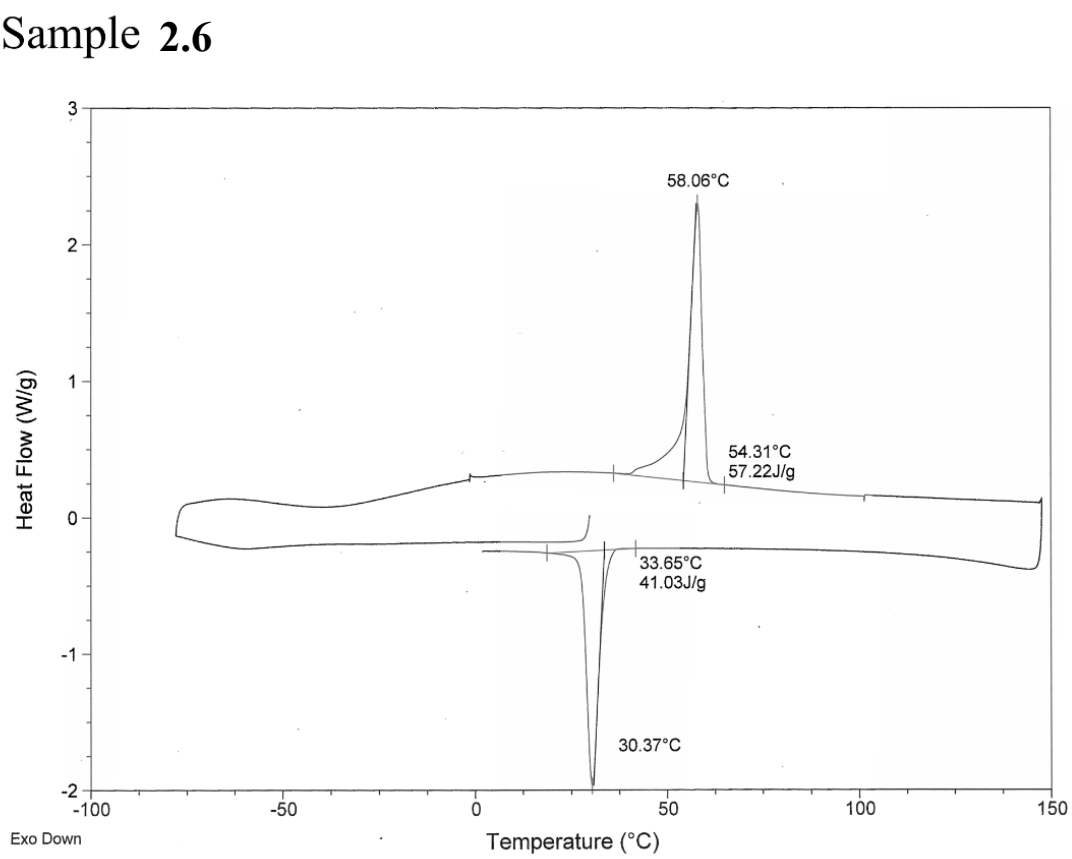

2.2 DSC thermograms for linear PCL 2.2

Linear PCL **2.2**

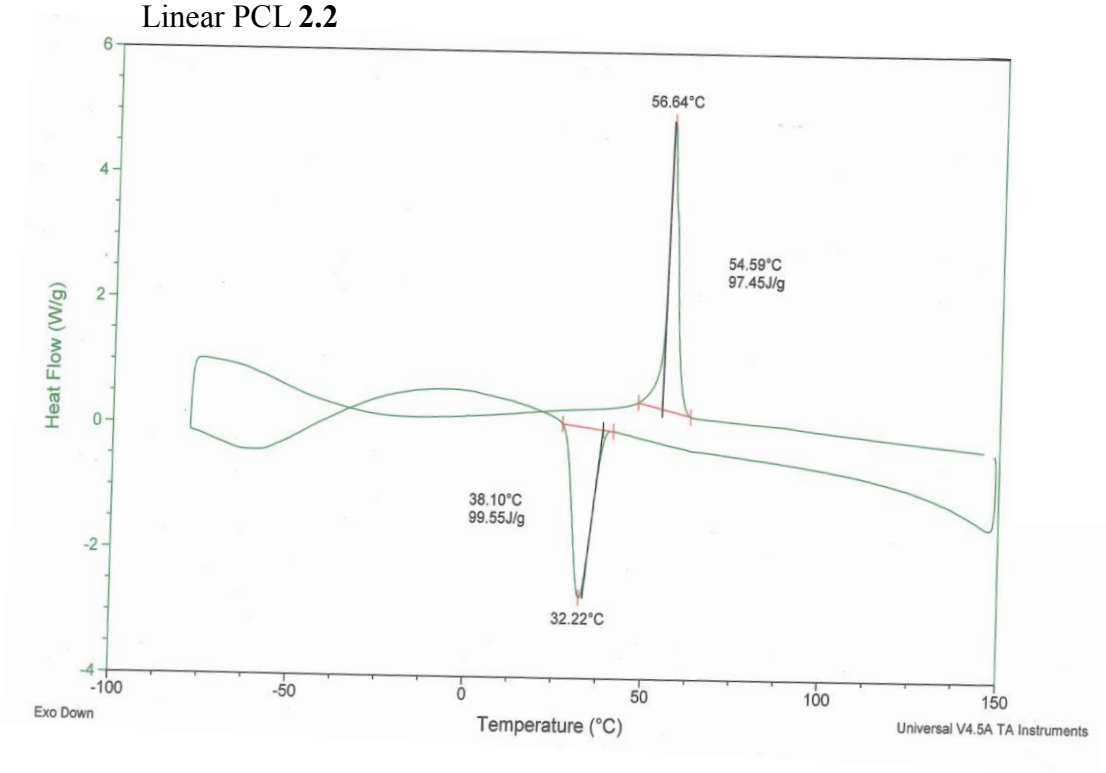

2.3 DSC thermogram of linear PCL 2.2 after 1 day of enzymatic degradation using *pseudomonas cepacia* lipase enzyme in PBS solution (pH 7.4) at 37 °C

Linear PCL **2.2** after 1 day of enzymatic degradation

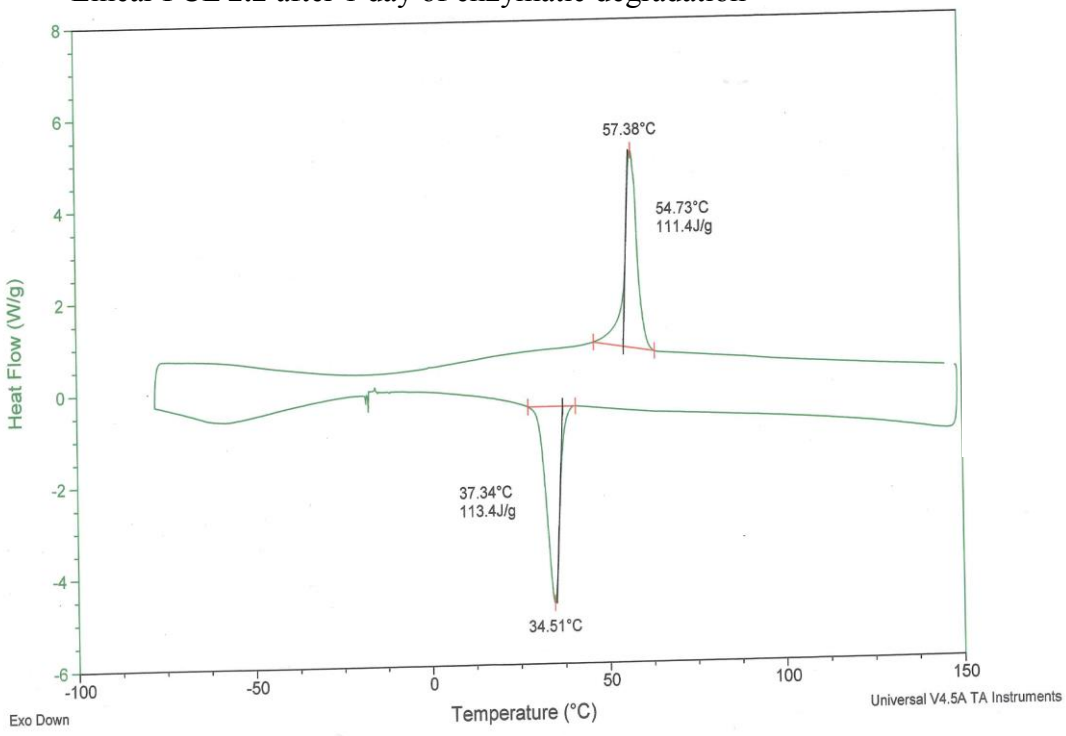

3.0 Appendices for Chapter 3

3.1 FT-IR spectra of hydroxyl-protected PEG macro-initiator 3.8 and tetra-hydroxyl PEG macro-initiator 3.9

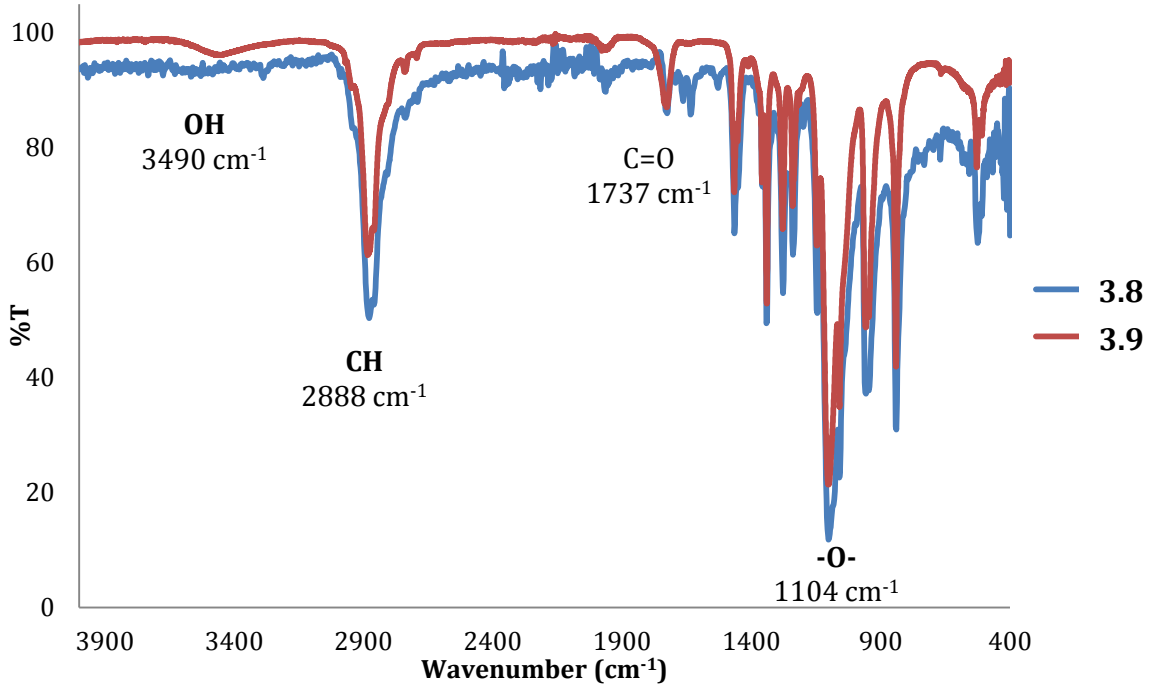

3.2 FT-IR spectrum of four-arm star PCL with a central PEG moiety 3.10

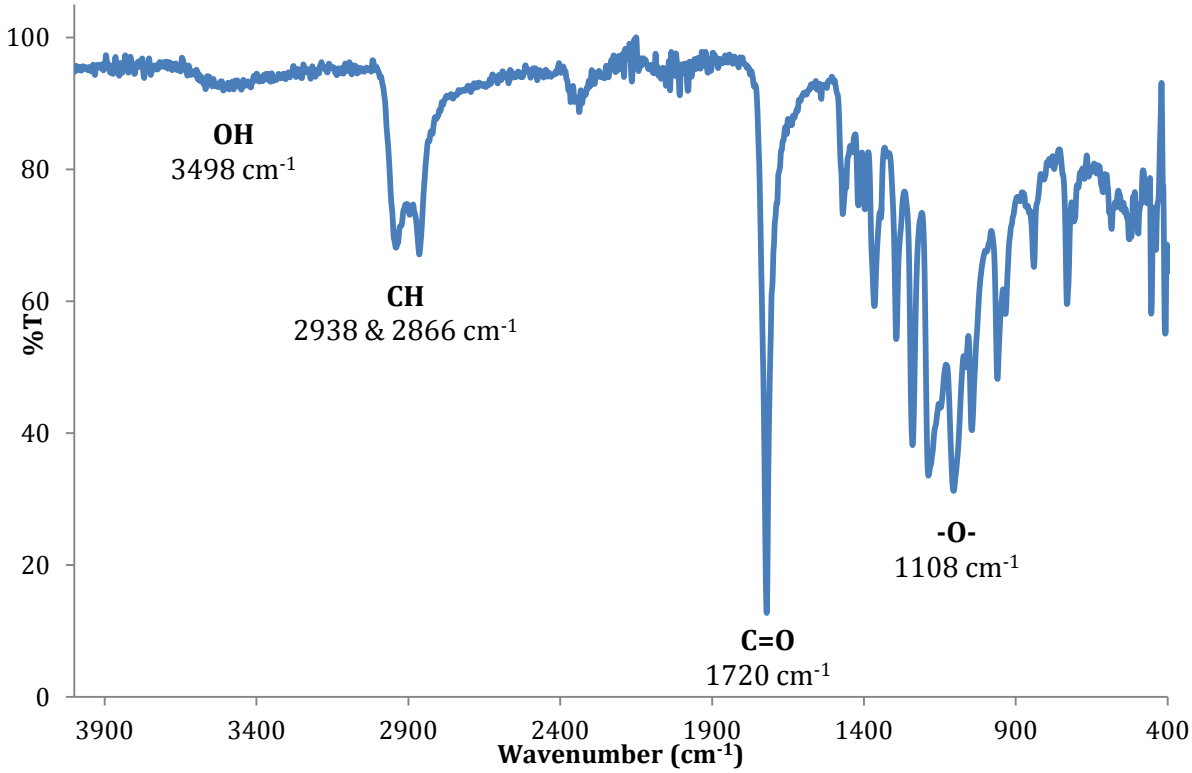

3.3 DSC thermogram for star copolymer 3.12 after 1 day of enzymatic degradation using *pseudomonas cepacia* lipase in PBS solution (pH 7.4) at 37 °C

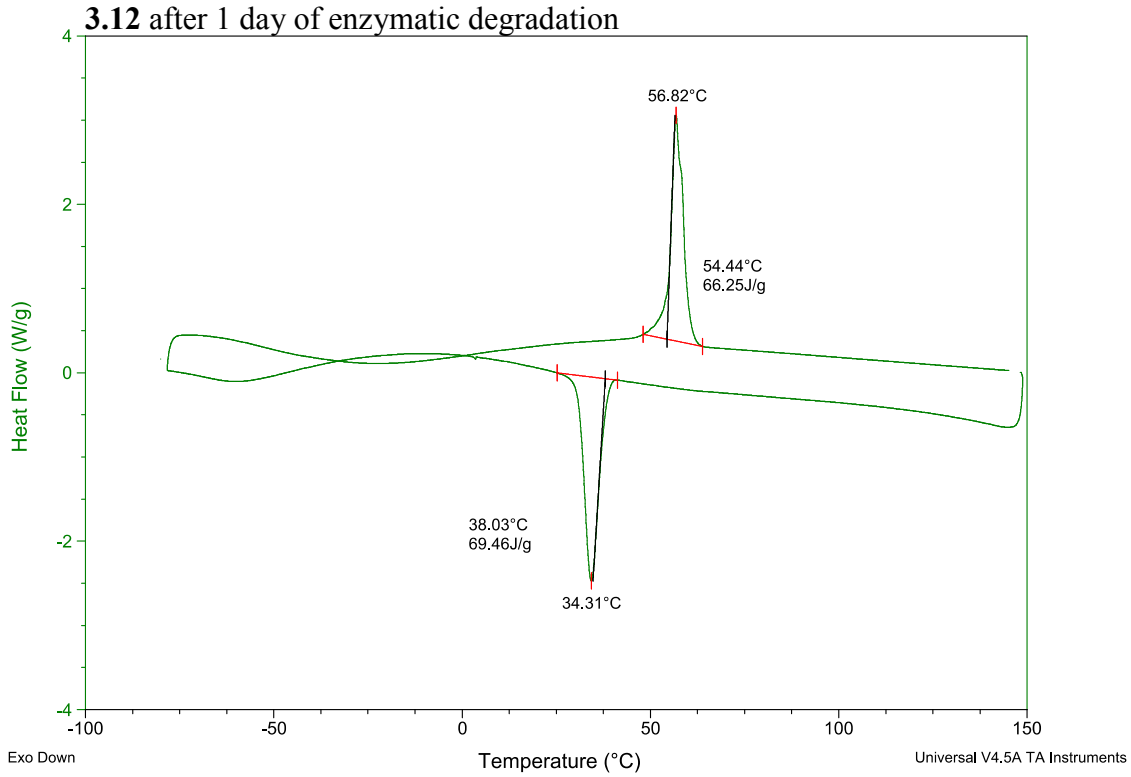

3.4 DSC thermogram for star copolymer 3.12 after 2 days of enzymatic degradation using *pseudomonas cepacia* lipase in PBS solution (pH 7.4) at 37 °C

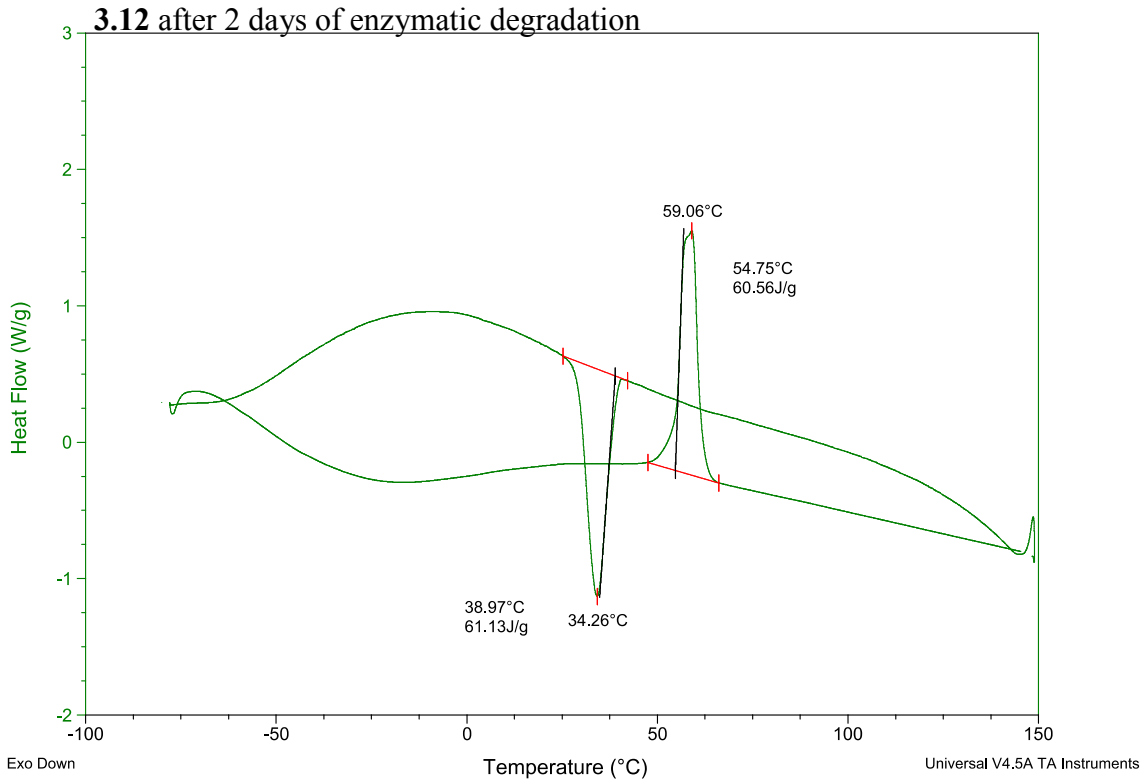

3.5 DSC thermogram for star copolymer 3.12 after 4 days of enzymatic degradation using *pseudomonas cepacia* lipase in PBS solution (pH 7.4) at 37 °C

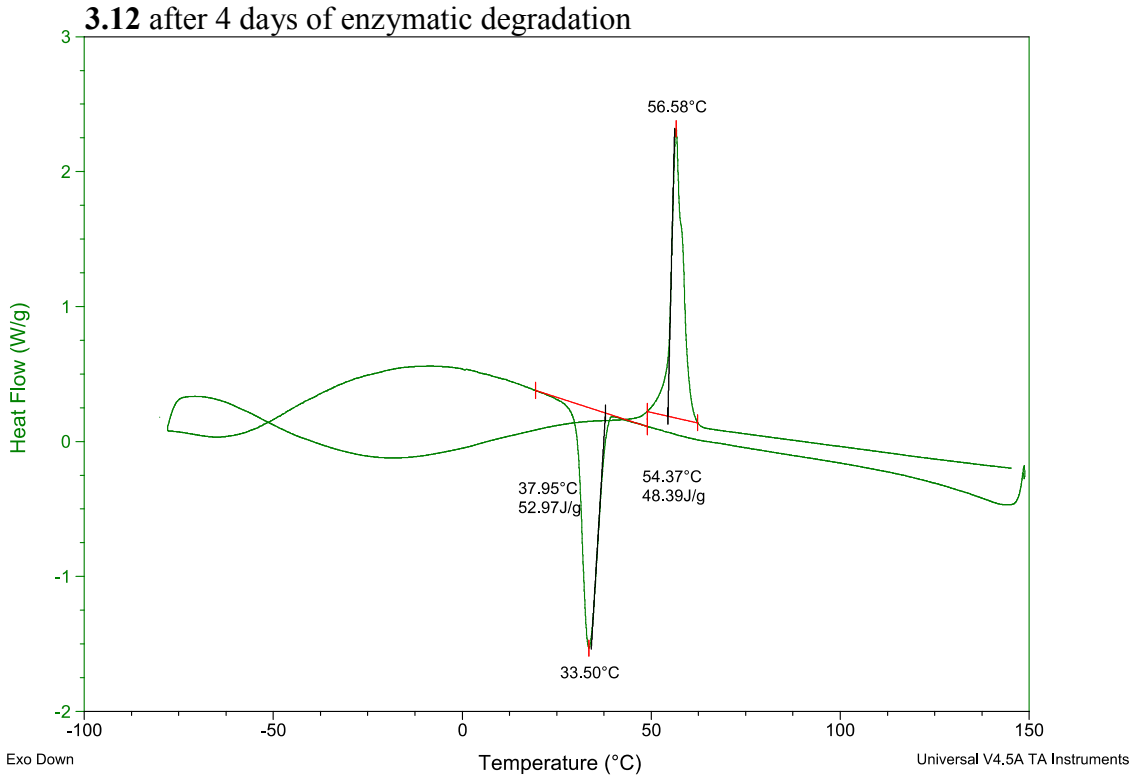

3.6 DSC thermogram for star copolymer 3.12 after 6 days of enzymatic degradation using *pseudomonas cepacia* lipase in PBS solution (pH 7.4) at 37 °C

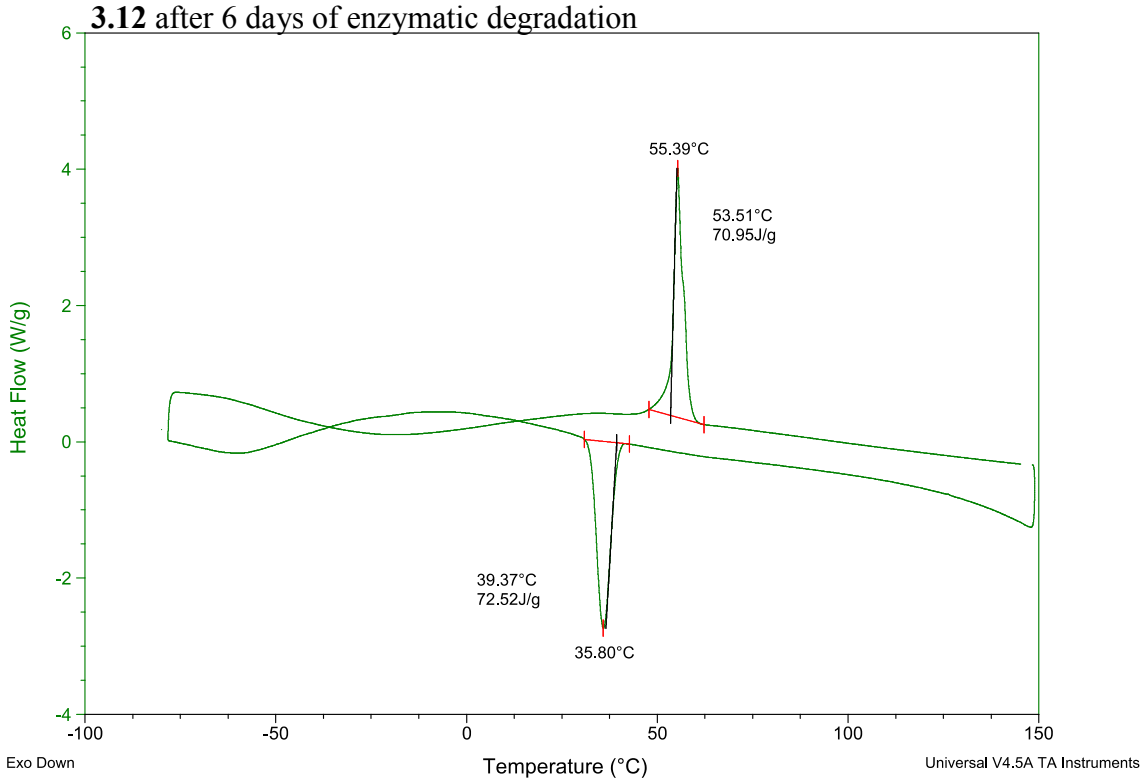

4.0 Appendices for Chapter 4

4.1 100 MHz ^{13}C NMR spectrum of 4.2 in $CDCl_3$

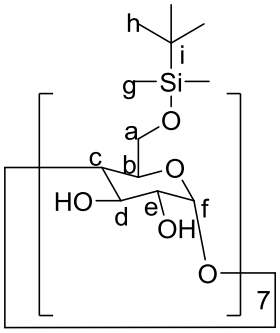

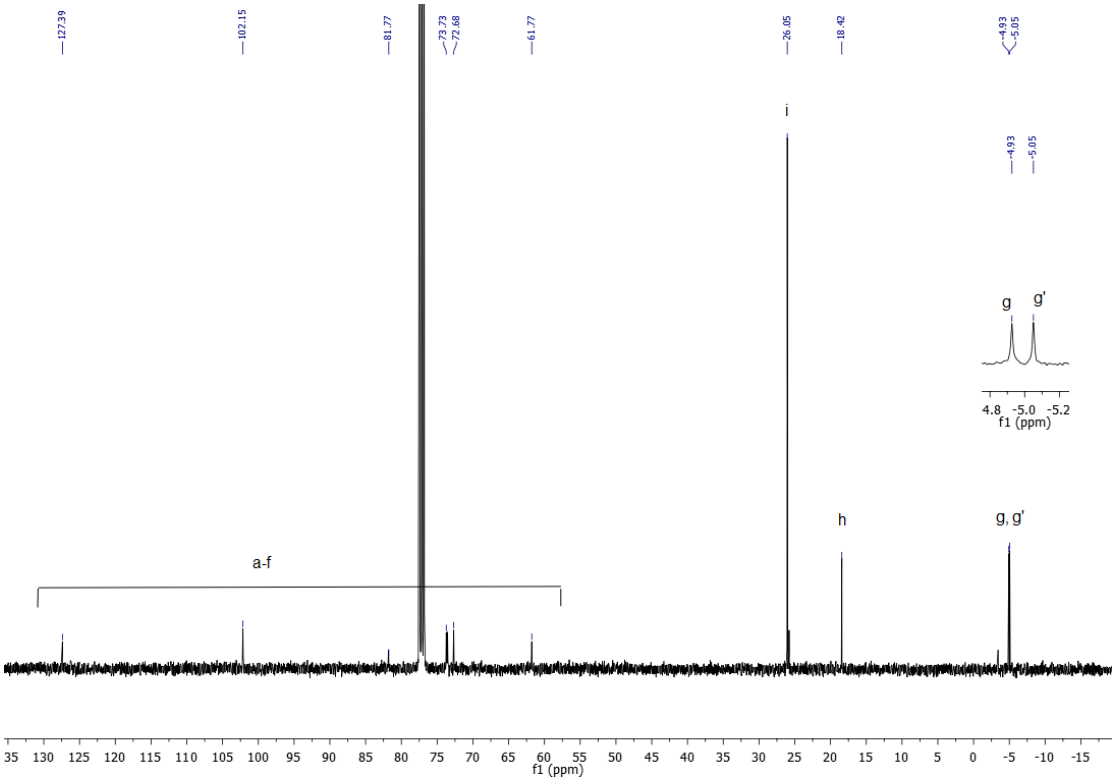

4.2 FT-IR spectra of 4.2 – 4.4

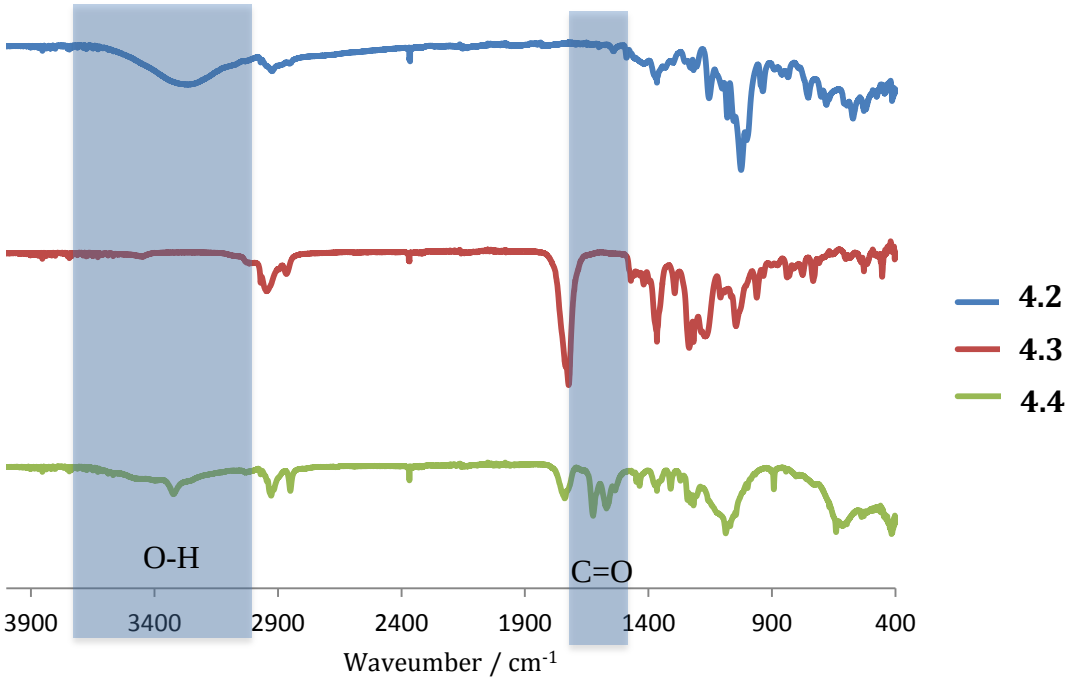

5.0 Appendices for Chapter 5

5.1 400 MHz ^{1}H NMR spectrum of 5.6 in $CDCl_3$

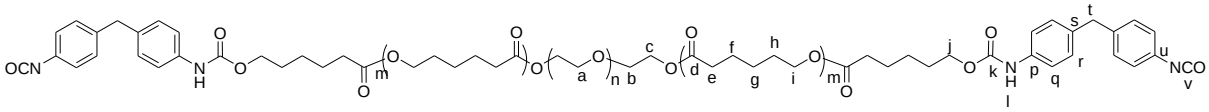

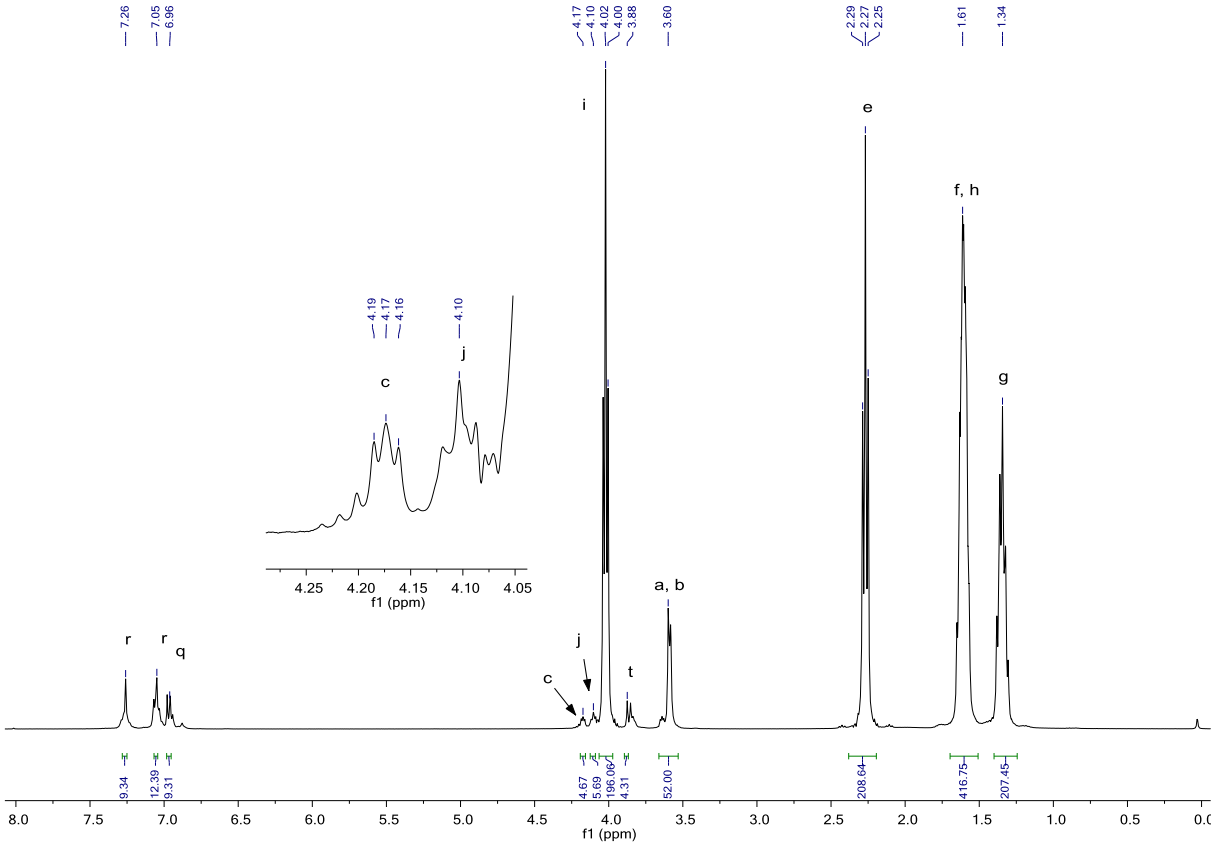

5.2 100 MHz ^{13}C NMR spectrum of 5.6 in $CDCl_3$

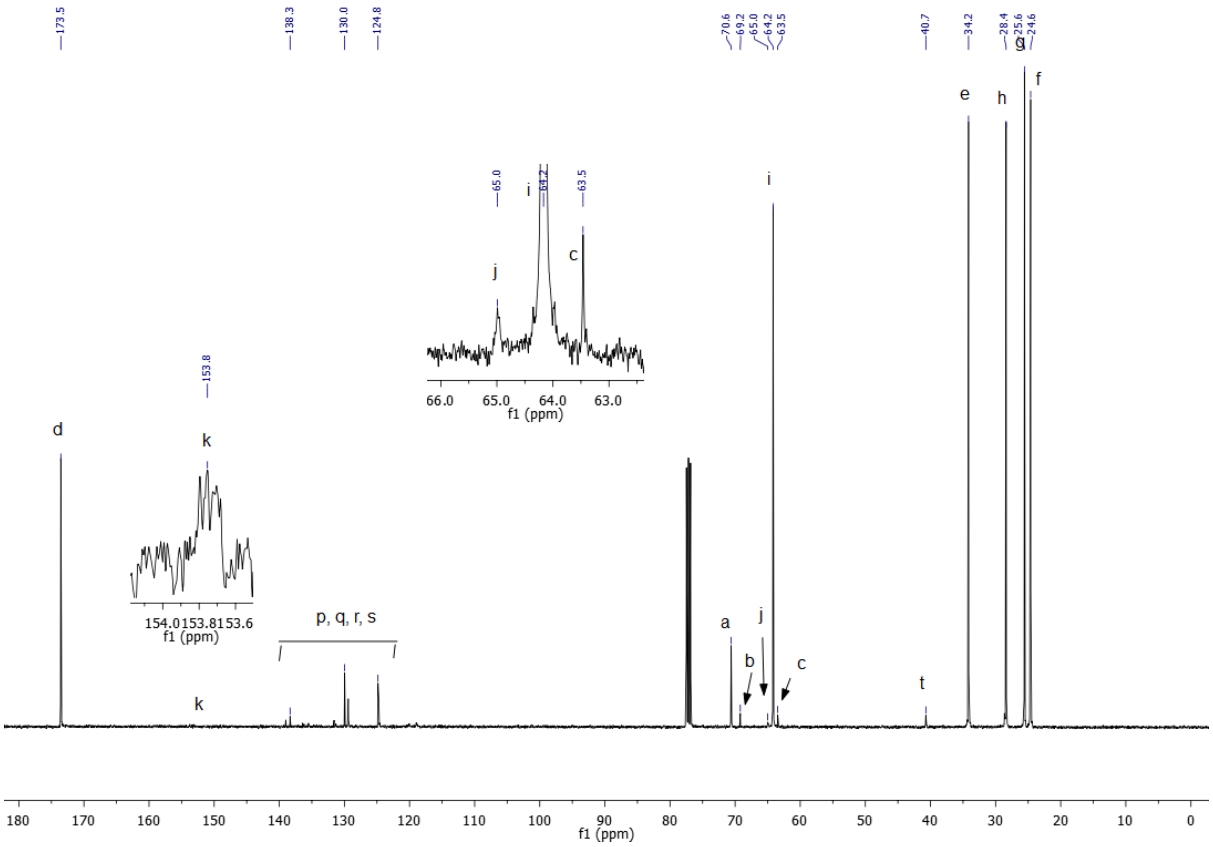

5.3 400 MHz ^{1}H NMR spectrum of 5.7 in $CDCl_3$

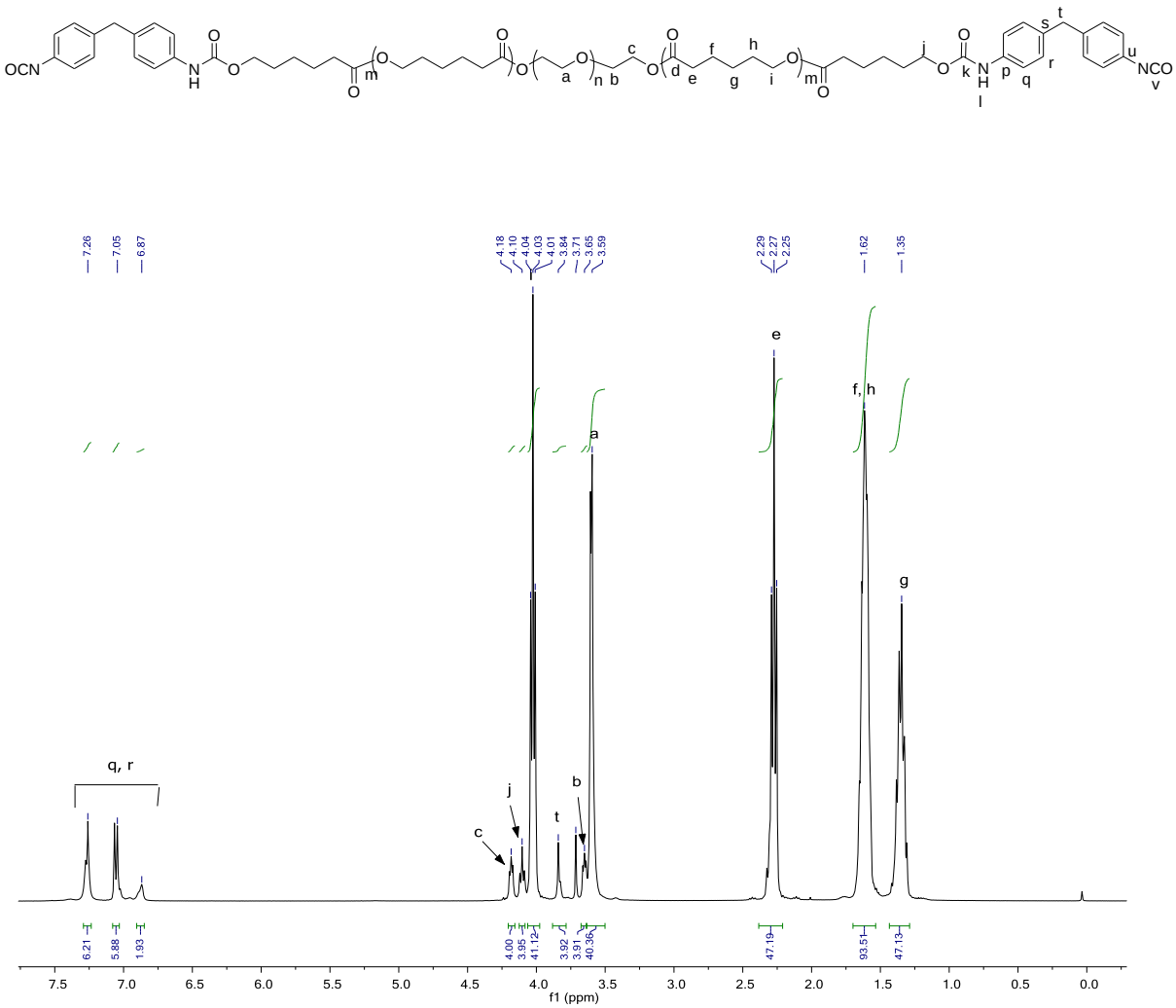

5.4 100 MHz ^{13}C NMR spectrum of 5.7 in $CDCl_3$

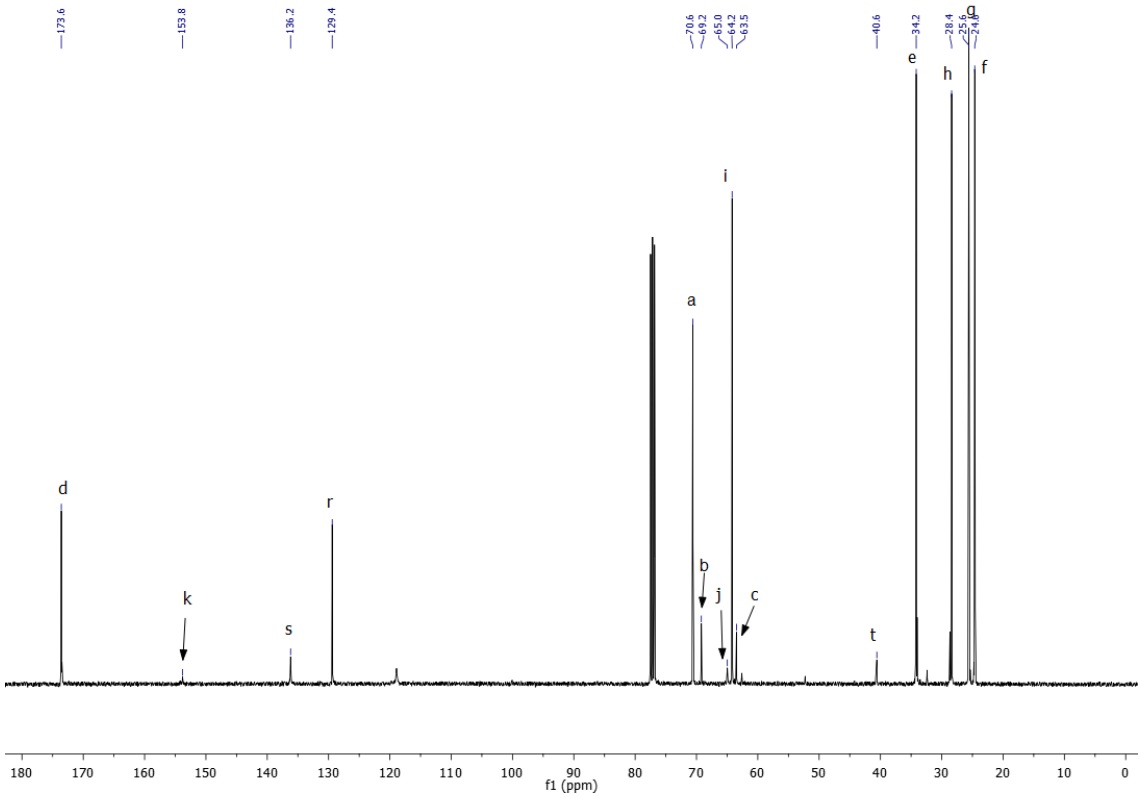

6.0 Appendices for Chapter 6

6.1 FT-IR spectrum of PU 6.1

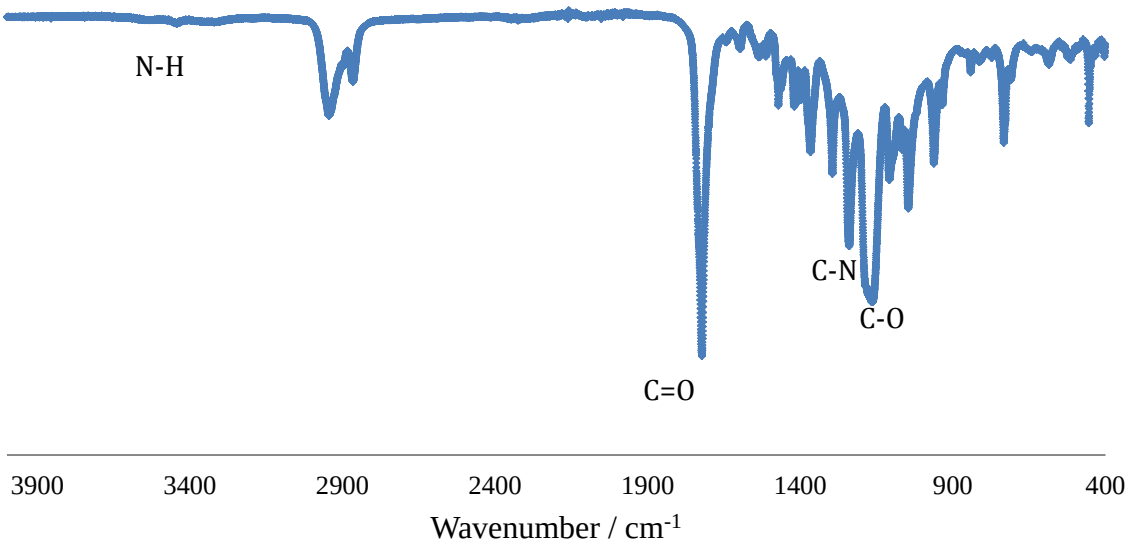

6.2 FT-IR spectrum of PU 6.2

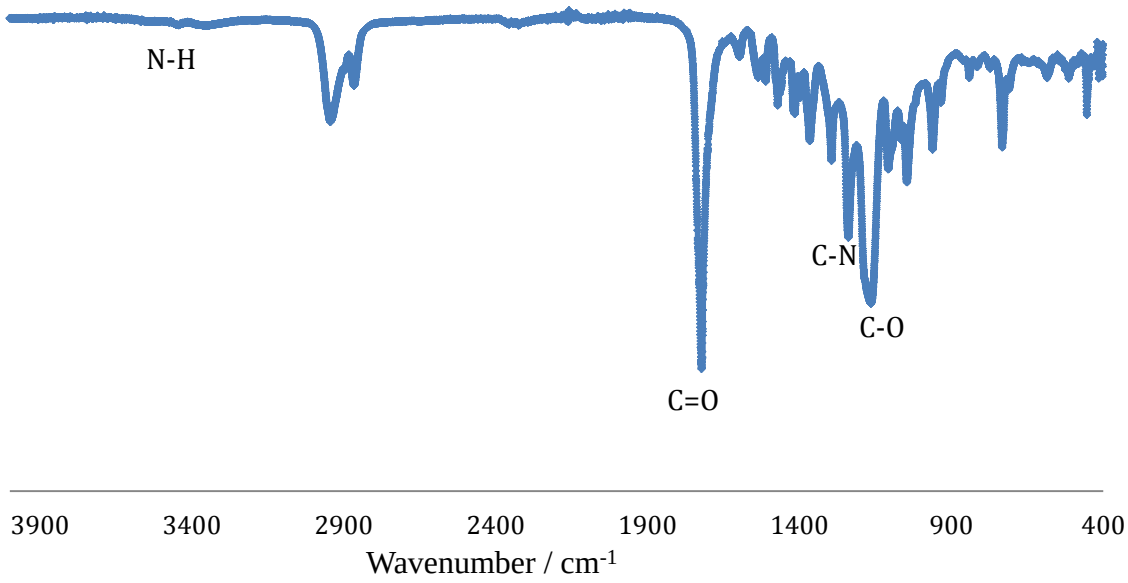

6.3 FT-IR spectrum of PU 6.3

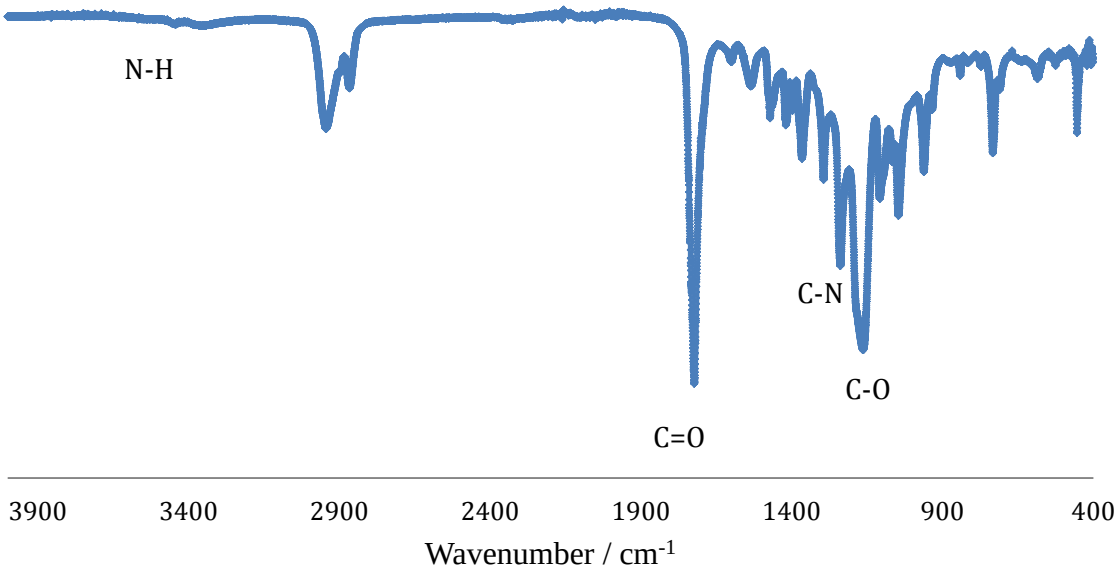

6.4 FT-IR spectrum of PU 6.4

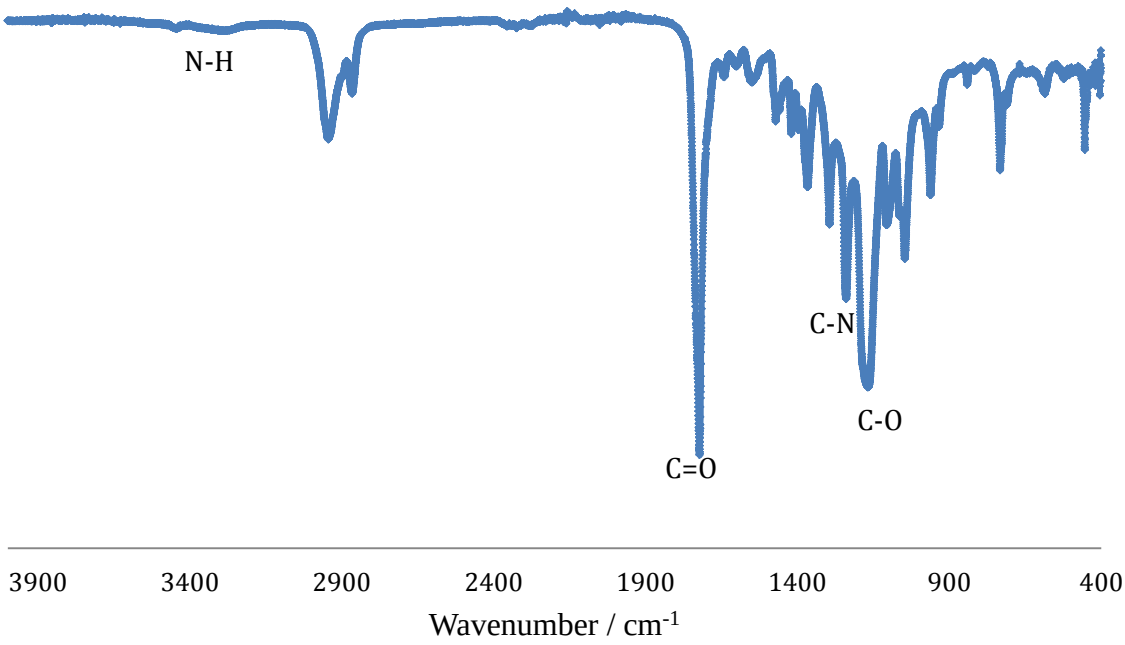

6.5 FT-IR spectrum of PU 6.5

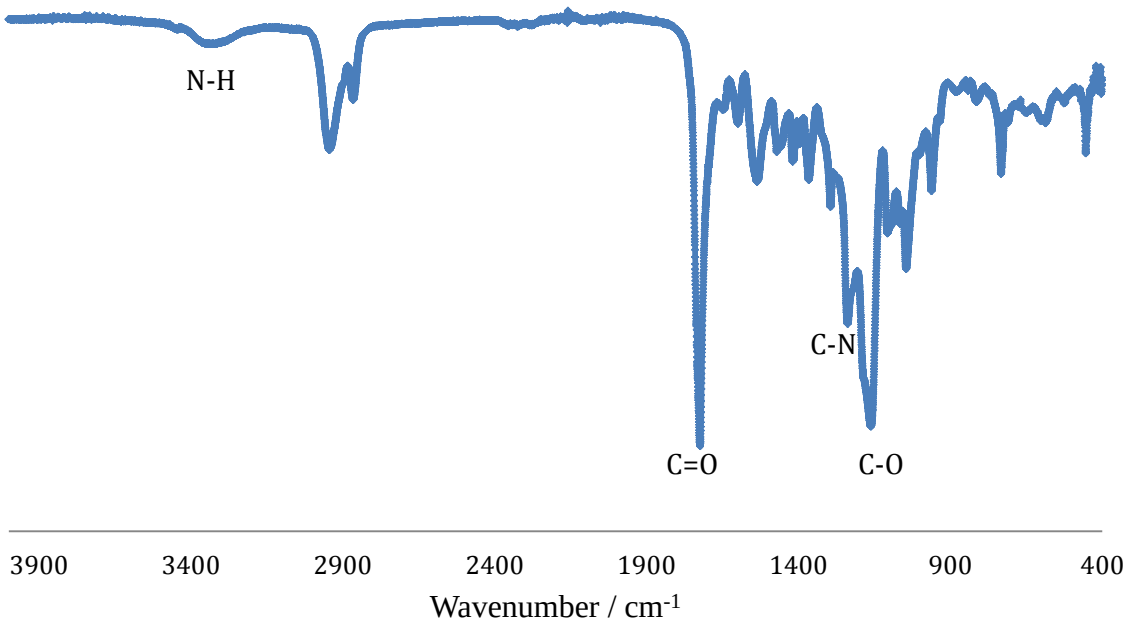

6.6 FT-IR spectrum of PU 6.7

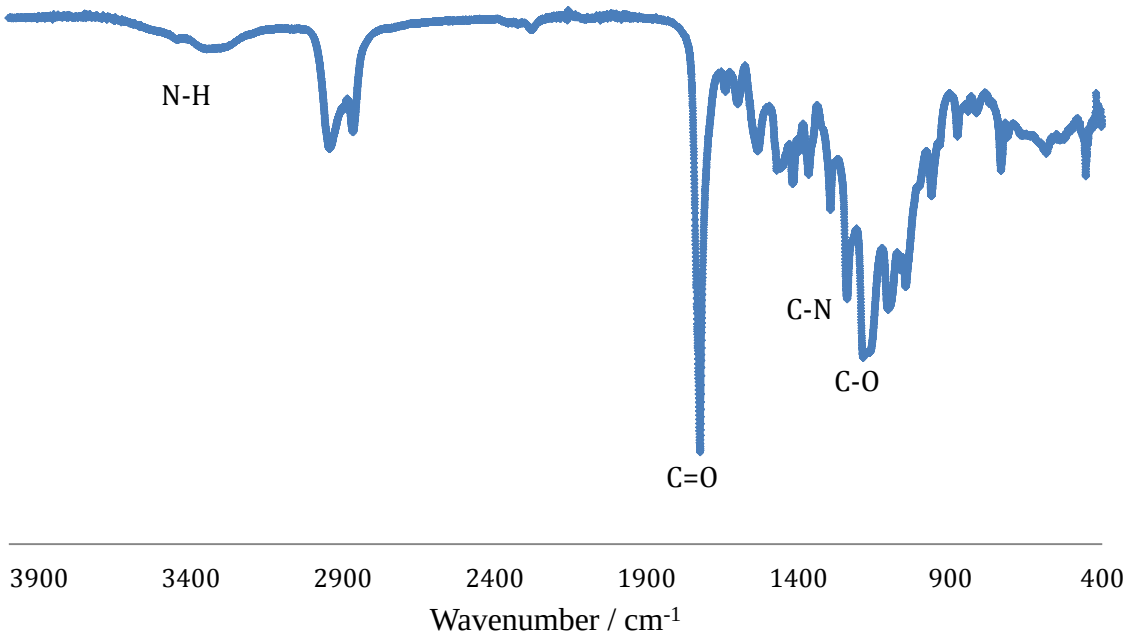

6.7 FT-IR spectrum of PU 6.8

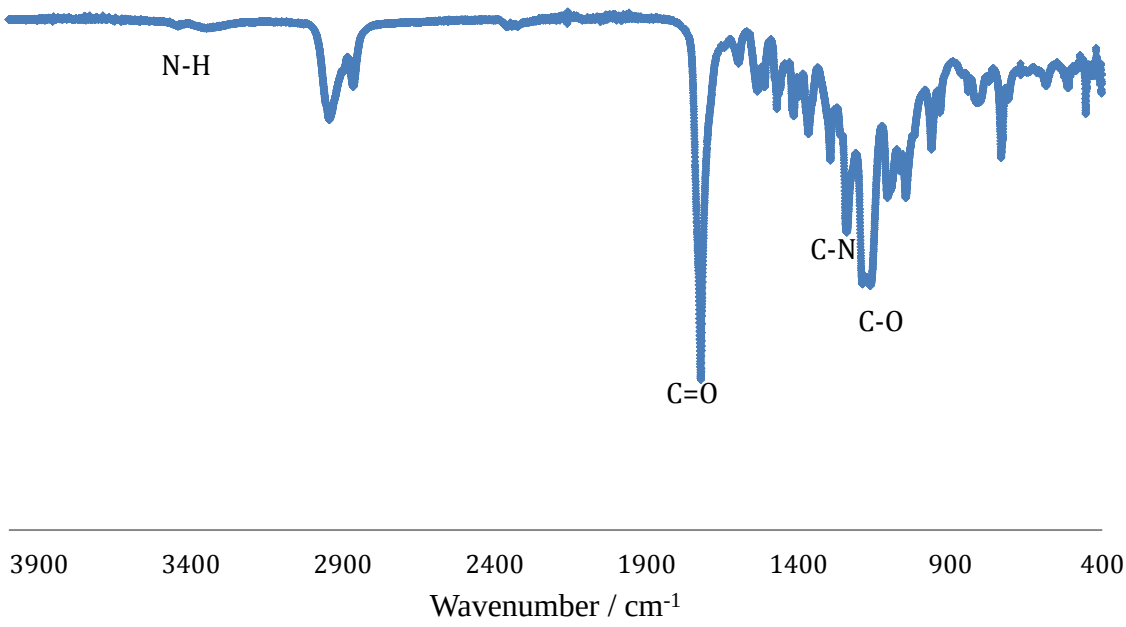

6.8 FT-IR spectrum of PU 6.9

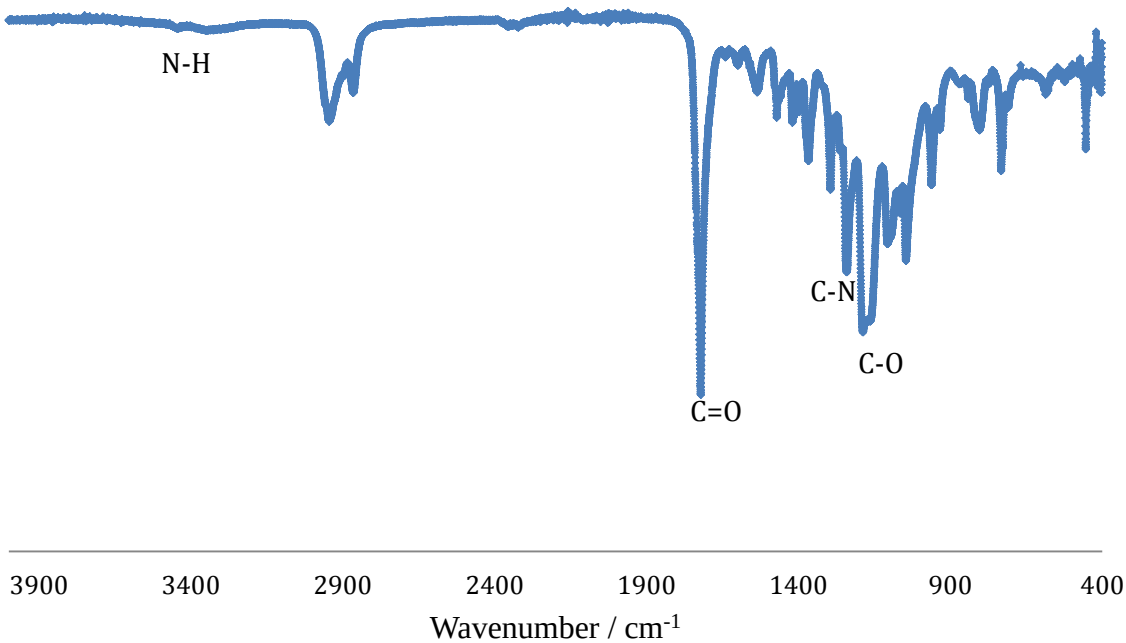

6.9 FT-IR spectrum of PU 6.10

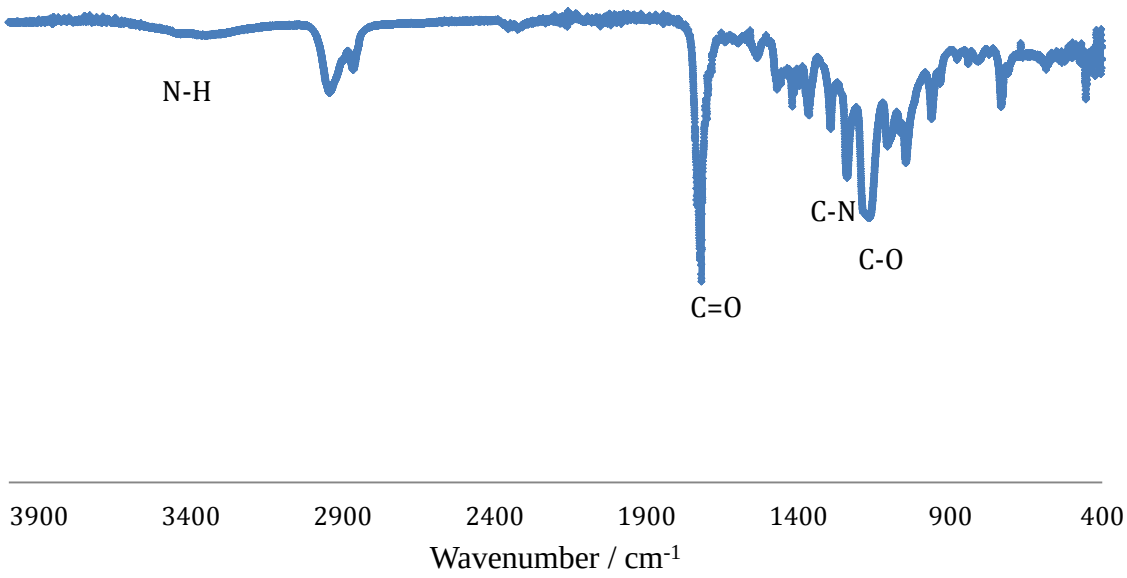

6.10 FT-IR spectrum of PU 6.11

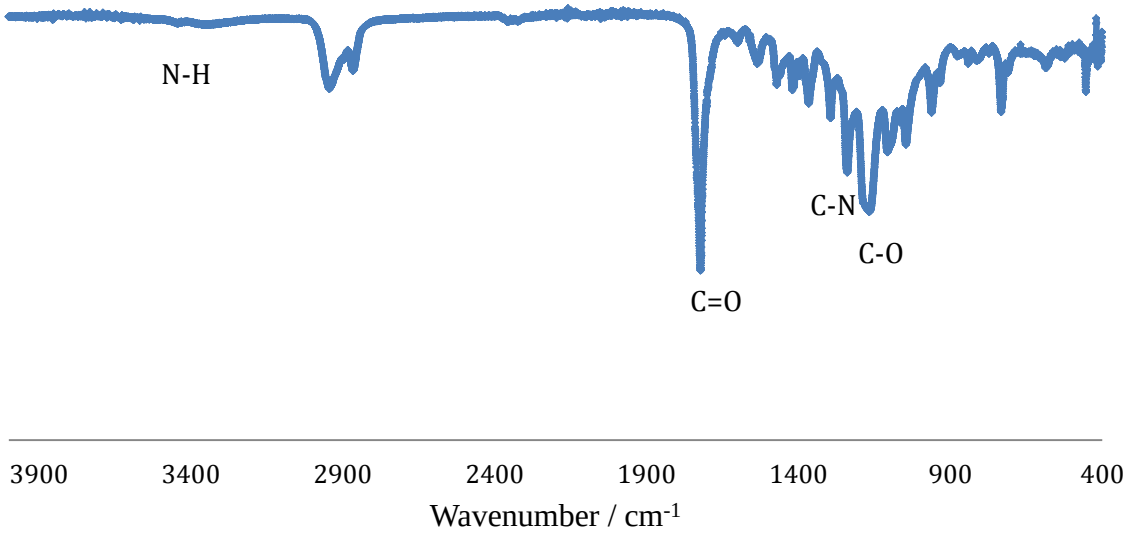

6.11 Table of thermal decomposition temperatures (T_d) for PU 6.1 – 6.11

PU	Component used in the synthesis of PU				T_d / °C
	Polyol			Diisocyanate	
	Central core moiety	No. arms	$\overline{DP}$ per arm (PCL)		
6.1	Dipentaerythritol **2.3**	6	20	MDI **5.1**	311
***6.2**					331
6.3				TDI **5.2**	318
6.4			10 (7 PCL, 3 PBL)		274
6.5	Acetylated β-CD **4.4**	7	30		315
6.6	Dipentaerythritol **2.3**	6	10 (7 PCL, 3 PBL)	MDI-PCL-MDI **5.4**	323
6.7				TDI-PCL-TDI **5.5**	310
6.8			20	MDI-PCL-PEG-PCL-MDI **5.6**	301
6.9				TDI-PCL-PEG-PCL-TDI **5.5**	292
6.10			10 (7 PCL, 3 PBL)		304
6.11	PEG **3.4**	4	20		291

T_d = Thermal decomposition temperature, determined by TGA analyses

* 1.5:1 ratio of OH:NCO groups used. All other samples are 1:1 of OH:NCO